Structural and Diffusion Magnetic Resonance Imaging in Mitochondrial Disease: Validation, Optimisation, and Implementation

Catherine Louise Hossain CSci CPhys MRes MPhys (Hon) BSc (Hon)

Wellcome Centre for Mitochondrial Research

Institute of Neuroscience, Newcastle University

September 2018

This thesis is submitted for the degree of Doctor of Philosophy at Newcastle University

Acknowledgements

Firstly I would like to thank my whole supervisory team of Professor Doug Turnbull, Professor Andy Blamire, Dr Gràinne Gorman, Dr Nichola Lax, and Dr Julie Hall for their support and guidance across a highly multidisciplinary project. I would also like to single out Gràinne, for all the weekly meetings that actually led to this thesis being written in time for the deadline, and also to Andy for introducing me to the 7 T preclinical scanner and letting me loose on it!

I would also like to thank Dr Roger Whittaker and Professor Bobby McFarland for being my internal assessors throughout my PhD and asking awkward questions during my annual reviews that, again, have led to the finishing of this PhD on time.

There have been a large number of people who have supported and guided me technically over the past three years, but there are a few I would like to thank individually: Dr Eoin O'Keefe, for providing the introduction to the GEMSIR Look-Locker sequence that allowed me to carry out the high-resolution scanning of Nichola's post mortem brain sections; Dr Peter Taylor, for patiently explaining DTI processing and providing me with a whole raft of useful command line prompts; Heather Thompson for carrying out the manual cerebellar segmentation of the entire cohort and control group; and finally to the Institute of Neuroscience IT department who have rescued my computer on a number of occasions when it decided it no longer wanted to play with the virtual machines that were so vital to my work.

Finally, I would like to thank the Wellcome Trust for sponsoring me through the whole experience.

Author's Declaration

This thesis is submitted for the degree of Doctor of Philosophy at Newcastle University. The research was sponsored by the Wellcome Trust and was conducted in the Wellcome Centre for Mitochondrial Research, Institute of Neuroscience, and unless otherwise stated is my own work. The research was completed under the supervision of Professor Sir D. M. Turnbull, Professor A. Blamire, Dr. G. S. Gorman, Dr. J. Hall, and Dr. N. Z. Lax from September 2015 to September 2018.

I certify that none of the material offered in this thesis has been previously submitted by me for a degree, or any other qualification, at any other university.

Abstract

Mitochondrial DNA mutations lead to a group of diseases that are both genetically and phenotypically heterogeneous. The m.3243A>G point mutation is one of the most common and is also present in around 80% of patients with mitochondrial encephalomyopathy, lactic acidosis and stroke-like episodes (MELAS), which is a phenotype characterised by symptoms that affect multiple systems and are either progressive or recessive progressive in nature. The aim of this thesis was to develop analysis methodologies to quantitatively characterise the structural properties of the brains of controls, carriers, and MELAS patients using non-invasive MRI techniques to then determine

I developed robust segmentation protocols from first principles for the global segmentation using FSL 5.0, and also for the regional segmentation using FreeSurfer 5.4. Global segmentation results shows that total intracranial volume may provide a surrogate marker for susceptibility to the onset of stroke-like episodes. Grey and white matter volumes showed significant difference in brain composition between controls and carriers despite the absence of overall brain volume differences. Regional segmentation highlighted that MELAS patients showed an almost global thinning of the cortex compared to both controls and carrier, but all carriers of the m.3243A>G point mutation showed significant thinning of the temporal pole and entorhinal cortex irrespective of the symptoms presented.

The TBSS analysis repeated this finding of a global difference in white matter fractional anisotropy between carriers and MELAS patients, indicating that although stroke-like episodes lead to localised lesions, the degenerative effects are felt throughout the brain.

The ultra-high-resolution MRI of post mortem sections highlighted the potential for the use of this technique in the future to allow the co-registration of MRI and neuropathological imaging despite the condition of the brain sections being suboptimal due to mounting in hydrogel.

This study provides a protocol for the systematic, quantitative characterisation, along with initial data capture and analysis, of brain volumes in people harbouring the m.3243A>G point mutation. This can be used as a starting point to more effectively investigate much larger populations of people with mitochondrial disease.

Publications

Published abstracts

1. Hossain, C. L., Hall, J., Ng, Y., Bright, A., Blamire, A., Turnbull, D. M., McFarland, R., Gorman, G. S. (2017) ‘Identification of biomarkers in patients with mitochondrial disease using non-invasive imaging’, Conference Proceedings EuroMIT 2017.

2. Hossain, C. L., Hall, J., Ng, Y., Bright, A., Blamire, A., Turnbull, D. M., McFarland, R., Gorman, G. S. (2018) ‘Structural analysis of m.3243A>G patients using 3D anatomical brain scans’, Conference Proceedings ISMRM, Paris 2018, Neurodegeneration 3622.

List of Figures

List of Tables

List of Equations

Abbreviations

AD	Alzheimer's Disease
ADC	Apparent diffusion coefficient
ASL	Arterial spin labelling
ATP	Adenosine tri-phosphate
BET	Brain extraction tool
BMI	Body mass index
CKD	Chronic kidney disease
CNN	Convolutional neural network
CNS	Central nervous system
COX	Cytochrome c oxidase
CPEO	Chronic progressive external ophthalmoplegia
CSF	Cerebrospinal fluid
DICOM	Digital imaging and communications
DKI	Diffusion Kurtosis Imaging
DNA	Deoxyribonucleic acid
DTI	Diffusion tensor imaging
DWI	Diffusion-weighted imaging
DW-MRS	Diffusion-weighted magnetic resonance spectroscopy
EEG	Electroencephalography
ETC	Electron transport chain
FA	Fractional anisotropy
FAST	FMRIB's automated segmentation tool

FSL	FMRIB Software Library
GABA	Gamma-aminobutyric acid
GEMS	Gradient echo multi-slice
GEMSIR	GEMS inversion recovery
GLM	General linear matrix
GM	Grey matter
GUI	Graphical user interface
IVF	In-vitro fertilisation
LVH	Left ventricular hypertrophy
MD	Mean diffusivity
MEG	Magnetoencephalography
MELAS	Mitochondrial encephalopathy, lactic acidosis and stroke-like episodes
MIDD	Maternally inherited deafness and diabetes
MPRAGE	Magnetisation prepared rapid acquisition gradient echo
MR	Magnetic resonance
MRA	MR Angiography
MRC	Medical research council
MRI	Magnetic resonance imaging
MRS	Magnetic resonance spectroscopy
MS	Multiple sclerosis
mtDNA	Mitochondrial DNA
NIfTI	Neuroimaging informatics technology initiative
nDNA	Nuclear DNA

NMDAS	Newcastle Mitochondrial Disease Scale for Adults
OXPHOS	Oxidative phosphorylation
PET	Positron emission tomography
POLG	Polymerase γ (gamma)
POLRMT	Mitochondrial RNA polymerase
PRESS	Point resolved spectroscopy
RNA	Ribonucleic acid
ROI	Region of interest
ROS	Reactive oxygen species
RVI	Royal Victoria Infirmary, Newcastle upon Tyne
SD	Standard deviation
SIENA	Structural brain change analysis tool
SNHL	Sensorineural hearing loss
SNR	Signal to noise ratio
SPACE	Sampling perfection with application optimised contrasts using different flip angle evolutions
SPECT	Single photon emission computed tomography
SPM	Statistical parametric mapping
STEAM	Stimulated echo acquisition mode
T1W	T1-weighted
T1W_SE	T1-weighted spin echo
T2W	T2-weighted
T2_FLAIR	T2-weighted fluid attenuation inversion recovery

TBSS	Tract-based spatial statistics
tCho	Total choline
tCr	Total creatine
TE	Echo time
TFAM	Transcription factor A
TFB2M	Transcription factor B2
TI	Inversion time
TICV	Total intracranial volume
TLE	Temporal lobe epilepsy
tNAA	Total N-acetyl acetate
TPV	Total parenchymal volume
TR	Repetition time
tRNA	Transfer RNA
UMDF	United mitochondrial disease foundation
VDAC	Voltage dependent anion channels
VBM	Voxel-based morphometry
VOI	Volume of interest
WM	White matter
WPW	Wolff-Parkinson-White Syndrome

Contents

Chapter 1. Introduction

1.1 Mitochondrial Disease

Mitochondria are intracellular organelles that are integral to cellular energy metabolism including the urea cycle, fatty acid β oxidation and the final common pathway for adenosine tri-phosphate (ATP) production in the mitochondrial respiratory chain. Mitochondrial diseases are an important group of neurometabolic disorders characterised by dysfunctional mitochondria that manifest marked genotypic-phenotypic heterogeneity. They are classified into two major groups due to their causative genetic aetiology: primary mitochondrial disorders (caused by point mutations or deletions in mitochondrial DNA (mtDNA) and nuclear mitochondrial disorders (caused by mutations in nuclear DNA (nDNA)). (McFarland *et al.*, 2010). The point mutation m.3243A>G in the *MT-TL1* gene encoding $tRNA^{Leu(UUR)}$ is the most common cause of adult mtDNA disease and the most prevalent point mutation within the Medical Research Council (MRC) MitoCohort, a cohort dedicated to patients with mitochondrial disease established in Newcastle upon Tyne and now extended to other mitochondrial disease centres across the country, but determining the prevalence of the mutation in the general population is not easily achieved due to the heterogeneous nature of the disease (Gorman *et al.*, 2015a). The best estimate of prevalence in the UK to date is provided by Gorman *et al.* (2015a) through a long-term study carried out from 1990 to mid-year period of 2011, in which all adults over the age of 16 years with suspected mitochondrial disease in the north east of England were all sent to a single centre for neurology for assessment. Two minimum prevalence rates were determined: 20 per 100 000 for mtDNA mutations; and 2.9 per 100 000 for nuclear mutations leading to clinically overt mitochondrial disease (Gorman *et al.*, 2015a). In total, mitochondrial and nuclear DNA defects have a prevalence of around 1 in 4300, which makes mitochondrial disease one of the most common forms of inherited adult neurological disorder (Gorman *et al.*, 2015a), and in addition to this, around 1 in 200 may be carrying pathogenic mtDNA mutations, which potentially puts mitochondrial disease high up the list of commonly inherited neuromuscular diseases (Gorman *et al.*, 2015a). As of September 2018, there are 680 mutations in mtDNA with disease associations in the human mitochondrial genome MITOMAP database (Lott *et al.*, 2013; Lott, 2016), a number that will inevitably continue to expand with continued genetic research.

The prevalence of the m.3243A>G point mutation does not, however, directly translate into prevalence of associated phenotypes. Mitochondrial encephalomyopathy with lactic acidosis and stroke-like episodes (MELAS) is often associated with the m.3243A>G point mutation, but only around 10% of those harbouring the m.3243A>G point mutation will go on to develop the MELAS clinical syndrome (McFarland *et al.*, 2010). However, the m.3243A>G point mutation accounts for around 80% of patients manifesting with MELAS (Tuppen *et al.*, 2010), making this a key mutation to study in depth to better understand the stroke-like episodes suffered by this patient group, which are neurologically devastating. Yet the heterogeneity of symptoms and lack of defined disease progression pattern makes treatment and prevention strategies extremely difficult to formulate and implement.

Neuropathology of human brain tissue has provided vital insight into our understanding of the neurological structural end stages of the disease, and vitally has facilitated interrogation of potential underlying mechanisms. But these techniques are limited to staining and imaging of post mortem samples, and are able to provide little information regarding the initial changes and triggers, particularly within the brain, that lead to symptoms such as seizures, stroke-like episodes, and encephalopathy.

Non-invasive neuroimaging is able to provide both structural and functional information about the brain *in vivo* and in real time. Magnetic resonance imaging (MRI) in particular offers a method to study high resolution structural details without the use of ionising radiation. To date it has been used extensively in other neurological diseases such as multiple sclerosis (MS), epilepsy, and various forms of dementia, but to date the latest developments in MRI scanning and analysis techniques have not been adequately brought to bear on mitochondrial disease. Diffusion tensor imaging is also of interest as it allows the investigation of white matter tracts, which form the microstructure of the brain. The technique has the potential to allow detection and visualisation of early, and potentially also pre-clinical, changes. Through the investigation of the structural and micro-structural features of people harbouring the m.3243A>G mutation, it is possible to add to, and provide supporting evidence for, clinical observations and information, and potentially improve the prognostic prediction for individuals, particularly for those at risk of central nervous system (CNS) involvement.

The neurodegenerative nature of MELAS led to the hypothesis that by quantitatively analysing the brains of those carrying the m.3243A>G point mutation and comparing to a healthy control group it would be possible to identify regions, and properties thereof, that either provide more information about the mechanisms of the progressive nature of neurodegeneration in patients with MELAS compared to the relative neurological stability of non-MELAS carriers of the m.3243A>G point mutation, or that highlight more generic differences in those who carry the m.3243A>G point mutation that may then provide further information on the overall nature of the effects of carrying this point mutation.

This thesis describes the work I carried out to quantitatively investigate the brain volumes of healthy controls and those carrying the m.3243A>G point mutation as both non-MELAS carriers, and those with a MELAS diagnosis. I developed robust segmentation protocols to provide both reliability and accuracy. The automated protocols were validated against manual segmentation techniques to assess accuracy and to justify the selection. I then used these to carry out global and regional segmentation to analyse, at multiple scales, what the differences were between the three study groups to begin to understand the effects on the brain of having the m.3243A>G point mutation. I decided to address the whole brain rather than an individual region, for example the cerebellum, due to the number of papers that state they have measured global effects across the brain.

1.1.i Mitochondria

Overview

Eukaryotic cells contain mitochondria, which are cytoplasmic organelles. Within each organelle is a double-membrane structure where ATP production takes place. This is only one of the roles that mitochondria fulfil; they also have a number of other functional roles including in apoptosis, the formation of iron sulphur clusters, and calcium handling. Mitochondrial function is maintained through the encoding of vital proteins, some of which are encoded by the non-nuclear mtDNA, but the vast majority are actually coded by nDNA (Anderson *et al.*, 1981). This dual source of protein encoding leads to mitochondria being affected by diseases caused by either mutations or deletions within the mtDNA, which not only affect the mitochondria themselves, but also the overall functioning of the cell (Park and Larsson, 2011).

Origins and Evolution

There are a number of theories that have been proposed to explain the presence of mitochondria within mammalian eukaryotic cells (Martin *et al.*, 2015). The most widely accepted theory is that proposed by Margulis (Margulis, 1971) in the form of endosymbiosis, defined as a mutually beneficial relationship between two organisms that is carried out by one of the partners 'swallowing' the other without digesting it. The fact that mitochondria contain DNA unrelated to that of the cell nucleus suggests supportive evidence that the mammalian eukaryotic cell began as two separate organisms, free-living bacteria and an ancestral host, that developed a hereditary symbiosis resulting in the development of mammalian cells (Margulis, 1971). The reasons for this endosymbiosis likely stems from the different respiration mechanisms of each of the organisms; the anaerobic ancestral host cell, and the aerobic prokaryote. This combination then allowed more efficient respiration and generation of ATP (Reece *et al.*, 2011) with the host cell benefitting from the ATP production and the prokaryote an environment rich in metabolites.

A second theory is the autogenous theory that proposes that a single prokaryote ancestor led to the development of eukaryotes through functions being compartmentalised through folding of the plasma membrane of the prokaryote and the enslavement of purple non-sulphur bacteria. This hypothesis suggests the evolution of mitochondria within the protoeukaryote cell when cell membranes have created compartments containing plasmids or vesicles of DNA that have then been pinched off and the endosymbionts developed into organelles because of the complex machinery required for protein import and the insertion of this into the inner membranes of protein carriers to extract energy (Cavalier-Smith, 2006).

Structure and oxidative phosphorylation

Mitochondria are found in every nucleated cell within the human body, with the exception of mature red blood cells. They are usually simplistically represented as rod- or ovoid-shaped double-membraned structures with a length of 1-4 μm, and a diameter of 0.5-1 μm (Palade, 1952). The structure comprises the outer membrane, the inner membrane, which folds to form 'cristae', the intermembrane space, and the matrix (Figure 1). This classical depiction is seen in most electron microscope (EM) imaging due to the 2D nature of the image (Figure 2). However, this depiction is somewhat misleading as mitochondria are actually highly dynamic (Figure 3) and

usually form complex networks to allow exchange of ions and molecules between mitochondria (Bereiter-Hahn and Voth, 1994; Chen and Chan, 2004). Mitochondria undergo both fusion and fission to facilitate transfer of mitochondria into daughter cells, to remove any mitochondria that are damaged, and may also, at least partially, modulate the production of ATP (Skulachev 2001). Disruption in the balance of fission and fusion leads to suboptimal performance of the mitochondria, which in turn has been linked to neurodegeneration (Chen and Chan, 2009).

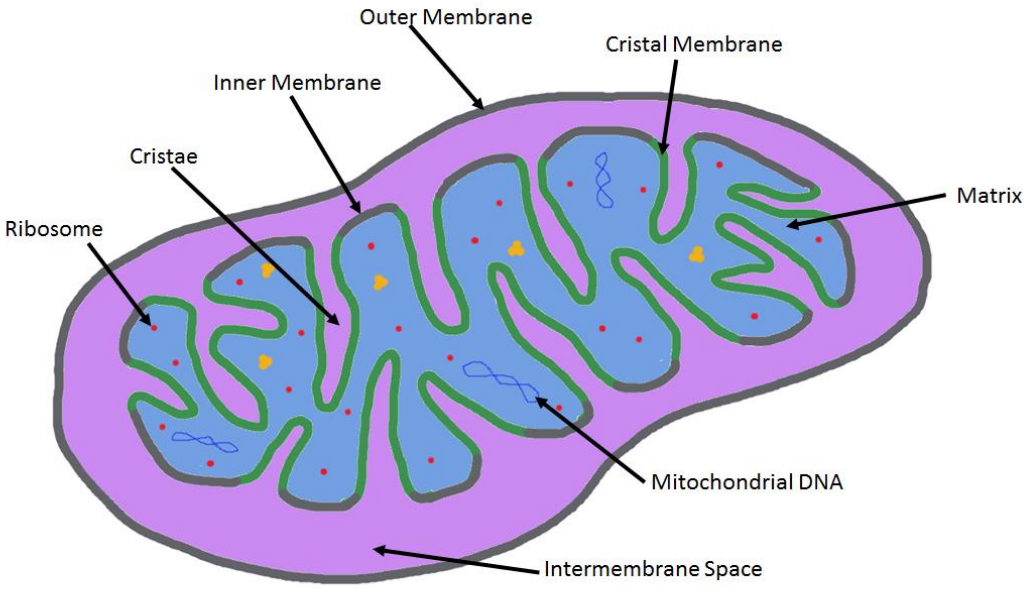

Figure 1. Schematic representation of the main elements of a mitochondrion.

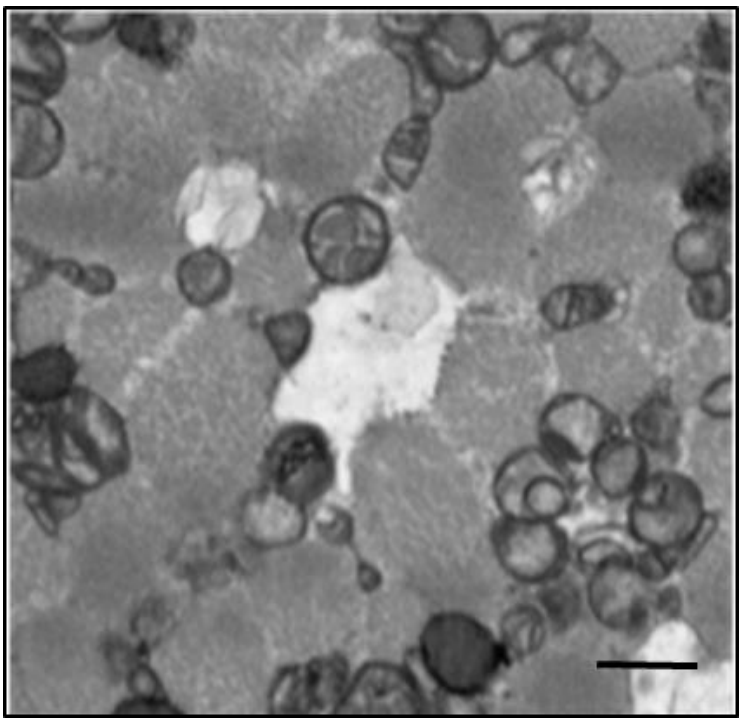

Figure 2. Classical EM image showing mitochondria as ovoid and rod-shaped structures (Image provided courtesy of Dr Amy Vincent).

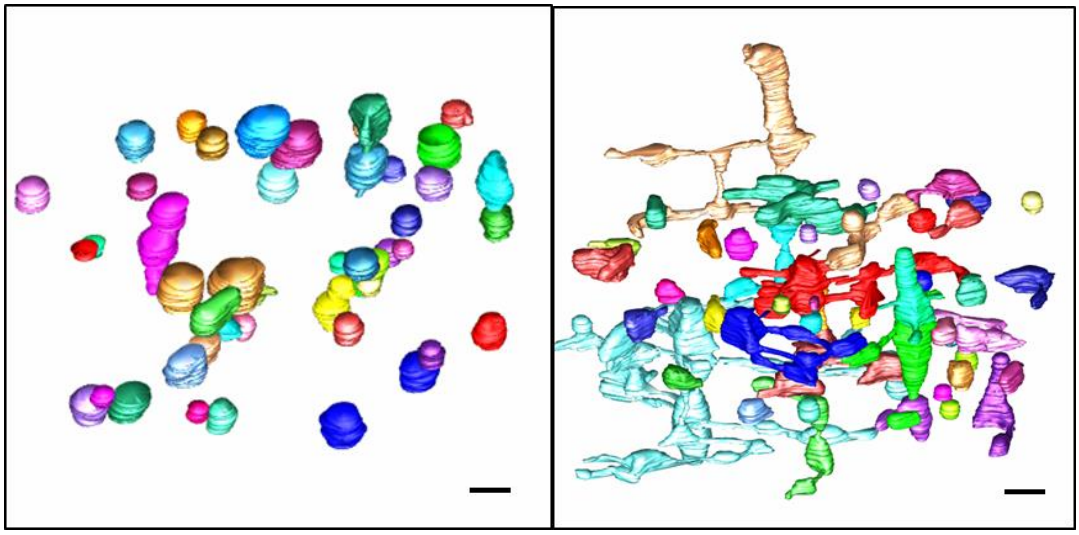

Figure 3. 3D volumetric rendering of EM imagery demonstrating the large variation in mitochondrial shape, size and connectivity Image provided courtesy of Dr Amy Vincent).

The outer membrane of the mitochondrion separates the cytosol and the organelle and also contains in the order of 10 000 voltage dependent anion channels (VDAC), one of the classes of porin ion channel. Small hydrophilic molecules and ions, up to 10 kDa in size, pass through these channels forming the exchange mechanism between the intermembrane space and the cytosol (Alberts *et al.*, 2008). The inner

membrane, which sits between the intermembrane space and the matrix, is selectively permeable, only allowing water, oxygen and carbon dioxide to pass through, thus there are a number of transport proteins associated with the inner membrane to allow material to enter the matrix from the intermembrane space, and also to help maintain the electrochemical gradient between the two. These features are essential for the formation of ATP (Alberts *et al.*, 2008).

The mitochondrial matrix hosts most of the mitochondrial processes. The content of the matrix consists of numerous copies of the mitochondrial genome and along with the essential components for replication, transcription, and translation. Other processes that take place in the mitochondrial matrix are iron-sulphur cluster biogenesis, β-oxidation of fatty acids, and the Krebs cycle (Llopis *et al.*, 1998).

Mitochondria have a large number of functions, but it can be argued that the most crucial one is the generation of energy via oxidative phosphorylation (OXPHOS). ATP, the end product of this process, is generated in the inner membrane using the OXPHOS system, which comprises five multimeric protein complexes, and two electron carriers (Hatefi, 1985).

Biogenesis

The metabolic demand of cells does not remain constant over time, therefore the synthesis of mitochondria, also referred to as mitochondrial biogenesis, also does not occur at a constant rate, instead it is a process that is regulated to ensure adequate production of ATP.

Neuronal Mitochondria

Neurons, compared to other types of cell, demand large supplies of energy but not at a constant rate. Therefore, to maintain neuronal health it is required that mitochondria are in the right locations when they are needed. The length of neuronal cells and their structural complexity make the transport of mitochondria key to the proper functioning of the cell. To add to the navigational complexity, mitochondria are produced predominantly, but not solely, in the soma and so then must be transported out as far as the neuronal distant terminals through anterograde transport mechanisms (Course and Wang, 2016).

In the same way, retrograde transport is also required for damaged mitochondria, which if not properly repaired by fusion with healthy mitochondria, or disposed of

either back in the soma or at the terminals, can cause oxidative stress to the neuron (Course and Wang, 2016).

The multiple functions of mitochondria in neurons include calcium buffering, detoxifying ammonia, and production of certain steroids (Rossier, 2006), haem compounds (Oh-hama, 1997), heat, and ROS. They are vital to the metabolism of neurotransmitters glutamate and gamma-aminobutyric acid (GABA) (Kugler and Baier, 1992), and also send signals for apoptosis, proliferation, and cell survival (McBride *et al.*, 2006). The combination of these multiple roles and the long, thin nature of the neuronal cell, as well as the neuron being post-mitotic, means that it is imperative that mitochondrial function and location is optimised. There is increasing evidence to indicate that if the mitochondria within neurons are not properly distributed to provide the correct energy amounts at the right time, that this may lead to neurodegenerative and neuropsychiatric disorders (de Vos *et al.*, 2008; Morfini *et al.*, 2009; Deheshi *et al.*, 2013) as a result of physical changes to the brain vasculature that includes impaired blood-brain barriers and lack of vascular response to changing oxygen demands (Nelson *et al.*, 2016).

Phenotypic expression

Mitochondria are found in all cells in the body with the exception of mature red blood cells, and provide localised energy production. This therefore means that mutations in either mtDNA or nDNA involved in the OXPHOS process, can be present in any part of the body, frequently leading to symptoms that affect multiple organs and tissues. The central nervous system (CNS) is particularly susceptible as when the body is at rest, the CNS will use up to 20% of all energy produced (Lax *et al.*, 2017). Hence organs with high energy demands are more often affected, such as the brain, muscles, and the heart. However, symptoms do not occur predictably and even patients with identical mtDNA heteroplasmy levels and genetic mutations can present with symptoms varying in both type and severity. Neurological manifestations include seizures, stroke-like episodes, encephalopathy (altered mental state), dementia, atrophy, and developmental delay. Other commonly seen symptoms include diabetes, cardiomyopathy, ptosis, and ophthalmoplegia (McFarland *et al.*., 2002). Childhood onset of mitochondrial disease generally involves more severe symptoms including developmental delay and/or regression, with an increased likelihood of disease expression (Chi *et al.*., 2010).

m.3243A>G mt-tRNA$^{Leu(UUR)}$ mutation

Around 77% of mitochondrial disease cases in adult patients result from mutations in mtDNA, with the most common of those being related to the m.3243A>G point mutation (Gorman *et al.*, 2015a). In addition to being the most prevalent, the m.3243A>G point mutation is also associated with patients who experience a wide spectrum of symptoms. Patients with this mutation comprise around 80% of those that are diagnosed with MELAS; however the m.3243A>G mutation can also give rise to other clinical syndromes, including Leigh syndrome, chronic progressive external ophthalmoplegia (CPEO), maternally inherited diabetes and deafness (MIDD) or a cardioencephalomyopathy syndrome (Gorman *et al.*, 2016).

mtDNA mutations affect both the quality and quantity of respiratory-chain protein production (DiMauro and Schon, 2003; Taylor and Turnbull, 2005). Research indicates that patients with the m.3243A>G point mutation have a decreased rate of protein synthesis, which in turn leads to a reduction in the complexes available for OXPHOS, thus reducing overall energy production (Ciafaloni *et al.*, 1992). There is also research to support disease onset being related to the mutant load, with higher mtDNA heteroplasmy levels leading to an earlier onset (Morgan-Hughes *et al.*, 1995); however, it is now recognised this does not fully explain the heterogeneity in disease expression, onset or progression.

1.1.ii Neuropathology

Further to focal lesions detected macroscopically in the brains of patients with MELAS, microscopic neuropathological investigations are indicative of profound neuronal cell loss, spongiform degeneration (mainly in the white matter), glial cell proliferation and axonal demyelination (Lax *et al.*, 2017). Respiratory chain deficiencies and decreased electron transport chain (ETC) protein expression in vulnerable neuronal, inter-neuronal and vascular cell populations have also been documented (Tanji *et al.*, 2001; Betts *et al.*, 2006; Lax *et al.*, 2012b; Lax *et al.*, 2012c; Lax *et al.*, 2015). These are usually associated with high heteroplasmy[1] , cellular loss, cortical necrosis, astrogliosis, and secondary axonal loss (Lax *et al.*, 2017).

[1] Heteroplasmy level = % of mutated DNA

m.3243A>G

Patients with the m.3243A>G point mutation, and more specifically, those with MELAS, have a characteristic presence of pan-necrotic foci, which are themselves characterised by any combination of neuronal loss, activation of the inflammatory response (although the response is not massive, as in the cases of other diseases such as MS (Steinman, 1996; McFarland and Martin, 2007), and proliferation of astrocytes and capillaries (Lax *et al.*, 2017). These foci are often described as being 'infarct-like' and are most commonly observed in the cerebral cortices, both unilaterally and bilaterally depending on disease development, and also in the cerebellum. Other areas may also be affected, including the basal ganglia, thalamus, brain stem, and subcortical white matter (Lax *et al.*, 2017). Calcification, particularly of the basal ganglia, is also a relatively common observation in neuropathological investigations in patients with MELAS, in addition to vacuolation, also known as spongiform degeneration due to the sponge-like appearance, which is observed in the cortex (Lax *et al.*, 2017).

There are a number of observed vascular abnormalities that include calcification of vessel walls (Sue *et al.*, 1998; Tanahashi *et al.*, 2000), a decrease in the immunoreactivity against mtDNA-encoded respiratory chain subunits (Sparaco *et al.*, 2003) and blood vessels that are both cytochrome c oxidase (COX)-deficient and have high levels of mtDNA heteroplasmy (Betts *et al.*, 2006; Lax *et al.*, 2012b). There is no specific association between COX-deficiency and the presence of lesions as COX-deficient blood vessel walls can be found globally throughout the brain in both cortical and subcortical white matter, as well as meningeal tissue (Betts *et al.*, 2006; Lax *et al.*, 2012b). In addition to COX-deficiency, the physical properties of mitochondria within the vasculature throughout the brain are altered as the mitochondria are enlarged and also aggregated (Ohama *et al.*, 1987; Mizukami *et al.*, 1992; Tanahashi *et al.*, 2000). Autophagy[2] is a key process in the maintenance of the health of mitochondria by removing old and damaged mitochondria and the aggregation of enlarged mitochondria indicates that the maintenance process is defective as it is not working quickly enough to remove them before they start to accumulate (Youle and van der Bliek, 2012).

[2] The removal of damaged components of cells, or those that are no longer required

Post mortem neuropathological investigations show generalised cerebellar atrophy (Sparaco *et al.*, 1993; Tanahashi *et al.*, 2000; Lax *et al.*, 2012a, Lax *et al.*, 2017). Even within neurons that are preserved there is a high percentage of mutant mtDNA and these neurons also show severely compromised respiratory chain protein expression, particularly for complexes I and IV (Lax *et al.*, 2012a; Chrysostomou *et al.*, 2015).

Aberrations in the inhibitory neurotransmission in the region of lesions are indicated by defects in complex I protein expression in GABAergic presynaptic terminals (Chrysostomou *et al.*, 2015). Compensation mechanisms may be present in the form of intracerebellar synaptic remodelling of residual inhibitory synapse through enlargement (Chrysostomou *et al.*, 2015).

In patients with the MELAS phenotype, profound inhibitory interneuronal loss has been found in the occipital, temporal, and frontal cortices, which is accompanied by complex I deficiency and high levels of heteroplasmy of around 79% in residual neurons (Betts *et al.*, 2006).

1.1.iii Human Mitochondrial Genetics and DNA Mutations

The Mitochondrial Genome

Multiple copies of mtDNA molecules make up the mitochondrial genome. Each molecule is made up of 16 569 base pairs and has two strands; an inner light (L) strand containing 9 genes, and an outer heavy (H) strand containing 28 genes. Of the 37 genes in mtDNA only 13 are used to encode mitochondrial respiratory chain polypeptide subunits, the other 24 are required for mtDNA translation and mitochondrial protein synthesis (Anderson *et al.*, 1981).

The mitochondrial genome has a number of distinctive properties that set it apart from the nuclear genome (Taylor and Turnbull, 2005), namely, mtDNA heteroplasmy, threshold effect and the mitochondrial genetic bottleneck. mtDNA is inherited entirely from the mother (Giles *et al.*, 1980) and the copy number of mtDNA molecules varies depending on the type of cell and its current energy demands. The bottleneck effect allows successive generations to show a random, and rapid, drift of mutation, making the inheritance and progression of the disease unpredictable. To add to the unpredictability, some heteroplasmic mtDNA mutations, such as m.3243A>G, show heteroplasmy drift due to vegetative segregation in dividing cells (Matthews *et al.*,

1995; Rajasimha *et al.*, 2008; Stewart and Chinnery, 2015). Finally, it is also known that mtDNA replication occurs independently of the cell cycle (Bogenhagen and Clayton, 1977). The key mtDNA properties are discussed in the rest of this section in relation to mitochondrial disease.

Transcription and Translation

Transcription is the initial process that occurs in gene expression and involves making a copy of a DNA sequence to create an RNA molecule. There are three sites where mtDNA transcription is initiated, with one promoter for the light strand and two for the heavy strand. Two of the promoters cover almost all of the coding regions, with one of the H strand promoters covering a much shorter transcript.

There are three proteins, mitochondrial RNA polymerase (POLRMT), transcription factor A (TFAM), and transcription factor B2 (TFB2M), that have been shown to be essential for transcription initiation and formation of the mitochondrial transcription initiation complex (Falkenberg *et al.*, 2002; Shi *et al.*, 2012; Yakbovskaya *et al.*, 2014). The process is begun with the binding of TFAM close to the promoter site to fold mtDNA. This then allows POLRMT to be recruited and bound to the promoter region as well as the TFAM. The POLRMT is also changed in shape through this process, which then allows TFB2M to bind to the incomplete pre-initiation complex to complete it (Yakubovskaya *et al.*, 2014).

Mitochondrial genome translation has a number of features that separate it from nuclear genome translation, but it still follows the recognisable steps of canonical initiation, elongation, and termination (Smits *et al.*, 2010) within mitoribosomes, the mitochondrial equivalent to the protein-rich nucleolar ribosomes (O'Brien, 2003).

Impairment of the mitochondrial transcription and translation processes due to either mitochondrial or nuclear DNA genetic mutations usually leads to malfunctioning of the proteins encoded by mtDNA, which results in dysfunction of the entire respiratory chain, although there are some nuclear genetic defects that only affect the translation of individual mitochondrial-encoded proteins (Boczonadi and Horvath, 2014). The resultant effect of mitochondrial proteins that are defective is that ATP production is lower than required, which has the knock-on effect of an overall energy deficit within the cell (Boczonadi and Horvath, 2014).

mtDNA Replication

mtDNA replication has its own cycle that is independent from the nuclear DNA and cell cycles. This independence has led to the term ‘relaxed replication’ being coined (Bogenhagen and Clayton, 1977; Birky, 1994). In post-mitotic cells, such as neurons, the turnover of mtDNA is much slower than is found in cells that are actively dividing (Wang *et al.*, 2009). In fact, there is some evidence to indicate that neuronal mtDNA synthesis may take up to 20 hours (Calkins and Reddy, 2011). The exact mechanism for mtDNA replication has yet to be agreed upon, but the most popular current models are the asynchronous, or strand-displacement, model (Holt and Reyes, 2012), and the synchronous, or strand-coupled, model (Brown, 2005).

In the asynchronous/strand-displacement model polymerase gamma (Polγ) is believed to carry out replication of mtDNA solely using one mechanism, which involves a few proteins and two priming events (Holt and Reyes, 2012). Synthesis of the leading strand DNA starts at an exact location and synthesis goes around about two thirds of the way before the synthesis of DNA is started on the ‘lagging’ strand, which although believed to be coated with protein for many years, it has now been proposed that it is RNA instead (Holt and Reyes, 2012).

In contrast, the synchronous, or strand-coupled, model involves bidirectional synthesis of DNA through the formation of replication forks in the directions of both the leading- and lagging- strand (Brown *et al.*, 2005).

Maternal Inheritance and the Bottleneck Effect

mtDNA is inherited wholly through the maternal germline (Giles *et al.*, 1980). Paternal mtDNA is destroyed, with mechanisms being species-specific and are known to take place both pre- and post-fertilisation (Sato and Sato, 2013). In mammals there is selective proteasomal degradation for paternal mtDNA destruction (Kaneda *et al.*, 1995; Sutovsky *et al.*, 1999).

Any pathogenic mtDNA mutations carried by a mother will be transmitted to any children she may have, however there is a significant amount of variability in the extent of the transmission to the next generation (Taylor and Turnbull, 2005). The existence of this variability may in part explain the phenotypic heterogeneity amongst patients carrying the same genetic defect (Chinnery *et al.*, 1997), for which the current explanation is the genetic bottleneck phenomenon, in which the number of

mtDNA molecules is reduced by around 1000 times between oocyte and embryo (Chinnery *et al.*, 2000; Floros *et al.*, 2018). The exact mechanisms underlying the genetic bottleneck are still being debated, but it is relatively widely accepted that during embryonic development the rapid mtDNA replication is one of the key factors (Cree *et al.*, 2008). Recent work by Floros *et al.* (2018) has shown that low levels of mitochondrial mutations are present within the primordial germ cells (PGCs) in healthy embryos, and that evidence of selection against mutated mtDNA variants is seen in these despite the heteroplasmy levels being below the threshold conventionally considered to be required for a change in biochemical properties. This work also indicates that the mtDNA bottleneck may be less stringent in human embryonic somatic cells and that selection against mutated mtDNA in these tissues is less effective, which perhaps indicates that there is some sort of selection advantage to this (Floros *et al.*, 2018). Mutations that are not removed by this mechanism will be characterised by heteroplasmy level shifts within the space of a single human generation, which explains the extreme variation in phenotype seen in family lines that have inherited mitochondrial disorders (Floros *et al.*, 2018). This new evidence of mtDNA selection provides further insights into the factors that dictate the level of pathogenic mutations, such as inheritance patterns for some mtDNA defects, in addition to the effects of random genetic drift (Brown *et al.*, 2001; Floros *et al.*, 2018).

mtDNA Mutagenesis and Repair Mechanisms

mtDNA is susceptible to acquiring defects for two major reasons; its close proximity to the electron transport chain (ETC), and also its compact structure. mtDNA has also been shown to have less robust repair mechanisms compared to nuclear DNA (Clayton, 1982), which leads to an order of magnitude higher mutation rate than chromosomal DNA (Brown *et al.*, 1979). The proximity of reactive oxygen species (ROS) production sites under normal OXPHOS conditions also has a negative impact on mtDNA integrity.

DNA strand breaks can lead to a variety of mtDNA defects, including point mutations, deletions, insertions, and duplications (el-Khamisy and Caldecott, 2007; Kasparek and Humphrey, 2011). There is also the possibility of replication errors or modified nucleotides being incorporated (Kamiya, 2003, Boesch *et al.*, 2011). The normal ageing process can also cause somatic mtDNA mutations to be acquired, and even environmental conditions can trigger ancient genetic variants to occur as part of an adaptive response (Wallace, 2010).

The repair mechanisms used in mtDNA repair are, in general, similar in nature to nuclear ones (Larsen *et al.*, 2005) and include direct reversal (Yasui *et al.*, 1992), base excision repair (Stierum *et al..*, 1999), mismatch repair (Mason *et al..*, 2003) and single-strand break repair (Hegde *et al.*, 2012). Mitochondria have also evolved a unique repair mechanism where damaged mtDNA fractions are degraded and replaced by replicated segments of the healthy genome (Gross and Rabinowitz, 1969).

mtDNA Heteroplasmy and the Threshold Effect

There are multiple copies of mtDNA within each cell, which means that a mixture of wild type and mutant mtDNA are able to co-exist within the same cell. This concept is called heteroplasmy and is the basis for the theory of the 'threshold effect', in which it is theorised that if the mutant mtDNA exceeds a certain percentage, this then leads to the presentation of a particular phenotype (Larsson and Clayton, 1995). In addition to heteroplasmy, it is also possible to have a homoplasmic state if all mtDNA molecules within a cell are either wild type or mutant (Taylor and Turnbull, 2005).

The levels of heteroplasmy are not constant over time and are affected by random genetic drift[3] through the process of clonal expansion[4] (Elson *et al.*, 2001). Clonal expansion allows for the mutant genome to be selectively multiplied, which then leads to higher heteroplasmy levels in post-mitotic tissue (Weber *et al.*, 1997). The threshold effect is a key concept in explaining the presentation of a phenotype, but in itself is complex as the actual heteroplasmy threshold varies between individuals, tissue type within an individual, and also between mutation types. Studies indicate that for tRNA point mutations that the threshold effect occurs at around 90% heteroplasmy, but for single large-scale mtDNA deletions the threshold effect is much lower at around 60% (Rossignol *et al.*, 2003). Tissue specific thresholds also vary in the type of deficiency they are sensitive to, with mitochondria in the brain having a lower threshold for complex I deficiency, when compared to other organs, and muscle mitochondria being more susceptible to complex IV defects (Rossignol *et al.*, 1999).

[3] The random fluctuations within a population in the number of variants of a specific gene.

[4] Clonal expansion refers to a population of cells, known as daughter cells, that all originate from a single cell.

1.1.iv Current Treatment and Prevention Strategies for Neurological Symptoms

Overall there is a lack of treatments that are effective, thus leaving clinicians with few options once patients have presented with symptoms. Pharmacological treatments have generally been found to have either low efficacy or high toxicity in patients with mitochondrial disease (Horvath *et al.*, 2008), with the exception of patients with a coenzyme Q10 deficiency. Non-pharmacological strategies for treating mitochondrial disease include diet modification along with exercise (Tarnopolsky, 2016; Ratnaike *et al.*, 2012; Murphy *et al.*, 2012; Gorman *et al.*, 2016), and also strategies for preventing the transmission of mitochondria between generations (Gorman *et al.*, 2015b).

Symptomatic Therapy

There are a number of relatively common neurological symptoms in m.3243A>G patients, which include seizures and stroke-like episodes, encephalopathy, cognitive dysfunction, dementia and ataxia. The neurological symptoms are characterised by a number of changes within the brain, such as lesions, global neurodegeneration, and global atrophy. Treatment for seizures usually comes in the form of anticonvulsants, with valproate being one a commonly used anti-epileptic drug. While this has generally been shown to provide effective seizure treatment, it has been associated with fulminent liver failure, mainly in polymerase γ (*POLG)* patients, and therefore clinicians advocate against its use (Stewart *et al.*, 2010). L-arginine has also been used in patients with MELAS to reduce the severity of acute stroke-like episode symptoms and to prevent recurring stroke-like episodes when in the chronic phase and its use is recommended by the United Mitochondrial Disease Foundation (UMDF) (Yoneda *et al.*, 2012), however evidence to support the routine use of L-arginine is still lacking.

Through ongoing monitoring and clinical care of patients, which is complex and multidisciplinary, there are several therapeutic strategies that have been investigated, but very few that are directly aimed at slowing, or preventing, neurological symptoms, particularly the neurodegenerative symptoms. In addition to anticonvulsants, anti-depressants have also been trialled, as mood disorders are a possible symptom in all mitochondrial disease (DiMauro *et al.*, 2006).

Additional treatment approaches

In addition to the traditional symptomatic therapy, there are a number of additional treatment possibilities that are also worth mentioning. These are: upregulation of mitochondrial proliferation for enhanced mitochondrial biogenesis to increase the numbers of wild-type mtDNA, which are able to assist in compensating for the mutated mtDNAs even though production of these are increased as well; increasing mitophagy through the use of rapamycin; the use of mildly hypoxic environments that could potentially restore locomotor function; novel gene therapy approaches that include targeting of mutated mtDNA for digestion, prevention of transmission of mice mtDNA haplotypes, and reducing oocyte heteroplasmy levels, which may offer an alternative to replacing mitochondrial DNA in the prevention of transmission of mitochondrial diseases through the maternal line (Gorman *et al.*, 2016).

Prevention of mitochondrial disease

The gold standard for mitochondrial disease is the prevention of mutation inheritance and recently prevention strategies to mitigate the transmission of serious mitochondrial disease have been developed (Gorman *et al.*, 2015b; Zhang *et al.*, 2017). As all mtDNA is inherited from the mother, the use of pro-nuclear transfer can be used, which essentially removes the mtDNA of the mother and replaces it with healthy mtDNA from a donor (Craven *et al.*, 2010), or alternatively spindle transfer can be carried out in which the nuclear DNA of the oocyte can be transferred to a donor oocyte without the transfer of the mitochondrial DNA (Zhang *et al.*, 2017). There are also additional reproductive choice options available for women with mtDNA mutations to have children via egg donation, or to have the option of either pre-implantation genetic diagnosis if conception is through in-vitro fertilisation (IVF), which totally eradicates the risk except, or prenatal diagnosis. These techniques allow the chances of having severely affected children to be reduced, but these also may involve decisions about termination and neither pre-implantation genetic diagnosis nor prenatal diagnosis are of benefit for women who have high levels of heteroplasmy (Steffann *et al.*, 2006), or for those women who have mutations that are homoplasmic.

1.2 Magnetic Resonance Imaging

Magnetic resonance imaging (MRI) is a technique that allows non-invasive imaging of the brain *in vivo*. The technique is indirect, which has both advantages and

disadvantages. The main disadvantage is that all output images are dependent on the MR scanner sequence used and so this must be carefully selected to ensure contrast may be observed between the desired tissues, for example between a tumour and healthy brain tissue. However, as MRI is sensitive to a range of brain tissue properties, it is possible to investigate a number of different brain properties using the same equipment, but varying the scan sequences chosen. MRI may be used to investigate both structural and functional aspects of the brain making it a powerful tool in brain research both in a healthy population and also to probe how disease affects the brain.

1.2.i Basic Principles of Magnetic Resonance Imaging

The basic concepts behind how MRI works are rooted in quantum mechanics, but it is possible to gain an understanding of these by using analogies in a more easily understandable classical mechanical system. In this section I will introduce the essential aspects of structural and diffusion MRI, consider how typical images are acquired, and also describe some of the standard clinical observations that are made in patients with mitochondrial disease.

Proton Spin and its Manipulation

The human body is made up of around 75-80% water. Within each water molecules are two hydrogen atoms, and each hydrogen atom contains one proton. It is the inherent properties of these protons that make MRI possible. A proton can be thought of as a charged ball, spinning on an axis, although in the quantum world ‘spin’ is not a literal term. The ‘right hand rule’ then dictates that this ball then also has an associated magnetic moment with a defined size and direction. Normally, proton spin direction will be random, and there will be zero net magnetisation. In an MRI scanner a strong magnetic field is present and this causes the protons to align with that field. Once aligned, the nuclei can exist in two possible states; low energy in which the proton is aligned with the field, and high energy in which the proton is aligned against the field. If there is no further change of field it is found that there are slightly more protons aligned with the applied field compared to against it. Overall, this creates a net magnetisation of the protons that is aligned with the applied field.

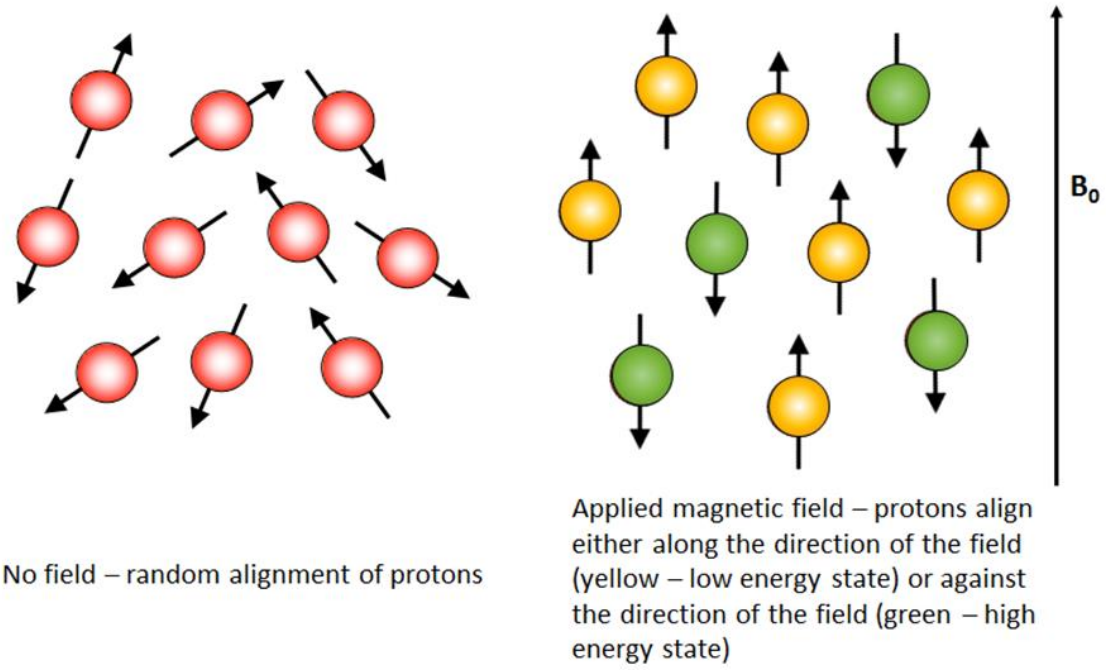

Figure 4. Proton spin orientations without external magnetic field (left) and with applied external magnetic field (right).

When in the presence of an externally applied magnetic field, there are fractionally more protons in the low energy state so when the magnetic moments are added together, they do not fully cancel each other out. This slight excess of protons in the low energy state is known as the 'spin excess'. This excess is very small, for example when the magnetic field is 3 Tesla (one of the most common magnetic fields found in clinical MRI machines) the spin excess is only around 3 in 100 000 (Equation 1). At first glance it does not seem likely that there will a measurable signal. However, there are of the order of Avogadro's number (6.022×10^{23}) of protons in only 24.7 grams of brain tissue, assuming that the brain is made up of approximately 73% water. Therefore, the net magnetisation then becomes measurable.

$$Spin\ excess = N\frac{\hbar\omega_0}{2kT}$$

Equation 1. Equation for spin excess where N = total number of spins in the sample, ħ = Planck's constant / 2π, ω_0 = Larmor frequency, k = Boltzmann's constant, and T = temperature in Kelvin.

The properties, and manipulation, of the net magnetisation vector is key to the magnetic resonance imaging technique.

The application of an external magnetic field alone is not enough to create a measurable signal, therefore an additional RF pulse must be applied, using a transmission coil, to temporarily shift the orientation of the protons so they precess around the axis of the applied magnetic field.

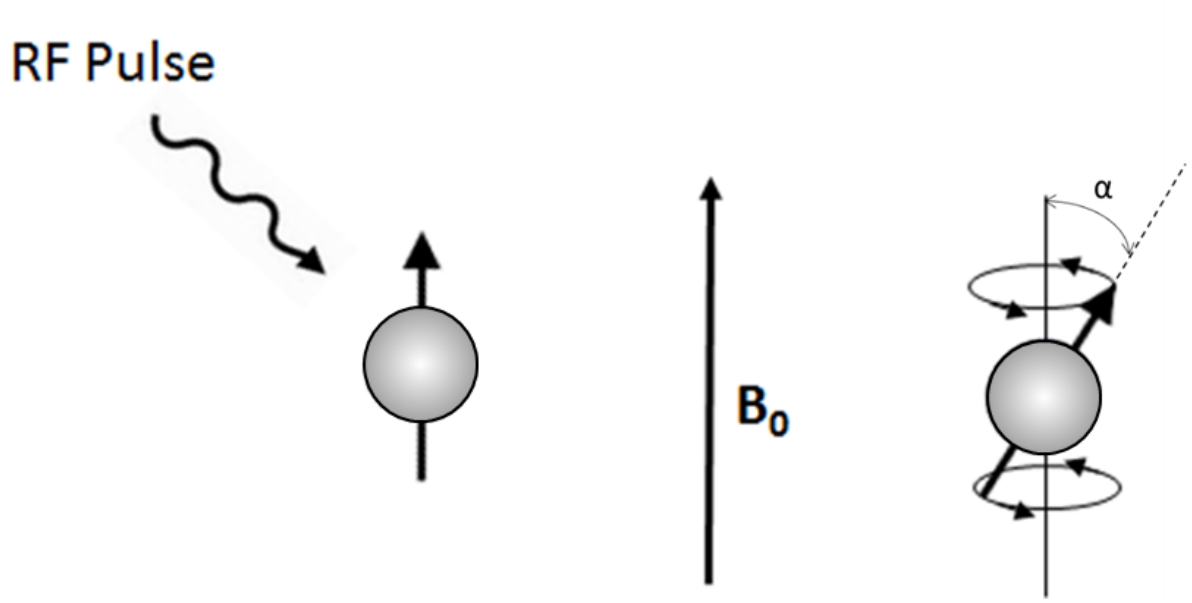

Figure 5. An RF pulse applied at a specific frequency imparts energy to the protons causing them to flip through an angle, α, and precess around the axis of the external magnetic field.

The RF pulse must be applied at a specific frequency, known as the Larmor frequency, for the proton to absorb the energy and shift from its original orientation with the precise frequency scaling with the strength of the applied static magnetic field. The duration of the pulse then dictates how far from the original orientation the proton moves (Figure 5), which is known as the 'flip angle', α. Detection coils are placed around the area of interest on the body in which a current is created via electromagnetic induction. This current provides the magnetic resonance (MR) signal. The angle through which the pulse tips the spins is not maintained over time and the protons eventually return to their original alignment with the external field and lose their phase cohesion, a process known as relaxation.

There are two relaxation processes that are important in image formation. These processes are described by the time-constants T_1 and T_2. The T_1 constant describes the *spin-lattice relaxation*, which is the loss of energy from the protons to the surrounding material. The T_2 constant describes the *spin-spin relaxation*, which describes the dephasing of the spins by the protons interacting with each other. Both

of these processes happen at the same time, but images are weighted to one or the other by setting the RF pulse sequence appropriately. The differences in the structural properties in the tissues allow good contrast in both T_1 and T_2-weighted images, but where pathological changes, such as lesions in patients with mitochondrial disease, are present one of the modalities often provides better contrast between the pathology and the healthy tissue. This is possible because the T_1 process takes longer than the T_2 process. It should also be noted that the T_1 relaxation time is significantly affected by the strength of the external magnetic field, while the T_2 relaxation time is relatively independent of it.

The contrast within an image is dictated by the physical properties of the tissue, with more solid tissue having distinct T_1 and T_2 values as compared to tissue with more fluid in it.

1.2.ii Structural MRI

Anatomical Scans

Most clinicians are familiar with the most commonly used clinical MRI sequences that produce anatomical scans with contrasts derived from either T_1 or T_2 weighting. By using multiple radiofrequency pulses within a single scan with specific repetition times (TR), the measured signals can be optimised for the type of contrast being looked for, whether that is contrast between healthy tissue types, for example grey and white matter, or contrast between damaged tissue, for example healthy grey and white matter, and a lesioned area (Figure 6). This method of creating an image uses the relative difference between the relaxation times of different tissues and therefore provides a qualitative ‘snapshot’ rather than a true measure of the T_1 and T_2 values for each tissue visible on the scan, although quantitative scan protocols are available.

To appreciate the differences between these two weighting types and their clinical relevance we shall first consider the longitudinal relaxation time, T_1.

$$M_z = M_0\left(1 - e^{-\frac{TR}{T_1}}\right)$$

Equation 2. Equation describing the longitudinal relaxation time, T_1, where M_z = measured magnetisation in the z direction, M_0 = maximum magnetisation value, TR = relaxation time.

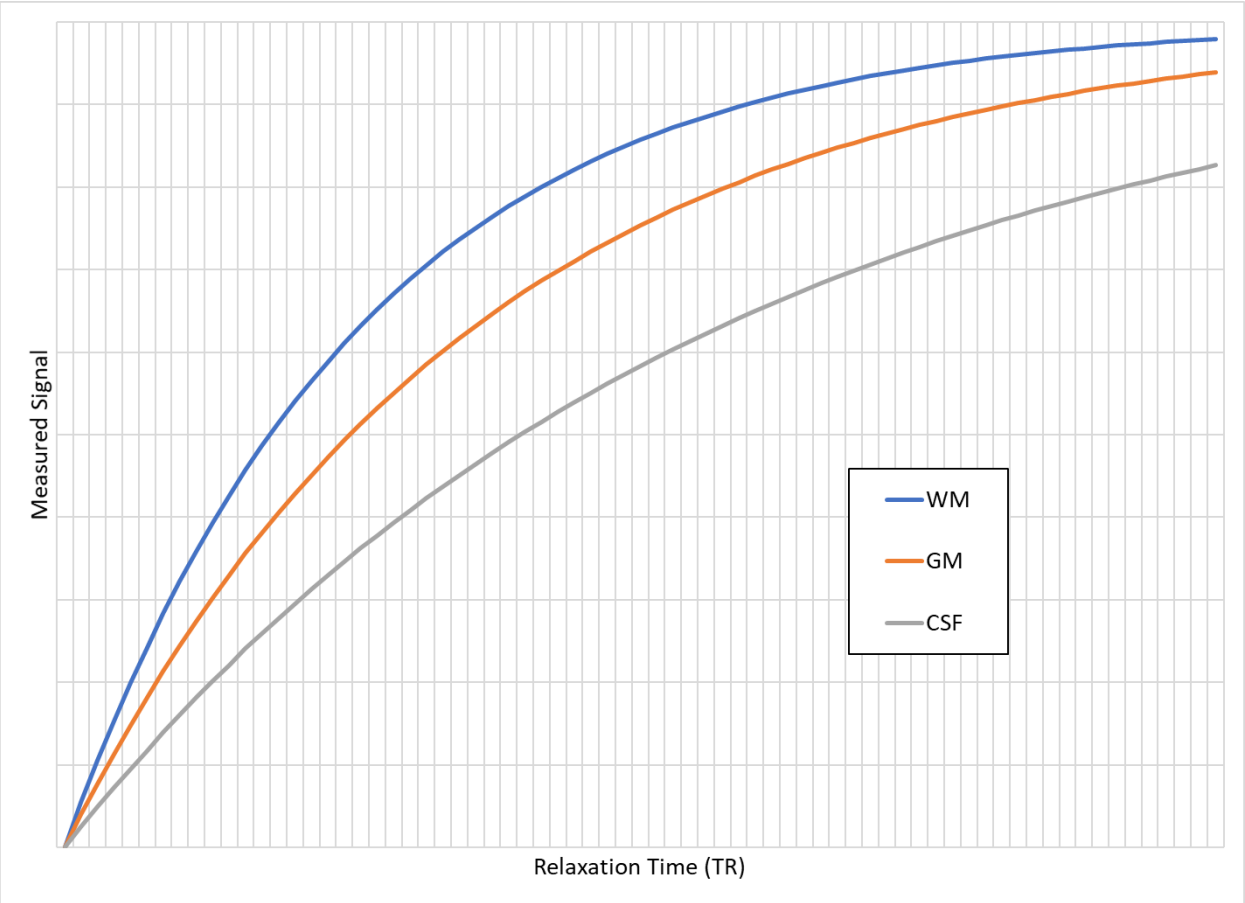

Figure 6. T_1 relaxation curves for white matter (WM) (blue), grey matter (GM) (orange), and CSF (grey). In a T_1-weighted image a short TR is used to maximise the contrast between all tissue types, which is better suited to carrying out volumetric analysis as tissue contrast is optimised.

Using short TR and echo time (TE) values weights the imaging to T_1, which provides good contrast, particularly between grey and white matter, and this is key if volumetric analysis is to be carried out as there needs to be as clear a distinction as possible between the tissue types. The T_1 of a specific tissue is defined as the time taken for the signal to increase to around 67% of its final value.

Next, we shall consider the transverse relaxation time, T_2.

$$M_{xy} = M_0 e^{-\frac{TE}{T_2}}$$

Equation 3. Definition of the transverse relaxation time, T_2, where M_{xy} = measured transverse magnetisation, M_0 = maximum magnetisation value, TE = echo time.

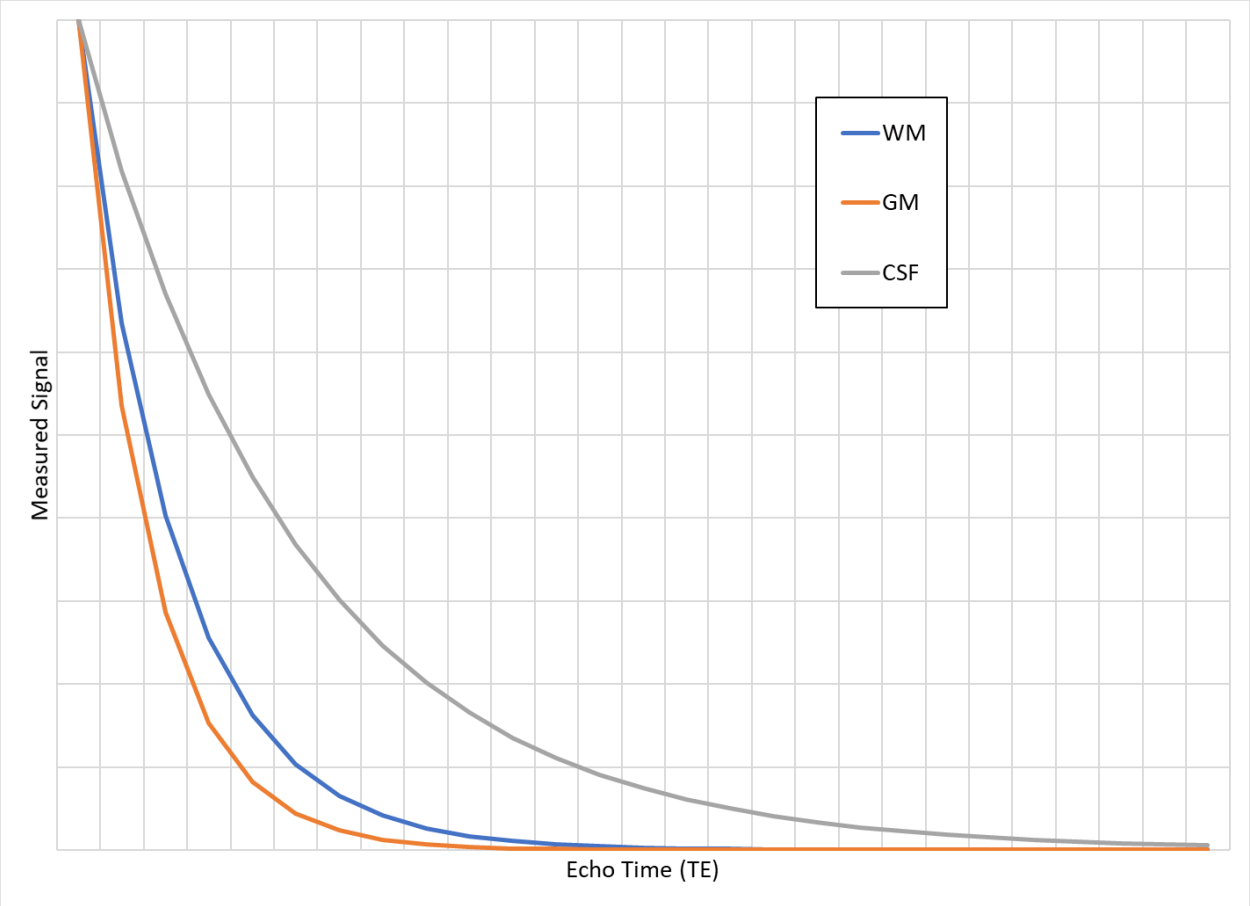

Figure 7. Graph showing the increased contrast between grey and white matter, and CSF when using T_2-weighted imaging.

To weight an image to T_2, long TR and TE values are selected for the scan, with the T_2 value of a tissue or fluid being defined as the time taken for the signal to drop to around 33% of its starting value. The difference between tissue and cerebrospinal fluid (CSF) signal in T_2-weighted imaging allows for better contrast to be seen between healthy tissue and lesioned regions in the brains of patients with mitochondrial disease. However, the brightness of the CSF can cause some problems with image interpretation as it is sometimes not clear whether an area is lesioned, or if it is an area appearing to be particularly bright where it is not expected to be, which occurs due to partial volume effects, particularly in images with large voxels as each voxel can contain signal from more than one tissue or fluid.

The differences between the weighting types can be best appreciated by inspecting output images from each, as can be seen in Figure 8.

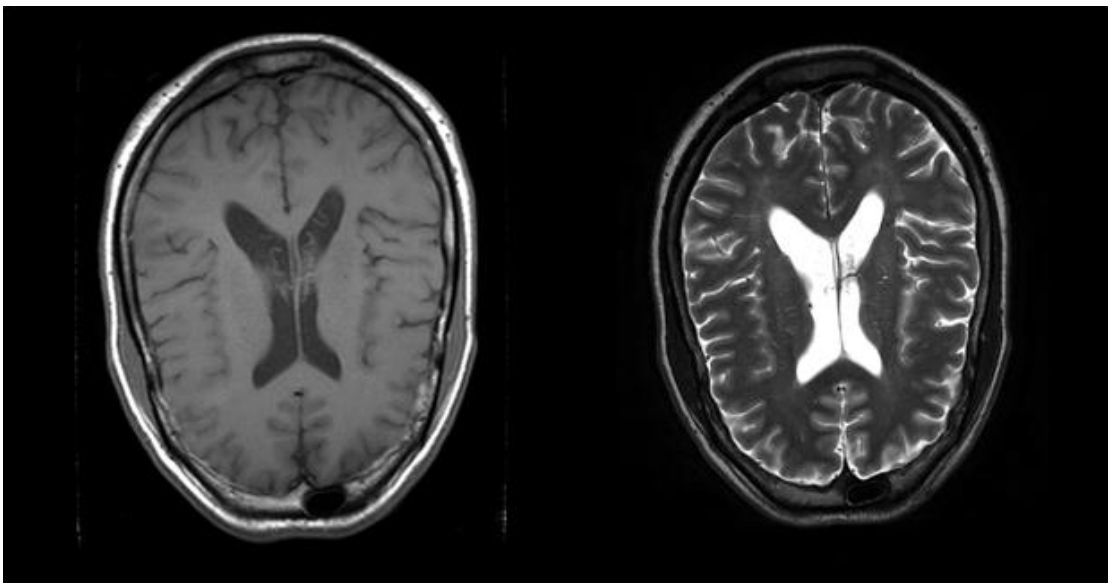

Figure 8. Example T_1-weighted (left) and T_2-weighted (right) images generated from the study cohort scan set for Patient 6. The difference in intensity associated with each tissue type and the contrast between tissues can clearly be seen.

These anatomical scans can show obvious changes to tissues, but this still relies on the skill and experience of a neuroradiologist to identify and interpret. The visual interpretation of these images is also entirely qualitative and therefore also subjective. When attempting to assess something like atrophy, the definition of the amount of atrophy that has occurred is highly problematic as the volume loss occurs three-dimensionally but is assessed using two-dimensional slices. The classical changes seen in patients with the m.3243A>G point mutation are the appearance of lesions, associated with stroke-like episodes, and also atrophy. While these observations may assist clinicians in assessing the effect and impact on the patient of these changes to the brain, they do nothing to explain the underlying mechanisms and do not provide a predictive capability prior to the onset of stroke-like episodes or global atrophy.

T_2 Fluid-attenuated Inversion Recovery (FLAIR)

T_2 FLAIR is an MR imaging technique in which the usually bright CSF is suppressed by utilising even longer TR and TE values, thus improving the image contrast within the image for the other tissues present. This is achieved by setting the inversion time (TI) to be equal to the time taken for the CSF signal to equal zero. This effectively nulls the normal CSF signal, while allowing abnormal tissues to remain bright within the image. This type of scan is particularly useful for clinicians to detect the location

and size of lesions within the brain and improves the ability to delineate between CSF and lesions, which are often difficult to distinguish in a standard T_2 image.

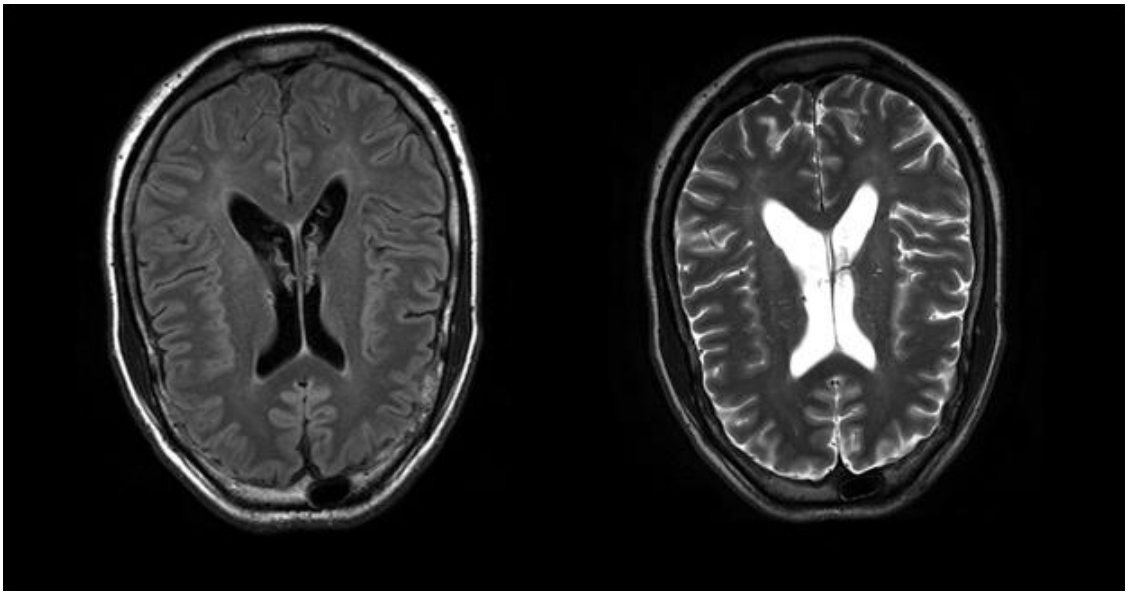

Figure 9. Example T_2-FLAIR (left) and T_2-weighted (right) images generated from the study cohort scan set for Patient 6. While the grey and white matter contrast are maintained, the bright CSF of the T_2-weighted image is suppressed, thus making it easier to observe the details in and around the areas of CSF.

1.2.iii Diffusion Tensor Imaging (DTI)

Diffusion Weighted Imaging (DWI)

In contrast to the qualitative imaging techniques described in Section 1.2.ii, there are also quantitative magnetic resonance techniques that have been developed to look at the pattern of water diffusion within the brain at a microscopic level. Although it has been possible to measure the self-diffusion of molecules using magnetic resonance since 1965 (Stejskal and Tanner, 1965), it was not until 1990 that it was employed in a clinical setting to interrogate the brain to ascertain where local water diffusion patterns had been disrupted during ischaemic stroke (Neil, 2008).

To obtain a diffusion image the location of the water molecules within the brain are encoded using one magnetic gradient pulse, then applying a second magnetic gradient pulse after a delay of around 60 ms to locate them again. Water molecule movement in the time between the two gradient pulses leads to attenuation of the MR signal due to diffusive processes, which then allows quantitative information about the general direction and degree of movement of the water molecules to be

calculated. The value is known as the diffusion coefficient and provides an average measure of how far the water molecules move due to Brownian motion. The scans are diffusion-weighted, and by modifying the diffusion times it is possible to, at least partially, target the specific environment in which the water molecules are moving, for example intracellular compartments. The environment within which a water molecule is moving is important as a freely moving water molecule will have a different pattern of movement to one moving in a more structured environment. A structured environment restricts molecular movement and so is termed the apparent diffusion coefficient (ADC).

To carry out this type of scan additional parameters have to be set. The first of these is the b-value. This defines the strength and duration of the gradient. Most diffusion scans that are used to estimate ADC use b-values between 0 and 1000 s/mm^2. To calculate an estimate of the ADC values Equation 4 is used.

$$\frac{I_2}{I_1} = e^{(-b.ADC)}$$

Equation 4. Equation for the estimation of ADC values where I_1 = signal at lower b-value, I_2 = signal at higher b-value, b = b-value, and ADC = apparent diffusion coefficient.

Principles of DTI

Diffusion tensor imaging (DTI) is a more robust extension of DWI and allows quantification of localised water molecule diffusion properties within the highly structured environment of the brain where there are both intra- and extracellular barriers that are encountered by a diffusing water molecule. In an unstructured environment the movement of a water molecule can be described by a sphere, but in a structured environment the movement is then modelled as an ellipsoid as diffusion is no longer isotropic (i.e. the same in all directions), as seen in Figure 10.

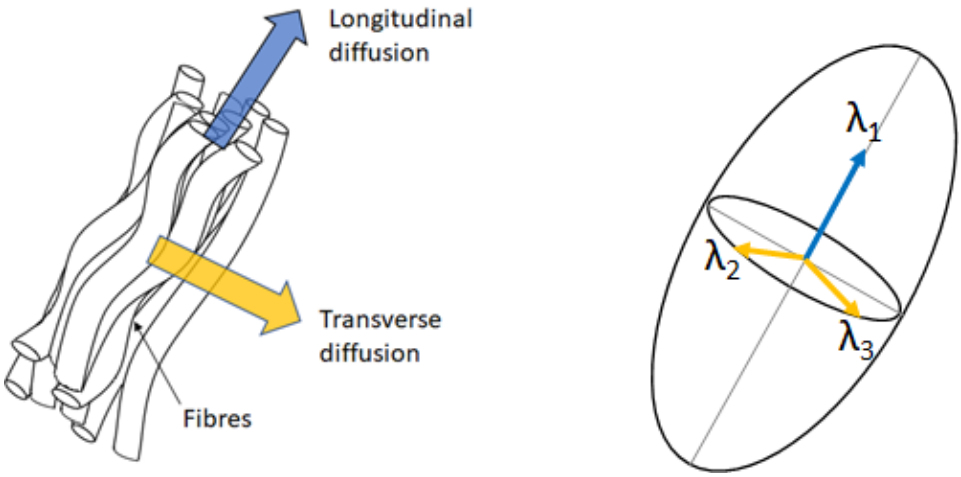

Figure 10. A model of anisotropic diffusion of water molecules (left) and its associated representation by a tensor (right).

To mathematically define the ellipsoid a number of measurements of water diffusion are required in multiple directions that are distributed throughout the three-dimensional space, and a diffusion tensor model applied to their analysis. The application of the diffusion tensor model allows the production of orthogonal measurements in the x, y, and z planes, and the magnitudes of these are the eigenvalues λ_1, λ_2 and λ_3. By combining the direction and magnitude the overall direction and movement of the water molecules can be described using the eigenvectors v_1, v_2, and v_3. In the white matter of the brain the myelinated axons run in a specific direction and water moves most freely in this direction, and is restricted across the axons. Therefore, the largest eigenvector will run parallel to the axon. The eigenvector values can then be used to calculate rotationally invariant diffusion values throughout the brain volume. Examples of the types of measure include the mean diffusivity (MD), as defined in Equation 5, which is a measure of isotropy, and the fractional anisotropy (FA), as defined in Equation 6, which is a measure of diffusion restriction. FA values can be anything from 0, totally isotropic, to 1, total anisotropy.

$$MD = \frac{\lambda_1 + \lambda_2 + \lambda_3}{3}$$

Equation 5. Equation describing the calculation of mean diffusivity (MD)

$$FA = \sqrt{\frac{3}{2}} \frac{\sqrt{(\lambda_1 - \langle\lambda\rangle)^2 + (\lambda_2 - \langle\lambda\rangle)^2 + (\lambda_3 - \langle\lambda\rangle)^2}}{\sqrt{\lambda_1^2 + \lambda_2^2 + \lambda_3^2}}$$

Equation 6. Equation describing the calculation of fractional anisotropy, where ⟨λ⟩ = one third of the trace of the tensor.

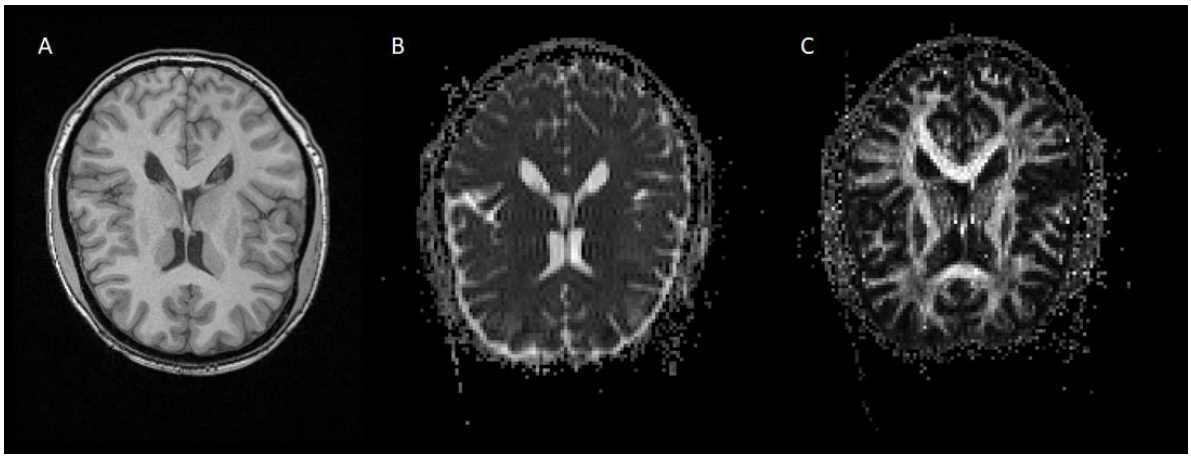

Figure 11. Example slices from Patient 1 of (A) T_1-weighted, (B) MD, and (C) FA.

Figure 11 shows the different types of information available using different scan types. The T_1-weighted image shows the familiar brain tissue with grey matter being darker grey, white matter a lighter grey, and CSF being almost black. The central mean diffusivity image can indicate regions of the brain that have altered diffusion properties showing up as brighter regions within the darker grey and white matter regions, which have very similar MD. The FA image highlights the pathways of the white matter tracts, which can also be presented in a colour version showing the different orientations of the fibres.

It has been proposed that the diffusion patterns of water molecules in the brain may provide additional information about the underlying microstructure of the tissue (Nucifora *et al.*, 2007; Lebois, 2014). In particular, a technique, known as tractography, uses patterns of local anisotropy to define the orientation of white matter tract pathways. FA has been of some interest in studies of patients with mitochondrial disease and recent studies have shown microstructural changes to white matter tracts that appear to be unique to a specific phenotype, and possibly genotype but many more studies would be required to fully assess this as no post mortem neuropathological correlates have yet been established (Virtanen, 2011; Rocca, 2011). Perhaps of most interest is the study that looked at a group of patients, all with the m.3243A>G point mutation, and compared them to a control

group. The main finding was a decreased FA in the inferior longitudinal fasciculus (see Figure 12) (Virtanen, 2011), which correlates to clinical observations of the symptoms experienced by many m.3243A>G patients relating to the areas of the brain linked by this particular tract.

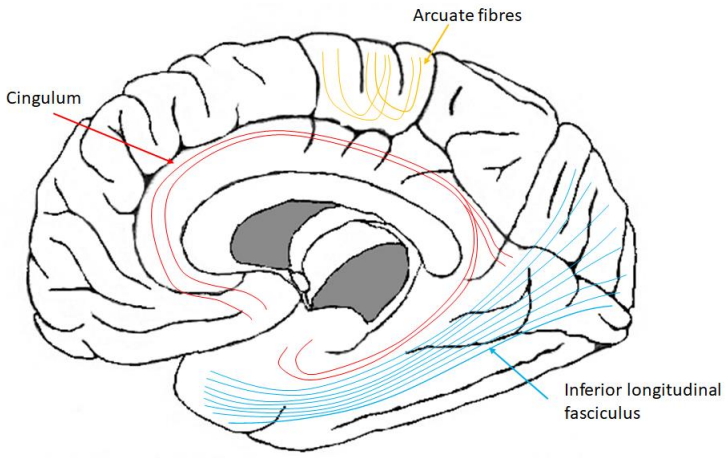

Figure 12. Schematic diagram of the route of the inferior longitudinal fasciculus joining the temporal and occipital poles.

Perhaps one of the most useful aspects about FA is that the relevant scans can be taken *in vivo* and so tissue structures in living patients can be mapped. With the information available from the eigenvectors a virtual map of white matter tracts can be rendered in three dimensions, also known as tractography. These maps may then potentially highlight whether the white matter tracts have been disrupted in some way, for example showing evidence of shearing after traumatic brain injury (Gold and Lipton, 2008).

DTI Analysis Techniques

MD and FA values that are obtained using DTI are measures of water molecule movement within the brain and are hypothesised to differ in different tissue types (Jeurissen *et al.*, 2012). A single value for the whole brain would be meaningless as this would average together all tissue types, including any areas of pathology, and although there may be an indication of the presence of pathology from the absolute value provided, there would be no information about the size, location, or structural nature, so a number of techniques have been developed to break down the analysis so that values can be obtained for specific structures and regions of interest (ROIs).

The most prevalent technique is to register DTI data with a conventional T_1- or T_2-weighted scan and then to place ROIs for which mean MD and FA values can then be extracted. These values can then be compared within regions, between regions, and also between patient and control groups (Levin *et al.*, 2008, Matsushita *et al.*, 2011, Newcombe *et al.*, 2011, Niogi *et al.*, 2008).

An increasingly popular method of data analysis is to automatically segment scans into tissue types, grey matter (GM), white matter (WM), and CSF, to then obtain mean values for each one; or to use a software program to carry out tractography to define and map the white matter tracts (Chu *et al.*, 2010, Goetz *et al.*, 2004, Hong *et al.*, 2009, Newcombe *et al.*, 2011).

For analysis to be meaningful between individuals or groups, differences in size and head geometry between individuals must be compensated for. To achieve this, scans are translated into “standard space”, which maps the test brain onto an ‘ideal’ brain that has been averaged from many scans so that the test brain aligns with the reference brain and thus regions can be more accurately defined. This then facilitates a direct comparison between specific brain regions. However, there are some research groups that advocate the use of patient space, or real space, instead to provide a more accurate determination of the values being measured in each individual (Aribisala *et al.*, 2011).

1.2.iv Arterial Spin Labelling (ASL)

ASL works on the principle that the water in blood can be magnetically labelled. The water in the blood just below the area that is to be imaged is given a magnetic label by applying a 180° RF inversion pulse. Over time this magnetically labelled water exchanges with tissue water, thus altering the properties of the water within the tissue as the magnetically labelled water has an inverted spin. This exchange reduces the overall magnetisation of the tissue which then also reduces the MR signal and the associated image intensity. This process is then repeated without the magnetic labelling step to create a control image. The labelled image is then subtracted from the control image to produce an image showing the perfusion within the tissue and also reflects the volume of arterial blood that is delivered to the location within each voxel during the image measurement time.

1.3 Thesis Aims and Scope

Mitochondrial diseases are a collection of heterogeneous diseases in which symptoms may occur in any tissue, with age of onset varying across the lifespan with few clear indicators of the underlying mechanisms that trigger the presentation of symptoms. Despite the advances of understanding in terms of genotypes, phenotypes, and disease end-state neuropathology, there is still a large gap in mitochondrial disease knowledge in terms of reasons for susceptibility to neurological symptoms, the early mechanisms of these, and thus also any early warning biomarkers that may be used to develop and utilise preventative treatments.

The main aims of this thesis were to develop, validate, and utilise cutting edge MRI analysis techniques to non-invasively investigate the volumetric properties of the brains of carriers and patients with MELAS with a confirmed m.3243A>G genetic diagnosis against a healthy control group to ascertain whether there are identifiable biomarkers for susceptibility to stroke-like episodes. The outputs are as defined below:

- Identification and validation of an accurate and repeatable automatic segmentation protocol.
- Analysis of global brain volumes in the form of whole brain, grey matter, and white matter.
- Analysis of regional brain volumes in the form of cortical thicknesses.
- Basic analysis of white matter tracts using tract-based spatial statistics applied to DTI scans.
- Looking beyond single mode imaging to assess the challenges associated with registering ultra-high-resolution MRI with CLARITY images.

Within the analysis of all of the above areas, there are a number of underpinning themes. These themes are the clinically relevant outputs that will assist clinicians in understanding mitochondrial disease better in terms of progression and prognosis. These themes are:

- Determining those at risk of stroke-like episodes using risk biomarkers.
- Tracking the disease trajectory from the point at which a specific mutation is identified rather than at first clinical presentation.

- Providing insights into the evolution of underlying mechanisms of stroke-like episodes and their development over time.
- Identifying any potentially easy-to-measure biomarkers, or surrogate biomarkers that may potentially be used in clinical practice.

The scope of the thesis was to not only utilise the analysis techniques, but also to assess them for validity in this particular field. The patient cohort was made up of 17 individuals, some of who had experienced stroke-like episodes, patients with MELAS (n = 7), and those who had not, carriers (n = 10). In addition, there was also a control cohort formed from age- and sex-matched controls from the general population.

Chapter 2. Magnetic Resonance Imaging of individuals harbouring the m.3243A>G point mutation

2.1 Introduction

Patients with mitochondrial disease may have any one of a large number of mitochondrial genetic defects, either in the form of point mutations or large-scale deletions (McFarland *et al.*, 2010). The most common genetic mutation is the m.3243A>G point mutation, which makes up around a third of all genetic diagnoses within the mitochondrial disease patient and family populations (Gorman *et al.*, 2015a). Although many of the phenotypes associated with the m.3243A>G point mutation, such as MELAS and MIDD, have been relatively widely discussed in the literature (El-Hattab *et al.*, 2015; Zhang *et al.*, 2015; Nelson, 2017), m.3243A>G as a standalone genotype, and the prediction of symptoms and the long-term prognosis prior to symptom onset, has not. There are a number of neurological symptoms that are associated with this genotype that have been well characterised (McFarland *et al.*, 2010), but there are yet to be reliable biomarkers identified to allow the probability of CNS symptom development to be assessed.

2.2 Aims

This chapter systematically reviews the use of MRI scans and the associated analysis techniques in the characterisation of the brains of patients harbouring the m.3243A>G point mutation and also considers relevant research carried out in other diseases that provides evidence to highlight methods that should be considered for in depth research into the mechanisms and processes of the development and clinical presentation of neurological manifestations of symptoms in patients harbouring the m.3243A>G point mutation.

2.3 Methods

2.3.i Paper Selection

Published clinical studies were identified using the following criteria: adult patients, defined as >18 years old; a genetic diagnosis of the m.3243A>G point mutation; have had a brain MRI; additional descriptors, including ‘stroke-like episodes’ and ‘MELAS’ were also used to identify relevant papers. The reason for only including adults within this literature search is due to the adult-only composition of the study cohort and the requirement to identify research relevant to this group.

Additional papers from research into other diseases, and also other techniques, were identified via the more general search terms: ‘lesion detection’; ‘lesion measurement’; ‘metabolite ADC’; ‘water ADC’; ‘brain MRI’.

2.3.ii Literature Search Strategy

Searches were carried out using online literature databases; PubMed, Scopus, and Web of Science. Publication dates from 1st Jan 1980 through to 26th October 2017 were included in the search. This wide date range was chosen to cover the main development period of MRI and its use in clinical practice. Articles in English, French, and German were included, and any duplicate articles were excluded. Reporting of patients in multiple papers was not considered to be an issue unless the findings in each were contradictory. The following keywords were used for searches: ‘m.3243A>G’, ‘A3243G’, ‘brain’, ‘MRI’, ‘adult’, ‘MELAS’.

Non-m.3243A>G paper searches were carried out using the same literature databases using search terms: ‘lesion’, ‘MRI’, ‘ADC’, ‘atrophy quantification’, ‘abnormal connectivity’. Papers were selected for the relevance to research into m.3243A>G neurological symptoms, along with the quality of methodology and insights provided into non-m.3243A>G disease.

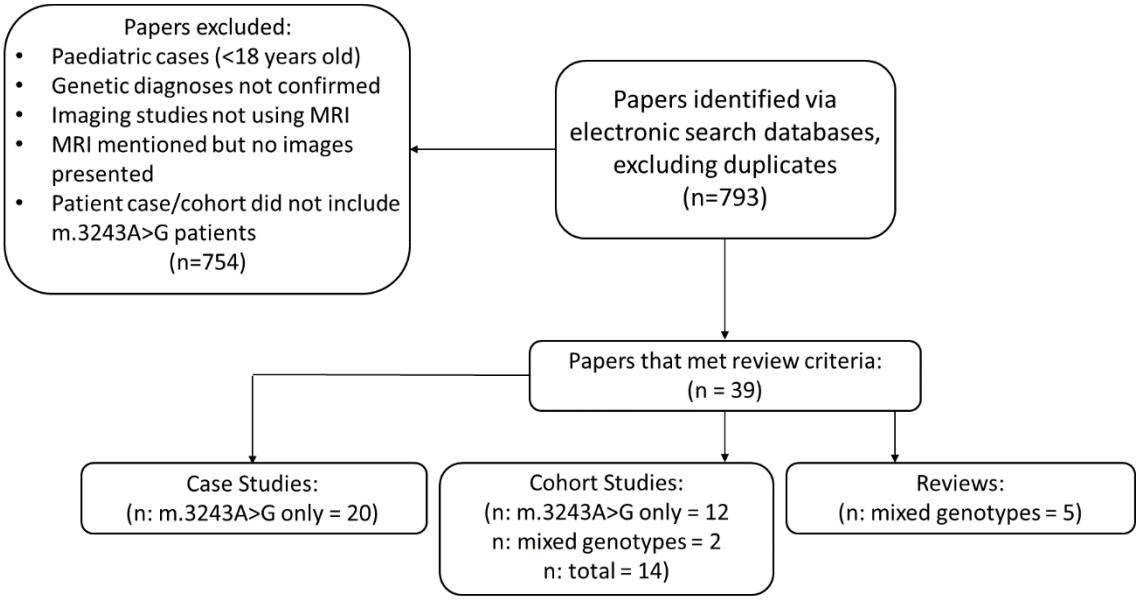

Figure 13. Flow chart showing breakdown of articles identified through a systematic search (1st January 1980 to 26th October 2017) before and after the application of the exclusion criteria.

Volumetric Studies	3 (46 Patients)
DWI/DTI Studies	1 (15 Patients)
Other – including SWI and ASL	0

Figure 14. Breakdown of papers that have quantitative analysis by subject matter. Papers may appear in more than one category depending on the study conducted.

An additional 22 papers were identified through a wider scope literature search and investigation of citations that covered research outside m.3243A>G, but provided additional information and evidence to allow a more in depth understanding to be formed of the current MRI research into the effects of the m.3243A>G point mutation on the brain. This was a search that utilised both systematic searching of databases, but also utilisation of reference lists within those papers that were identified as adding relevant information to the discussion of topics identified within the MRI in mitochondrial disease papers.

2.4 Data Extraction and Analysis

The selected articles were arranged by cohort type, with further categorisation carried out to identify the type of MRI scan and analysis used in each of the papers with regards to the investigation and understanding of the brains of patients with the m.3243A>G point mutation. Case studies are defined as papers that discuss one, or more, specific individual patients, while cohort studies are papers that discuss patients as a group and report group characteristics rather than characterise the individual.

To provide an overview of the findings to date a meta-analysis was attempted. The data collected showed that this would not be possible as the sample sizes for each possible parameter was very small, generally numbering less than 10, and with data coming from a maximum of n = 3 papers per parameter. Therefore, quantitative analysis was not possible due to the predominance of observational findings and, in many cases, small sample size. Therefore, analysis of papers will consist of a qualitative analysis of the methods used and the findings in each of the areas of interest.

2.5 Results

2.5.i Use of MRI in the study of mitochondrial disease in patients with the m.3243A>G point mutation

The search terms yielded a total of 793 articles within the electronic databases selected. Of these, 20 articles described 31 patients in case studies, which are defined as papers discussing specifics of each individual. There were also 14 articles describing 182 patients in cohort studies, defined as papers discussing group characteristics of the participants, along with five relevant reviews containing overviews of MRI findings and use of MRI in patients with mitochondrial disease with the m.3243A>G point mutation. It is perhaps interesting to note that datasets for only 211 patients harbouring the m.3243A>G point mutation have ever been published, and yet if the prevalence estimate from Chapter 1 is used, along with the m.3243A>G point mutation making up around a third of that number, there are approximately 670, 000 people with the m.3243A>G point mutation.

Application of the search criteria led to a large number of papers being removed from the analysis. Around half of these were papers using paediatric subjects, while the rest were removed due to insufficient information being contained within the paper to be of any value to a larger study. In many cases an MRI scan was mentioned either in the abstract or methods, but no image was presented, nor was the scan discussed, or alternatively it was simply stated that the MRI scan did not show anything of interest. These papers also made no statement of the scan sequence used, or the scanner type. n = 7 papers were removed due to there being no verification of the genetic mutation of the patient(s) in question, thus making it impossible to know whether the paper is relevant to a study of purely patients with the m.3243A>G mutation.

2.5.ii Case Studies, Cohort Studies, and Reviews

Case Studies

The 20 case study papers covered a total of 31 individuals, 12 of these utilised T_2-weighted MRI scans, of which three carried out longitudinal follow-ups over time periods ranging from three weeks to 12 months (Apostolova *et al.*, 2005; Bi, *et al.*, 2006; Choi *et al.*, 2012; Clark *et al.*, 1996; Fabrizi *et al.*, 1996; Hanna *et al.*, 1997; Kim *et al.*, 2016; Kobayashi *et al.*, 2005; Kolb *et al.*, 2003; Miceli *et al.*, 2008). Of the

31 individuals covered in these studies, the dominant observations were the presence of temporal and occipital lobe lesions, in 15 and 14 individuals respectively. Seven were reported with lesions within the parietal lobe, and only two with lesions in the frontal lobe. Of the 18 symptoms reported, three were reported in around a third of cases, which were headaches, epileptic seizures, and aphasia, with the others only being reported for a couple of individual cases, most of which were reported due to their unusual presentation. This collection of reporting backs up the anecdotal clinical reports of temporal and occipital lesions being the most common. There was also approximately even reporting of cortical and cerebellar atrophy (in eight and nine patients respectively), however it was rare that both types of atrophy were reported in a single individual. Seven of the studies utilised apparent diffusion coefficient (ADC) mapping techniques (Bi *et al.*, 2006; Choi *et al.*, 2012; Kolb *et al.*, 2003; Ohshita *et al.*, 2000; Oppenheim *et al.*, 2000; Tzoulis *et al.*, 2009; Uehara *et al.*, 2014) to analyse the diffusion properties of water in the brain and the findings were somewhat contradictory as equal reporting was given for both increases and decreases of ADC associated with lesions caused by stroke-like episodes. The Tzoulis *et al.* (2009) paper did however suggest that these differences are due to the time between the stroke-like lesion forming and the measurement being made as they monitored the lesions in their patient over time and noted a change from a decrease in ADC to an increase in ADC compared to healthy controls over time (see Section 2.6.i for further discussion of the literature ADC values), four studies utilised ASL to analyse the perfusion properties of the brain (Ikawa *et al.*, 2013; Li *et al.*, 2017; Tsujikawa *et al.*, 2012; Uehara *et al.*, 2014). All four found that in acute lesions there was hyperperfusion, and two also noted that in old lesions hypoperfusion was seen. Ikawa *et al.* (2013) and Li *et al.* (2017) noted regions of hyperperfusion in a total of five patients prior to their next stroke-like episode, so these patients already had a history of stroke-like episodes and were being actively monitored. Tsujikawa *et al.* (2012) also noted an interesting case in which hyperperfusion was observed in the contralateral cerebellum to the location of the lesion, which then resolved over time no lesion was noted in the cerebellum itself. The final case study used MR angiography (MRA) (Minobe *et al.*, 2015) and observed increased vasodilation within the lesion forming in the occipital lobe compared to other regions of the brain.

Cohort Studies

The 14 cohort studies involved a total of 182 patients who had MRI scans as part of the study and ranged in sample size from 3 up to 33 patients with m.3243A>G related mitochondrial disease. Some of the studies contained a mixed genotype cohort and only where patients with the m.3243A>G point mutation could be separated out were the studies deemed to be valid for use in this review. All bar two of the cohort studies utilised structural MRI scans to analyse the patient brains qualitatively by eye (Abe *et al.*, 2004; Iizuka *et al.*, 2002; Iizuka *et al.*, 2003; Majamaa-Voltti *et al.*, 2006; Sue *et al.*, 1998; Suzuki *et al.*, 1996; Tatlisumak *et al.*, 2016; Tschampa *et al.*, 2013; Tsujikawa *et al.*, 2016; Virtanen *et al.*, 2011; Chinnery *et al.*, 2000; Fromont *et al.*, 2009).

In the qualitative observations there was a slightly different weighting to the reporting of the location of lesions with equal numbers being reported in all of the temporal, occipital, and parietal lobes. Interestingly there were 12 reported cases of having a confirmed m.3243A>G point mutation with symptoms such as headaches and epileptic seizures, but with MRI scans that were reported as looking normal. In terms of symptoms, reporting of stroke-like episodes (58 individuals), epileptic seizures (33), and cognitive impairment (38 individuals) dominated the cohort literature.

The differences seen between the case studies and the cohort studies is likely to be due to the selection of ‘interesting cases’ for the case studies, while the cohort studies perhaps used patient groups that are more representative of the patient population as a whole, although the patient selection is heavily weighted towards those with MELAS or histories of stroke-like episodes.

Four of the studies had a longitudinal element to them in addition to the main case study, but timeline details were only given in one of these (Abe *et al.*, 2004; Iizuka *et al.*, 2002; Iizuka *et al.*, 2003; Majamaa-Voltti *et al.*, 2006) and although they did describe the progression of the lesions in the patients that were followed up in terms of size and location, most often beginning in the temporal lobe and spreading unilaterally, without timelines associated with those it is impossible to begin to ascertain whether there are any patterns in terms of lesion development.

Five studies looked at water ADC mapping techniques (Abe *et al.*, 2004; Iizuka *et al.* 2003; Liu *et al.*, 2010; Virtanen *et al.*, 2011; Fromont *et al.*, 2009) in which all found

that ADC values were decreased in acute lesions, but Liu *et al.* (2010) also investigated non-lesioned areas compared to controls and found the ADC values to be elevated (further discussion of ADC values can be found in 2.6.i).

Of these cohort studies, three carried out voxel-based morphometry (VBM) to statistically volumetrically compare the brains of those with stroke-like episodes, to carriers, and to controls (Tsujikawa *et al.*, 2016; Virtanen *et al.*, 2011; Haast *et al.*, 2018), but only one of those actually presented a full quantitative presentation of their results that included actual values in addition to statistical comparisons (Virtanen *et al.*, 2011). The regions highlighted by Tsujikawa *et al.* (2016) were the left superior parietal lobe, the right precuneus, the right middle temporal gyrus, and the bilateral posterior lobes of the cerebellum, which were significant in all four of their patients with MELAS, and found in three, one, two, and five of their carrier group respectively. In contrast Virtanen *et al.* (2011) found the predominant changes between their control and patient groups in the occipital lobes and the cerebellum, with no apparent dominance in either hemisphere. All three of the papers found significant differences between the control and patient group grey matter volumes, although Haast *et al.* (2018) did not find a significant difference between their controls and their 'low heteroplasmy' group.

The paper by Virtanen *et al.* (2011) provided a methodology that was well-described and repeatable, with the measures being clearly defined and also quantified. In the analysis conducted in this paper, the patients were all consolidated into a single group that included both carriers and patients with a history of stroke-like episodes and significant atrophy. The paper reported the patient group to have significantly less grey matter than the control group.

The cohort studies mostly consisted of patient groups with a mixture of clinical histories and within each group there were patients with, and without, histories of stroke-like episodes (Majamaa-Voltti *et al.*, 2006; Suzuki *et al.*, 1996; Tatlisumak *et al.*, 2016; Tschampa *et al.*, 2013; Tsujikawa *et al.*, 2016; Virtanen *et al.*, 2011; Chinnery *et al.*, 2000; Fromont *et al.*, 2009). Most of these clearly defined the number of patients that were included who had histories of stroke-like episodes (Tsujikawa *et al.*, 2016; Virtanen *et al.*, 2011; Chinnery *et al.*, 2000; Fromont *et al.*, 2009), but some did not (Majamaa-Voltti *et al.*, 2006; Suzuki *et al.*, 1996; Tatlisumak *et al.*, 2016; Tschampa *et al.*, 2013), hence precluding a meta-analysis of the published data. In

addition to this, only around half of the cohort studies papers included a patient table with information such as symptoms, age at diagnosis, age at first stroke-like episode, and so on.

Comparison and Discussion of Case and Cohort Studies

The vast majority of the reporting is from clinical sources and there is a heavy emphasis within the case studies of 'interesting cases'. The trend of publishing these 'interesting' case studies has now almost ceased, and there is now a much larger emphasis being placed on cohort studies to attempt to gain a more in depth understanding of the neurological, and in particular the neurodegenerative, symptoms experienced by patients with the m.3243A>G point mutation, whether they have suffered from stroke-like episodes or not.

All reported case studies within this review, except one case study presentation of a patient with MIDD (Kobayashi *et al.*, 2005), were of patients who had suffered from a stroke-like episode, or who had lesions reported on their MRI scans. Therefore, the vast majority of case studies reported some type of lesion being present on the MRI scans. Unfortunately the details of when the stroke-like episodes occurred in relation to the date of the MRI scan were not reported in the majority of cases, with only seven of the case studies (Bi *et al.*, 2006, Clark *et al.*, 1996; Ikawa *et al.*, 2013; Kolb *et al.*, 2003; Li *et al.*, 2017; Tsujikawa *et al.*, 2012; Tzoulis *et al.*, 2009) and 3 of the cohort studies (Abe *et al.*, 2004; Iizuka *et al.*, 2003; Liu *et al.*, 2010) providing timelines relative to the first recorded stroke-like episode within the study timeline.

The studies that included structural MRI scans provided clinical observations of the general location, and in the case of the longitudinal studies, the spread or development of lesions, but the longitudinal studies carried out no further analysis of the images to provide information about the size of the lesions present, the lesion location, the shape or coverage of the lesion, details of the size changes of the lesion, or any other observations about the longitudinal changes that occurred.

The seven case and cohort studies that captured longitudinal structural data simply captured observational comments and cannot be combined to provide further information about the longitudinal progression of stroke-like episodes (Bi *et al.*, 2006; Clark *et al.*, 1996; Kitamura *et al.*, 2016). The only structural longitudinal aspect of stroke-like lesions that was commented on was the development of atrophy (Bi *et al.*,

2006; Clark *et al.*, 1996; Fabrizi *et al.*, 1996; Hanna *et al.*, 1997; Kim *et al.*, 2016; Kitamura *et al.*, 2016; Kobayashi *et al.*, 2005; Majamaa-Voltti *et al.*, 2006), with three of the papers observing significant, but unquantified, atrophy over time in the regions of the lesion formation (Bi *et al.*, 2006; Liu *et al.*, 2010; Majamaa-Voltti *et al.*, 2006). Cortical laminar necrosis was reported by some of the longitudinal studies (Bi *et al.*, 2006; Majamaa-Voltti *et al.*, 2006) even though cortical laminar necrosis is a pathological diagnosis and there have yet to be imaging correlates established. With a combined sample size of seven the data presented states that up to half of lesioned areas caused by stroke-like episode lesions will show cortical laminar necrosis, however this should be read as the T_1-weighted images showing hyperintensities in the grey matter surrounding lesions.

Atrophy is another measure that is frequently commented upon in the selected case studies. All of these studies only made qualitative visual assessments of the presence, and extent, of the atrophy. These most commonly qualitatively described atrophy in the region of the lesions, in addition to descriptions of both cerebellar (Kim *et al.*, 2016; Kobayashi *et al.*, 2005) and brain stem (Kobayashi *et al.*, 2005) atrophy.

One of the difficulties of studying patients with mitochondrial disease who do not have significant symptoms is identifying them. One method that may be of use to increase the cohort of people with the m.3243A>G point mutation is to look in other disease groups including diabetes (Tatlisumak *et al.*, 2016) or ischaemic stroke (Tschampa *et al.*, 2013). While these studies are relatively rare, they indicate that m.3243A>G point mutation carriers could make up 15 - 45 patients per thousand within the diabetic and stroke patient groups (Suzuki *et al.*, 1996; Tatlisumak *et al.*, 2016). These results indicate that the prevalence of the m.3243A>G point mutation within the general population may be somewhat higher than currently thought and these patient groups may provide a useful clinical insight into the differences in symptomatic presentation between those who are carriers, and those who are diagnosed with phenotypes, such as MELAS, due to their more extreme symptoms.

Comments on Review Papers

Relevant reviews identified in this process are few, and are also somewhat varied in nature (Goodfellow *et al.*, 2012; Haas *et al.*, 2004; Malhotra *et al.*, 2016; Parry *et al.*, 2003; Saneto *et al.*, 2008). One review discusses the use of MRI in MELAS only to discuss the most common initial clinical features of stroke-like episodes, which are

stated to be headaches, seizures, acute neurological deficits, which agrees with both the case and cohort study findings in this review, and the associated lesions seen on MRI (Goodfellow *et al.*, 2012). The four reviews concentrating on imaging modalities provided a lot of information about the imaging techniques available, but in general there are only a couple of useful published papers providing data to allow any sort of assessment of the usefulness of each technique to be made (Haas *et al.*, 2004; Malhotra *et al.*, 2016; Parry *et al.*, 2003; Saneto *et al.*, 2008). The main findings include the use of T_2-weighted FLAIR images for effect visual assessment of the location and size of lesions associated with stroke-like episodes as well as highlighting the potential for techniques such as quantitative T_1-mapping. The papers also only summarise the observations from the papers they have reviewed without acknowledging that these are specifically related to the occurrence of stroke-like episodes in the form of lesions and significant atrophy, and also fail to add any additional value to the original research either through a meta-analysis, or by stating what the observations mean for either a patient group focus (Haas *et al.*, 2004; Malhotra *et al.*, 2016), or for mitochondrial disease in general, for which the other two papers discusses the use of imaging techniques in the diagnosis of the disease (Parry *et al.*, 2003; Saneto *et al.*, 2008). The most important observation made in these imaging papers is that to date there is still no pathonomic correlation between specific neuroimaging changes seen in the brain and the genetic defects present in patients with mitochondrial disease (Saneto *et al.*, 2008).

2.5.iii Volumetric Studies

There are three cohort studies that state they have carried out quantitative volumetric analysis on high resolution MRI scans (Tsujikawa *et al.*, 2016; Virtanen *et al.*, 2011; Haast *et al.*, 2018). Tsujikawa *et al.* (Tsujikawa *et al.*, 2016) and Haast *et al.* (Haast *et al.*, 2018) carried out VBM on their scans, which although strictly speaking is a quantitative analysis technique, the results presented were simple a statement of the brain areas that were highlighted as having statistically significantly different volumes between the patient groups. Tsujikawa *et al.* (2016) split patients into those with, and without, documented stroke-like episodes, while Haast *et al.* (2018) split their patient group by degree of blood heteroplasmy with a low heteroplasmy group (<23%) and high heteroplasmy group (≥23%), with no justification for splitting the patient group in this manner, although examination of the presented data by eye appears to indicate that 23% represents the median heteroplasmy level, and other than a single paper

finding correlation between hearing loss symptoms in patients with MIDD and heteroplasmy, all other papers have found a lack of strong correlation, which further adds to the questions arising from this choice of patient grouping.

The second quantitative volumetric analysis paper to be considered (Virtanen *et al.*, 2011) utilised both segmentation and VBM analysis methods to ascertain whether there were significant volumetric differences between the patient and control groups. In this study the patient group was kept as a single group containing both those with, and without, a history of stroke-like episodes. The number of patients with histories of stroke-like episodes was not stated, but it was stated that nine of the patients were neurologically asymptomatic. The lack of patient information means that is it also unknown how many were of short stature, and therefore have smaller heads, which would bias the patient results. The results showed that there was significantly smaller volumes of grey matter in patients compared to controls (after normalisation for head size) and that these were concentrated in the occipital pole region and the cerebellum (Virtanen *et al.*, 2011). The methodology used was clearly stated and could easily be repeated by any other group. The results were also presented as quantitative outputs, which could allow simple comparison to output from other studies if the scan type and parameters are suitably matched. However, it needs to be stated that the grouping of patients into a single group and the lack of attention to additional patient details means that this research is highly biased towards patients with histories of stroke-like episodes and significant atrophy.

2.5.iv DWI and DTI Studies

Seven case studies looked at the ADC properties of water in the brains of patients who had suffered stroke-like episodes (Bi *et al.*, 2006; Choi *et al.*, 2012; Kolb *et al.*, 2003; Ohshita *et al.*, 2000; Oppenheim *et al.*, 2000; Tzoulis *et al.*, 2009; Uehara *et al.*, 2014). The presented results of these were that around half found restricted diffusion, identified through the observation of a reduction in ADC values, (Bi *et al.*, 2006; Choi *et al.*, 2012; Tzoulis *et al.*, 2009) in and around lesions, while the other half found increased diffusion (Kolb *et al.*, 2003; Ohshita *et al.*, 2000; Oppenheim *et al.*, 2000; Uehara *et al.*, 2014). Those finding restricted diffusion postulated that in the region of a lesion vasogenic oedema was occurring, while those finding increased diffusion postulate that cytotoxic oedema is the dominant mechanism within a lesion. Unfortunately, the lack of reporting on specific timelines does not allow any

conclusions to be reached about whether the difference in reported diffusion characteristics are due to the timing of the scans in relation to the stroke-like episode.

Two cohort studies have been carried out that provide more details about the nature of changes in water ADC (Iizuka *et al.*, 2003; Liu *et al.*, 2010). The cohort study comparing the water ADC values between lesioned and non-lesioned areas found that the values were lower in lesioned areas (0.7 - 1.2 x 10^3 mm^2/s) than apparently non-affected areas (0.9 - 1.7 x 10^3 mm^2/s), and therefore that diffusion was more restricted in the lesions than in the surrounding tissue (Iizuka *et al.*, 2003). The study also found that the mean ADC values in normal appearing regions with no previous lesions were lower than in previously affected regions (0.9 – 1.1 x 10^3 mm^2/s, compared to 1.2 – 1.7 x 10^3 mm^2/s) (Iizuka *et al.*, 2003). In a second scan taken five days after the stroke-like episode the newly appearing lesions were measured as having water ADCs of 0.73 – 0.89 x 10^3 mm^2/s compared to 0.92 – 0.98 x 10^3 mm^2/s in normal appearing regions (Iizuka *et al.*, 2003). The other cohort study solely looked at water ADC values in the apparently normal areas of the brain of patients with lesions and compared these to controls (Liu *et al.*, 2010). This paper found that water ADC values in patients with MELAS were significantly higher across ten regions of the brain than in the control group, with the overall average water ADCs being 0.793 ± 0.054 x 10^3 mm^2/s for the patients with MELAS and 0.740 ± 0.038 x 10^3 mm^2/s for the controls. This paper also noted that other studies (Ohshita *et al.*, 2000; Wang *et al.*, 2003) looking at water ADC values have traditionally taken the water ADC values from non-lesioned parts of the brain as the ‘normal’ value to compare the lesioned values against (Liu *et al.*, 2010). Traditional explanations for the formation of lesions were discussed, along with the possibility of the combination of impaired cerebral perfusion with the increased neuronal metabolic rate leading to disruption of the OXPHOS process and then on to neuronal death in the lesioned regions (Liu *et al.*, 2010). There are also a number of pathological assumptions that have been made to justify the use of water ADC as an MRI marker for the presence of oedema, either cytotoxic or vasogenic, and also to attempt to explain the local cellular conditions.

One of the cohort studies (Virtanen *et al.*, 2011) carried out analysis of DTI data in addition to the volumetric analysis that was also carried out. Again, the patient group was kept in a single group to compare against the control group with not enough patient information to allow understanding of the composition of this group. The

analysis was carried out using tract-based spatial statistics (TBSS) and the results indicated that significant differences in fractional anisotropy (FA) were seen in a number of areas, but the most significant being along the length of the inferior longitudinal fasciculus approximately connecting the occipital and temporal poles (Virtanen *et al.*, 2011).

2.5.v Additional MRI protocols

ASL was used in four case studies to investigate perfusion within the brains of patients suffering from stroke-like episodes (Ikawa *et al.*, 2013; Li *et al.*, 2017; Tsujikawa *et al.*, 2012; Uehara *et al.*, 2014), with two of those papers (Ikawa *et al.*, 2013; Li *et al.*, 2017) claiming that ASL maps may show hyperperfusion up to 3 months prior to the onset of a stroke-like episode. One further paper utilised MRA to look at the vascular system during a stroke-like episode and found vasodilation of the cerebral arteries, which then reverted to normal as the symptoms reduced in severity (Li *et al.*, 2017). All of these papers utilised patients who had already had a stroke-like episode and were therefore being actively monitored, with some being scanned at 3 month intervals, allowing the longitudinal tracking of perfusion. However, none of the papers had scanned a patient prior to the first presentation of a stroke-like episode, and therefore the observations made cannot be assumed to be an initial indicator of a stroke-like episode.

2.6 Findings from non-m.3243A>G research

2.6.i ADC values

With a number of m.3243A>G research papers looking at water ADC, some further information was sought on this parameter, particularly due to the often-contradictory results presented.

Specifically looking at water ADC values to begin with, it is known that although water is almost omnipresent throughout both the microscopic and macroscopic brain tissues, it is for this very reason inherently non-specific (Shepherd *et al.*, 2012). In addition to this ubiquity, there is also work that has been carried out by Lampinen *et al.* (2017) and Reisart *et al.* (2017), which claims that the exact diffusion properties and coefficients of water in the various cellular environments are not yet accurately known, and therefore diffusion measurements of water in the brain offer little solid information about the specific cellular environments of interest, particularly the

division between the intra- and extracellular components of a diffusion signal. In addition to these issues, there is also the problem that there are a number of different models utilised in order to quantify the diffusion properties of water in the brain, and all of which incorporate a large number of assumptions within them (Shepherd *et al.*, 2012).

It therefore seems obvious that water alone is unlikely to ever provide a complete picture of all cellular environments of interest within the brain. If metabolite ADCs are also used, the combination of all of these could provide detailed insights to the microstructure of the brain *in vivo* (Shepherd *et al.*, 2012).

To further undermine the usefulness of water ADC, Table 1 and Table 2 show ADC values that have been quoted in the literature.

Tissue type	Average value ($x10^{-3}$ mm^2/s)	Range ($x10^{-3}$ mm^2/s)
Cortical grey matter	0.89 ± 0.04	0.78-1.09
Deep grey matter	0.75 ± 0.03	0.64-0.83
White matter	0.70 ± 0.03	0.62-0.79

Table 1. Typical water ADC values in a healthy population (Helenius et al., 2002). These ADC values did not vary significantly with age, gender, or hemisphere.

Tissue type (mixture of GM and WM)	Average value ($x10^{-3}$ mm^2/s)	Range ($x10^{-3}$ mm^2/s)
Lesioned (2-5 days post stroke-like episode)		0.7 – 1.2
Contralateral to lesion – previously unaffected		0.9 – 1.1
Contralateral to lesion – previously affected		1.2 – 1.7
Normal appearing		0.92 – 0.98
Average across the brain	MELAS 0.79 ± 0.05 Control 0.74 ± 0.04	

Table 2. Published water ADC values in patients with MELAS with confirmed m.3243A>G point mutations (Iizuka et al., 2003; Liu et al., 2011).

The values provided in the literature show that in general the ADC values found in any patient with a history of stroke-like episodes are higher than those in healthy controls. This may be indicative of global changes that occur in association with stroke-like episodes.

Although diffusion-weighted magnetic resonance spectroscopy (DW-MRS) measurements to ascertain metabolite ADCs are highly challenging, if accurate metabolite diffusion data are acquired, it can then be combined with geometric and computational modelling to provide unique information about specific types of cells and the microstructure in the tissue of the brain both in healthy and diseased brains (Shepherd *et al.*, 2012).

Now addressing metabolite ADCs specifically in ischaemic regions of the brain, there are a number of papers that have begun to tackle research in this area.

One of the earliest papers to look at metabolite ADCs in ischaemic regions of the brain is Wick (1995) and used a rat model. Metabolite ADCs were measured over an 80-minute period, with ischaemia being induced after 20 minutes, and lasted for 20 minutes. The final measurements were made 60 minutes after the onset of the

ischaemic attack. ADCs were recorded for water, total N-acetyl aspartate (tNAA), total creatine (tCr), total choline (tCho), and *myo*-inositol.

The water ADC value initially decreased, but gradually returned to its starting value by the time the final measurement was made. In contrast, all of the metabolite ADCs initially decreased, then returned to their starting value for a very short period of time, and then decreased again, indicating that the cellular changes were not as simple as water moving between the cellular environments, and also perhaps that there are some permanent cellular changes are induced as part of the process (Wick, 1995).

To support this finding, Abe *et al.* (2000) also carried out DW-MRS measurements of metabolite ADCs during the early stages of focal ischaemia in rat brains to observe the temporal changes that occur. ADCs for water, tNAA, tCr, and tCho were measured over a period of 2 hours. The main findings are that all ADC values dropped immediately within the ischaemic regions and were then followed, after a delay, by decreases in all ADCs of the non-ischaemic region and the metabolite ADCs in the contralateral hemisphere, thus indicating that although the ischaemic region was well defined, that there was a global effect observed (Abe *et al.*, 2000).

Liu *et al.* (2011) have carried out a study of metabolite ADCs in patients with MELAS who were all interictal, and therefore had well-established lesions within their brains (Liu *et al.*, 2011). This study was carried out on *in vivo* brains, and examined the metabolite ADCs of tNAA, tCho, and tCr. In this study all of the metabolites were found to have significantly higher ADCs both in lesioned and non-lesioned areas than the control group (Liu *et al.*, 2011).

Looking more in depth at the diffusion properties of water within the brain shows that there is a dependence of ADC on the diffusion time with longer diffusion times showing a decrease in water ADC, thus indicating more restricted movement of the water molecules, which is then theorised to be predominantly attributed to the intracellular environment (Branzoli *et al.*, 2013). Shorter diffusion times are therefore theorised to be predominantly associated with diffusion in extracellular space and larger ADCs (Branzoli *et al.*, 2013). In reference to metabolite ADCs, this paper suggests that their diffusion is not dictated by the cell size, type, and associated structure, but also by additional compartmentalisation on a sub-cellular level along with varying distributions of metabolites in either a ‘free’ or a ‘bound’ state. It is also theorised that the presence of macromolecules and lipids within an environment

could also affect the quantitative measurement of metabolite diffusion (Branzoli *et al.*, 2013).

Metabolite ADCs appear to offer a great level of information about their cellular environments, but there are yet more factors that have to be considered, and one of these is that metabolite ADCs are different in grey and white matter, which considering their different cellular makeups should be expected (Deelchand *et al.*, 2017). When defining volumes of interest (VOIs) within which to measure metabolite diffusion, there are cross-term effects that must be considered and which are directly proportional to the volumes of grey and white matter within the VOI. To add further complexity to the cross-term factor, some scan sequences are more greatly affected than others, with the examples of STEAM[5] and PRESS[6] sequences being given in this case as examples of scan sequences that are affected to a greater and lesser extent respectively (Deelchand *et al.*, 2017).

In real terms, metabolite diffusion measured in grey matter is found to be significantly more restricted than in white matter and therefore any VOI containing multiple types of tissue must therefore have cross-term effects considered for absolute values to be valid along with relative values compared to other VOIs within the same brain or VOIs from the same region in a different subject (Ercan *et al.*, 2015; Kan *et al.*, 2012).

One of the reasons for the attraction of measuring metabolite diffusion properties is because, on the whole, metabolites are confined within cells, and are not found in the extracellular environment (Najac *et al.*, 2016). The location of metabolites can further be determined through experimentation with diffusion times. By varying diffusion times from very short (a few milliseconds) up to over a second it can be seen that there is no dramatic dependence upon these, thus indicating that the majority of the metabolites found within cells in the brain are actually within the long fibres of cells rather than the cell bodies (Najac *et al.*, 2016; Valette *et al.*, 2018). This metabolite distribution reflects the distribution of mitochondria within the neuron as although mitochondria start in the soma they then travel along the fibres to provide localised energy production for each part of the cell, only returning to the soma to be repaired or recycled (Lin and Sheng, 2015). The lack of dependence on short diffusion times

[5] STEAM – Stimulated echo acquisition mode, is a 90° - 90° - 90° slice selective pulse sequence.
[6] PRESS – Point resolved spectroscopy, is a 90° - 180° - 180° slice selective pulse sequence, which is less susceptible to motion, diffusion and quantum effects and has a better signal to noise ratio (SNR) than STEAM.

also indicates that metabolites are also not dominantly transported by active mechanisms around the cell (Valette *et al.*, 2018).

This predilection for metabolites to be in the long fibres of cells also means that there is an age-dependency of their ADCs as neuronal cell properties change significantly over time losing dendritic length, surface area, volume, diameter, and spine numbers and density (Zheng *et al.*, 2012). Therefore, metabolite ADCs decrease as the brain ages, while in contrast water ADCs are not significantly affected (Zheng *et al.*, 2012). It is also stated that neuronal apoptosis could begin as soon as 30 minutes after the onset of ischaemia, with a peak occurring between 24 and 48 hours, and at timescales longer than 48 hours the lesion is considered to be fully mature and necrotic.

While this technique appears to offer a method to gain in-depth insight into the microstructure of the brain in patients carrying the m.3243A>G point mutation, the scanning protocols are not yet routinely available on clinical scanners and so could not be utilised within this study, but should definitely be considered in the planning for any future work.

2.6.ii Alternative theories for restricted diffusion

Changes in dendritic morphology, which could be caused either by age or ischaemia, may decrease the internal neuronal space across a number of dimensions, in which metabolite diffusion may occur, which then leads to the decrease of metabolite ADCs (Zheng *et al.*, 2012). In addition to the morphological changes already described, it is also stated that apoptotic neurons are smaller in size than healthy neurons, which in itself could account for an overall decrease in metabolite ADCs while the water ADC is able to return to normal (Zheng *et al.*, 2012).

One theory about long term changes in metabolite ADCs is in the case of a chronic (necrotic) lesion, there is liquefaction of the neuronal debris, which then reduces the viscosity of the extracellular space. The number of apoptotic neurons also decreases, which could then result in a net increase of metabolite ADCs over time assuming that apoptosis ceases, which could provide an explanation for the relapsing/remitting nature of mitochondrial disease. However, this would require a large-scale longitudinal study to investigate further (Zheng *et al.*, 2012).

In high grade gliomas, there is another alternative mechanism for the production of reduced metabolic ADCs proposed. In these gliomas there is the possibility of the presence of volume reduction caused by hypoxia within the glial cells, with an associated shift of cytoplasmic water (Gadda *et al.*, 2016).

One final theory for the reduction of metabolite ADCs actually comes from the study of lesions in patients with POLG (Tzoulis *et al.*, 2016). It was found in these lesions that there was a significant increase in the cerebral vascular density, which was more pronounced in regions of chronic neurodegeneration, in other words, within lesions as identified on structural T_1 and T_2 FLAIR MRI scans. The vascular density correlated with the severity of the neuronal loss, but it was also observed in acute lesions and so either occurred very quickly, or was an ongoing process prior to the full development of the lesion and associated stroke-like episode (Tzoulis *et al.*, 2016). These results suggest that in patients with mitochondrial disease that at least some lesions do not have ischaemia as a contributing factor to the pathogenesis of either chronic neurodegeneration or acute lesions, particularly in *POLG* encephalopathy and that these lesions are more likely to reflect energy production insufficiency driven in large part by underlying seizure activity (Tzoulis *et al.*, 2016).

2.6.iii Quantification and mechanisms of atrophy

Quantifying atrophy is not necessarily a straightforward task, but a large study carried out into the quantification of atrophy in Alzheimer's Disease (AD) attempted to identify reliable methods to quantify the progression of atrophy in this patient group. A number of methods were proposed, all looking at the quantitative measure of atrophy, however the methods proposed were more designed to quantify the overall rate of atrophy in patients with AD, rather than to quantify the rate of progression in a single patient and also only considered atrophy progression over short timescales of up to a year (Cash *et al.*, 2015). The paper found that there were large differences between the proposed techniques in terms of the number of samples required for the technique to work, but the smallest sample sizes stated for a trial that has a subsequent 12-month monitoring period is 242 for the full brain. It should also be stated that these techniques were designed to be able to identify volume changes down to around 1%.

It has also been observed in patients with temporal lobe epilepsy (TLE) that there is ongoing grey matter atrophy even when there is no recordable seizure activity (Alvim

et al., 2016). The patients with TLE have MRIs that appear normal, in terms of lesion presence, and also in patients both with and without hippocampal sclerosis. This appears to suggest either a separate atrophy process, or one that is due to sub-clinical activity within the temporal lobe (Alvim *et al.*, 2016). Interestingly, it has been noted that some patients with AD suffer so-called 'silent' seizures and spikes in the hippocampus during sleep (Lam *et al.,* 2017), which indicates that seizure activity during sleep may be a factor in apparent seizure-less atrophy processes. One area that does not appear to have been studied in any detail is the effect of seizure control on the rate of atrophy, with no papers having been found addressing this question, either qualitatively or quantitatively, within the current literature.

TLE research has also employed quantitative segmentation techniques to assess differences between patient and control populations in very large cohorts (Whelan *et al.,* 2018) and have found patterns of atrophy associated with each of the epilepsy subgroups identified within the patient population. In addition to this definition of atrophy patterns, other work has shown that grey matter atrophy is networked, which may also be linked to seizure frequency and aetiology (Coan *et al.,* 2014) and which may provide some insights into the mechanisms of seizure-related atrophy in patients with mitochondrial disease.

2.6.iv Abnormal connectivity

The previous example of ongoing atrophy without seizure activity may perhaps be linked to the findings of work that has been carried out into looking at the hippocampal-thalamic wiring in patients with medial temporal lobe epilepsy, which shows enhanced connectivity per hippocampal voxel (Freund *et al.*, 2012). This study found pronounced enhancement of connectivity between the sclerotic hippocampus and the ipsilateral thalamus in patients with either left or right TLE compared to a control group. The differences were most apparent in the number of absolute fibres and was most pronounced when correcting for hippocampal volume (Freund *et al.*, 2012). It was also noted in this study that the increased connectivity also negatively correlated with cognitive performance on a number of executive function tasks.

A further study has also been carried out in patients with TLE using connectivity-based segmentation to determine the connectivity patterns of the thalamus to ipsilateral cortical regions; occipital, parietal, prefrontal, precentral, postcentral, and temporal (Keller *et al.*, 2014). It was noted that patients had a significant decrease in

volume of the ipsilateral hippocampus and entorhinal cortex. There was also a preferential volumetric loss of the thalamic segment connected to the temporal lobe (Keller *et al.*, 2014).

Further analysis also showed that the thalamotemporal segment volume significantly correlated with the volume of ipsilateral, but not contralateral, mesial temporal structures, which indicates that the degree of thalamic pathology is related to the extent of mesial temporal lobe damage in TLE (Keller *et al.*, 2014).

Research has also been carried out in patients with Parkinson's Disease with, and without, hallucinations to attempt to pinpoint the regions involved in this phenomenon. Despite previous assumptions that the mesial temporal lobe is involved, this work showed that the hallucinations in these patients are actually related to disruption of the visuoperceptual pathway (Goldman *et al.*, 2014). The areas that were shown to have a significant relationship to hallucination severity were: left inferior parietal lobule; left cuneus; right lingual gyrus; and right precentral gyrus. These affected regions play essential roles in both primary and secondary visual processing and visuoperceptual functions (Ungerleider and Mishkin, 1982). The secondary visual pathway is of most interest relating to mitochondrial disease patients, and particularly the disruption to the lingual gyrus, and their hallucinations as the pathway is involved in object recognition and movement detection and from anecdotal clinical reports appears to correlate with the types of visual hallucination experienced by patients with mitochondrial disease (unpublished data). Unfortunately, to date there has not been a cohort study formally investigating the nature of hallucinations and any related changes in the microstructure of the brain in patients with mitochondrial disease to allow any further analysis of this phenomenon.

2.6.v Individualised approach to scanning and mapping

There is ongoing work to develop a robust method for lesion segmentation utilising shape priors from both offline and online learning (Shepherd *et al.*, 2012). The technique combines radial shape parameterisation combined with machine learning techniques from the field of non-linear time series analysis and offers the potential for quantifying the volume of a lesion (Shepherd *et al.*, 2012). This could provide a robust method for assessing the location, size, and spread of a lesion over time.

Taking an individual approach further into the future and considering the requirements for a system that could potentially be applied to clinical practice,

Cantor-Rivera *et al.* (2016) propose the use of patient-specific mapping to allow addressing clinically relevant individual pathologies, thus facilitating a detailed patient-specific automated quantitative assessment using MRI scans. For each genotype, phenotype, or disease, it is theorised that it is possible to carry out baseline imaging to then identify and define regions of interest that can then be interrogated for volumetric, relaxometry, and diffusion features that may differ from healthy control groups. Direct comparison of these regions with healthy control groups can then identify and provide visualisation of any significant differences in specific regions of clinical interest and importance through the use of individual feature maps (Cantor-Rivera *et al.*, 2016).

2.7 Discussion/Conclusions

There are a number of learning points that can be taken away from this literature review to improve both the way MR research is carried out in patients with the m.3243A>G point mutation, and also to improve and increase the awareness that is required to ensure that all relevant research is taken into consideration when stating that a parameter appears to be of significance in indicating a neurodegenerative process is either about to occur, or is occurring.

The early literature predilection for reporting on case studies of patients who have already suffered from stroke-like episodes means that there is only piecemeal, inconsistent information regarding the following research parameters:

- The exact symptoms and their durations, or timelines, during a stroke-like episode
- Subsequent reporting of disease progression, for example the formation of lesions within the affected area of the brain, which migrate over time in many cases and are not constricted by vascular boundaries
- The rapid atrophy that occurs in a large number of cases, although the proportion in which this happens is still completely undefined

The sum total of the information from this style of reporting on individual cases is not enough to provide any real insight into the causes and mechanisms of the onset of stroke-like episodes.

The consistent reporting of lesions being more common in the temporal and the occipital lobes may provide an indication that these regions are most susceptible to

stroke-like episodes, and therefore should be of greatest interest for more in-depth analysis, particularly in those carrying the m.3243A>G point mutation but who have not yet suffered a stroke-like episode.

Despite these initial clues, identifying a suitable technique to interrogate whether these mechanisms are in progress, and at what stage they are at, is something of a guessing game. The aim of this type of reporting should be to create a clinical database of symptoms, and the number, and progression, of patterns, to establish whether there are any specific markers to allow definition of which of these a patient may be likely to experience.

Despite the move to larger cohort studies there is a clear lack of standardisation in the way that patient information is analysed. Of the three papers claiming to have carried out quantitative analysis of their patients, two simply carried out VBM and stated the areas found to have a statistically significant difference in volume without providing justification of what they considered to be statistically significant or why, with absolutely no consideration of what may be clinically significant. This was also reflected in the lack of attempt to explain what the volumetric difference might mean in terms of the symptoms suffered by patients, or why the m.3243A>G point mutation would affect these areas in both carriers and patients (Tsujikawa *et al.*, 2016; Haast *et al.*, 2018). In addition to this, the methodology that was used in each of these was far from being reproducible, and in Haast *et al.* (2018), there was also an unexplained and unjustified split in the patient group made by blood heteroplasmy levels, despite the only correlation between heteroplasmy and symptoms being found in patients with MIDD (Chinnery *et al.*, 2000) and relating to deafness, no other papers have found significant correlations between heteroplasmy and individual symptoms.

Table 14 also provides supporting evidence for the lack of correlation between heteroplasmy level and susceptibility to stroke-like episodes. In addition to the points already mentioned there is also a lack of timeline reporting for both cross-sectional and longitudinal studies for the time elapsed between the presentation of a stroke-like episode and the subsequent imaging, which means that the information presented cannot be analysed in a meaningful way to then provide additional information within a clinical setting relevant to the onset of stroke-like episodes. This is especially true in water ADC studies as there appears to be some evidence

showing that water ADC changes over time (Tzoulis *et al.*, 2009), but there has yet to be any definition of timelines, or variations of these, within the MRI literature for mitochondrial disease.

There are a number of theories for the underlying mechanism of stroke-like-episodes that include mitochondrial cytopathy, mitochondrial angiopathy, non-ischaemic neurovascular cellular mechanism, or even some combination of any of these (Koga *et al.*, 2010; Lax *et al.* 2012) and it is clearly an important task to identify which of these it may be; however there have been no MRI correlates for any of these established for patients with the m.3243A>G point mutation that may provide an early warning that a stroke-like episode will occur in the future. There has also been no reported work on attempting to establish the order in which subclinical seizure activity, activation of rapid atrophy, formations of lesions, and clinical presentation of stroke-like episodes occur, or if they do in fact occur in a specific order. In addition to the cellular mechanisms previously mentioned, there are also mechanisms by which subclinical seizure activity occurs, which may alter the underlying white matter structure, or general connectivity, which then exert influences over other processes. Therefore, while it is important to understand the formation and development of stroke-like episodes on a cellular level, I have identified a distinct need to identify potential non-invasive imaging biomarkers indicating an underlying susceptibility that exists prior to a stroke-like episode reaching clinical significance as otherwise it will never be possible to formulate effective treatments that could stop the occurrence of stroke-like episodes rather than attempting to limit the devastating effects they have on the brain once they have occurred. However, it is acknowledged that any biomarkers are likely to be identified through more in-depth longitudinal research into all of the microstructural parameters that may be measured through non-invasive imaging.

It should also be noted that in MS tCr ADCs potentially indicate problems with energy regulation and that the primary attempt at treatment would be to rectify this (Zhu *et al.*, 2009). The same could be true for all mitochondrial disease, as the regulation of energy production should be seen as the optimum treatment.

There is also a potential issue of either sub-clinical activity that never fully manifests as a stroke-like episode, or an additional unidentified process, that is significant enough to cause lesions within the brain along with also triggering the rapid and

severe atrophy seen in the majority of patients who have had clinical presentations of stroke-like episodes.

In addition to this, there is work that was carried out in the mid-1990s that indicates that there are fundamental changes to the intracellular environment in the presence of oedema and that permanent regional damage to the cells is caused within 20 minutes (Wick, 1995). This highlights that in order to identify the optimal method for predicting stroke-like episode susceptibility requires a multi-disciplinary approach that includes pinning down at least some of the pathological correlates of stroke-like lesions. It has been questioned whether cellular swelling alone can account for all water ADC changes in tissue that is assumed to be ischaemic (Wick, 1995). In fact, a number of papers have gone on to investigate the ADC of various metabolites, which allows the separation of extra- and intracellular diffusion coefficients, as normally metabolites are only found within cells, such as neurons and glial cells (Wick, 1995; van der Toorn *et al.*, 1996; Valette *et al.*, 2018). The main outcomes of these studies was that although the water ADC returned approximately to normal, metabolite ADCs of N-acetyl-aspartate, myo-inositol, creatines, and cholines, all showed persistent changes, and in addition to this, in post mortem pathological tests nuclear chromatin showed clumping, mitochondrial swelling was frequently observed, and dilation of the endoplasmic reticulum was found in astrocytes, thus indicating that there may be some fundamental intracellular changes that take place when a region of the brain is ischaemic (Wick, 1995; van der Toorn *et al.*, 1996; Valette *et al.*, 2018). These changes have been observed in stroke animal models and indicate that in only a 20-minute global transient ischaemia model irreversible tissue damage occurs (Wick, 1995), and after induction of a 24 hour focal ischaemia, metabolite ADCs were so low that no measurement was possible, indicating that concentrations of these were extremely low within the ischaemic region (van der Toorn *et al.*, 1996), which provides supportive evidence of energy failure. This information shows that patients with mitochondrial disease, with an already impaired energy production system, may suffer an increased rate of irreversible damage compared to patients who have suffered from a conventional stroke. This is an important consideration to consider when attempting to apply ADC as either a predictor of stroke-like episodes, or as a measure of the status of the lesion as the exact mechanisms causing changes to ADC values are not yet understood.

Cerebellar atrophy is something that is highlighted in a number of papers with apparently no associated cerebral atrophy, but there is no mention of the fact that the cerebellum has much smaller features than the rest of the brain, and therefore is much more susceptible to distortion and appearing to be atrophied. When the details of the MRI scan in Kobayashi *et al.* (2005) are investigated, it is found that the slice thickness in all of the scans was 5mm. A quick reference to either anatomy or neuropathology texts (Romero-Sierra, 1986; Osborn, 2013) shows that the smallest structures around the outer edge of the cerebellum are only a couple of millimetres in size. This means that they will in no way be imaged, or presented, accurately in a scan using 5mm thick slices. Not only will the structures appear to blur into each other on the image being assessed, there are also the issues of how partial volume effects are considered in the formation of that image, which is a particular problem when it comes to the accuracy of cerebellar imaging. When combined, these effects often lead to the appearance of the cerebellum being more atrophied than the rest of the brain. After identifying these as issues, I have investigated them further in Chapter 4.

A parameter often quoted as being related to both lesions and atrophy is cortical laminar necrosis. The reporting of cortical laminar necrosis in imaging studies is incorrect as there has, to date, been no pathological correlation for cortical laminar necrosis with the cortical T_1 hyperintensities observed. Data on these cortical T_1 hyperintensities, and the likelihood of their development once a lesion has formed, is sketchy as it is often the most severely affected patients who are commented on and presented, even within a group of those who have suffered from stroke-like episodes, so there can be no further conclusions drawn from the reporting of cortical T_1 hyperintensities to further understanding of the clinical progression of lesions.

The Tsujikawa *et al.* (2016) paper was an attempt to carry out a quantitative analysis of the brain structure of patients with the m.3243A>G point mutation. While there may actually be significant volume differences in the highlighted areas of the brain, many of these were seen in both patient groups and so they can't be linked with susceptibility to stroke-like episodes without a longitudinal study as they could just be a feature of changes that are seen in the brain due to the m.3243A>G point mutation. This paper needed an assessment of what the highlighted brain areas are responsible for and whether they link to any specific symptom(s) commonly seen in patients with the m.3243A>G point mutation before any assumption can be made

that they are related to the susceptibility and subsequent onset of stroke-like episodes. This paper highlights the need for interpretation and meaning to be applied to any, and all, quantitative analysis results as there is little, to no, benefit in merely stating areas of statistically significant volumetric difference in which the requirements for 'significance' are neither stated nor discussed. This opens up a whole new question about the analysis methods utilised as statistical significance is highly unlikely to be the same as clinical significance, and yet every paper only states results by statistical significance. This lack of discussion about clinical significance partly stems from the difficulty in defining it and what it means when there are clinically significant differences between groups, but this is a key part of ensuring that the research output is able to provide information that is of clinical relevance and that may also potentially be used in further research to investigate in more detail regions of the brain that may provide further answers to the question of whether someone is susceptible to stroke-like episodes, in the first instance, but also susceptibility to a broader range of symptoms could potentially also be defined.

The Virtanen *et al.* (2011) paper, at first glance appears to take a much more robust approach to the analysis. However, the failure to separate the patients into two groups means that any subtle differences between the patients without a history of stroke-like episodes and the control group will be lost due to the very large volumetric changes that are seen in the brains of patients who have experienced stroke-like episodes and have suffered from significant and rapid atrophy after these. I have identified and demonstrated the importance of this separation in globally in Chapter 5, and regionally in Chapter 6. The diffusion results in this paper are interesting as they appear to indicate significant differences in the diffusion properties of the inferior longitudinal fasciculus between the patient and control groups. It would be of great interest to see whether this difference is seen only in the stroke-like episode patient group, or if it is seen in all, or a subset of, patients without a history of stroke-like episodes. The results of the TBSS analysis are of more interest than the volumetric results as they appear to indicate a significant difference in the diffusion properties of the inferior longitudinal fasciculus, which connects the occipital and temporal poles. This white matter tract route is of particular interest as there is anecdotal clinical evidence that the temporal and occipital lobes are particularly susceptible and are usually the locations of the first onset of stroke-like episodes. The migration of lesions has often been seen along this pathway in past clinical histories, but there is

no comprehensive analysis of the nature and route of lesion migration due to the lack of longitudinal scan data. The high level of clinical anecdotes for the temporal lobe being the site of the first stroke-like episode indicate that the inferior longitudinal fasciculus should be the subject of further investigation, along with the temporal lobe itself. Their methodology is well-presented and makes sense as a process as I independently formulated this same methodology through validation of the segmentation software and techniques available, and have found that it is the only one to provide true quantitative outputs, allowing clinically relevant analysis to be carried out rather than purely statistical analysis, which does not in any way provide information about the clinical relevance or significance of differences that have been found between control, carrier, and patient groups.

Correct interpretation of results is also absolutely vital and an example of how incorrect interpretation can be misleading can be found in the Haast *et al.* (2018) paper. In a number of places significant correlation is stated, but the correlation values do not support these statements. Inspection of the data presented shows that some of the correlational values provided are significant, in other words, likely to be accurate with 95% probability, but significance of the correlational value does not equate to significant correlation. This appears to have been misinterpreted throughout the paper with correlation values of 0.3 and below being stated as showing significant correlation (Haast *et al.*, 2018). Although smaller correlation values are often accepted in biological sciences as showing a significant correlation, the smallest value for this to be the case is usually around 0.5 at the lowest, with most using 0.6. Therefore, any clinical significance postulated regarding the link between heteroplasmy and symptomatic presentation within the Haast *et al.* (2018) paper must be treated with caution and the size and significance of the correlational value clarified and confirmed. A number of correlation values have been determined to be significant, and so the values found are accurate within 95% confidence limits, but this does not mean that the correlation is significant in itself (Haast *et al.*, 2018).

There are occasionally papers that comment on the efficacy of a particular treatment in either the prevention of future stroke-like episodes, or a lessening of post-stroke-like episode progression of atrophy. These papers do not represent a full clinical trial, with a large patient cohort, in which the effects of L-arginine, or other drugs, are assessed objectively with measurable outcomes and so cannot be utilised as

evidence for which to use a particular treatment and the value of publishing these has to be questioned (Ohsawa *et al.*, 2018).

The reviews to date, unsurprisingly, are limited by the lack of in depth published literature regarding patients with mitochondrial disease who have no history of stroke-like episodes and so generally concentrate on the observations that have been highlighted throughout this chapter. What these reviews do not do is to identify the need for in depth studies looking at patients with confirmed genetic mutations and deletions associated with mitochondrial disease, but who have not had any stroke-like episodes, as without these there is very little chance of moving research forward to provide understanding of the changes in the brain that occur prior to a stroke-like episode occurring and also to be able to identify possible methods of seeing these changes long before the first presentation of a stroke-like episode. This, in turn, would then allow for the targeting of treatments to known processes, to either impede them, or potentially stop them altogether.

The main takeaway point from this systematic review of the use of MRI scans in the study of stroke-like episodes in patients with the m.3243A>G point mutation is that, to date, the overwhelming majority of papers have presented observations, often of individual case studies, without the benefit of any sort of quantitative baseline data of the m.3243A>G brain prior to the onset of any stroke-like episodes. There has also been a distinct lack of hypotheses in the presentation of the observational data, barring a couple of exceptions. Although a number of brain regions have been highlighted as potentially being different in those carrying the m.3243A>G point mutation, there have been no theories proposed as to why these areas may be important in the development of stroke-like episodes, or why they may also be susceptible to the development mechanisms.

Therefore, I have identified that in order to fully utilise any MRI scan data, whether that is related to the structure of the brain or its diffusion properties, there must be an associated investigation and attempt at explanation of why any highlighted areas are important for further investigation. To attempt to begin to rectify this I have identified the requirement to systematically collect and analyse data with respect to current clinical anecdotal information to put together a solid understanding of the similarities and differences seen in patient brains pre- and post-stroke-like episodes.

There is also an additional requirement to collect longitudinal scans to provide better information regarding the progression of changes in the brain over long time periods. With the recent work to identify carriers of the m.3243A>G point mutation prior to clinical presentation, there is the opportunity to build up a cohort of both asymptomatic and presymptomatic carriers, which currently cannot be differentiated from each other with any certainty.

While I have acknowledged the work carried out looking at brain metabolites, further investigation into this has not been carried out as part of this study due to time limitations.

Chapter 3. MRC Participant Cohort and Post Mortem Brain Sections

3.1 Participant Cohort

Participants were sourced from the MRC Mitochondrial Disease Patient Cohort (UK), either locally via the mitochondrial clinical team, or via a postal invitation to suitable candidates already within the cohort. The cohort for this specific study were opportunistically utilised from within a larger m.3243A>G study.

The inclusion criteria that had to be met for the study were:

- ≥18 at the time of the first appointment
- Have proven genetic disease (blood or urine mtDNA heteroplasmy levels were used to confirm)
- Have high levels of heteroplasmy
- All participants must be carriers of the m.3243A>G point mutation and either have the MELAS phenotype (n=7), or be an non-MELAS carrier of the point mutation (n=10)
- Provide informed consent to be included in the study

Scan details

All cohort participants were scanned on the Siemens Achieva 3 T clinical MRI scanner at the Royal Victoria Infirmary (RVI), and all controls were scanned on a Philips Intera 3 T research MRI scanner.

To minimise the differences due to being scanned on different scanners, the same 3D Anatomical T_1-weighted MRI scan parameters were used. In addition to this, MRI scans from a healthy control that had been scanned on both machines using this protocol were analysed to assess whether there were any significant differences in total intracranial, grey matter, and white matter volumes. Derived values were within ± 1.5 % of each other, which was deemed to not be significant in relation to the volume changes being assessed within the study.

Scan 1: 3D Anatomical T_1-weighted

Axial; TE: 5ms; TR: 8ms; Flip angle: 8°; voxel size $1mm^3$.

Scan 2: Diffusion Weighted (DTI)

TR: 9000ms; TE: 95ms; Number of averages: 2; Flip angle: 90°; b-values: 0, 1000; number of directions: 64

Control Participants

Each patient within the study cohort had at least one age- and sex- matched control identified. The control group was taken from the general population, but few demographic details were held regarding this population so it was not possible to match to any additional parameters of interest, such as height, BMI, lifestyle, and so on.

The lack of information about the handedness of the members of both the control group and the cohort may introduce a confounding factor as there are various documented differences in brain physiology between left- and right-handed individuals, with a larger corpus callosum in left-handers being most often noted (Khosravizadeh and Teimournezhad, 2011). The produced results must therefore be analysed with this in mind.

Carriers of the m.3243A>G point mutation details

Patient Number	Sex	Age	MELAS Diagnosis	Blood heteroplasmy	Urine heteroplasmy	BMI	NMDAS scaled score	Age of 1st stroke-like episode	Distribution of most recent stroke-like lesions (before this study)	Clinical features
P01	F	33	0	44%	65%	22	25.9	N/A	None	SNHL, diabetes mellitus, migraine, chronic constipation, exercise intolerance
P02	M	32	0	28%	90%	23.5	2.1	N/A	None	Asymptomatic
P03	M	55	1	28%	87%	25	45.1	42.3	Left parietal and temporal lobes	MELAS, SNHL, chronic constipation, diabetes mellitus, LVH, CPEO, ataxia, cognitive impairment
P04	M	61	1	5%	46%	36.9	58		None	Encephalopathy, chronic constipation, ataxia, myopathy
P05	F	30	1	21%	42%	22.1	57	28.3	Right parietal, temporal and occipital lobes	MELAS, SNHL, migraine, chronic constipation, ptosis, ataxia, myopathy
P06	M	50	1	16%	72%	22.7	35.2	46	Bilateral temporal lobes (more changes on the right)	MELAS, CKD, SNHL, diabetes mellitus, LVH, ataxia
P07	M	25	0	24%	80%	24.9	2.1	N/A	None	Asymptomatic
P08	M	36	0	6%	72%	28.5	2.1	N/A	None	Asymptomatic
P09	M	43	0	27%	85%	27.6	52.8	N/A	None	SNHL, WPW (had ablation), diabetes mellitus, chronic constipation, exercise intolerance, exercise intolerance, myopathy, ataxia
P10	F	38	0	20%	56%	30.9	7.5	N/A	None	Diabetes mellitus
P11	M	30	1	39%	95%	19.4	48.3	23.8	Bilateral temporal and occipital lobes, left insular cortex	MELAS, SNHL, migraine, chronic constipation, cognitive impairment
P12	F	37	0	10%	55%	24.4	17.6	N/A	None	Migraine, ptosis, CPEO
P13	F	61	0	n.d.	20%	32.9	22.8	N/A	None	SNHL, diabetes mellitus, migraine, chronic constipation, exercise intolerance
P14	F	30	1	23%	57%	17.4	19	29.1	Bilateral temporal lobes (more changes on the right), right parietal and occipital lobes	MELAS, SNHL
P15	F	28	1	33%	81%	19.8	24.9	27.2	Bilateral temporal (more changes on the left)	MELAS, SNHL, migraine, chronic constipation
P16	M	51	0	17%	76%	26.1	36.5	N/A	None	SNHL, diabetes mellitus, migraine, chronic constipation, exercise intolerance
P17	M	50	0	24%	85%	18.6	12.9	N/A	None	Migraine, chronic constipation, depression

Table 3. Details of participants involved in the m.3243A>G cohort study. SNHL = sensorineural hearing loss; WPW = Wolff-Parkinson-White syndrome; CPEO = chronic progressive external ophthalmoplegia; n.d. = not detectable; MELAS = mitochondrial encephalomyopathy, lactic acidosis and stroke-like episodes; LVH = left ventricular hypertrophy; CKD = chronic kidney disease stage 4/5

Patient Number	Stroke-like episode clinical history (date, location of lesions, other notes)
P03	10/2003 - LP, LT with report of bright objects seen in left field 03/2005 - RO
P04	No obvious lesions on MRIs, suspect encephalopathic episodes mimicking stroke-like episodes. Brainstem stroke was cause of death.
P05	05/2015 - RP, RT, RO 06/2015 - RO only, rest resolved
P06	01/2012 - BilatT (R>L), BilatO (L>R), LT (+ restricted diffusion) - note significant delay to seeking medical attention as patient was in Australia at the time. Date recorded is first presentation to clinic. 02/2012 - LP, with BilatT (R>L) still in evidence.
P11	01/2010 - LT 04/2010 - All resolved 06/2010 - RO (+ restricted diffusion) 06/2011 - All resolved 05/2012 - LF, LIns, BilatP, BilatT, BilatO 02/2013 - LP, LT, LO, all others resolved 07/2013 - LIns, BilatT, BilatO
P14	08/2012 - No lesions but scanned due to functional neurological problems 11/2015 - RP, BilatT (R>L), BilatO (R>L) 02/2016 - RP, BilatT (R>L), RO, others resolved 05/2017 - LP, BilatT (L>R), BilatO (L>R), LF
P15	01/2016 - RP, RT, RO 04/2016 - BilatT (L>R)

Table 4. Detailed histories and MRI scan notes for all patients with MELAS with histories of stroke-like episodes. L = left; R = right; Bilat = bilateral; P = parietal; T = temporal; O = occipital; F = frontal; Ins = insular.

3.2 Post mortem brain sections

Donor Details

This section details the post mortem brain sections used in the work carried out on the 7 T pre-clinical scanner to obtain very high-resolution structural MRI scans and quantitative T_1 maps of the same sections. There were 22 patient sections from seven patients with a variety of mitochondrial genetic diagnoses. These sections covered the frontal, temporal, and occipital lobes and had representative samples from macroscopically defined lesioned and non-lesioned regions of the left hemisphere of the fixed post mortem brain. There were also six post mortem brain sections from two controls covering the frontal, occipital, and temporal lobes. It is perhaps important to note that it is not common to have the clinical history of a brain donor for brain sections.

Label	Genetic defect	Brain region	Non-lesioned / lesioned *	Length of time in fixative	Status	Further information
Patient 1	m.3243A>G	Frontal	Non-lesioned	7 mnths	Fixed	Whole fresh brain has been scanned
		Temporal	Lesioned	7 mnths	Fixed	
		Occipital	Lesioned and non-lesioned	7 mnths	Fixed	
Patient 2	Multiple mtDNA deletions	Frontal	Non-lesioned	4 years	Fixed and hydrogel-embedded	Fixed right hemisphere scanned
		Temporal	Non-lesioned	4 years	Fixed and hydrogel-embedded	
		Occpital	Non-lesioned	4 years	Fixed and hydrogel-embedded	
Patient 3	*POLG*	Frontal	Non-lesioned	4 years	Fixed and hydrogel-embedded	Fixed right hemisphere scanned
		Temporal	Lesioned and non-lesioned	4 years	Fixed and hydrogel-embedded	
		Occpital	Non-lesioned	4 years	Fixed and hydrogel-embedded	
Patient 4	m.8344A>G	Frontal	Non-lesioned	4 years	Fixed and hydrogel-embedded	Fixed right hemisphere scanned
		Temporal	Lesioned	4 years	Fixed and hydrogel-embedded	
		Occpital	Non-lesioned	4 years	Fixed and hydrogel-embedded	
Patient 5	*POLG*	Frontal	Non-lesioned	5 years	Fixed and hydrogel-embedded	Fixed right hemisphere scanned
		Temporal	Non-lesioned	5 years	Fixed and hydrogel-embedded	
		Occpital	Non-lesioned	5 years	Fixed and hydrogel-embedded	
Patient 6	m.3243A>G	Frontal	Non-lesioned	3 years	Fixed and hydrogel-embedded	Fixed right hemisphere scanned
		Temporal	Non-lesioned	3 years	Fixed and hydrogel-embedded	
		Occpital	Non-lesioned	3 years	Fixed and hydrogel-embedded	
Patient 7	m.8344A>G	Frontal	Non-lesioned	9 years	Fixed and hydrogel-embedded	
		Occipital	Non-lesioned	9 years	Fixed and hydrogel-embedded	
Control 1	Control	Frontal	Non-lesioned	8 years	Fixed and hydrogel-embedded	
		Temporal	Non-lesioned	8 years	Fixed and hydrogel-embedded	
		Occipital	Non-lesioned	8 years	Fixed and hydrogel-embedded	
Control 2	Control	Frontal	Non-lesioned	9 years	Fixed and hydrogel-embedded	
		Temporal	Non-lesioned	9 years	Fixed and hydrogel-embedded	
		Occipital	Non-lesioned	9 years	Fixed and hydrogel-embedded	

*Table 5. Description of the post mortem brain sections used in the high-resolution MRI work in Chapter 9. * = defined macroscopically.*

3.3 Sample Size, Power, and Correcting for Multiple Comparisons

Clearly the sample size within this study is small and there are also multiple comparisons being made. To allow usable results to be generated the statistical hypothesis used in each case is that the comparison group of either carriers or patients with MELAS has a mean that is a minimum of three standard deviations away from the mean of the control group. This greatly reduces the number of

participants required for the sample sizes used to have adequate power. By using specific comparisons, and not assessing every possible comparison, as is done in automated voxel-based morphology, to assess whether a region has a significantly different volume, in addition to setting the statistical hypothesis to require the test group mean to be at least three standard deviations below the control group mean, the need to carry out correction for multiple comparisons is not required as the probability of a group mean occurring within these parameters becomes vanishingly small. In addition to this, the p-value for every comparison is stated and was assessed during analysis for any correction requirement.

Clearly, the statistical hypothesis used throughout this study is aimed at finding very large differences between groups. Therefore subtle, but consistent, differences in brain volumes will not be highlighted as statistically significant within this work as the power is not high enough to allow these to be reliably detected. The justification for this approach was to attempt to not only provide statistical significance, but also to highlight results that are of clinical significance and to ensure the power was high enough to generate valid results.

Chapter 4. Software Accuracy Assessment and Validation for quantitative volumetric analysis

4.1 Introduction

There has been a great deal of development of brain structure analysis techniques over the past 15 years. For many years the most commonly used tool to calculate brain volume, and also segmented brain volume, was the manual tracing method (Keller and Robert, 2009; Geuze *et al.*, 2005). These were popular because they allowed the operator the surety of specificity of the selected areas, particularly on poor quality images. This specificity allows for absolute brain volumes to be calculated more easily than for automated methods (Keller and Roberts, 2009). However, there are a number of disadvantages to using this method including the time burden to manually trace the sections, and operator wobble when tracing along boundaries, which can cut off areas desired for inclusion and include areas desired for exclusion (Keller and Roberts, 2009). A much faster manual method of calculating brain volume is to use the stereological point counting method (Keller and Roberts, 2009) in which areas are selected by superimposing a grid of points over the image and deselecting those that are not relevant to the area of interest (Garcia-Fiñana *et al.*, 2003; Garcia-Fiñana *et al.*, 2009; Roberts *et al.*, 2000). There is one final significant drawback of using manual methods, and that is the requirement for expertise in neuroanatomy, particularly for volumetric analysis of specific brain components, so despite manual methods offering greater specificity, they are often not used due to lack of expertise in neuroanatomy and also the difficulty of achieving high inter-rater reliability (Keller and Roberts, 2009).

There are a huge number of papers that have been published over the last 15 years detailing various different pieces of software and methods for carrying out semi-automated and automated volume and segmentation analysis (Keller and Roberts, 2009; Ashburner and Friston, 2000; Ashburner and Friston, 2001; Bookstein, 2001; Freeborough *et al.*, 1997; Smith *et al.*, 2004; Smith *et al.*, 2002; Taylor *et al.*, 2014). One thing is very clear, there are many different approaches employed when it comes to non-manual MRI analysis. This causes a number of problems in that results produced by different pieces of software are rarely directly comparable. This was demonstrated by the author by carrying out segmentation of the same set of brain MRIs with two different pieces of software and obtaining wildly different output

values. Therefore, there needs to be a good level of understanding of what a piece of software is outputting. Previous literature may be used as a guide to the type of processing to use so that new results may be compared to those previously published.

Most current automated processing of brain MRIs uses a reference set of healthy brains, the composition of which is important if a true population norm is to be established, which is used to create a 'standard'. The brain under investigation is then compared against the standard using either physical characteristics (FMRIB, 2015) or statistical techniques (Friston, 2007). This comparison to a standard based on a group means obtaining absolute values for parameters such as brain volume, ventricle size, etc., is not a reasonable aim for individual scans but identifying group trends is. However, obtaining relative changes over time for an individual is a reasonable activity as they are only referenced to themselves and not to a group standard. In summary, there is no standard automated method of processing MRIs, which causes a number of reproducibility issues.

In general, manual stereological analysis is considered to be more suited to individual cases, whereas the statistical nature and use of atlases makes automated processing more suitable for comparing groups of cases (Roberts *et al.*, 2000). Understanding of the different analysis techniques and how they can best be used is vital to ensure accurate and reliable information is output from any analysis. There are very few papers that have directly compared the output of manual, semi-automated/region of interest and fully automated volumetric analysis (Good *et al.*, 2002; Keller *et al.*, 2002) so it is difficult to know how the different techniques compare to each other, particularly with respect to the type and quality of images that are being used for the analysis. It is key, however, to remain consistent in the type of analysis method used for a particular measurement so that results are repeatable and comparable (Good *et al.*, 2002).

The method of processing is irrelevant if the images that are being worked with are not of a high enough quality in terms of resolution of features and contrast between tissues of interest. Irrespective of processing method, poor images will not provide robust, accurate volumetric analysis or segmentation (Keller and Roberts, 2009; Geuze *et al.*, 2005).

Despite a high level of interest in carrying out quantitative analysis of MRI scans within both the clinical research and the analysis tool development communities, there is a lack of quality assurance standards to provide standardised information about the accuracy, repeatability, and reliability of the various softwares available. There are a number of softwares that have been validated for very specific regions of the brain, most notably the hippocampus, amygdala, and corpus callosum (Mulder *et al.*, 2014; Velasco-Annis *et al.*, 2018), and some that have been validated for repeatability (Yang *et al.*, 2016), but to date I have not been able to find any that been validated for global segmentation volumetric accuracy, as opposed to repeatability, with the results published in open literature.

One of the underlying reasons for this is due to the speed of development of MRI analysis techniques with the research community moving to convolutional neural networks (CNNs) and the complex architectures required to carry out the deep learning processes required for increased accuracy, and also greatly increased speed (van Ginneken, 2018). This rapid development leaves little time for methods to be developed to the point where they have been quality assured for the purposes of clinical use, which is not helped by the use of bespoke software on the scanners themselves (Block, 2018). However, to reach the point of having a clinical use, the techniques first have to demonstrate a clinical value, which is likely to require a greater level of collaboration between the developers of these techniques and the clinicians who would be the ones using the outputs (Schmeirer *et al.*, 2018).

Clinicians are keen to move forwards from the technology that is currently available, should robust quantitative outputs providing useful and clinically relevant information be developed, and agree that an iterative process is for development is likely to be the most effective method of producing software and techniques that are fit for purpose, and also disease specific as each disease has different requirements from MRI (Schmeirer *et al.*, 2018).

In addition to all of the issues mentioned above, it is also the case that MRI scanners have not been developed as quantitative measurement devices, and each vendor has come up with different methods to achieve each type of scan so there is no easy way to standardise between scanner types (Chenevert, 2018).

This current state of affairs means that to carry out quantitative analysis on clinical MRI scans requires the use of automated software that is not only very slow and

takes up a lot of human effort as well, but also has no absolute accuracy limits provided, which are vital should any software be considered for use within a clinical setting.

The lack of standards relating to quantitative analysis of structural scans makes any quantitative project difficult, and therefore to allow my confidence to be established in my quantitative results, I carried out a time-consuming validation exercise to ascertain the most suitable segmentation software, as well as starting to gain an understanding of some of the intrinsic limitations of the quantitative outputs provided by the software.

The final justification for carrying out this type of validation is because there are inherent issues in attempting to segment a combination of healthy and diseased brains using the same atlas, and so there needs to be careful assessment of how the diseased brains are segmented by the software. An alternative approach has also been developed in which multiple atlases are used that are specific to the group being analysed, in terms of age, disease type, and any other significant factors that may affect the segmentation.

4.2 Aims and Methods

The most commonly available MRI scan type are thick-slice clinical scans used by radiologists to visually identify any abnormalities on the scans. However, for quantitative analysis there are issues with attempting to segment from this type of scan, and high-resolution anatomical scans are required.

The aims of this section are to carry out a validation exercise on the segmentation software commonly used in the volumetric analysis of brain MRI scans to assess the following:

Aim 1: To demonstrate why global tissue segmentation cannot be carried out on thick-slice scans.

Aim 2: To compare manual vs automated segmentation of global volumes of GM, WM, and CSF.

4.2.i Initial File Preparation

All files to be segmented were first converted from the digital imaging and communications (DICOM) file type to Neuroimaging Information Technology Initiative

(NIfTI) files using the DICOM to NIfTI file conversion capability within the MRIcroGL MRI viewing software (Rorden and Brett, 2000). Bias field correction was carried out as part of the automated segmentation processes, and was not carried out for the manual segmentation as variation across the image could be compensated for by the person carrying out the segmentation.

Eight 3D T_1-weighted anatomical scans were selected, all from people in their 30s and comprising four men and four women, for segmentation. Six of the scans were from healthy controls, and two scans were selected from the carrier group who did not have any visible lesions or histories of stroke-like episodes.

A 2D T_1-weighted spin echo (T1SE) with thick slices from a MELAS patient with no obvious lesions or atrophy was also selected to provide a comparison.

4.2.ii Comparison of 2D thick-slice and 3D anatomical scan types

To carry out tissue segmentation successfully there should ideally be a discernible difference in the intensity of each class of tissue, identified by the presence of a clear peak in the histogram output. These peaks can be spread by factors including noise in the image, motion artefacts, bias field effects, partial volume effects, in addition to true within class variation (Smith *et al.*, 2004). This spreading effect can lead to the mislabelling of voxels, which may lead to a significant distortion of the results if any of the contributing factors are particularly strong (Smith *et al.*, 2004).

The easiest method of assessing the size of the effect of the confounding artefacts is to take a histogram of the intensities seen within the image. To demonstrate some of the issues a histogram from a high resolution and low resolution scan were taken and can be seen in Figure 15 and Figure 16. These can be obtained by opening the MRI scan in FSLView and outputting the histogram of the image.

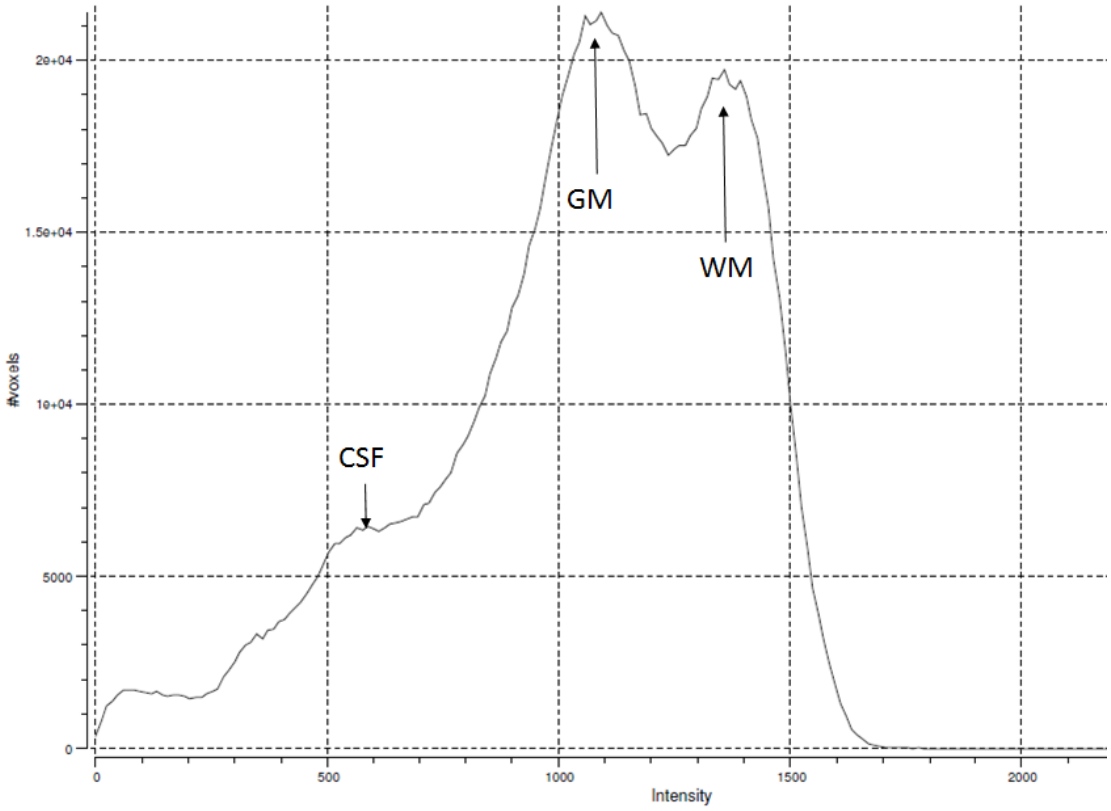

Figure 15. Histogram of a high resolution 1mm^3 voxel structural MRI scan. The separated peaks can clearly be seen for each of the different tissue types.

Figure 15 shows the resulting histogram from a high-resolution 3D anatomical scan. Separation of the peaks for each of the tissue types can clearly be seen, and therefore it is possible to differentiate between these when looking at individual pixels on each slice of the image as they have different intensities.

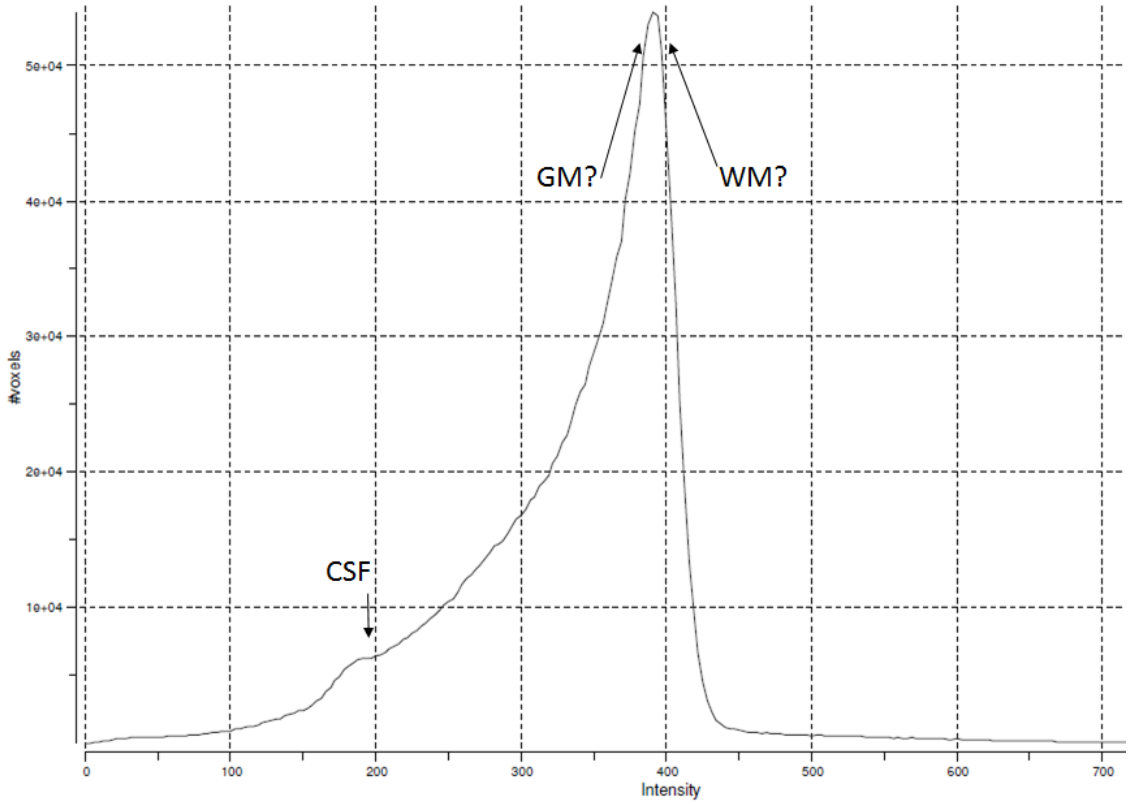

Figure 16. Histogram of a thick-slice T1SE scan using 3mm slices through the brain. The CSF can clearly be seen with a much lower intensity, but there is no clear separation between GM and WM intensity grouping, although some contrast may be observed.

Figure 16 shows the resulting histogram from a thick-slice T1SE scan using a slice thickness of 3 mm. Separation of the peaks for each of the tissue types can clearly be seen, and therefore it is possible to differentiate between these when looking at individual pixels on each slice of the image as they have different intensities.

When high-resolution and thick-slice scans are compared side by side as shown in Figure 17, the differences in contrast are also visibly very clear. The lack of contrast in the thick-slice scan can only lead to large error margins for any quantitative volumetric segmentation, particularly when contrast is used to define the tissue boundaries. It should be noted that there may also be contrast differences between different acquisition sequences, irrespective of slice-thickness, that may also have an impact on the contrast, for example the use of magnetisation prepared rapid acquisition gradient echo (MPRAGE) or sampling perfection with application optimised contrasts using different flip angle evolutions (SPACE) (Okada *et al.*, 2012).

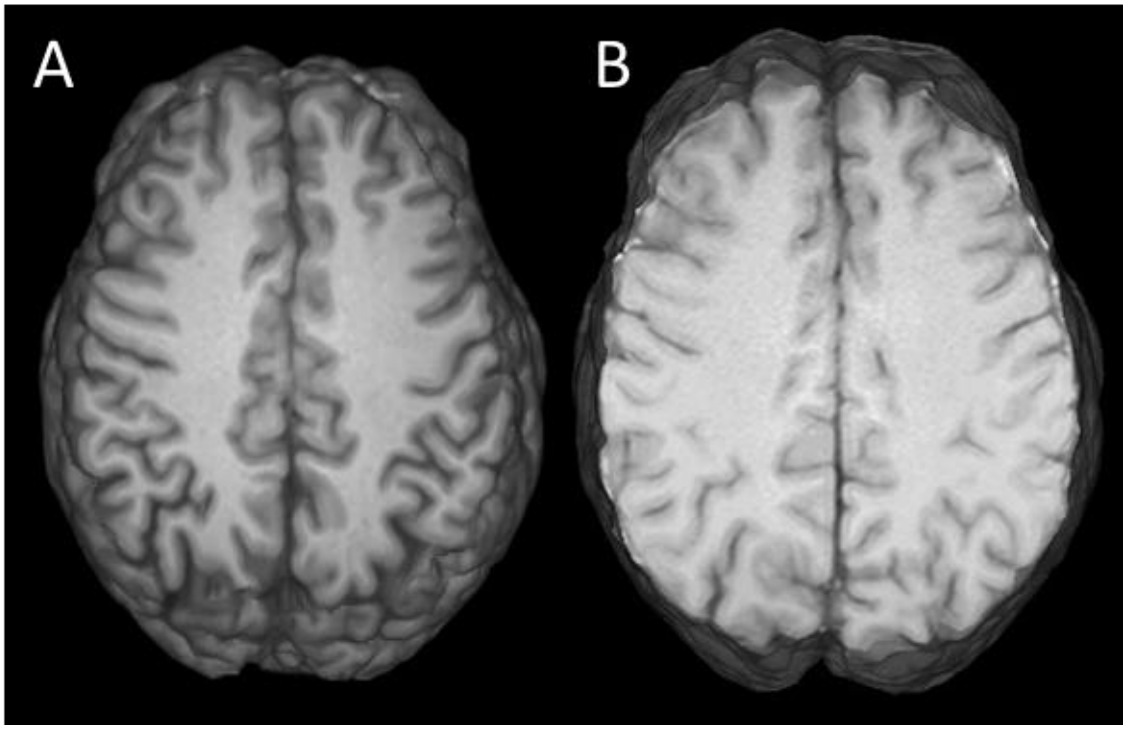

Figure 17. Single slices taken from a high-resolution (1mm^3 voxels) scan (A) and a thick-slice scan (4mm slice thickness with 1mm^2 pixels) (B). The differences in the contrast between grey and white matter are very clear and cannot be improved from the images above using contrast enhancement techniques.

The importance of bias field correction in automated segmentation can be appreciated if a histogram is taken of an uncorrected MRI, as shown in Figure 18. This shows clearly the regular peaks across the histogram, which if not corrected will lead to the segmentation algorithms incorrectly segmenting an image.

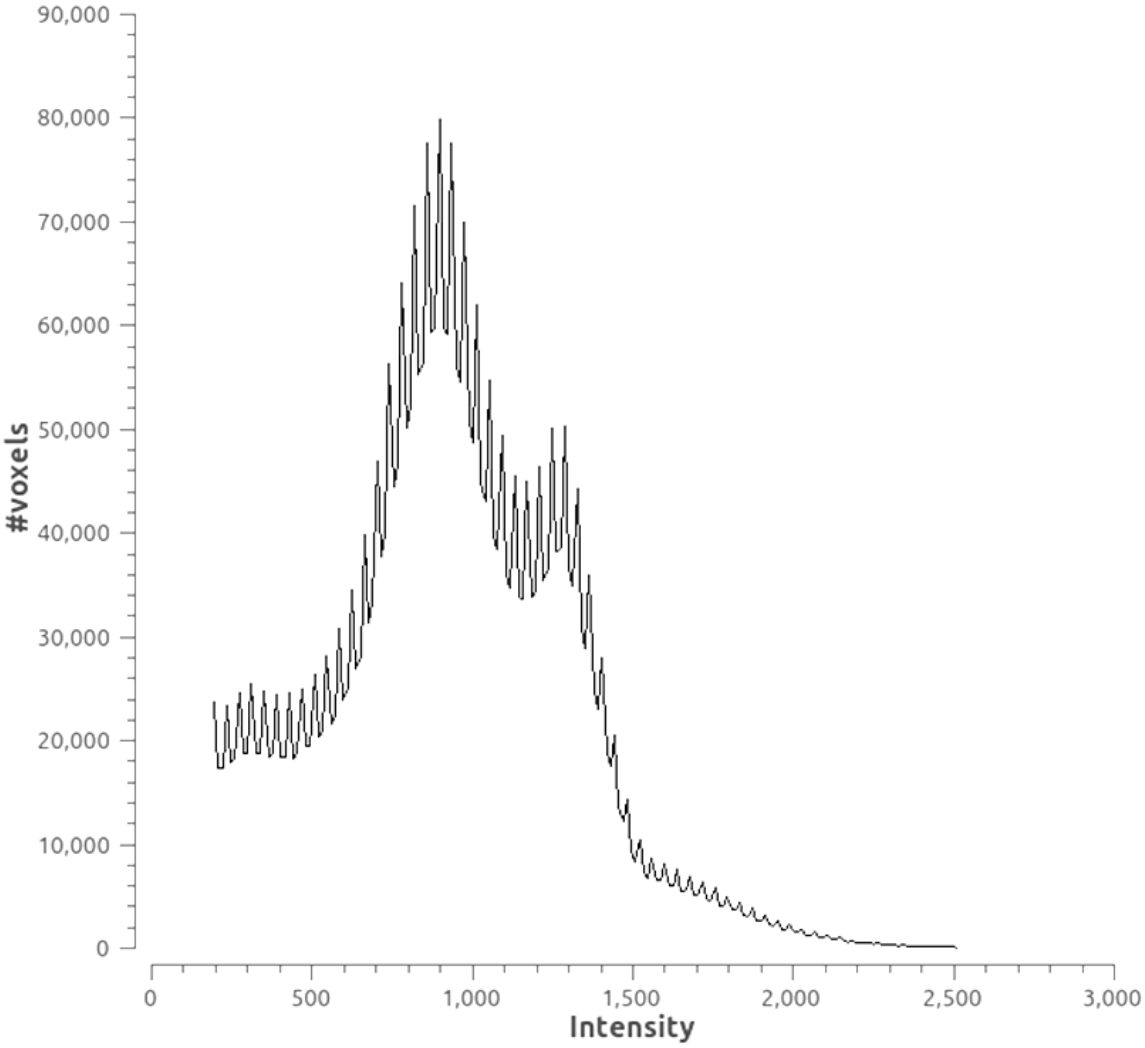

Figure 18. Image showing the interference of a bias field in the assessment of pixel intensity in the form of regular peaks across the slice histogram.

4.2.iii Manual Segmentation

3D Slicer 4.8 (Kikinis *et al.*, 2014; Fedorov *et al.*, 2012) was used to carry out the manual segmentation of the sample brains. Each pixel was inspected and allocated to a tissue category using individual pixel selection. These selections were used to define the region of each tissue type on each slice, with the segmentation being driven almost completely by the intensity of, and contrast between, tissues due to my neurological inexperience. The majority of the segmentation was carried out in the sagittal and axial planes, with the coronal plane being used periodically to double check that areas had not been selected erroneously.

The technique used was to segment the grey and white matter, with the deep grey matter being included in the grey matter volume, of the brain in a combined model, and then to segment the total intracranial volume (TICV) as a separate volume. This

method was chosen to keep the segmentation time to a minimum as the CSF volume could easily be derived from these values.

It took around seven to ten hours to carry out TPV segmentation of a scan to obtain values for TICV, and between 60 and 70 hours to carry out a grey and white matter segmentation.

Once each piece of segmentation had been completed, it was built into a 3D model from which the volumetric values could be extracted.

Manual segmentation was carried out three times per scan, with a gap of 4-6 weeks in between each segmentation to take into account intra-rater reliability between each segmentation attempt. The presence of any large discrepancies would be assessed and explained. To compare the results between the automated segmentation and the manual segmentation, an average of the manual segmentation values was taken.

4.2.iv Automated Segmentation

The software selected to carry out the automated segmentation were the two most prevalent available. While both offer essentially the same type of global segmentation into grey and white matter, and CSF, they carry out this process in slightly different ways, which can then lead to differences in the output results. The FMRIB software library (FSL) FMRIB's automated segmentation tool (FAST) (Zhang *et al.*, 2001) is based on a model called the Hidden Markov Random Field (HMRF) model that uses the Expectation-Maximsation algorithm to optimise it (Zhang *et al.*, 2001). The HMRF model is a finite mixture model and is generally considered to be more robust than similar models as it takes spatial information into account with respect to the mutual information found in local neighbourhoods to then use this information to carry out the segmentation of tissue into different classes (Tsang *et al.*, 2008). In contrast the SPM12 segmentation algorithm is based on a unified model that carries out all three stages; the segmentation, correction of bias, and spatial normalisation, within the same model (Ashburner and Friston, 2005). Statistical parametric mapping 12 (SPM12) also uses the Expectation-Maximisation algorithm to optimise the parameters that correspond to models comprising a mixture of Gaussians that each represent one of the tissue classes (Tsang *et al.*, 2008). SPM12 then utilises tissue probability maps to transform the brain anatomy into MNI152 standard space (Tsang *et al.*, 2008).

Automated segmentation protocols

The FSL segmentation was carried out by using the following protocol on each .nii file:

1. Carry out brain extraction using the FSL brain extraction tool (BET) (Smith, 2002) with a fractional intensity setting of 0.5 that was derived from empirical experiments to assess the optimal value for this setting to ensure that all of the brain remained in the extracted file.
2. Carry out the segmentation using FSL FAST (Zhang *et al.*, 2001) with all settings left at default.
3. Volumes were then extracted using the fslstats tool.

The SPM12 segmentation was carried out by running the SPM graphical user interface (GUI) through Matlab. Using the fMRI option, which also includes the structural processing features, batch processing was carried out using ‘Batch’ and selecting the Segmentation.mat option. All of the files to be processed are then added to the ‘Volumes’ list. The rest of the parameters were all left on the default settings. The ‘get_totals.m’ Matlab script was then run on the output files c1, c2, and c3, which are grey matter, white matter, and CSF volumes respectively, for each of the scans to output the volumes.

The segmentation output images were all visually inspected to assess the segmentation patterns and differences between them.

4.3 Results

4.3.i Manual vs Automated Global Tissue Segmentation

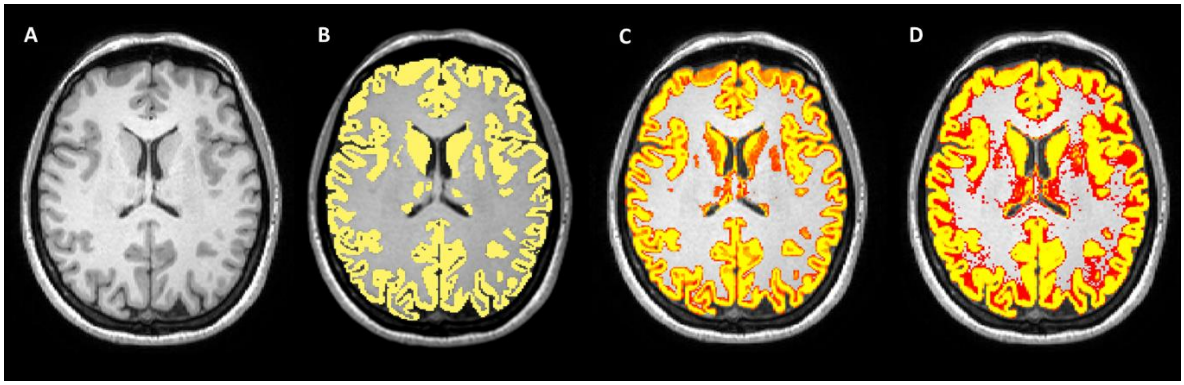

Figure 19. Single slice examples of GM segmentation output from manual (B), FSL 5.0 (C), and SPM12 (D) segmentation, with original T1 image also provided as a reference (A). The grey matter in the manual segmentation is shown in yellow. In the FSL and SPM images, the grey matter is shown in a red-yellow colour scheme in which the yellow areas represent high levels of confidence (0.95-1.0), and the red areas represent areas of lower confidence.

	FSL	SPM	Manual
HC01	673.624	796.131	658.472
HC02	597.761	666.015	584.369
HC03	598.417	675.354	604.856
HC04	652.495	755.671	665.342
HC05	660.995	769.5	650.142
HC06	643.927	715.521	639.934
Ca01	705.473	806.861	698.165
Ca02	602.954	697.926	608.364

Table 6. Grey matter volumes derived using each of FSL, SPM12, and manual segmentation. All values are given in cm^3.

	FSL vs SPM	FSL vs Manual	SPM vs Manual
Grey Matter	FSL < SPM p = 0.002	No significant difference p = 0.868	SPM > Manual p = 0.001

Table 7. Results of the 2-sample t-test to assess whether there are group differences between FSL, SPM12, and manual segmentation methods for grey matter.

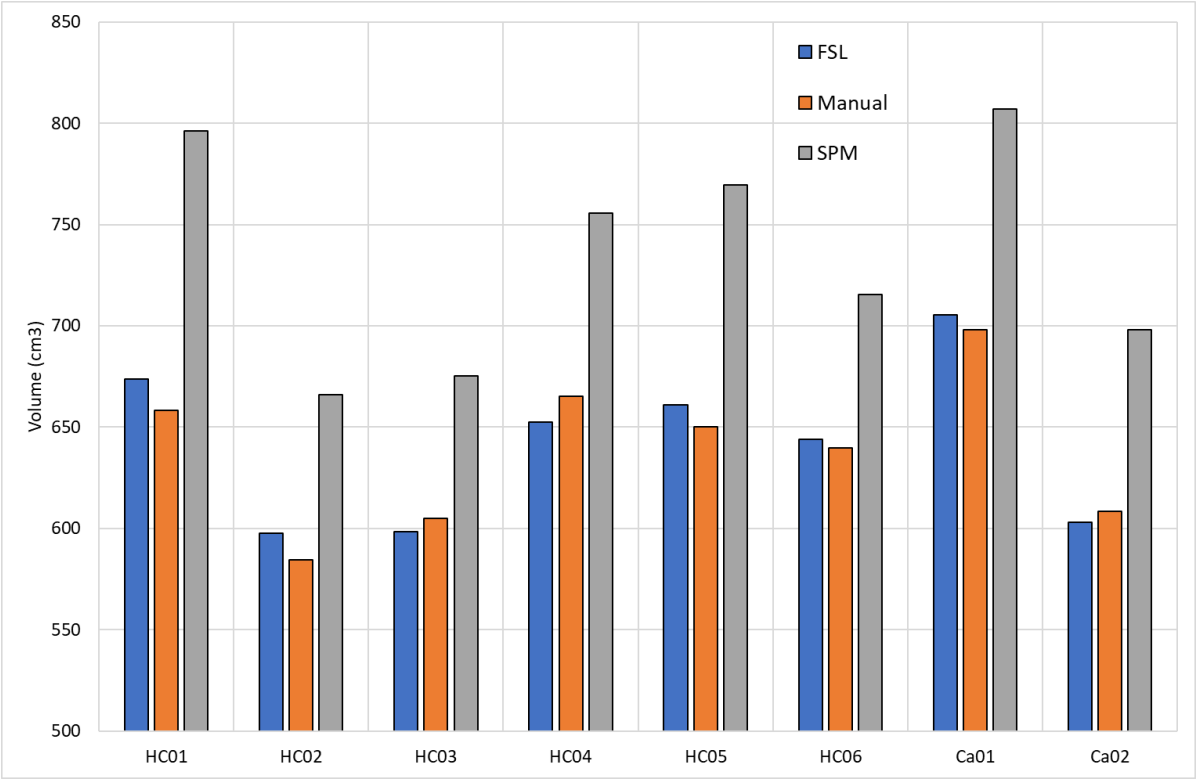

Figure 20. Output volumes of global segmentation of grey matter for FSL, manual, and SPM12 segmentation showing the similarity in volumes between the FSL and manual segmentation techniques.

The results shown in Figure 19, Figure 20, Table 6, and Table 7 show that there is a clear, and statistically significant, difference in the end results of the segmentation between FSL and SPM, and also between manual and SPM.

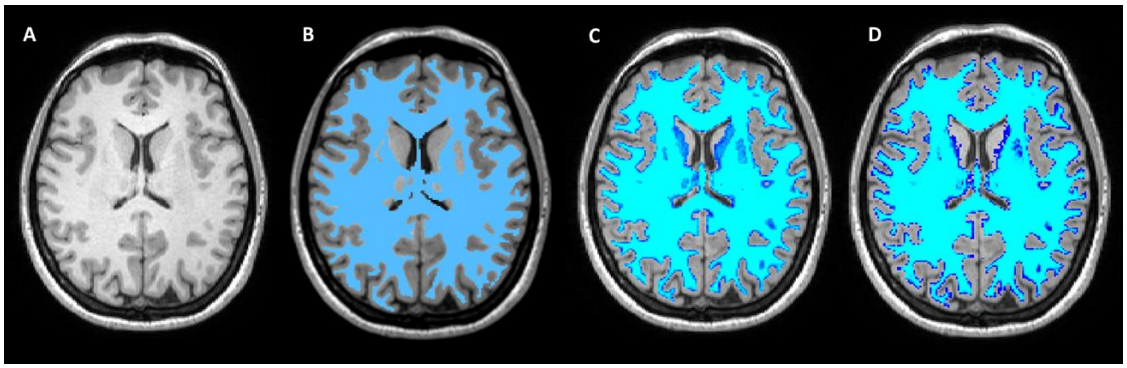

Figure 21. Single slice examples of WM segmentation output from manual (B), FSL 5.0 (C), and SPM12 (D) segmentation, with original T1 image (A) also provided as a reference. The dark blue regions in the FSL and SPM images represent regions of lower confidence in the classification of the white matter.

	FSL	SPM	Manual
HC01	619.901	592.95	632.158
HC02	549.954	480.88	555.694
HC03	549.756	495.821	561.74
HC04	694.186	546.148	678.144
HC05	621.479	534.799	631.251
HC06	607.149	494.571	615.316
Ca01	670.943	485.613	681.196
Ca02	556.571	425.193	568.615

Table 8. White matter volumes derived using each of FSL, SPM12, and manual segmentation. All values are given in cm^3.

	FSL vs SPM	FSL vs Manual	SPM vs Manual
White Matter	FSL < SPM p = 0.002	No significant difference p = 0.800	SPM > Manual p = 0.001

Table 9. Results of the 2-sample t-test to assess whether there are group differences between FSL, SPM12, and manual segmentation methods for white matter.

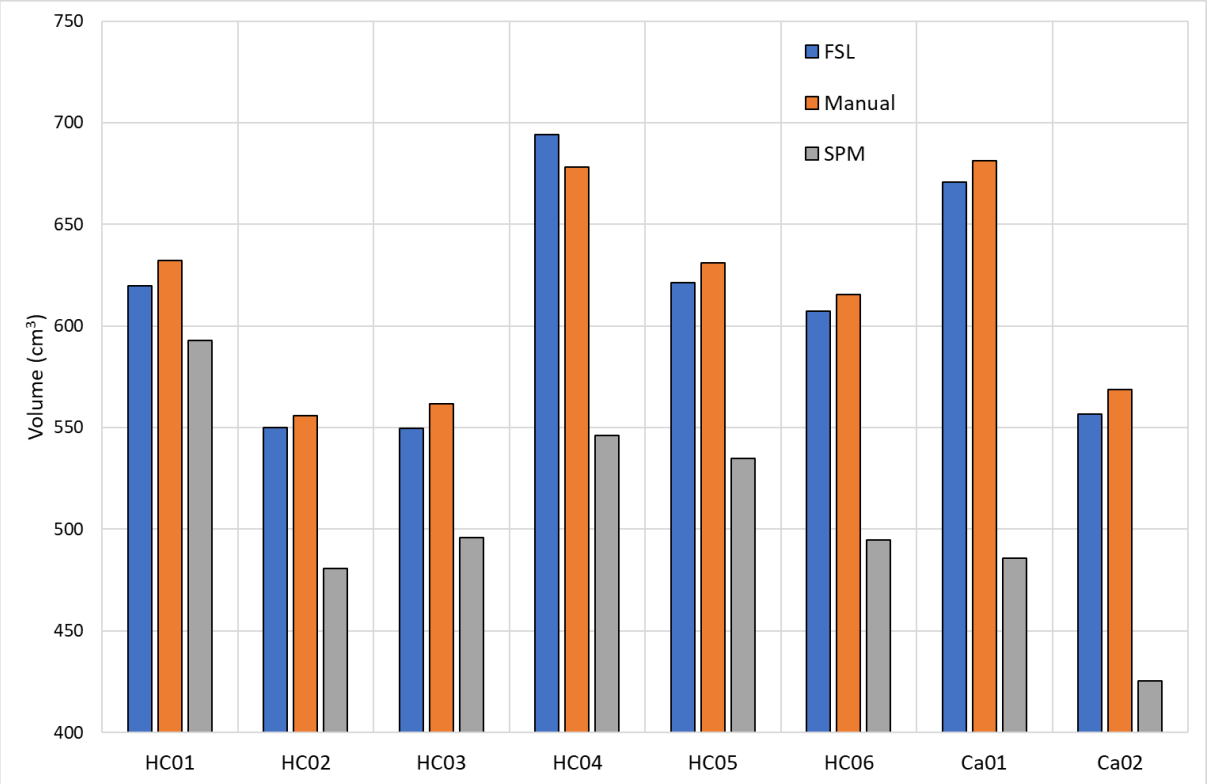

Figure 22. Output volumes of global segmentation of grey matter for FSL, manual, and SPM12 segmentation showing the similarity in volumes between the FSL and manual segmentation techniques.

Figure 21, Figure 22, Table 8, and Table 9 show a reversal of the findings in the grey matter results with both FSL and manual segmentation showing statistically significantly larger values than the SPM segmentation.

	FSL	SPM	Manual
HC01	1533.8	1704.67	1536.01
HC02	1373.16	1397.47	1371.05
HC03	1371.71	1405.75	1387.03
HC04	1660.81	1646.99	1639.1
HC05	1620.8	1746.07	1602.04
HC06	1504.05	1473.34	1501.63
Ca01	1669.36	1538.93	1668.96
Ca02	1419.52	1323.11	1428.61

Table 10. TICVs derived using each of FSL, SPM12, and manual segmentation. All values are given in cm^3.

	FSL vs SPM	FSL vs Manual	SPM vs Manual
TICV	No significant difference p = 0.885	No significant difference p = 0.969	No significant difference p = 0.855

Table 11.Results of the 2-sample t-test to assess whether there are group differences between FSL, SPM12, and manual segmentation methods for TICV.

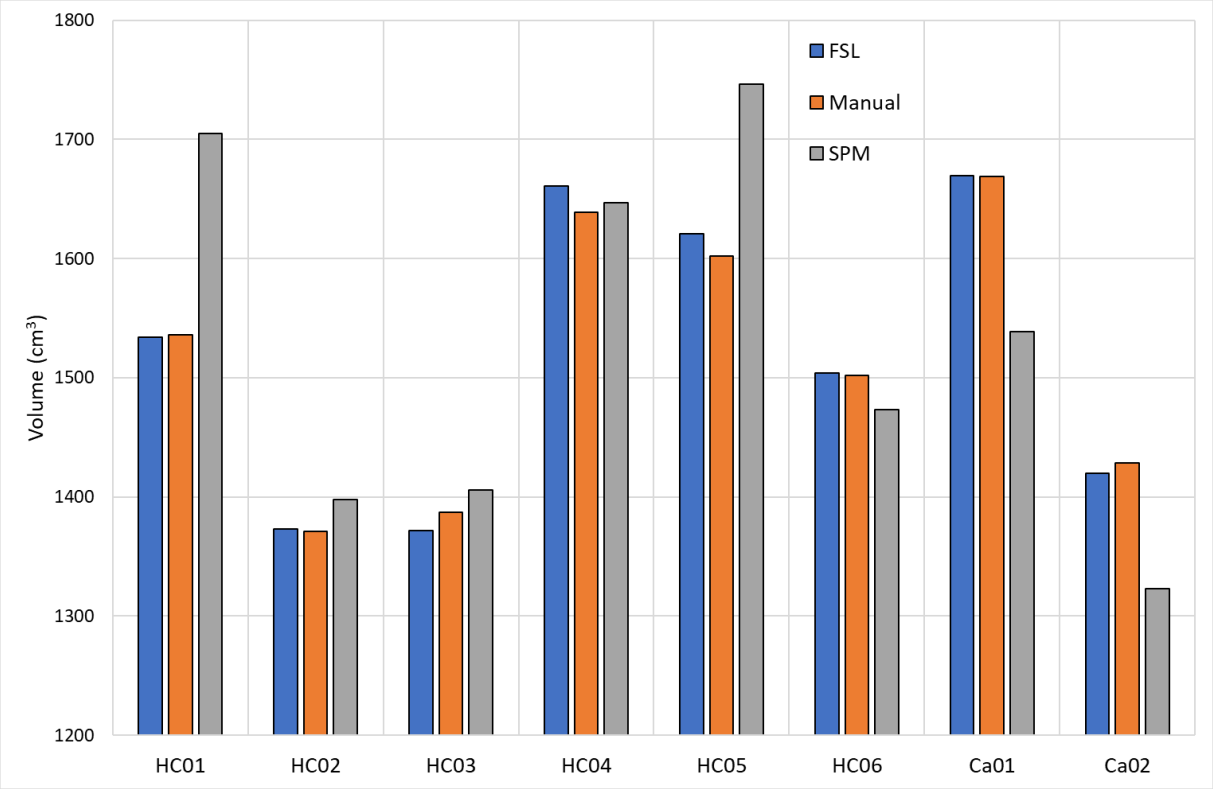

Figure 23. Output volumes of global segmentation leading to TICVs for FSL, manual, and SPM12.

Figure 23, Table 10, and Table 11 show that there are no statistically significant group differences between the different segmentation methods for the measurement of TICV, although Figure 23 does appear to indicate an overall better agreement between the FSL and manual segmentation methods.

4.4 Discussion/Conclusions

Due to the huge range of possible aims of automated segmentation it was not possible to find anything in the literature that specifically addressed the global volumetric accuracy of segmentation software, particularly in the presence of lesions, so, although time consuming, it was a matter of due diligence to be able to justify the

decisions made in this study with regards to the methods used to carry out volumetric analysis of the brain MRI scans of the participant cohort.

It is clear from Figure 20 and Figure 22 that the FSL 5.0 and manual segmentation results are very similar, with the SPM12 results apparently indicating a larger volume of grey matter, and a smaller volume of white matter. Inspecting the segmentation images in Figure 19 and Figure 21 indicates that both the manual segmentation, in which a voxel has to be 100% defined as a single tissue type, and FSL 5.0 segmentation define the grey/white matter boundary relatively tightly. This is in contrast to the SPM12 segmentation, which has a much larger gradient of tissue type probability at the location of any grey/white matter boundary.

It should be noted that this selection of software for automated segmentation is only valid for high-resolution (1mm^3 voxels or smaller) T_1 anatomical scans taken on either a 3 T Philips Achieva or a 3 T Siemens MRI scanner using the scanning parameters shown in Chapter 3. Lower resolution scans, or scans of different types, such as T_2 anatomical scans, would have to be assessed in a separate study. These scans were also all MPRAGE[7] scans. There have been anecdotal reports than some radiology departments are using SPACE[8] scans, which although are better for seeing lesions, do not provide as good a contrast between healthy tissue types (Okada *et al.*, 2011) and would also have to be assessed in a separate trial to ascertain whether they are suitable for this type of segmentation.

Therefore, the decision was made, on the basis of these results to utilise FSL 5.0 for all of the global volumetric analysis.

[7] MRPAGE: fast 3D gradient echo pulse sequence using a magnetisation preparation pulse.
[8] SPACE: fast 3D spin echo pulse sequence with reduced flip angles and partial Fourier imaging to decrease imaging time.

Chapter 5. Volumetric analysis of global volumes

5.1 Introduction

The literature review carried out in Chapter 2 discusses and summarises the state of current research into brain MRI analysis in mitochondrial disease. Only a single paper by Virtanen *et al.* (2011) provided any volumetric results, and even then the carrier and MELAS patient groups were combined so the results were dominated by the severe atrophy seen in patients with histories of stroke-like episodes and any, more subtle, changes in m.3243A>G mutation carriers would have been lost.

There are two papers in the literature that have carried out analysis of volumetric changes using VBM to highlight regions of significantly different volumes between controls, carriers, and patients with MELAS (Tsujikawa, 2016; Haast, 2018). It should be noted that hypotheses under test in these papers were both purely statistical in nature and further work would be required to establish the clinical significance, if any, of these differences.

To date, the published volumetric work in mitochondrial disease is somewhat thin on the ground, a mere three papers to date, and the findings from these do not agree on the details of significant differences between their groups. This is likely to be in part due to the different grouping methods used between the studies, and also the differences in symptom groupings found within the individuals in each study. Therefore using this information alone it is difficult to formulate a hypothesis. Adding in the qualitative reporting from the case and cohort studies in Chapter 2 does at least provide a good starting point for formulating regions of interest as stroke-like episodes, and their associated lesions are most commonly seen in the temporal and occipital lobes, thus indicating that there may be something about the structure, and also the function, of these regions that lead to a susceptibility to the occurrence of stroke-like episodes. Therefore, there are many questions to answer regarding the effect of the m.3243A>G point mutation on the volumetric properties of the brains of people with the m.3243A>G point mutation prior to the onset of stroke-like episodes, and in addition to this, which of those changes cause measurable clinical changes in the functioning of the brain and if any of those can be used as biomarkers for susceptibility to the future development of other neurological symptoms or the presentation of stroke-like episodes and the severe atrophy that is associated with these.

This work has therefore been planned in such a way as to allow results from existing studies to be assessed and compared to the outputs defined here, but also to carry out a broader assessment of the global properties of the head and brains of those carrying the m.3243A>G point mutation.

5.2 Aims

Due to the very small amount of quantitative volumetric baselining data available for anyone with the m.3243A>G point mutation, the aims for this initial piece of analysis were:

1. Carry out an analysis of total head size to ascertain whether the overall growth of people with the m.3243A>G point mutation is affected and where all carriers of the m.3243A>G point mutation lie within the normal distribution of head sizes of the healthy population.
    a. Justification for this comes from the anecdotal evidence gained from clinicians who regularly note that patients with MELAS seen in clinics are of short stature and generally have a very low body mass index (BMI).
2. Analyse the head size distribution to ascertain whether head size may be related to the eventual onset of stroke-like episodes.
3. Analyse grey and white matter volumes to ascertain what the differences are, if any, between controls, carriers, and patients with MELAS.
    a. It is hypothesised that in the MELAS patient group that atrophy will be the dominant measure and that all relative volumes will be significantly smaller than the control group.
4. Analyse cerebellar atrophy and compare to global atrophy to ascertain whether the trend in case reports for reporting visual cerebellar atrophy in the absence of cerebral atrophy is correct, or whether it is an artefact of the visual inspection process.
    a. Justification for this comes from continued reporting in the literature of standalone cerebellar atrophy with the absence of cerebral atrophy. There is also disagreement within the clinical community about the apparent predominance of cerebellar atrophy in addition to imaging factors that will affect smaller structures more and that are not taken into account in visual assessment of atrophy levels.

5.3 Methods and Materials

5.3.i Carriers and patients with MELAS

Seventeen participants from the MRC mitochondrial disease cohort were used for the TICV and total parenchymal volume (TPV) analysis. 10 of these participants were classed as carriers with no history of stroke-like episodes, while seven were classed as patients with MELAS and had a history of stroke-like episodes. Participant details can be found in Chapter 3.

5.3.ii MRI Scans

Cohort participant scans were taken on a 3 T Siemens MRI scanner. The scan parameters used were Gradient Echo, 3D sequence, TR = 50 ms, TE = 30 ms, FA = 15°, with 1 mm x 1 mm x 1 mm voxels.

5.3.iii Segmentation

Segmentation of global tissue volumes

Segmentation of the MRI scan images to produce the global tissue volumes was carried out using the FSL FAST (Zhang *et al.*, 2001) as justified by the work carried out in Chapter 4 regarding the accuracy of the volumetric outputs. A detailed protocol and relevant screenshots can be found in Appendix 1.

Skull stripping was carried out using the FSL BET (Smith, 2002). Fractional intensity threshold was set to 0.5, and ‘robust brain centre estimation’ was selected. The extracted brain files were each examined using FSLView to assess the accuracy of the brain extraction to ensure that all of the brain was present.

Segmentation of the extracted brains was then carried out using FSL FAST (Zhang *et al.*, 2001) with the outputs being partial volume maps for GM, WM, and CSF. The segmentation for each individual was then assessed using FSLView, loading up the extracted brain file and overlaying each of the segmented classifications on top to ensure that the segmentation was ok. The quantitative volumetric values were then extracted using the fslstats tool.

Patients with MELAS with obvious lesions were excluded from this analysis due to the inaccuracies introduced into the volumes by the misclassification of the lesioned areas.

This analysis used the raw values output from the FSL segmentation software that was validated for global tissue segmentation in Chapter 4. The definition of TICV using a slice from an MRI is shown in Figure 24, in which the TICV value is the volume encompassing all brain tissue and cerebral spinal fluid contained within the skull cavity with the ventral boundary being defined by the frontal and temporal lobes, the brain stem, and the cerebellum. The TICV includes the entire brain stem (Midbrain, Pons, and Medulla) and also the cerebellum. The reason for using this definition of the TICV is because that is how FSL segments the brain and it is also the definition used in Chapter 4 to validate the volumetric outputs from FSL. The image of the 3D model shows the relatively smooth appearance of the TICV, with no definition of sulci and gyri, or around the cerebellum.

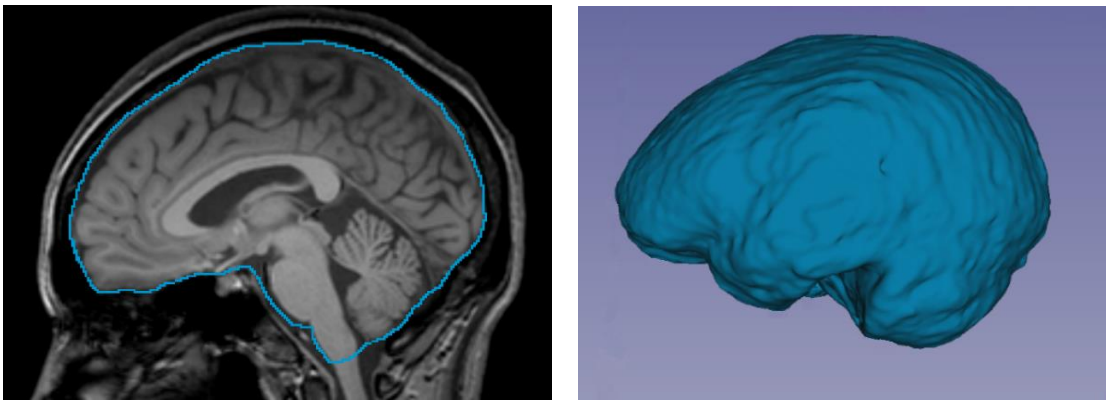

Figure 24. (A) 2D presentation of the definition of total intracranial volume, (B) 3D model of the total intracranial volume of the brain shown in the MRI in (A)

The definition of TPV using a slice from an MRI is shown in Figure 25, in which the TPV value is the volume encompassing all brain matter within the skull cavity, with the lower limits being bounded by the frontal and temporal lobes, the brain stem, and the cerebellum, and excluding all CSF. The image of the 3D model shows the clear definition of the sulci and gyri, but also shows the lack of definition of the finer details of the cerebellum, which reflects the $1mm^3$ voxels used in these scans being around the same order of magnitude as the cerebellar surface details, and so are not easily resolved.

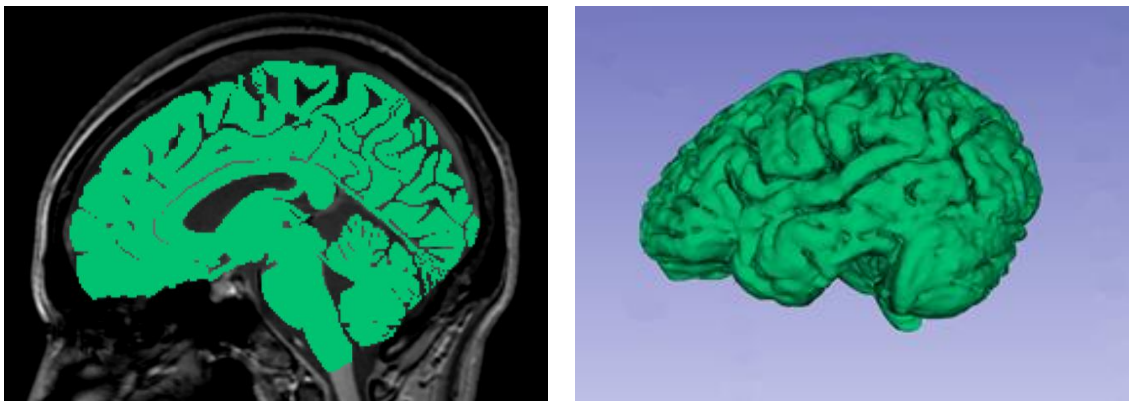

Figure 25. (A) 2D presentation of the definition of total parenchymal volume, (B) 3D model of the total parenchymal volume of the brain shown in the MRI in (A). Note that the definition of the cerebellum is relatively poor, this is due to the small size of the detailed structure leading to blurring due to the partial volume effect.

The TPV was defined as consisting of all of the brain tissue within the skull cavity from the brain stem upwards, including the cerebellum, and excluding all CSF.

The raw TPVs were divided by the TICVs for each individual to normalise the volumes to head size to remove any confounding effect of differing head sizes, which also removes the requirement to calculate separate means for males and females as any gender differences have already been taken into account.

Segmentation of cerebellum

The cerebellar volume for each of the controls, carriers, and patients with MELAS was measured using manual segmentation, with the segmentation being kindly carried out by Heather Thompson (BSc Biomedical Sciences, final year undergraduate), as a complete volume rather than attempting to segment it into grey and white matter. Heather carried out work to define the boundary of the cerebellum, and to ensure reproducibility the cut-off point was positioned at anterior edge of the meeting point of the pons and lingual of the superior cerebellar hemisphere and a straight line dropped down from this point using sagittal images as shown in Figure 26.

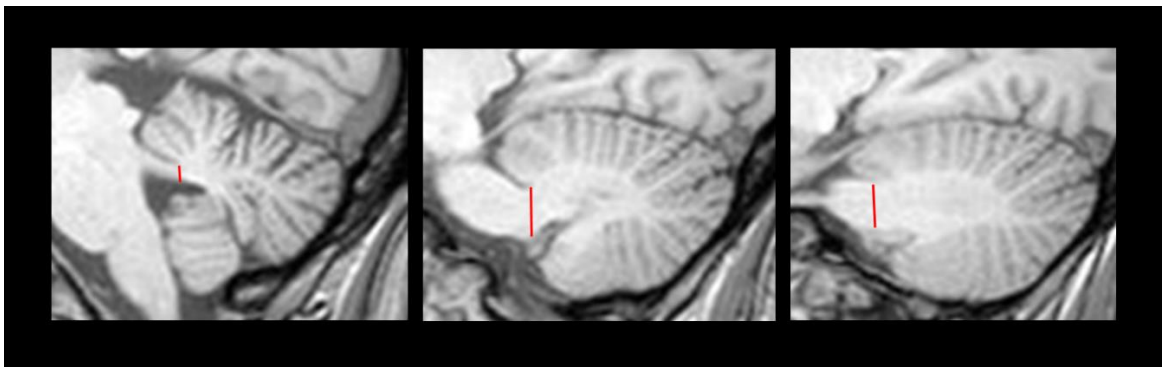

Figure 26. Images taken from ImageJ showing the cut-off position for the cerebellar measurements.

ImageJ software (Schneider *et al.*, 2012) was used to carry out the segmentation and volumetric measurements by initially reslicing the axial scan into the sagittal plane. The cerebellar volume for each individual was then measured by manually tracing around the edge of the cerebellum on each slice in which it was visible using the polygon feature to create a region of interest (ROI), which could then be summed to provide a volumetric output.

I analysed the volumes obtained by Heather using my methodology of utilising z scores, and so all analysis of the volumes was carried out by the author. The cerebellar volumes were normalised against TICV to remove any confounding effect of head size, corrected for age, and the z scores were then calculated.

Analysis

The raw volumetric data were input into Excel so that each control and MELAS patient had a gender, age, grey matter volume, white matter volume, CSF volume, TPV, and TICV listed for them.

The TPV was calculated by adding together the grey and white matter volumes, and the TICV was calculated by adding together the TPV and CSF volume.

For the TICV analysis, gender effects had to be taken into account as, on average, women have significantly smaller head sizes than men, so the groups were not only split into control, carrier and MELAS patient groups, but also subdivided into gender categories within these. The control group was used to calculate the male and female mean and standard deviation, which was then subsequently used in the calculation of both the individual, and group, z scores.

$$z\ score_{individual} = \frac{(x - \bar{x})}{SD}$$

Equation 7. The equation used to carry out the calculation of the z score for an individual, where, x = individual value, $\bar{x}$ = group mean of the control group, SD = standard deviation of the control group.

$$z\ score_{group} = \frac{(x - \bar{x})}{SD/\sqrt{n}}$$

Equation 8. The equation used to carry out the calculation of the z score for a group, where x = individual value, $\bar{x}$ = group mean of the control group, SD = standard deviation of the control group, n = number in test group.

The z scores for the carrier and MELAS patient individuals and groups were then plotted onto a graph using Excel. One of the advantages of this type of analysis, is that the control group are always represented on the graphical output as having a z score of 0, which then removes any requirement to plot any control data and provides an easy way to see exactly how far away, or how close, the carrier and MELAS patient data lies to the control group.

The rationale behind using z scores rather than any other statistical test, is because z scores provide an easy to visualise statistical output relating the cohort groups to the normal Gaussian population, defined by the control group. Population statistics allow for the easy identification of participants with abnormal characteristics, particularly when there is clustering of participant characteristics in a region of the distribution that may indicate clinical relevance to either the presence of the m.3243A>G point mutation or symptomatic disease progression.

The selection of the statistical hypothesis being three standard deviations was also chosen to take into account lifestyle factors that may also cause generalised brain shrinkage over time, such as drinking alcohol, smoking, and having diabetes. The literature shows that although these can cause relatively large amounts of brain shrinkage compared to healthy controls, even in severe cases of long-term alcoholics, smokers, and sufferers of diabetes, the mean TICVs only lie around one standard deviation away from the control mean and longitudinal data show that the

decrease in brain volume occurs over timescales of several decades, compared to the seven to ten years observed in patients with mitochondrial disease (Oscar-Berman and Marinkovic, 2003; Biessels and Reijmer, 2014; Duriez *et al.,* 2014).

5.4 Results

Total intracranial volume (TICV)

Using the definitions and measurements in Section 5.3.iii, the carrier and MELAS patient TICVs can be presented in the form of z scores as in Figure 27. The carrier group as a whole have TICVs that are well within the normal distribution of the control group, even if the group average does lie on the low side of that normal distribution, however there is one carrier with a TICV that is closer to those of the MELAS patient group. The MELAS group shows a very different trend, with all of the MELAS group having TICV z scores below -2, and half of that group having z scores below -4, which represents a vanishingly small percentage of the population considering that only 0.15% of people will have head sizes with z scores of less than -3 and standard z score tables only go as far as -3.4.

	Controls	Carriers	MELAS
	1514.010934	1373.161132	1168.823791
	1589.222312	1588.93062	1317.752912
	1772.567801	1571.175255	1325.690229
	1669.356447	1669.092139	1343.869776
	1693.052217	1437.952649	1323.261746
	1682.62982	1508.187093	1167.453067
	1486.548344	1533.802205	1167.340458
	1518.623386	1344.750416	1138.138908
	1657.084203	1427.858664	
	1580.490013	1311.229395	
	1744.412677		
	1460.726604		
	1457.860499		
	1487.796431		
	1335.606485		
	1443.618577		
	1381.586921		
	1402.136365		
	1570.835958		
	1420.285963		
	1379.88648		
	1419.518661		
	1445.221626		
	1400.627351		
Male Mean	1602.04502	1524.749815	1295.879691
Female Mean	1426.101893	1404.41017	1157.644144
Group Mean	1521.40442	1476.613957	1244.041361

Table 12. Absolute TICVs for control, carrier, and MELAS groups. Male TICVs are above the double line, female TICVs are below the double line for each of the groups.

	Controls vs Carriers	Controls vs MELAS	Carriers vs MELAS
Male	No significant difference p = 0.166	Controls > MELAS p < 0.0005	Carriers > MELAS p = 0.003
Female	No significant difference p = 0.618	Controls > MELAS p < 0.0005	Carriers > MELAS p = 0.009
Group	No significant difference p = 0.342	Controls > MELAS p < 0.0005	Carriers > MELAS p < 0.0005

Table 13. 2-sample t-test to ascertain whether the differences in overall head size (TICV) between groups are statistically significant.

Table 13 shows that although there is some difference between the carrier and control groups, this does not reach significance. It also shows that both the control TICVs and carrier TICVs are significantly larger than for the MELAS group.

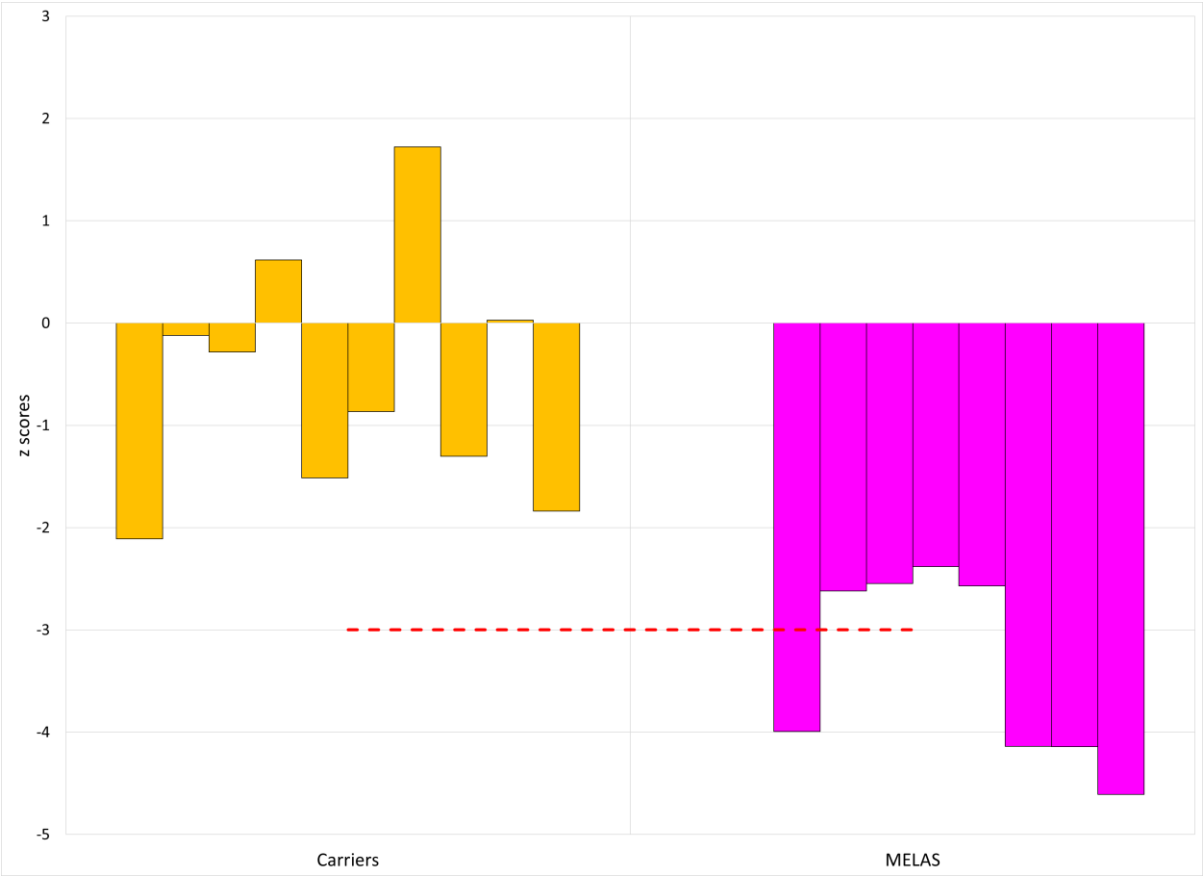

Figure 27. Breakdown showing individual z scores of the carrier and MELAS participants compared to the control group (group z score of 0) showing the individual differences in head size compared to a healthy population. The red dashed line denotes a z score of -3, below which only 0.15% of the control population will lie.

TICV and other physical attribute correlations with stroke-like episodes.

There are some who believe that, in addition to head size, height, BMI, heteroplasmy levels are also appropriate biomarkers for disease severity prediction, and in particular the onset of stroke-like episodes. Therefore, I have also carried out a correlational analysis to provide further information about the measures that are often referred to in patients with histories of stroke-like episodes.

	Correlation with SLE	p-value
TICV	-0.784	<0.001
Height	-0.629	0.009
BMI	-0.588	0.017
Head Circumference	-0.551	0.022
Blood Heteroplasmy	-0.015	0.957
Urine Heteroplasmy	0.160	0.57

Table 14. Spearman Rho correlational values for some of the commonly referred to measures in mitochondrial disease. Strong correlation can be considered to be present for Spearman Rho values of around ±0.8 and upwards.

Table 14 shows that the only measure approaching a strong correlational value is TICV. While height, head circumference, and BMI indicate some level of correlation, the values are not high enough to justify using these as surrogate measures of susceptibility to stroke-like episodes. The blood and urine heteroplasmy correlations are so low as to be meaningless in the context of predicting susceptibility to stroke-like episodes within this cohort.

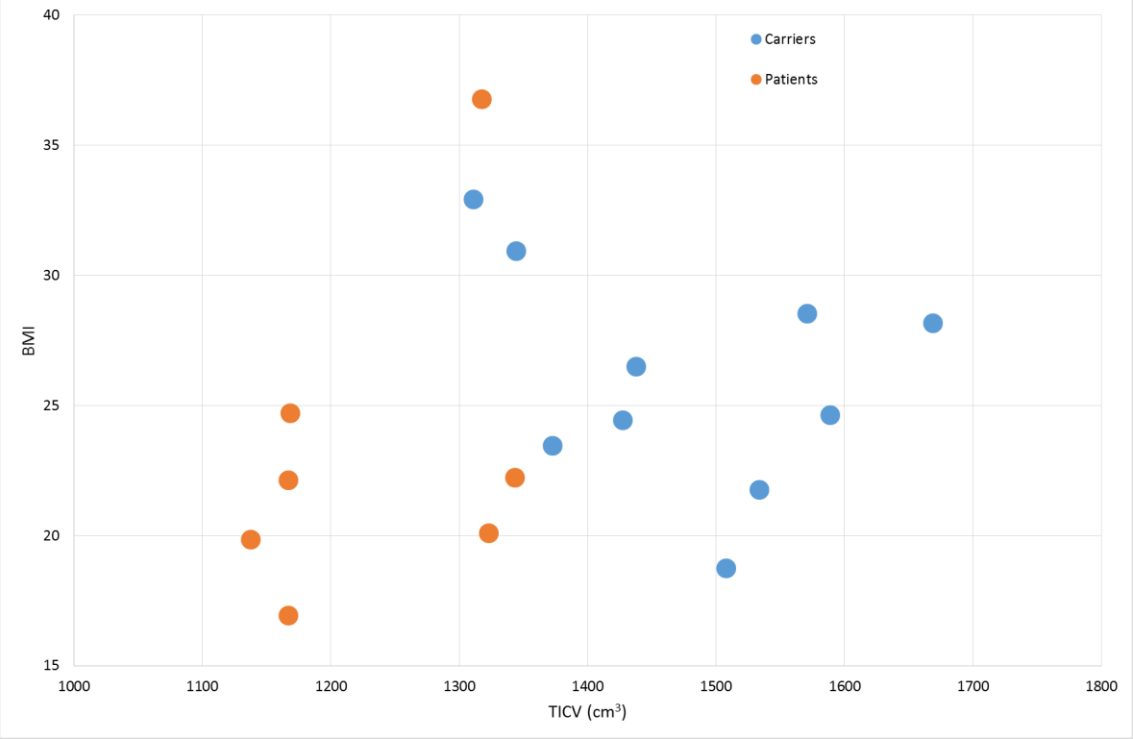

Figure 28. Plot of BMI against TICV, showing graphically the overall lack of correlation between BMI and TICV, and that 'outliers' with high BMIs are present in both the carrier and MELAS patient groups.

Total parenchymal volume (TPV)

This analysis used the raw values output from the segmentation software that was validated for global tissue segmentation in Chapter 4 and the definition of TPV as defined in Section 5.3.iii.

Patient 3 was removed from this analysis due to the very large regions of lesioned brain tissue, which was shown to be misclassified by the FSL segmentation software. Figure 29 shows a manually segmented 3D model of the left hemisphere of Patient 3 and has had the temporal lobe lesion removed for demonstrative purposes. The model also serves to show the physical, observable changes due to the severe, and rapid, atrophy experienced by patients with MELAS, which generally begins around the time of the first stroke-like episode, but currently the exact timing and relationship between the two are unclear.

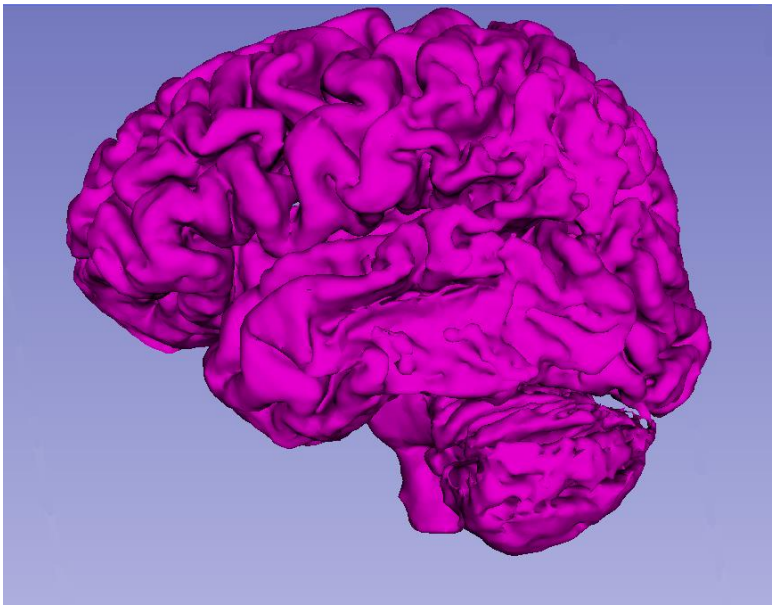

Figure 29. 3D model of the TPV of a MELAS patient brain that has undergone significant atrophy throughout the brain. The differences between this and the healthy brain in Figure 1Figure 25 (B).

The rest of the individual TPVs were then corrected for age and the z scores calculated using the mean and standard deviation calculated from the control data using Equation 7 and Equation 8.

	Controls	Carriers	MELAS
	0.775968636	0.797584588	0.742669688
	0.75022562	0.779145269	0.690250799
	0.773852936	0.786974575	0.677451625
	0.76803736	0.778201538	0.736133233
	0.774278709	0.727115041	0.658765467
	0.74843789	0.801783727	0.699083914
	0.780928097	0.765780975	0.725224586
	0.801055467	0.751419244	0.708454824
	0.799796234	0.779411618	
	0.732535587	0.723978481	
	0.782019304		
	0.801065187		
	0.793804658		
	0.782102403		
	0.776312995		
	0.803502072		
	0.795039189		
	0.792329142		
	0.738292617		
	0.784403918		
	0.767105875		
	0.785211712		
	0.793455118		
	0.749259618		
Mean	0.777042514	0.769139506	0.704754267

Table 15. TPVs normalised to TICV for the control, carrier and MELAS groups

Controls vs Carriers	Controls vs MELAS	Carriers vs MELAS
No significant difference p = 0.359	Controls > MELAS p < 0.0005	Carriers > MELAS p = 0.003

Table 16. 2-sample t-test to ascertain whether the differences in normalised TPV between groups are statistically significant.

Table 16 shows that even after head size is corrected for by normalising to TICV, that there is no significant difference between TPVs of controls and carriers. Both the control and carrier groups show significantly larger TPVs than the MELAS group, indicating that the MELAS group, as a whole, shows atrophy compared to a population with no history of stroke-like episodes.

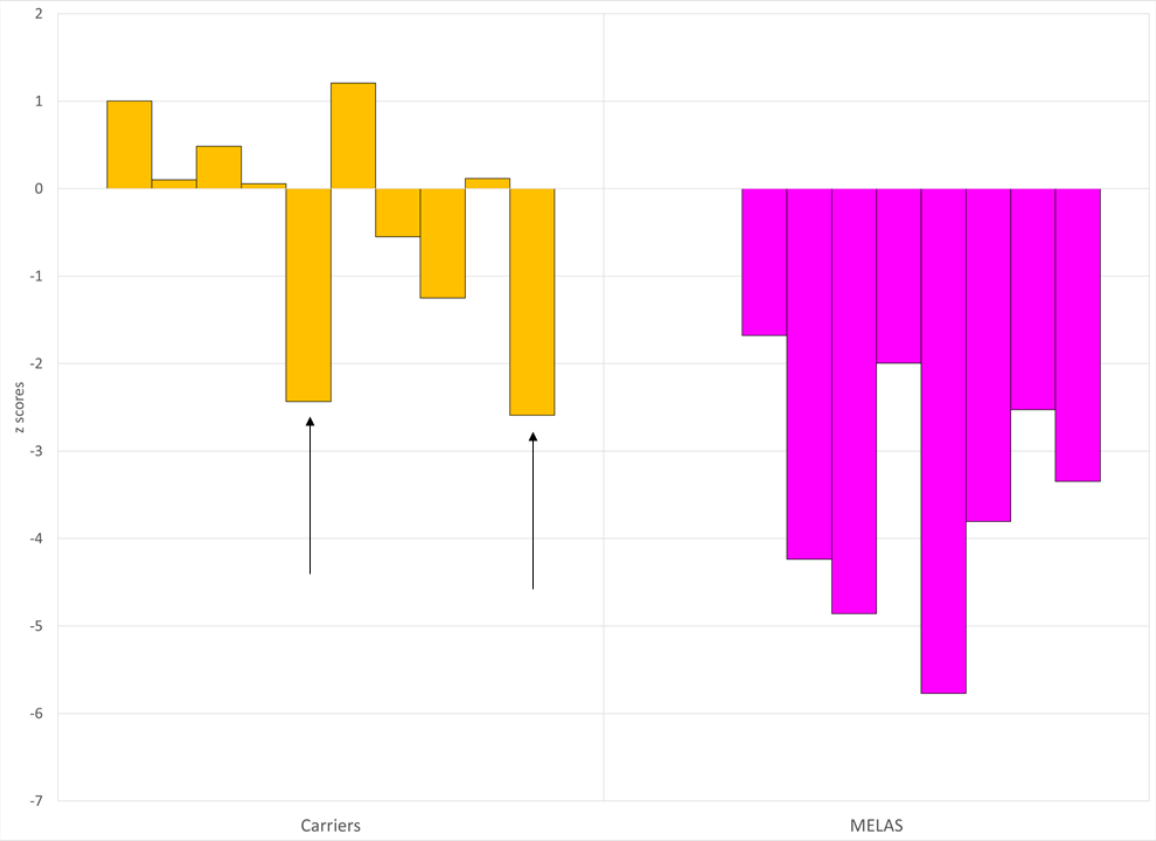

Figure 30. Plot of age and gender corrected z scores comparing the relative TPV between the carrier and MELAS groups. The two carriers with relative TPVs in the smallest 2.5% of the population are highlighted.

The results show a clear difference between the mutation carrier and MELAS patient groups, with the MELAS patient group having TPVs with a z score of -3 or lower,

which is indicative of the fact that all of these patients have had stroke-like episodes and have large amounts of atrophy. The carrier group shows that most of the group have relative TPVs that are well within the limits of the healthy control group, however there are two carriers that show relative TPVs that are much smaller than would be expected in healthy controls. In these cases only a longitudinal study would provide further information about these patients with regards to whether they either just have small brains for their head size that are stable, or normal sized brains for their head size that are undergoing atrophy.

Longitudinal changes in TPV

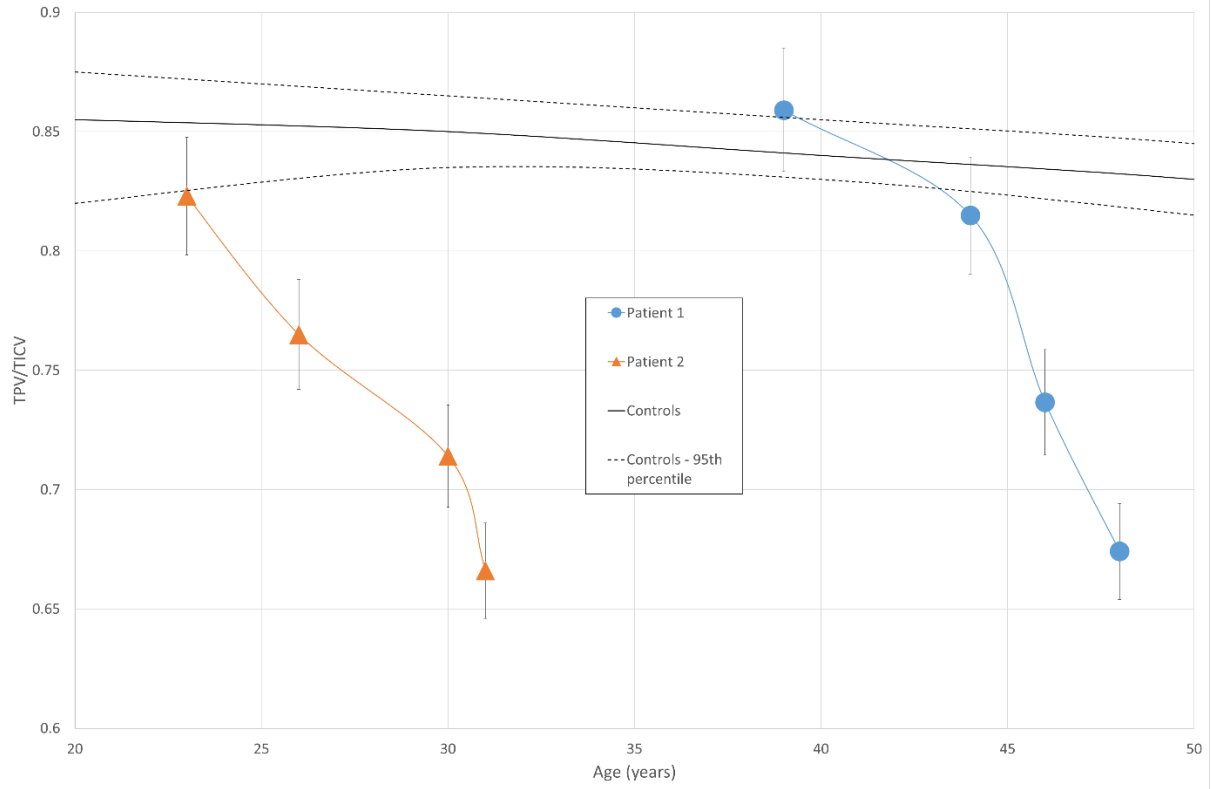

Figure 31. Graph showing two examples of patients with MELAS showing a rapid longitudinal change of brain volume over time with the healthy population mean and 95th percentile limits derived from the meta-analysis paper: M. Vågberg et al., PLOS One, 17 Jan 2017: 5878 (3102 Female) healthy individuals.

The characteristics of Figure 31 show that atrophy can be very rapid in patients with MELAS, although from this sample size of only two patients it is impossible to ascertain whether this is the most common pattern, or if there are other patterns of atrophy progression. The atrophy measures shown in Figure 30 could potentially be

at any position along this longitudinal atrophy path, including a stable position without rapid atrophy.

Grey matter (GM) and white matter (WM)

The MELAS group had to be modified for this section of analysis as three of the patients with MELAS had lesions that misclassified the grey and white matter in around the regions of the lesions, which led to misleading value for the segmented volumes of grey and white matter. The three patients with MELAS with lesions visible on their images were therefore removed from this section of the analysis.

The raw volumes were normalised against TICV to remove any confounding effect of head size and were also corrected for age before calculating the z scores.

	Controls	Carriers	MELAS
	0.42195468	0.442474915	0.391817005
	0.387825907	0.3802001	0.366170007
	0.424226751	0.435971207	0.415581588
	0.4347478	0.437559717	0.382222188
	0.415630963	0.363118959	0.404265241
	0.404249629	0.43630996	
	0.43192424	0.43556832	
	0.454810257	0.415325497	
	0.447549115	0.39920786	
	0.413525344	0.392298146	
	0.431956567		
	0.448315431		
	0.456997583		
	0.460172684		
	0.432329268		
	0.437691472		
	0.449317966		
	0.443675978		
	0.418517036		
	0.446051198		
	0.446054078		
	0.466760841		
	0.437411079		
	0.430014395		
Mean	0.435071261	0.413803468	0.392011206

Table 17. Grey matter volumes normalised to TICV for each of the control, carrier, and MELAS groups.

Controls vs Carriers	Controls vs MELAS	Carriers vs MELAS
Controls > Carriers p = 0.014	Controls > MELAS p < 0.0005	No significant difference p = 0.148

Table 18. Results from a 2-sample t-test showing significance, or otherwise, of the differences between the groups.

Table 18 shows, perhaps unexpectedly considering the results in Table 16, which both the carrier and MELAS groups show significantly less grey matter relative to head size compared to the control group. This is despite the carrier group showing no significant difference to controls in the overall amount of brain tissue within the skull cavity.

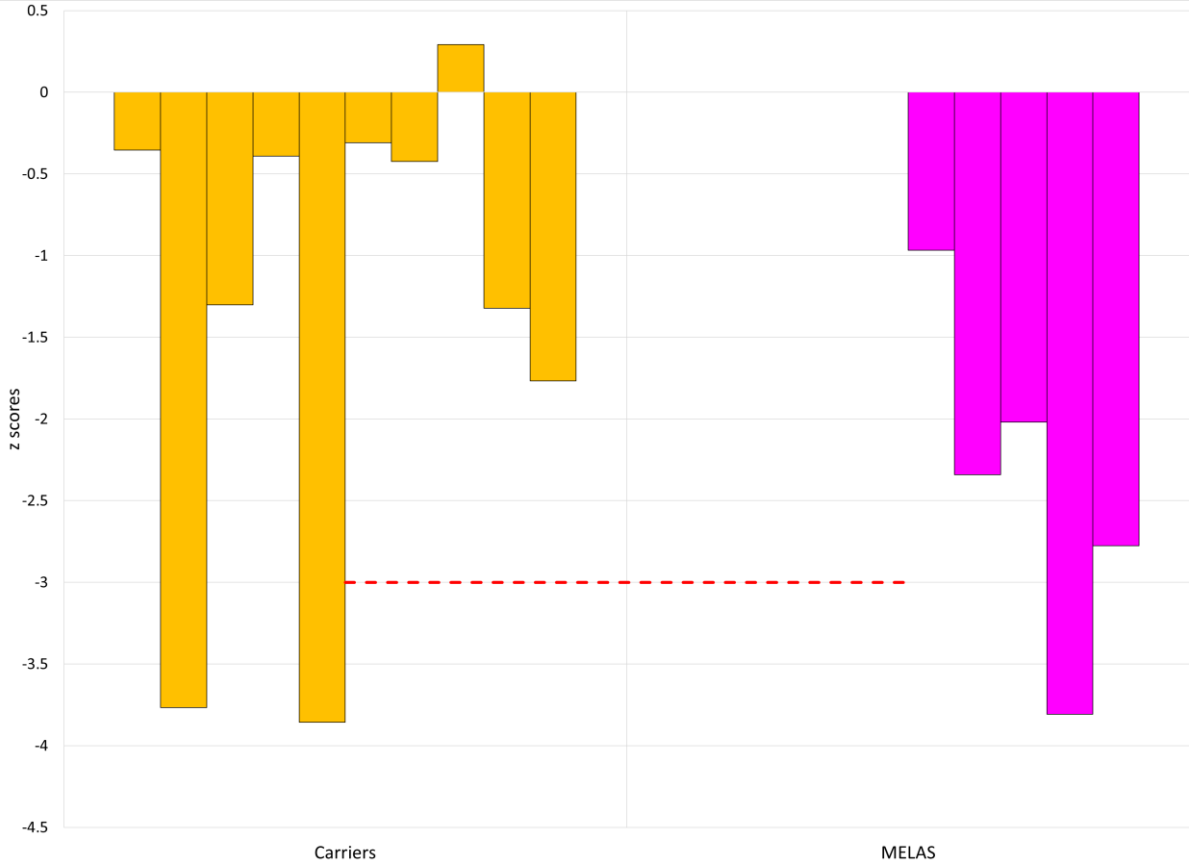

Figure 32. Plot of z scores of GM volumes normalised to TICV for the carrier and MELAS patient groups.

Figure 32 shows a large variation in the amount of grey matter present in each brain in the carrier group, and a generally small amount of grey matter present in MELAS patient brains compared to the control group.

	Controls	Carriers	MELAS
	0.333405122	0.339314938	0.284003926
	0.339113598	0.3778952	0.297147849
	0.329144104	0.334995747	0.301787721
	0.313542654	0.324947837	0.303425986
	0.340199729	0.352289719	0.291019837
	0.319953087	0.348266113	
	0.326580456	0.315727327	
	0.325061821	0.320124001	
	0.329313731	0.362301221	
	0.301850702	0.318553316	
	0.330937912		
	0.331144062		
	0.313558588		
	0.302720875		
	0.321569054		
	0.345967387		
	0.321705637		
	0.329736769		
	0.294846718		
	0.315678837		
	0.299810072		
	0.298626897		
	0.340488767		
	0.301311408		
Mean	0.321094499	0.339441542	0.295477064

Table 19.White matter volumes normalised to TICV for each of the control, carrier, and MELAS groups.

Controls vs Carriers	Controls vs MELAS	Carriers vs MELAS
Controls < Carriers p = 0.007	Controls > MELAS p = 0.001	Carriers > MELAS p = 0.001

Table 20. Results from a 2-sample t-test showing significance, or otherwise, of the differences between the groups.

Table 20 shows that the carrier group has a greater amount of white matter within their overall brain volume than the control, thus indicating that there are significant differences in the structure and make-up of the brains of those carrying the m.3243A>G point mutation compared to those who do not.

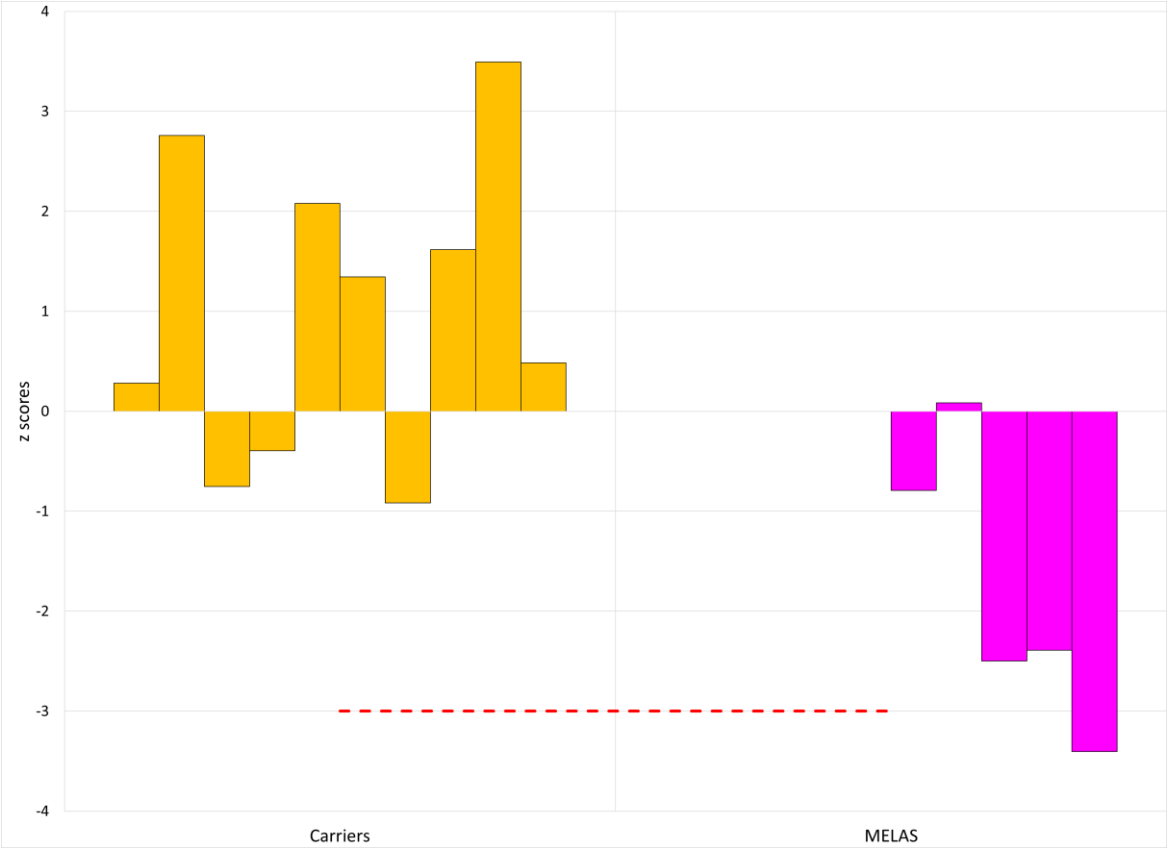

Figure 33. Plot of z scores of relative WM volumes for the carrier and MELAS patient groups.

Combining Figure 32 and Figure 33 it is clear to see that despite the apparently normal TPVs of the carrier group seen in Figure 30, there are differences in the relative grey and white matter volumes of some of the carrier group compared to the control group, which consist of reduced grey matter volumes and increased white matter volumes that are then combined to show TPVs within the healthy control group range. In contrast, the MELAS patient group show the expected characteristics of having reduced volumes overall compared to the control group.

Grey matter to white matter ratio (GM : WM)

To further demonstrate the differences between the control and carrier group the grey to white matter ratio was also looked at. The MELAS patient group was removed from this analysis due to atrophy being clearly dominant in the grey and white matter analysis.

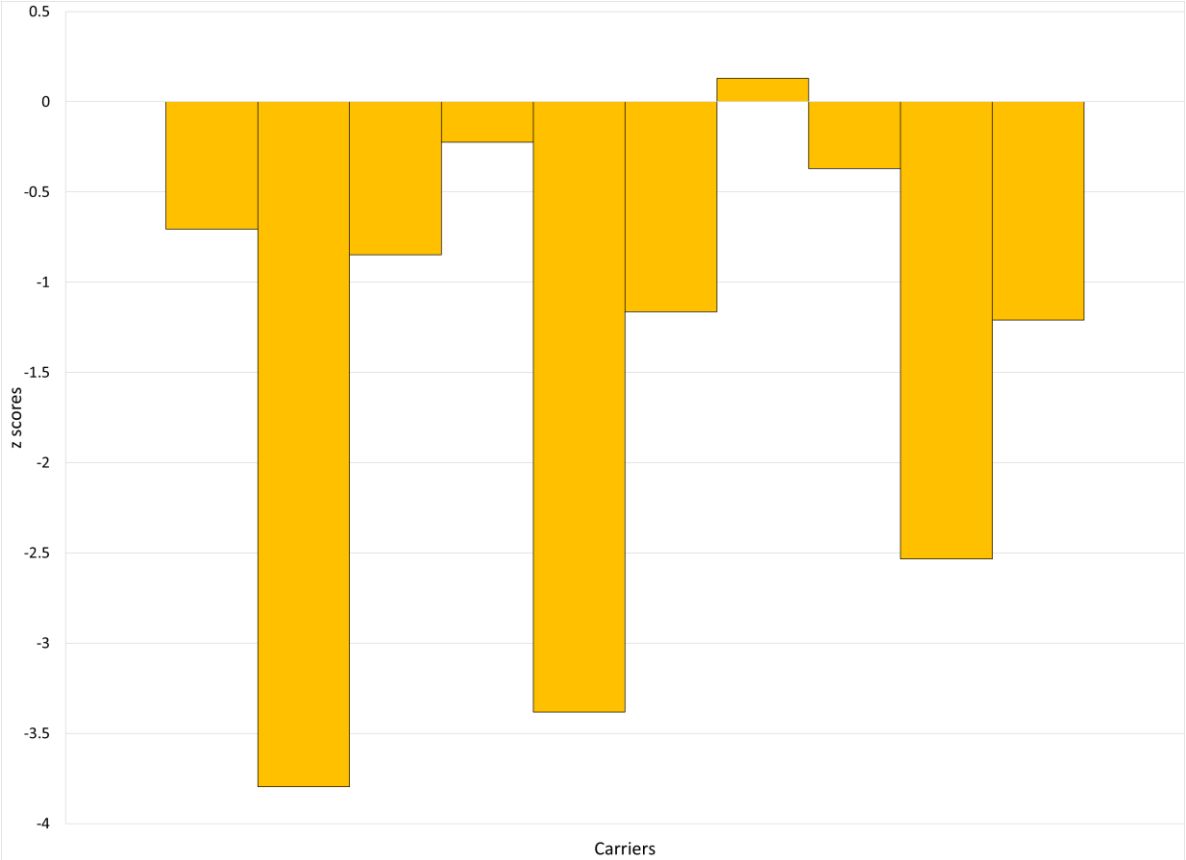

Figure 34. Graph of carrier GM:WM z scores showing that some carriers have a normal ratio, while others show large reductions in GM volumes compared to the control group, which appear to dominate the statistical analysis carried out. In a group-wise analysis, the control group have a significantly larger grey to white matter ratio (p = 0.003).

Figure 34 highlights that within the carrier group there are significant differences between individuals, highlighting the unpredictable and heterogenous nature of mitochondrial disease.

Cerebellum

The cerebellum has often been quoted as showing atrophy in isolation to the rest of the brain (Sue *et al.*, 1998; Majamaa-Voltti *et al.*, 2006; Fromont *et al.*, 2009), with

the results presented here looking at whether these are true observations, or if it is at least partly an observational illusion caused by the size of the structures being imaged.

	Control	Carrier	MELAS
	0.078941965	0.07659084	0.063425455
	0.087887881	0.102796734	0.073324641
	0.076128189	0.086966868	0.096025239
	0.077978649	0.090514664	0.062220314
	0.072934541	0.063494541	0.061169576
	0.081545279	0.091640262	0.076044036
	0.079537297	0.072309678	0.068731997
	0.079480572	0.081768027	
	0.078440863	0.072989107	
	0.0803817	0.070246988	
	0.079153403		
	0.079891355		
	0.080784003		
	0.083431218		
	0.076862843		
	0.073471243		
	0.076231985		
Mean	0.079004882	0.080931771	0.071563037

Table 21. Cerebellar volumes normalised to TICV for each of the control, carrier, and MELAS groups.

Controls vs Carriers	Controls vs MELAS	Carriers vs MELAS
No significant difference p = 0.538	Controls > MELAS p = 0.028	No significant difference p = 0.136

Table 22. Results from a 2-sample t-test showing significance, or otherwise, of the differences between the groups.

Table 22, combined with observations from Figure 35, again shows the large individual differences between carriers of the m.3243A>G point mutation and

indicates that some carriers, in addition to a reduced grey matter volume, also have either a smaller cerebellum, or one that has undergone some atrophy.

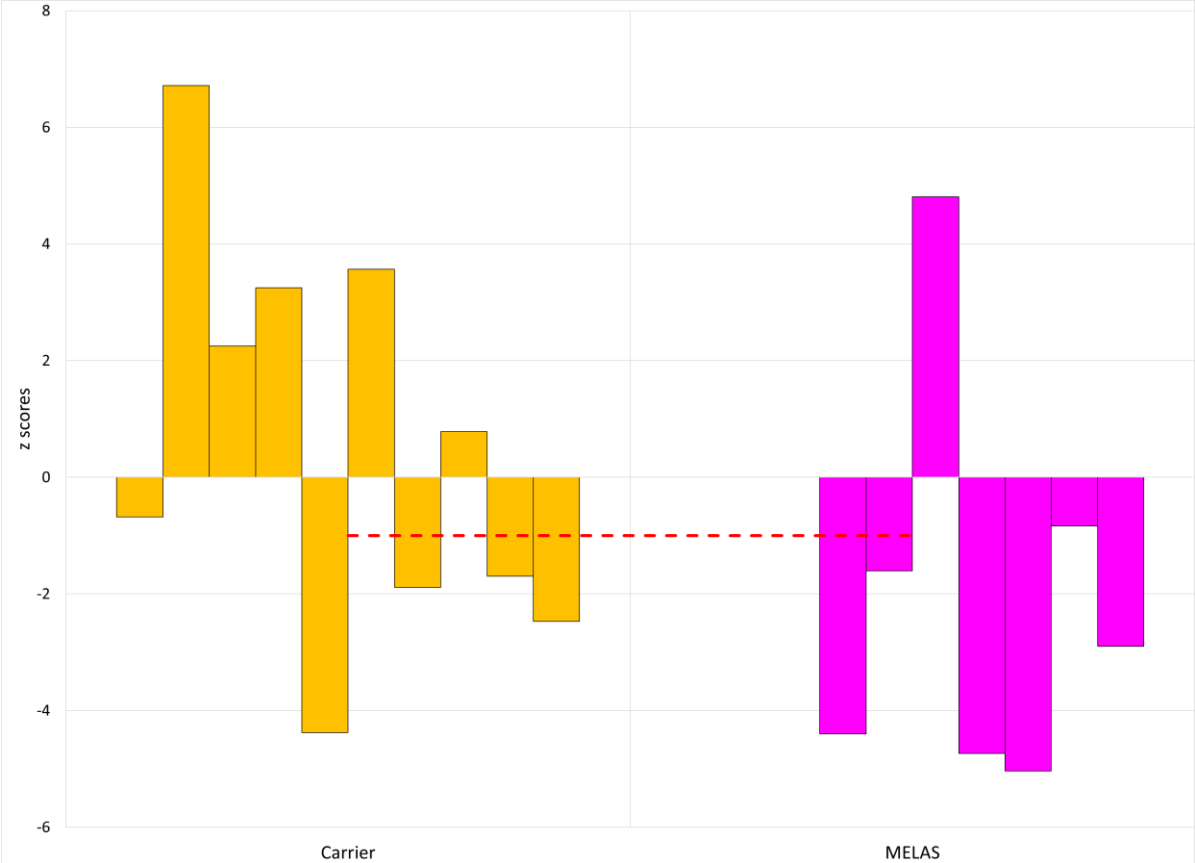

Figure 35. z scores of cerebellar volumes corrected for age, gender, and head size.

Comparing Figure 35 to Figure 32 and Figure 33 shows that in this group of patients with MELAS and carriers that cerebellar atrophy does not occur in isolation and in most cases reflects the atrophy state of the rest of the brain.

5.5 Discussion

The heterogeneous nature of mitochondrial disease makes it very difficult to predict disease progression for any individual patient. Despite a large amount of anecdotal clinical evidence, I identified that, at the time of writing, the head sizes of patients with MELAS has not yet been quantitatively investigated, and theorised that the overall growth of carriers and patients with MELAS may provide some sort of insight into their overall prognosis. Examining Figure 27 clearly shows that the MELAS patient group, who have suffered stroke-like episodes, all have head sizes more than two standard deviations away from the control group mean. This means that these patients with MELAS have head sizes that sit in the bottom 2.5% of the population. With these patient with MELAS head sizes being very small, this implies a

developmental factor associated with the m.3243A>G point mutation, however, as the carrier group in general have head sizes that sit well within the control group normal range, this indicates that there is either a threshold, or an additional mechanism that is exceeded or present in carriers of the m.3243A>G point mutation who go on to develop stroke-like episodes.

Looking back at the correlation data in Section 5.3.iv, it can clearly be seen in

Table 14 that TICV and BMI are not equivalent as measures of possible susceptibility to stroke-like episodes as there is a much stronger correlation between TICV and stroke-like episodes than between BMI and stroke-like episodes.

While it has been shown that blood, urine, and muscle heteroplasmy levels are correlated (Grady *et al.* 2018), what has not yet been established is whether these are either correlated, or representative, of heteroplasmy levels within the brain. The blood-brain barrier could provide an effective isolation mechanism to prevent the heteroplasmy levels in the blood from taking on a correlational component from the brain. It could easily be hypothesised that heteroplasmy levels within the brain could provide significant insights into both the current status, and the future prognosis, of the brains of those carrying the m.3243A>G point mutation. Localised, and unilateral, thinning of the cortical thickness, and in particular the thinning of the temporal pole, could point to significant differences in heteroplasmy levels between hemispheres of a single brain, and possibly even between regions, however the observed progression of lesions across boundaries implies a mechanism to facilitate this, which may well be associated with the local heteroplasmy characteristics.

While TICV does not provide any information about the mechanisms in play that define who is susceptible to stroke-like episodes, it does provide a simple measure, using the MRI method described here that could effectively highlight those people carrying the m.3243A>G point mutation who are more likely to develop stroke-like episodes at some point, which would allow them to be more closely monitored and potentially benefit from more timely interventions due to this. Substituting head circumference for TICV has been suggested as an alternative method, however a basic literature search has revealed that there are no equivalent head circumference percentile charts for adults, and the Tanner growth charts are not suitable (Busby *et al*, 1992). One paper attempts to derive percentiles, but uses a Turkish population, which from the data presented does not appear to be suitable for a UK population

(Örmeci *et al*, 1997). Papers using either UK, or comparable, populations, show correlation values of 0.28 to 0.39 for males and 0.53 for females (Bale *et al*, 1991; Nguyen *et al*, 2012), and so height and head circumference do not appear to be strongly correlated and therefore the current approach of combining head circumference with height to generate percentiles within population norms is not suitable to provide a substitute for TICV. Head circumferences for each of the m.3243A>G population within this study were also assessed for correlation with stroke-like episodes, and it came out at a similar correlation to BMI, see Table 14 for details, thus showing there is some level of correlation, but not one that is strong enough to use a predictor.

The abnormally small TICVs seen in the MELAS patient group also indicate that the effects of having the m.3243A>G point mutation is not just about the development of stroke-like episodes or brain shrinkage due to atrophy, and highlights that there are developmental factors in play from birth that appear to influence whether someone with the mutation is going to be susceptible to stroke-like episodes or not. To fully understand the effects of having the m.3243A>G point mutation it is going to take a multi-disciplinary approach to understand exactly how the point mutation affects someone right from the OXPHOS chain, through to global effects throughout the body and the brain.

Within the systematic review in Chapter 2, I highlighted papers that carried out and reported on visual measures of atrophy within their patient populations (Iizuka *et al.*, 2002; Majaama-Volti, 2006; Sue, 1998; Tschampa *et al.*, 2013; Tsujikawa *et al.*, 2016) and also that there currently does not exist any robust quantitative measure of atrophy to replace this. I have used the fact that once someone has finished growing, their head, and therefore also their TICV, does not change during their adult life to provide a stable volumetric reference against which atrophy may be effectively measured. In contrast to the complex analytical methods to assess atrophy put forward in the MIRIAD atrophy challenge (Cash *et al.*, 2015), and also to the somewhat variable performance of completely automated measure of longitudinal brain volume changes (Durand-Dubief *et al.*, 2012), I have defined a simple measure of total brain atrophy that is calculated by using global segmentation of brain tissue to provide a volumetric measure of brain tissue, that can then be normalised to the TICV to give the proportion of the TICV filled with brain tissue. In this case I used all of the brain tissue including the brain stem and the cerebellum due to the use of FSL

and the inclusion of these structures in the segmentation. It would not be a difficult task to define atrophy for different regions of the brain as desired either using manual segmentation or other segmentation software to divide the brain tissue up into a number of regions, which I go on to do in Chapter 6. Obtaining an accurate measure of atrophy in those with the m.3243A>G point mutation may provide an early warning that significant changes are occurring that are not immediately obvious through qualitative visual inspection. There are a number of reasons for this, with the main reason being that the brain can lose a significant amount of volume, up to around 10% if loss is spread globally, before the atrophy would be visually classed as being of note. The longitudinal data presented in Figure 31 provides evidence that it could be the first few percent of brain volume loss that could be the most important in terms of being able to provide earlier intervention and also how quickly brain volume is lost once the rapid atrophy process has begun.

The percentage of brain volume lost in these patients with MELAS is an important value as it takes the changes well outside volumetric changes that are seen due to dehydration and weight loss. A study into a healthy group of runners before, during, and after a 9 week, 4487 km ultra-marathon, found that even after running in these extreme conditions for several weeks, the athletes only showed a maximum of a 6% brain volume loss, which was quickly restored are hydration levels and weight were regained after the race (Freund *et al.*, 2014). The clinical relevance of the volume changes seen in patients with MELAS is that there are processes occurring that are outside of normal changes caused by environmental factors, and therefore are likely to be permanent. However, the major limitation of this work is that it is cross-sectional in nature and so the longitudinal element of the analysis is not possible, which would provide individualised analysis of brain volume changes over time

There do exist possible automated evaluations of atrophy, such as the structural brain change analysis tool (SIENA) in FSL (Smith *et al.*, 2002), however due to the lack of high resolution 3D anatomical scans for the carrier and MELAS patient groups it was not possible to investigate the accuracy, reliability, or usability of these, however as they use previous scans of each individual as the baseline it may be possible to use these to not only provide a quantitative measure of volumetric loss, but also to pinpoint specific regions that have atrophied more, or less, than the rest. I have noted that many automated quantitative methods utilise statistical hypotheses,

and so any future work to look at these must make sure that any statistically significant results can be clearly linked to clinically relevant changes.

The grey matter, white matter, and grey to white matter ratio results further demonstrate the high level of variability between individuals carrying the m.3243A>G point mutation in the carrier group, while the MELAS patient group clearly show the effects of atrophy with both grey and white matter volumes being reduced compared to the control group. The only previous quantitative volumetric work that I identified in the systematic review by Virtanen *et al.* (2011) kept all of the participants grouped together in a single group, with no information about who had a history of stroke-like episodes, and so the atrophy from those who had suffered from stroke-like episodes may have dominated their results and only indicated significant reductions in both grey and white matter compared to their control group. In themselves these measures do not provide much additional information other than the fact that carriers tend to have less grey matter and more white matter than the control group, but do indicate that further investigation is required into specific regions to ascertain whether there are some that are more, or less, affected than others and their potential implications. I have taken this work forward and it will be discussed in the next chapter.

I have brought the predilection of reporting cerebellar atrophy in the absence of cerebral atrophy into question here as the results here indicate that there is cerebellar atrophy when there is also cerebral atrophy. There are a number of reasons why this may be the case and they are all related to the fact that the features of the cerebellum are usually around the same order of magnitude as the size of the voxels. This causes issues as there will be significant partial volume effects, which may be exacerbated by the fact that viewing software usually smooths the image.

To better understand the relationship between cerebral and cerebellar atrophy higher resolution MRI imaging protocols will be required so that the cerebellar volume can be more accurately assessed. If cerebral and cerebellar atrophy are intrinsically linked, this potentially makes identifying atrophy in the cerebellum using standard MRI protocols and visual inspection clinically important as it could provide an easily identifiable indicator of global atrophy as the observed level of atrophy in this cohort lies well outside that of atrophy during healthy ageing.

5.6 Conclusions and Further Work

The simplicity of the apparent correlation between TICV and presentation of stroke-like episodes could be a potentially powerful clinical tool. The next step for this work is to greatly expand the m.3243A>G carrier and MELAS patient groups to ascertain whether this trend is seen throughout the wider population with the m.3243A>G point mutation.

The quantitative atrophy measurement that I have defined and developed allows for the monitoring of atrophy using simple percentage relations rather than requiring statistical hypotheses to test against to assess the significance of changes, and is therefore more easily carried out and understood. It would be feasible to automate the calculation of the TPV/TICV measurement, which would facilitate the longitudinal investigation of atrophy progression and which would also be an initial step in the standardisation of quantitative atrophy assessment.

Analysis of the global grey and white matter volumes yielded little specific information about the carrier group, therefore this group is investigated in much more detail in the next chapter.

I have shown that visual inspection of atrophy is not straightforward due to the effect of overall volume on the visibility of atrophy, and that quantitative assessment of atrophy of both cerebellar and cerebral tissues is required to not only understand the relationship between them, but also to assess whether the visible changes in the cerebellar volume can be used as an indicator of associated global atrophy.

While the findings within this chapter have provided some clear differences between the control, carrier, and MELAS patient groups, the major limitation here is that there are no longitudinal high-resolution scans available for any of the individuals within this baselining cohort yet to allow a much more in-depth study of similarities and differences in the disease progression between individuals. The lack of longitudinal data in addition to the relatively small group size, particularly of the MELAS group when patients with obvious lesions have been removed, is also a limiting factor in this study.

Chapter 6. Regional analysis of volumetric and cortical thickness data

6.1 Introduction

The work I carried out in Chapter 5 showed that there are differences between the control, carrier, and MELAS patient groups in the global volume measures that required further investigation. One possible option was to carry out voxel-based morphology (VBM) analysis between the different groups, but as with the work in Chapter 5, there is no clinical baseline. Therefore I tested the following hypotheses: 1) that there are specific regional differences between patients with MELAS and controls caused just by the presence of the m.3243A>G point mutation that are not related to having a history of stroke-like episodes; and 2) that despite the regional specificity of the presence of lesions there are in fact global changes to the brain.

The VBM work that has been done by Tsujikawa *et al.* (2016) and Haast *et al.* (2018) did not systematically assess the volumes of the regions of the brain they were quoting as being statistically significantly different. Without quantitative results to go on it is impossible to build up a clinical picture of the actual differences that are present that are clinically significant, and instead all that is possible is to provide a list of the areas that have been highlighted.

To my knowledge, no-one has attempted this type of analysis on brain MRI data in mitochondrial carriers and patients with MELAS, which makes this an important study to carry out so that mitochondrial disease research may benefit more fully from a multidisciplinary approach.

6.2 Aims

The aims of the work carried out in this chapter are as follows:

1. Ascertain whether there are differences in overall cortical thickness for each lobe between the control, carrier, and MELAS patient groups.
    a. Cortical thickness was chosen over grey matter volume in each region as it is a far simpler task to verify cortical thickness measurements in FreeSurfer outputs than it is to verify volumes.

2. Break the lobes down into sub-regions to ascertain whether there are specific regions showing cortical thinning in carriers, or if the cortical thinning is spread evenly across the lobe, and therefore across the entire cortex.
3. Devise and utilise a methodology that is easily repeatable.

6.3 Methods

6.3.i Carrier and Patients with MELAS

17 participants, the same as used in Chapter 5, from the mitochondrial disease cohort were used for the TICV and TPV analysis. 10 of these were classed as carriers with no history of stroke-like episodes, while 7 were classed as patients with MELAS with a history of stroke-like episodes. Carrier and MELAS patient details can be found in Chapter 3.

6.3.ii MRI Scans

Cohort participant scans were taken on a 3 T Siemens MRI scanner. The scan parameters used are Gradient echo, 3D anatomical, TR = 50 ms, TE = 30 ms, FA = 15°, with 1 mm x 1 mm x 1 mm voxels.

6.3.iii Regional Segmentation

Volumetric and cortical thickness measurements were carried out using the FreeSurfer 5.4 software (Dale *et al.*, 1999; Fischl and Dale, 2000; Fischl *et al.*, 2002; Fischl *et al.*, 2004). This version of the software was used for all analysis within this section as studies into previous FreeSurfer versions have found significant differences in the outputs available and the accuracy of these (Gronenschild *et al.*, 2012).

The cortical parcellation was carried out using the Desikan-Killiany Atlas, which splits the brain into 35 cortical areas based on the morphology of the gyri (Desikan *et al.*, 2006).

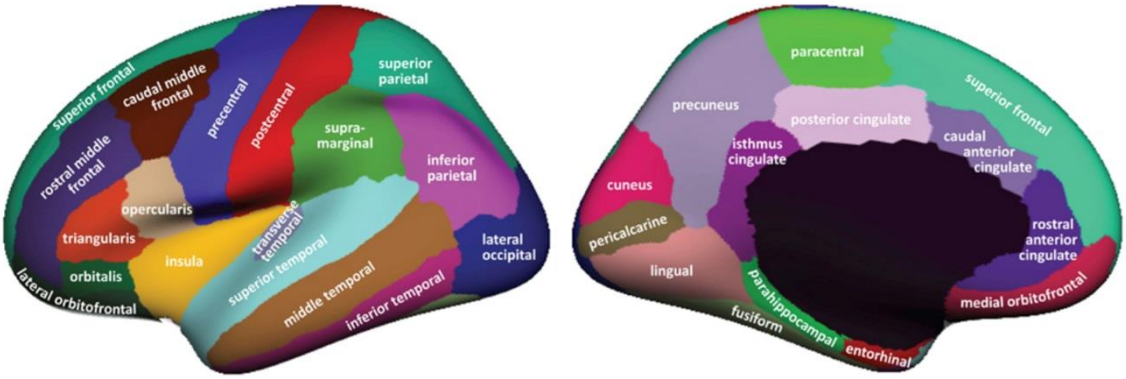

Figure 36. Visual representation of the Desikan-Killiany Cortical Parcellation Atlas in an inflated brain

These 35 cortical areas can then be combined to provide data by lobe (Frontal, Parietal, Temporal, and Occipital). This is valid for both cortical volumetric measurements of the grey matter volume, and also for the cortical thickness measurements.

All of the FreeSurfer segmentation is carried out using the command line prompt. All of the control, carrier, and MELAS patient files were converted to .nii for the FSL segmentation and were used in this format for this analysis. Each file was run through the full FreeSurfer cortical reconstruction process using the following command:

recon-all –subject ‘output file name’ –i input_file.nii –all

Where the ‘output file name’ is used to name the folder where all of the output files for a specific input file will go. These were set to match throughout, so Control1.nii would be output to folder Control1.

Manual assessment of the cortical thickness measurements output by FreeSurfer across random sections of each region was carried out to ascertain the accuracy and validity of the automated measurements.

The volumetric and cortical thickness values then had to be extracted from their output text files, which are located in the ‘stats’ folder within the output folder for each individual. The relevant stats files are ‘aseg.stats’, ‘lh.aparc.stats’, and ‘rh.aparc.stats’. The ‘aparc.stats’ files contained a list of all of the regions and the associated measures, which then have to be transferred into Excel and reordered by lobe. Table 23 shows all of the measured regions and the lobe to which they are

allocated, and Table 24 shows all of the sub-cortical segmentation measures from the aseg.stats output file.

Frontal	Parietal	Temporal	Occipital
superiorfrontal	superiorparietal	inferiortemporal	lateraloccipital
caudalmiddlefrontal	inferiorparietal	middletemporal	lingual
rostralmiddlefrontal	supramarginal	superiortemporal	cuneus
parsopercularis	postcentral	bankssts	pericalcarine
parsorbitalis	precuneus	fusiform	
parstriangularis		entorhinal	
lateralorbitofrontal		temporalpole	
medialorbitofrontal		parahippocampal	
insula			
precentral			
paracentral			
frontalpole			

Table 23. Output regions from the FreeSurfer aparc.stats files grouped by lobe.

Left-Lateral-Ventricle
Left-Inf-Lat-Vent
Left-Cerebellum-White-Matter
Left-Cerebellum-Cortex
Left-Thalamus-Proper
Left-Caudate
Left-Putamen
Left-Pallidum
3rd-Ventricle
4th-Ventricle
Brain-Stem
Left-Hippocampus
Left-Amygdala
CSF
Left-Accumbens-area
Left-VentralDC
Left-vessel
Left-choroid-plexus
Right-Lateral-Ventricle
Right-Inf-Lat-Vent
Right-Cerebellum-White-Matter
Right-Cerebellum-Cortex
Right-Thalamus-Proper
Right-Caudate
Right-Putamen
Right-Pallidum
Right-Hippocampus
Right-Amygdala
Right-Accumbens-area
Right-VentralDC
Right-vessel
Right-choroid-plexus
5th-Ventricle
WM-hypointensities
Left-WM-hypointensities
Right-WM-hypointensities
non-WM-hypointensities
Left-non-WM-hypointensities
Right-non-WM-hypointensities
Optic-Chiasm
CC_Posterior
CC_Mid_Posterior
CC_Central
CC_Mid_Anterior
CC_Anterior

Table 24. List of outputs from the aseg.stats file.

z scores were then calculated and plotted in the same way as described in Chapter 5.

6.4 Results

Frontal			Parietal			Occipital			Temporal		
Controls	Carriers	MELAS	Controls	Carriers	MELAS	Controls	Carriers	MELAS	Controls	Carriers	MELAS
2.755521	2.65625	2.443063	2.17625	2.05045	1.876625	2.143083	2.15115	1.883063	2.783854	2.7182	2.599063
2.542063	2.48415	2.272625	2.455271	2.48515	2.26225	1.954458	1.9925	1.686438	2.876708	2.7494	2.61225
2.442792	2.4043	2.21425	2.559438	2.5205	2.279875	1.812458	1.7656	1.5645	2.840688	2.67115	2.231125
2.638875	2.5997	2.327813	2.072104	1.8785	1.787688	1.530083	1.46925	1.35875	2.536729	2.433	2.229063
2.733667	2.8126	2.566625	2.359479	2.31325	2.055375				2.683646	2.5139	2.331313
2.537146	2.4867	2.297375							2.359417	2.2884	1.780938
2.697896	2.6978	2.5375							3.297313	2.8888	2.707438
2.554188	2.52835	2.320625							3.815708	3.06175	2.925063
2.964708	2.9784	2.796688							2.734583	2.61385	2.482563
2.485708	2.18345	2.1415									
2.291625	2.0192	1.939875									
2.76	2.8848	2.794813									

Table 25. Table showing the cortical thickness (the average of the right and left hemisphere) for each lobe by lobe region, as detailed in Table 23.

Frontal Lobe		
Controls vs Carriers	Controls vs MELAS	Carriers vs MELAS
No significant difference p = 0.149	Controls > MELAS p < 0.0005	Carriers > MELAS p < 0.0005

Parietal Lobe		
Controls vs Carriers	Controls vs MELAS	Carriers vs MELAS
No significant difference p = 0.124	Controls > MELAS p < 0.0005	Carriers > MELAS p = 0.003

Occipital Lobe		
Controls vs Carriers	Controls vs MELAS	Carriers vs MELAS
No significant difference p = 0.554	Controls > MELAS p = 0.002	Carriers > MELAS p = 0.014

Temporal Lobe		
Controls vs Carriers	Controls vs MELAS	Carriers vs MELAS
Controls > Carriers p = 0.018	Controls > MELAS p < 0.0005	Carriers > MELAS p = 0.001

Table 26. Tables showing the outputs of a paired t-test for each lobe, and between each of the control, carrier, and MELAS groups.

Table 26 shows that there is no significant difference in cortical thickness between the control and carrier groups in the frontal, parietal, or occipital lobes, but that there is a significant difference in the temporal lobe. All lobes show significant differences between the control and MELAS groups, and also the carrier and MELAS groups.

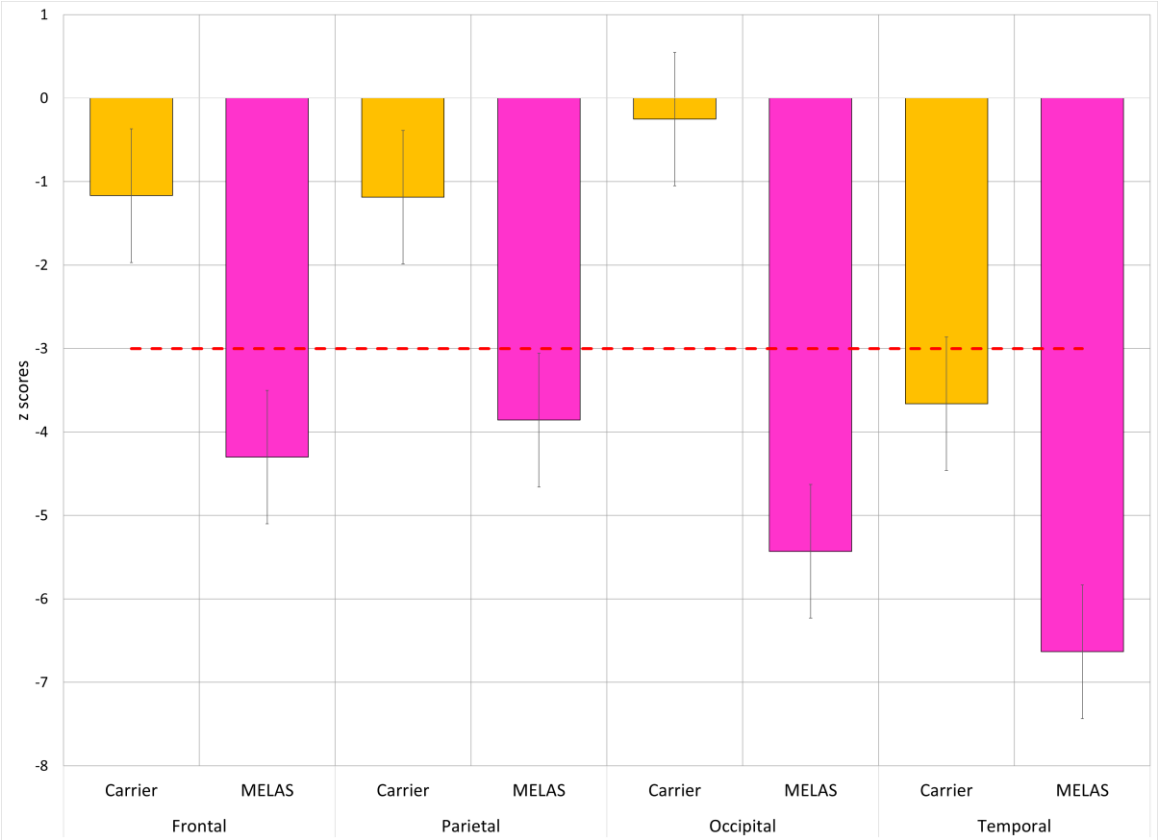

Figure 37. z scores of the cortical thickness by lobe of the carrier and MELAS patient groups, corrected for head size, age, and gender.

Figure 37 shows that in the carrier group the frontal, parietal, and occipital lobe cortical thicknesses are slightly thinner than the control group, but are still within the normal cortical thickness distribution. The carrier group temporal lobe cortical thickness is much thinner than would be expected as it is more than three standard deviations smaller than the control group. The MELAS patient group has much smaller cortical thicknesses than the control group across all lobes. The raw values show that there is approximately a 10% difference in cortical thickness in all lobes between the carrier and MELAS patient groups, which demonstrates that whatever the atrophy mechanism is, it globally affects the cortex and not just the cortex that is local to the site of the stroke-like episode and any associated lesion.

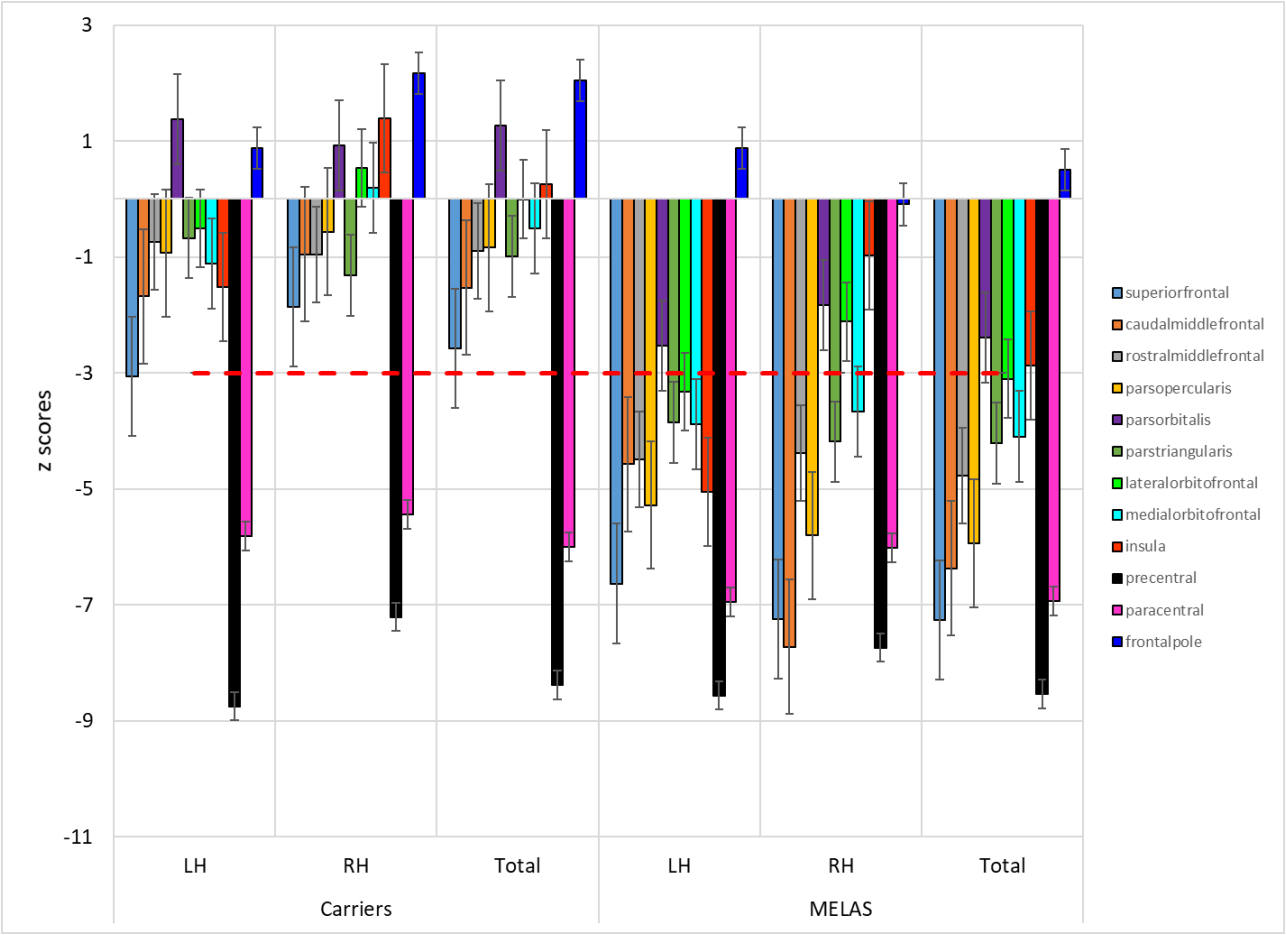

Figure 38. z scores for the cortical thickness of each sub-region, averaged across the sub-region, of the frontal lobe.

Figure 38 shows that most of the sub-regions of the frontal lobe are within normal ranges for the carrier group, but the precentral and paracentral gyri are both a great deal thinner in the carrier group than the control group (control (total) > carrier (total), precentral: $p < 0.0005$, paracentral: $p = <0.0005$). None of the other frontal lobe regions showed a significant difference between the control and carrier cortical thicknesses, although the superiorfrontal region was approaching significance ($p = 0.05$). The MELAS group results show that cortical thicknesses are greatly reduced across the frontal lobe, except for the frontal pole, which appears to be preserved, and also to some extent the pars orbitalis, which does not reach significance when compared to the control group ($p = 0.081$). There are also no significant group differences between the left and right hemispheres.

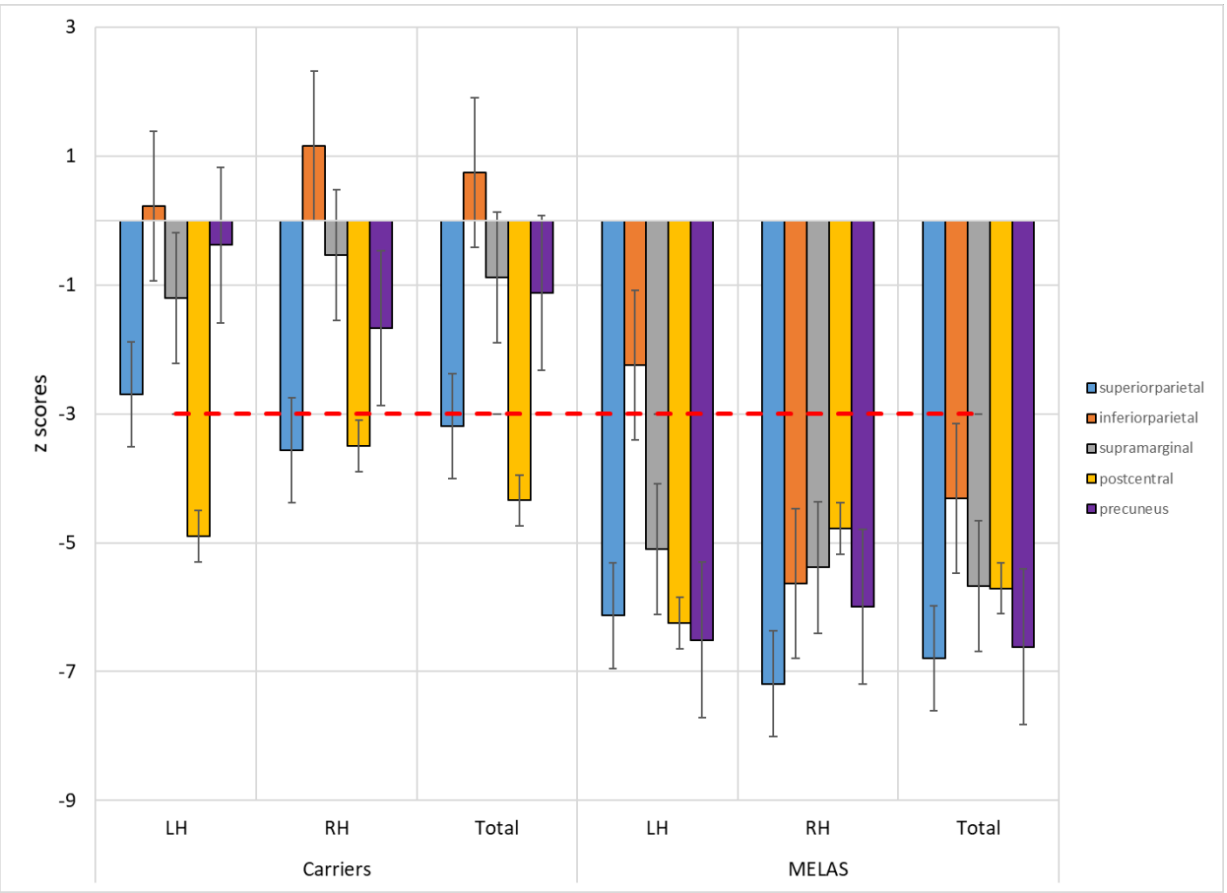

Figure 39. z scores for the cortical thickness of each sub-region, averaged across the sub-region, of the parietal lobe.

The cortical thickness in the parietal lobe of carriers, as shown in Figure 39, also shows a variation across sub-regions, with the postcentral gyrus and superior parietal region both being, on average, significantly thinner than in the control group ($p < 0.0005$ and $p = 0.006$ respectively). There do not appear to be any sub-regions that are preserved in the parietal lobes of patients with MELAS after the onset of stroke-like episodes. Again, there are no significant differences between the left and right hemispheres, although the inferior parietal region approaches significance ($p = 0.064$) and thus requires a larger sample size to reduce the uncertainty in the mean and clarify whether this is an artefact of this study population or a true group difference.

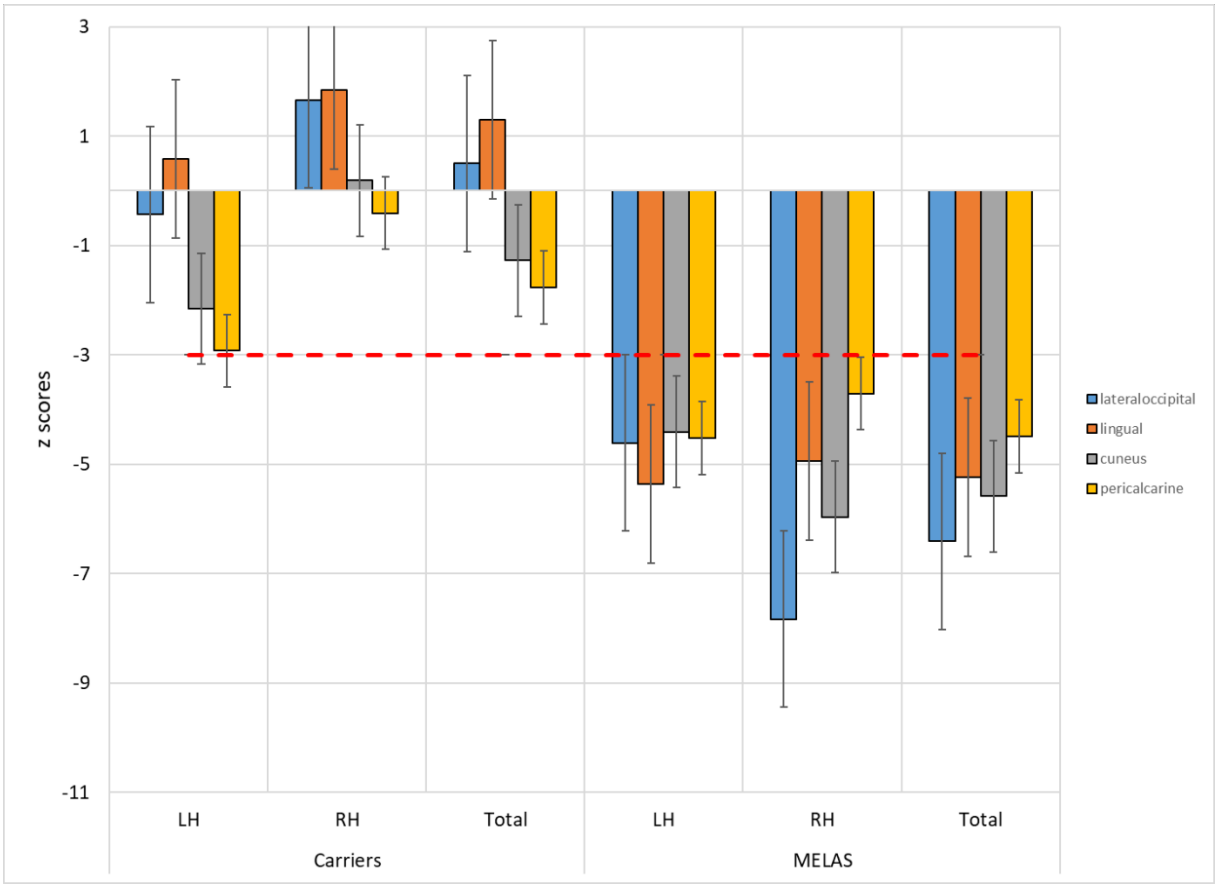

Figure 40. z scores for the cortical thickness of each sub-region, averaged across the sub-region, of the occipital lobe.

The cortical thickness in the occipital lobe of carriers is mostly well within the normal distribution, as shown in Figure 40, however there does appear to be a predisposition of the carrier group left hemisphere cuneus and pericalcarine regions to show thinning that are not seen in the right hemisphere. The hemisphere differences are statistically significant for the cuneus ($p = 0.031$) and the pericalcarine region ($p = 0.028$). The cortical thicknesses of the MELAS group clearly show that all regions have undergone significant thinning after the onset of stroke-like episodes (all occipital regions in the MELAS group are significantly thinner than the control group, $p \leq 0.001$ for all).

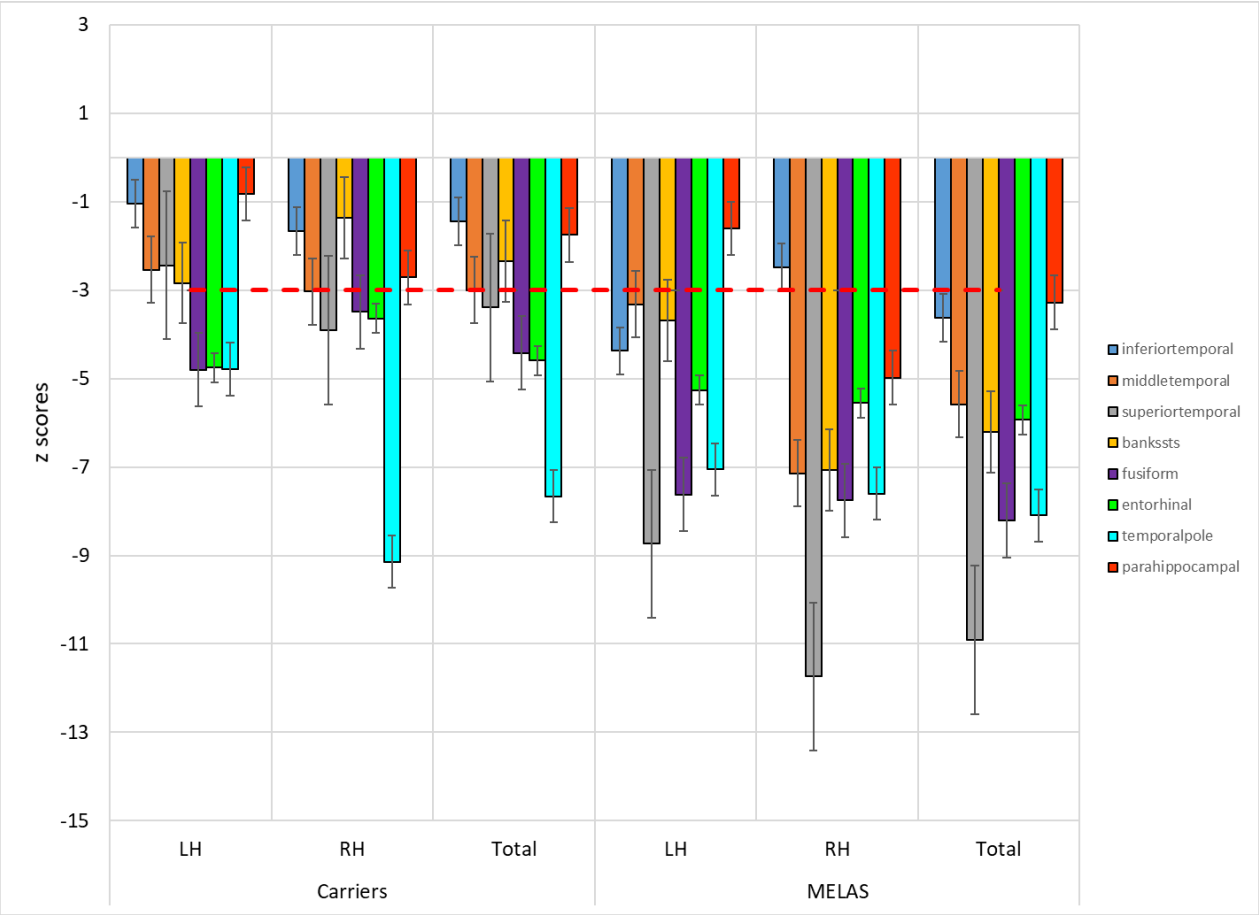

Figure 41. z scores for the average cortical thickness of each sub-region of the temporal lobe.

Figure 41 shows that even in carriers that the cortical thickness is much thinner than in the control group particularly in the temporal pole, the entorhinal cortex, and the fusiform gyrus. The temporal pole does not appear to thin much further in the MELAS patient group, but all of the other temporal sub-regions do show significant thinning after the onset of stroke-like episodes.

	Control vs Carrier	Control vs MELAS	Carrier vs MELAS
Inferior temporal	No significant difference 0.231	Control > MELAS 0.02	No significant difference 0.252
Middle temporal	Control > Carrier 0.009	Control > MELAS <0.0005	Carrier > MELAS 0.051
Superior temporal	Control > Carrier 0.01	Control > MELAS <0.0005	Carrier > MELAS <0.0005
Banks of Superior Temporal Sulcus	Control > Carrier 0.043	Control > MELAS <0.0005	Carrier > MELAS 0.036
Fusiform	Control > Carrier <0.0005	Control > MELAS <0.0005	Carrier > MELAS 0.057
Entorhinal	Control > Carrier 0.001	Control > MELAS <0.0005	No significant difference 0.209
Temporal pole	Control > Carrier <0.0005	Control > MELAS <0.0005	No significant difference 0.553
Parahippocampal	No significant difference 0.194	Control > MELAS 0.023	No significant difference 0.407

Table 27. Results of the 2-sample t-test for all of the areas of the temporal lobe.

Table 27 shows all of the statistical results for group comparisons across the temporal lobe. The full set of comparisons are shown as the patterns are unlike any of the other lobes, which all follow approximately the same pattern of the carrier group showing no significant difference to the control group, except in the highlighted regions, while the MELAS group shows significantly thinner cortex than either the control, or the carrier, group.

6.5 Discussion

The analysis method I chose to carry out regional assessment of the carrier and MELAS patient brains is very different to anything that has previously been presented

in the MRI literature as it does not utilise VBM to carry out the comparisons. There are a number of examples of VBM studies, including Tsujikawa *et al.* (2016) and Haast *et al.* (2018), in which carrier and/or MELAS patient groups are compared statistically to a control group. Within previous studies, both volumetric and also qualitative observation, a number of areas are identified as being different between the groups, but there is often little effort to ascertain the clinical relevance of these and to establish at what point the difference becomes clinically significant. My approach takes a step back from testing a specific statistical hypothesis and instead provides a robust, repeatable method to carry out quantitative measurements on the brains of both controls and carriers that provides an output that may be more easily related to the clinical significance of the results, and may also inform the formulation of more specific statistical hypotheses in which the hypothesis goes beyond 'mean ≠ 0' for use in future studies.

The results, even in this relatively basic format, already challenge some of the assumptions that exist both within the research and the clinical communities. If we first consider Figure 37, it shows that there is a very large difference in cortical thickness between the carrier and MELAS patient groups, and that this is global and not centred in the regions of previous stroke-like episodes (see Table 4). Only one of the patients with MELAS had a reported stroke-like episode centred in the frontal lobe, and removing their data from the MELAS patient frontal cortical thickness made very little difference to the resulting z score, showing that their result was not biasing the overall result. Up to now, it has often been assumed that the frontal lobe is relatively well spared, but my results indicate that while the underlying white matter may be relatively spared until later in the disease progression, there are significant changes to the grey matter once a stroke-like episode has occurred.

Figure 37 also shows that even in carriers, the temporal lobe is severely affected, which suggests that there are intrinsic differences between the brains of carriers and controls. This finding formed the rationale for my investigation of the sub-regions of the individual lobes to ascertain whether the smaller cortical thicknesses were throughout the lobe, or centred in any particular areas.

Figure 38 shows the results from the breakdown of the frontal lobe. Despite the assumption that the frontal lobe is relatively spared, these results clearly indicate that in both carriers and patients with MELAS the precentral and paracentral sub-regions

are both greatly thinned compared to the control group. The presence of this thinning fits in neatly with clinical observations of carriers of the m.3243A>G point mutation who are very often slow in both their movements and speed of mental processing. It is also interesting to note that the frontal pole, even in the brains of patients with MELAS who have a lot of atrophy, is preserved. This region has been identified through neuroimaging studies to be responsible for monitoring the expected outcomes from an ongoing action (Boorman *et al.*, 2009; O'Doherty, 2007; Daw *et al.*, 2006; Koechlin, 2002).

Figure 39 shows that two of the five parietal sub-regions, the postcentral gyrus and the superior parietal cortex, are much thinner than in the control group. All regions of the parietal cortex are then further thinned in the MELAS patient group compared to the carrier group.

Figure 40 shows the results for the sub-regions of the occipital lobe. The occipital lobe appears to show a large difference between the left and right hemispheres, with the left showing much thinner cortex than the right. Hemispherical differences are something that have not traditionally been addressed in neuropathological research due to the widespread practice of only fixing the left hemisphere of any donated brains, while the right hemisphere is frozen, but my results indicate that there may be significant differences between the left and right occipital lobes and that these differences may provide valuable information on the mechanisms that either lead to the cortical atrophy, or perhaps even the mechanisms involved in the onset of stroke-like episodes. These results indicate that handedness may be an influencing factor for occipital thickness, and also that the lack of significant thinning seen between carriers of the m.3243A>G point mutation and healthy controls perhaps indicates that the occipital cortex may already be critically thin and susceptible to influences of abnormal activity, particularly in the adjoining regions of the temporal lobe.

The temporal lobe, unlike the other lobes, is heavily affected in both carriers and patients with MELAS. These results provide a solid region of interest not only in patients with MELAS, but also in carriers to ascertain whether the cortical thinning in the temporal lobe is linked to whether there will be an onset of stroke-like episodes. The carriers frequently only show significant thinning in one hemisphere, but there is no specific pattern to whether this is the left or the right. In this small sample size and without any long-term longitudinal data for the carriers regarding whether they will go

on to develop stroke-like episodes, the results from this analysis are limited to defining regions of interest for future work, using both MRI and neuropathology to begin to tie together the data from the different disciplines.

All of the m.3243A>G carriers and patients with MELAS in this study were adults, with the youngest being 25, so one of the key questions that would need to be addressed is whether the thinner cortex is due to an early onset atrophy of the grey matter that is not related to the onset of stroke-like episodes, or if those regions of cortex did not develop fully in the first place.

With the results from this analysis, it gives the opportunity to devise very specific cognitive tests to use in addition to the volumetric results of an individual to begin to pin down exactly how big a change is required in cortical thickness before it becomes clinically significant, with clinically measurable changes in performance or behaviour. This type of 'back to basics' approach to attempting to gain an understanding of how carrier and MELAS patient brains is generally lacking in current mitochondrial disease MRI literature with methodology and approaches being chosen seemingly at random. The heterogeneous nature of mitochondrial disease means that the current scatter-gun approach to measurement and analysis is unlikely to yield any results that are of real value to the clinical community as without a clinical baseline or a standard, well-defined, methodology the outputs are highly likely to contain contradictory data simply due to different assumptions being made and different analysis methods being used.

My work here has highlighted the absolute requirement for a set of standard measurement protocols to be defined to allow a much more rapid progression of understanding to be achieved as data from multiple studies will be much more readily compared and/or combined and clinical significance can actually be defined so that meaningful statistical analysis may be carried out.

6.6 Conclusions

The results from this section have highlighted that assumptions cannot be made about volumetric and cortical thickness measurements from qualitative inspections of MRIs. I have shown that there are numerous quantitative differences between carriers and controls in very specific regions of the brain, which have not yet been explored or explained. It is possible that changes in one, or more, of these regions may be a deciding factor in whether stroke-like episodes develop. This study is

limited by it only covering a single time point, and also that it only used adult m.3243A>G carriers and patients with MELAS as there are many questions relating to whether the carriers show cortical thinning, or if they have a cortex that was never any thicker. These are questions that only a longitudinal multi-disciplinary study can begin to answer.

Chapter 7. Tract-based spatial statistical analysis in individuals with the m.3243A>G point mutation

7.1 Introduction/Hypothesis

There is a growing amount of evidence to show that white matter tract properties are affected by neurological disease (Turken *et al.*, 2008; Kim *et al.*, 2015; Rieckmann *et al.*, 2016). These changes can include thickening, or thinning, of the myelin around the white matter tract, and change to the tract itself, both in terms of diameter, directionality, and branching (Bourbon-Teles *et al.*, 2017; Barakovic *et al.*, 2018). Fractional anisotropy (FA) provides a gross measure of some of these parameters as it shows the level of anisotropy, in other words the higher the value, the more directional the properties of the tissue. In a completely isotropic material the fractional anisotropy will be zero.

With the evidence from temporal lobe epilepsy studies (Chiang *et al.*, 2016; Imamura *et al.*, 2016) showing changes in white matter tracts, it is not a large step to consider the effects on the white matter tracts of stroke-like episodes and the electrical and cellular activity leading up to these, and in particular in the lead up to the first stroke-like episode. There has only been one study to date that has looked at FA in patients with the m.3243A>G point mutation, and this found significant differences between controls and patients, particularly in the inferior longitudinal fasciculus (Virtanen *et al.*, 2014).

The hypothesis being test in this section of the work is:

1. That there are significant differences in the fractional anisotropy between each of the two groups, carriers, and patients with MELAS, demonstrating physical differences in the white matter tract connectivity and directionality.

This work forms a basis for further hypotheses to be developed that can utilise more in-depth white matter tract analysis to assess the connectivity between specific regions of interest, as identified in the preceding chapters of this thesis, with a particular focus on the connections to and from the regions showing much smaller cortical thicknesses compared to the control group.

7.2 Methods

No controls were available from locally held brain MRIs. Some control DTI scans were sourced but there were significant differences in the scan sequences used and due to the unknown amount of variation (Styner *et al.*, 2002; Vollmar *et al.*, 2010; Biberacher *et al.*, 2016) this would introduce I decided that the analysis for this section of the study should be limited to the carrier and MELAS groups as they were all scanned on the same scanner using an identical protocol.

7.2.i MRI DTI Scanner Protocol

Participant scans were taken on a 3 T Siemens MRI scanner. The scan parameters used were 2D Echo Planar, TR = 9000 ms, TE = 95 ms, FA = 90°, with 2 mm x 2 mm x 2 mm voxels, two b-values (0, 1000), 64 directions, and two averages.

7.2.ii TBSS Protocol

The full details of the TBSS protocol can be found in Appendix B, with only the key stages highlighted within this section.

The DTI files were converted from DICOM to NIfTI and as there were two averages taken, these were split into two separate files so that the number of b-values and b-vectors matched the number of images within the file to be analysed.

Each DTI file was then corrected for eddy currents, and the b-vectors rotated appropriately.

The b0 image was then skull-stripped to create a binary mask image that is used to define the brain area over which the rest of the analysis is run.

The diffusion tensors are then reconstructed by running the DTIFIT tool. This outputs a number of files including an FA file. The FA files for each scan are then collected into a single folder for further processing ensuring that each group has a distinct naming convention as this greatly simplifies future stages of the processing.

There are four stages of pre-processing that have to occur before TBSS can be run to output the associated statistics of the groups being compared. These stages are pre-processing, after which the ‘slicesdir’ folder should be opened and the images inspected to ensure that the process has run correctly (if it has not these images are usually blank), registration to align the images to the FMRIB58_FA standard space,

post-registration to bring the subjects into MNI152 space, and finally the thresholding, which is defined by inspecting the mean_FA_skeleton, although it is usually around 0.2, which should remove highlighted regions outside of the white matter tracts.

To run TBSS a general linear matrix (GLM) needs to be generated. This is achieved using the GLM option in the main FSL GUI. The two cases analysed were for the carrier FA to be greater than the MELAS FA, and vice versa.

The number of permutations used in this analysis was 5000, however this should be considered the minimum for each of the larger datasets and if time and processing facilities permit, larger n values should be used for large datasets such as these.

7.3 Results

While all groups were compared against all others looking for FA both higher and lower, only those group comparisons that showed any significant differences have been presented here in the form of a number of slices with regions of significant difference highlighted.

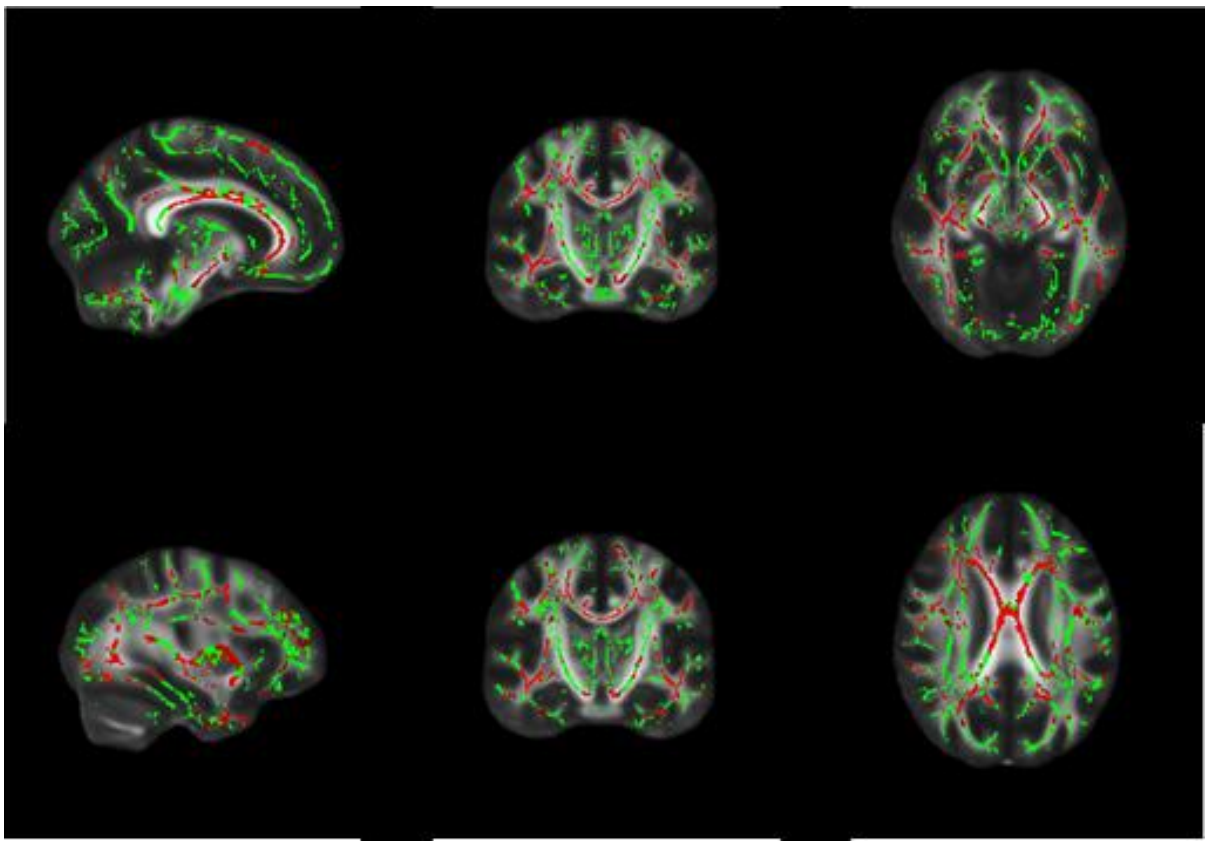

Figure 42. TBSS output showing the regions in which carriers have a significantly higher FA than patients with MELAS. The mean FA skeleton is shown in green. The regions indicate a significant difference between the Carrier and Patient groups with a confidence limit of over 95%.

The carrier group was shown to have significantly larger FA than both the control and the MELAS patient groups, with no significant difference being found between the control and MELAS patient groups. The difference between the carrier and control group is concentrated along the cingulum, with a couple of regions of arcuate fibres in the para- and pre-central gyrus region. The differences between the carrier and MELAS patient group are much more widespread and although the difference in FA is seen in the cingulum again, there is also evidence that both the superior and inferior longitudinal fasciculi also have altered FA values, as well as in arcuate fibres across the brain.

7.4 Discussion

The only previous TBSS analysis of patients with the m.3243A>G point mutation and controls found significant differences in the FA of the inferior longitudinal fasciculus between a combined carrier and MELAS patient group and a control group (Virtanen *et al.*, 2014). The main problem with this study is that participant clinical histories

were not included, so the prevalence of stroke-like episodes is unknown. In my study the carrier and MELAS patient groups were split and analysed against both a control group and each other. This was to separate out the effects on the white matter of stroke-like episodes.

The results showed that the carrier group had significantly larger FA values than both the control and MELAS patient groups. This may indicate that carrying the genetic mutation m.3243A>G causes white matter tracts to develop with greater levels of directionality than in controls, and that this is reduced and disrupted in the event of stroke-like episodes.

However, there are a number of factors that have to be taken into account when considering these results. The first is that the analysis was carried out using DTI scans, which are well known to be limited when it comes to tracing crossing fibres (Raffelt *et al.*, 2017) and so there may be differences between the control and MELAS patient groups within areas where fibres are crossing that are not detected using this method. The sample sizes for the carrier and MELAS patient groups are also small, so again details of differences may not be readily apparent.

Further resolution to these results could be obtained from in depth white matter tract analysis, but perhaps a better option would be to carry out DKI scans and analysis to gain more information about the white matter tract features. In addition to this, it would also be useful to carry out scans to allow for the measurement of white matter tract diameters and degree of myelination as it will be this type of analysis that will start to provide information about the white matter microstructure, which has been shown in other diseases to be altered by abnormal electrical and chemical activities (Rodriguez-Cruces and Concha, 2015; Hubbard *et al.*, 2017).

7.5 Considerations for Future Work

Although the work carried out in this chapter has provided some interesting initial results, it was not possible to utilise the technique to its full potential due to the scans being captured before the analysis technique was fully understood.

TBSS is, as defined in its name, a statistical technique and so larger scan sets than have been used in this study, are highly recommended. The presence of lesions in the scans of some of the patients with MELAS meant that they had to be removed from the TBSS analysis due to the altered structure in those regions.

It is also key to collect each of the DTI scans using the same MRI scanner for everyone to be included in the analysis, and to ensure that identical DTI scan protocols are used. This also includes any control group. Even though there are some freely available DTI scan sets for healthy controls, there are too many unknowns in the collection process, and attempting to combine scan sets from different scanners, even if they do use the same protocol, is not recommended. I did attempt to use some available control DTI scans, but ran into issues with the orientation of the scans, along with differences in the scan protocols, that led to outputs that were not possible to sensibly interpret.

Understanding what is captured, and what the limitations are, within a DTI scan is also important. White matter tracts that travel in approximately straight lines will dominate the data, which could easily lead to a false picture being painted of what is happening within the white matter. Crossing tracts, and tracts that change direction, are better identified using DKI scans, but they have the issue of taking longer to capture, and also being more complex to analyse.

It must also be understood that DTI analysis is a group analysis, and in its current form is not suitable for assessing individuals against group characteristics. This is perhaps one of the most limiting factors about this type of analysis as although group trends may be identified, individual differences may not.

In summary, to overcome the challenges above, the analysis technique needs to be understood prior to the scanning taking place to ensure scan sets will be numerous enough to provide enough power to the study. The level of detail of a DTI scan and its limitations should also be appreciated prior to analysis.

Chapter 8. 7 T MRI ultra-high-resolution scanning and quantitative T_1 mapping of post mortem brain sections

8.1 Introduction

It became very apparent early in this PhD that although MRI scanning is a very powerful investigative technique due to it being non-invasive and suitable for use *in vivo*, to be able to get more information out of the scans, the tissue being imaged needs to be better characterised and understood. Standard anatomical MRI scans only provide limited information, so to delve deeper a completely novel approach needs to be taken.

To better understand the underlying tissue, and potentially even the processes that lead to abnormal electrical activity and subsequent degeneration, it seems like a natural step to turn to neuropathology and to attempt to combine the outputs of neuropathological staining and very high-resolution MRI scans. Until very recently, this hasn't been practically feasible because MRI scanners could not scan at a high enough resolution, and neuropathological techniques required tissue slices so thin that MRI scans just could not image them.

The development of the CLARITY technique, allowing staining of up to 500 µm thick slices, opens up the possibility of being able to quantitatively investigate parameters such as protein deficiencies, cell death, cellular make-up, neuronal density, vascular characteristics to be measured through the use of optimised antibody staining (Lee *et al.*, 2014; Poguzhelskaya *et al.*, 2014; Spence *et al.*, 2014; Tomer *et al.*, 2014) at a cellular level, and to carry out ultra-high-resolution MRI scanning of these same sections.

Despite having a reasonable understanding of how the standard formalin fixation process affects tissue properties in that the T_1 relaxation times decrease significantly compared to fresh tissue (Schmierer *et al.*, 2008; Schmierer *et al.*, 2010; Birkl *et al.*, 2016; Yong-Hing *et al.*, 2005; Pfefferbaum *et al.*, 2004; Tovi and Ericsson, 1992; Blamire *et al.*, 1999), and T_2 relaxation times develop a temperature dependence (Birkl *et al.*, 2016; Dawe *et al.*, 2009), the impact of the first stage of the CLARITY process of mounting tissue samples in hydrogel on the tissue properties that define an MRI image was neither understood nor documented.

It is unfortunate that this section of the study was again opportunistic in nature as post mortem samples became available that were ear-marked for future CLARITY staining, but they had already undergone the first stage of the process, namely mounting in hydrogel.

The original rationale behind this section of the work was to begin to put together a set of protocols that would allow neuropathological staining of specific cell types, or activity, to, ultimately, be linked to specific MRI characteristics *in vivo*. The complexity of achieving this is outlined in the rest of the introduction, and the specific findings of this study detailed in the results and discussion sections.

Carrying out MR imaging of unfixed post mortem brains would be ideal, but there are a number of issues associated with this. Firstly, if the brain is removed from the skull it will not retain its shape unless it is placed in some sort of carriage system (Schmierer *et al.*, 2008). Secondly, the brain tissue will begin to decay (D'Arceuil and de Crespigny, 2007), which will also affect the MRI metrics and downstream neurohistopathological studies. It is clear that there are advantages to imaging both unfixed and fixed brains, but this can only be accomplished successfully if the conditions the brain is being imaged in are fully understood. In particular, the understanding that imaging post mortem fixed brains and brain tissue cannot be directly mapped onto *in vivo* imaging is key (Birkl *et al.*, 2016).

While there has been some in depth imaging studies of healthy post mortem brains and also of patients with multiple sclerosis, there have not, to date, been any post mortem imaging studies carried out on patients with m.3243A>G point mutations. There have also not been any imaging studies to look at the effect of embedding brain sections in hydrogel, which is part of the CLARITY (Phillips *et al.*, 2017) process, to ascertain what effect that has on the imaging parameters. This is important as the process of mounting a brain section in hydrogel significantly alters the tissue properties by removing the lipids from the section.

There are recently published papers that have looked in depth at various elements of multiple sclerosis, including cortical atrophy (Popescu *et al.*, 2015), and myelination and cellular characteristics (Schmierer *et al.*, 2008). The techniques utilised in these studies are directly applicable to the brains of patients with mitochondrial disease and could potentially yield a large amount of information about the underlying mechanisms of neurodegeneration and also perhaps something about the order in

which they occur. In addition to these studies in multiple sclerosis, there is other developmental work in which high resolution MRI can be used to image individual layers of the cortex *in* vivo (Waehnert *et al.*, 2016). Applying this technique to the brains of patients with m.3243A>G could provide vital information in differentiating how the cortex of a patient has been affected before, during and after the formation of a lesion, and also generally throughout their lifetime.

Combining MRI with CLARITY is something that has only been done in a couple of studies, and only in one of relevance to this PhD. Spence *et al.* (2014) used a combination of *in vivo* MRI with post mortem CLARITY to investigate grey matter atrophy in multiple sclerosis.

It is clear from the rather complex picture of atrophy progression in patients with mitochondrial disease discussed in Chapter 5 that this type of multi-disciplinary methodology is likely to be the only way to build up a comprehensive picture of the longitudinal progression of mitochondrial disease. Previous histopathological work indicates observed features in MELAS, a phenotype frequently associated with the m.3243A>G point mutation, as being multifocal necrosis (Sparaco *et al.*, 1993; Brown and Squier, 1996; Tanji *et al.*, 2001), loss of neurons (Sparaco *et al.*, 1993; Tanji *et al.*, 2001), vacuolation (Sparaco *et al.*, 1993), astrogliosis (Brown and Squier, 1996; Lax *et al.*, 2016), calcification (Tanji *et al.*, 2001; Lax, 2011) and disruption to the vascular network and blood-brain barrier (Lax *et al.*, 2016; Lax, 2011). Clearly there are a number of processes involved and the order and causality of these is a long way from being identified and pathological investigations are limited to post mortem and biopsy samples.

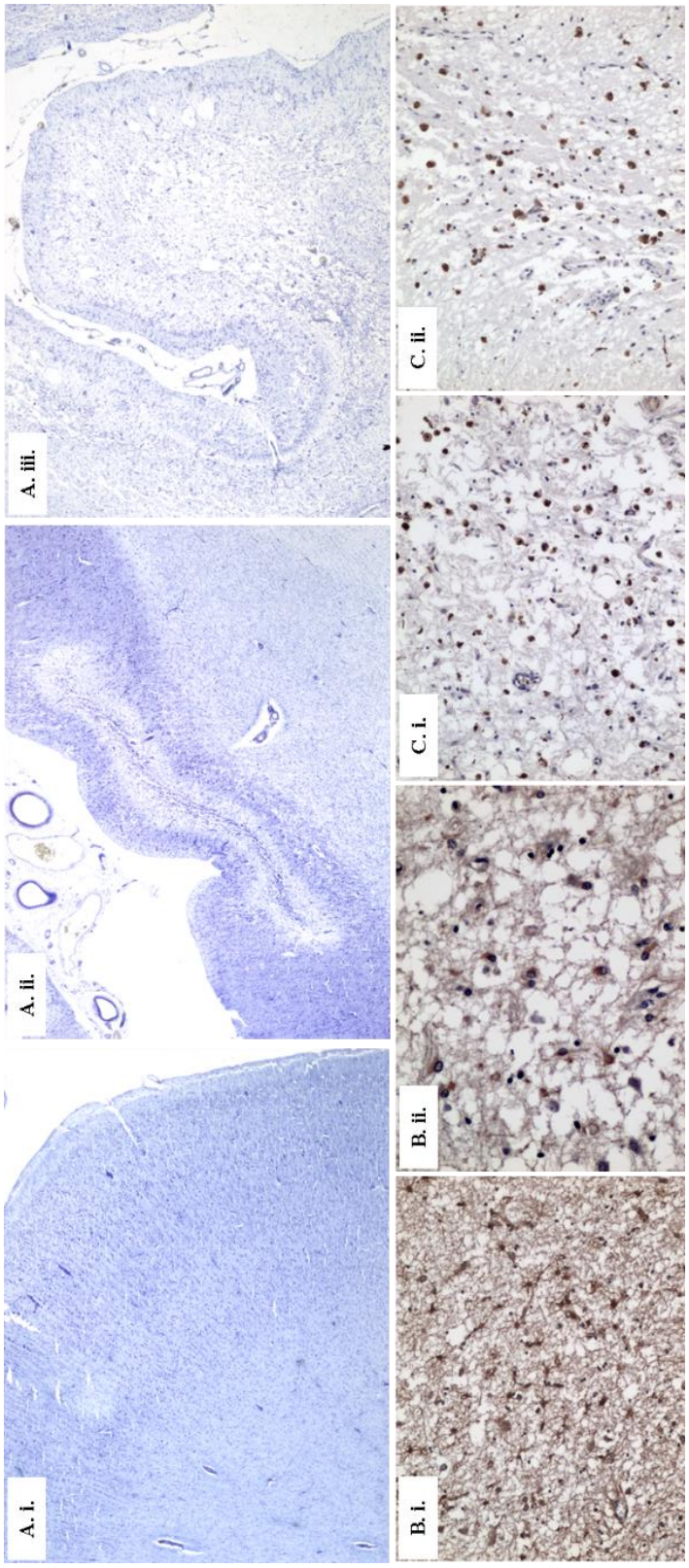

Figure 43. Documented characteristics of lesions seen in patients with mitochondrial disease. A.I. shows normal cellular layers in the temporal cortex while A.II. and A.III. show loss of neuronal cells and tissue necrosis. B.I. and B.II. show severe astrogliosis. C.I. and C.II. show tissue inflammation. [Images courtesy of Dr N. Z. Lax]

Therefore, the combination of multiple investigation techniques is the only way of taking the large body of neuropathological knowledge forwards to the next stage. This will begin by starting to tie together pathological observations made in volumetric samples, as opposed to thin slices, using the CLARITY neuropathological processing technique and initially combining that with MR images taken of the same post mortem volumetric samples. In the long term it is envisaged that high resolution MRI of fresh post mortem brains from patients with m.3243A>G can then be linked to the fixed tissue MRI and CLARITY observations, with the final step being the application of this information to provide details of MRI features that indicate the beginnings and progression of very specific changes within the brain, which may aid diagnosis, prognosis and the development of treatments.

The level of detail attainable in immunofluorescent staining of thick sections of post mortem tissue prepared using CLARITY is extremely high (Figure 44).

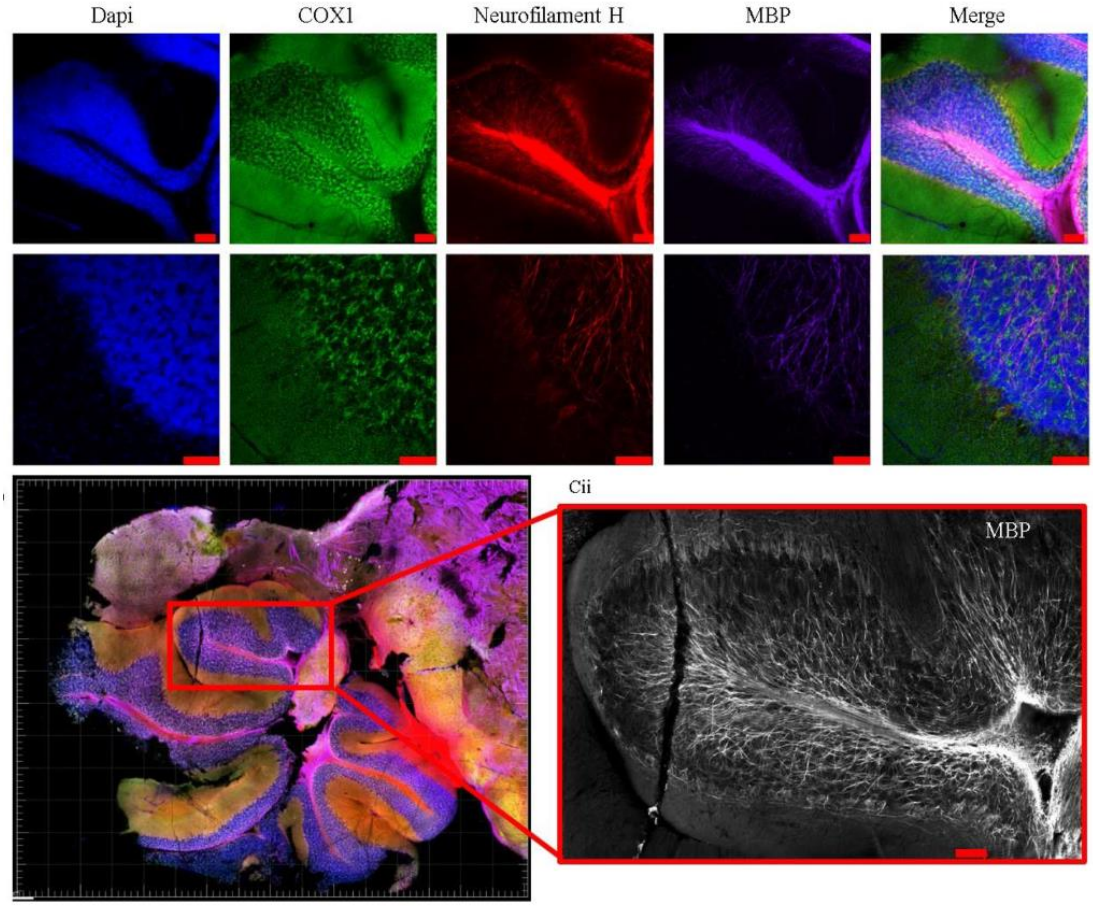

Figure 44. Images of a mouse cerebellum obtained using the CLARITY technique combined with immunofluorescent staining and also the use of confocal microscopy (red scale bar = 100 µm). Reproduced with permission from Phillips (2015).

In order to relate the cellular level observations back to *in vivo* brains it would be ideal if this type of imaging could be registered with a non-invasive imaging modality, such as MRI, to gain a better understanding of the processes in the brain as they happen.

All imaging work to date using MRI to investigate the brains patients with the m.3243A>G point mutation has been whole brain, in contrast to diseases such as multiple sclerosis in which many studies have focussed upon various deep grey matter structures (Haider *et al.*, 2014; Debernard *et al.*, 2015; Van de Pavert, 2017), and low resolution, of the order of $1mm^3$ voxels, compared to neuropathological techniques, which allows imaging on the scale of just a few microns (Phillips, 2015). There has also been no work carried out correlate the anomalies seen on MRI scans in these patients with the underlying neuropathological changes, particularly in relation to observations of assumed cortical laminar necrosis, which has been commented on in MRI papers even though this is a purely neuropathological finding. For this reason, there are still a number of different theories for the cause and proliferation of stroke-like episodes and little real understanding of the mechanisms involved.

While the previous work in this thesis has shown a number of potentially informative changes that occur in the brains of patients with the m.3243A>G point mutation and subsequent changes that occur after stroke-like episodes, the lack of understanding of the types of cellular changes that lead to changes in the brain that then lead to abnormal signals that are picked up on an MRI scan means that as things stand MRI is of relatively limited use in the assessment of the cellular state of the brain.

The introduction of 9 T clinical scanners opens up the option of carrying out higher resolution structural scans and also of achieving greater contrast between brain tissues, but also the opportunity to utilise other MRI scan types that can provide additional information about the brain tissue in each area, such as quantitative T_1 mapping. To inform which of these are the most relevant scans to carry out, it is suggested that carrying out MRI scans on post mortem tissue, in conjunction with neuropathological techniques, and registering the output images can begin to provide details on the cellular changes that lead to each type of anomaly observed. As it is likely that multiple types of scan will be required to gain specific combinations of quantitative values as biomarkers, scanning of post-mortem tissue provides an

opportunity to use long scan times and ultra-high-resolution imaging techniques to optimise the types of scan required without initially having any patient involvement.

The aims of this piece of work were:

- To develop and assess a very high-resolution MRI scanning sequence for post mortem brain sections already mounted in hydrogel.
- To assess how closely MRI and neuropathology structural image resolutions could potentially be matched.
- To investigate the methods required for high resolution structural MRI scans and CLARITY and to ascertain whether they are compatible for carrying out imaging, and registration of those image, on the same section.
- To optimise a scan sequence to carry out quantitative T_1 mapping of the post mortem brain sections and identify whether this may be a useful technique for investigation of the cortex both post mortem and ante mortem.
- To discuss the future potential insights that the combination of these techniques may provide.

8.2 Methods and Materials

The post mortem brain sections used in this work are as detailed in Table 5 in Chapter 3.

The MRI scanner used was a pre-clinical 7 T Agilent (Varian) scanner using a 28 mm birdcage coil (Rapide Biomedical).

Prior to each scan being carried out, including between samples scanned on the same day, the scanner was calibrated by carrying out a manual shim to optimise the signal, checking the position of the peak frequency and adjusting as necessary to centre on 50 kHz, using a single pulse (SPULS) scan, and checking the power of the pulse to ensure transmission and detection is optimal. Should the frequency and/or power be abnormal this was an indication that there was something wrong with the overall setup and functioning of the scanner.

Each post mortem sample was placed in a 20 mm diameter falcon tube filled with phosphate-buffered saline (PBS) solution after trials were carried out to assess the effect of imaging with this solution around the sample. The samples were not secured to the tube in any way, but were positioned in the tube so they presented their largest

face uppermost. The falcon tubes then had a collar placed around them so they fitted into the centre of the coil and would not move during the scanning process. The sections were then inserted into the scanner with the centre of the section at the centre of the coil. To assess the position of each slice, SCOUT scans were run, each taking around 10 s, with adjustments of the section in between these, until the section was in the correct position for the main scan to be carried out.

8.2.i Structural Imaging

The scan sequence used for the structural imaging was a gradient echo multi-slice (GEMS) sequence using the following parameters:

Parameter	Value
Repetition Time (TR)	799.84 ms
Echo Time (TE)	10.04 ms
Flip angle (α)	20°
Averages	92
Slices	20
Gap	0 mm
Slice thickness	0.5 mm
Resolution	512 x 512 pixels
Field of view	20 x 20 mm
Pixel size	39 x 39 µm

Table 28. Table of GEMS scan parameters used to obtain the structural T1 MRIs of post mortem brain sections.

The output files for these scans were standard .nii files and so the images were viewed and analysed in ImageJ.

8.2.ii Quantitative T1 mapping

For the quantitative T_1 mapping a Gradient echo multi-slice inversion recovery (GEMSIR) Look-Locker scanning sequence was used. Inversion recovery sequences are the gold standard for quantitative T_1 mapping, but in this case the GEMSIR Look-Locker sequence was chosen because it allowed the measurement of T_1 values from a single inversion recovery. The magnetisation is inverted, and then is sampled a number of times using multiple relaxation times during its recovery. As this type of scan sequence is sensitive to the flip angle (α), α was kept as small as possible as the sensitivity decreases with α. The GEMSIR Look-Locker scan sequence had been pre-defined on the Agilent (Varian) scanner and was not designed as a bespoke sequence for this work.

Parameter	Value
Repetition Time (TR)	8.37 ms
Echo Time (TE)	4.2 ms
Flip angle (α)	8°
Averages	20
Dummy slices	2
Slices	2
Gap	0.5 mm
Slice thickness	0.5 mm
Resolution	128 x 128 pixels
Field of view	20 x 20 mm
Pixel size	156 x 156 µm
Sweep width	50 kHz
Receiver gain	10 dB

Table 29. Scanner settings to run the GEMSIR Look-Locker scan to measure the quantitative T1 values of the post mortem brain sections.

In addition to the scan settings, an array is also required to be defined:

Start inversion time (TI): 5.00 ms

End inversion time (TI): 2000.00 ms

The array values were chosen so that a balance of measurements between the negative and positive magnetisation states was taken during the inversion recovery, hence the exponential nature of the array values. A representation of this is shown in Figure 45. The processing of the data requires that the inversion of the magnetisation is taken into account, which was done in this case by using an algorithm in which the data was analysed to find the null point, which was also visible by eye as the point at which the contrast of the images was inverted, to restore the polarity (Bakker *et al.*, 1984; Nekolla *et al.*, 1992; Clare and Jezzard, 2001). Polarity restoration also reduces any potential noise-induced systematic errors (Tofts, 2003).

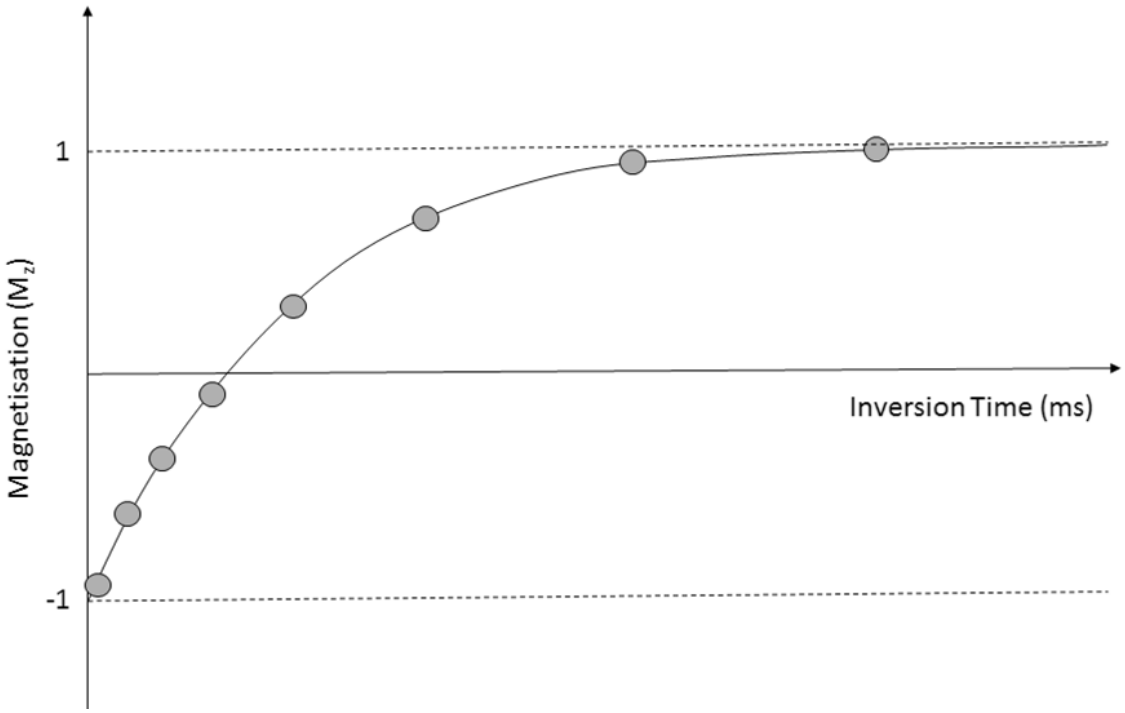

Figure 45. Basic representation of a perfect magnetisation inversion recovery to demonstrate the array requirement to contain an exponential set of inversion times to cover both the negative and positive magnetisation regions equally during the scan.

For the quantitative T_1 mapping scans the scanner room was kept at a constant temperature (21.8 ± 0.4 °C) throughout the scans and all of the samples were allowed to thermally equalise with the scanner room temperature before a scan was commenced.

After the scan had completed it was then necessary to generate the T_1 map from the measurement files captured within the NMRJ software on the scanner computer. In this process the sequential images were opened to check their quality. Due to the long T_1 of the PBS dominating the image if automatic thresholding was selected, the threshold was set at 100 ms to optimise the contrast of the brain tissue in the images.

Using the 'Math' tab functions to generate .nii files for M0 and S0, it was then possible to generate NIfTI libraries of each quantitative T_1 scan and output single slice quantitative T_1 maps in the .nii file format. Scale bars for the images could only be generated using the NMRJ software, and the colour scales could also only be altered with ease within the NMRJ software.

8.3 High Resolution Structural Imaging

At the time of writing, the most recent high-resolution MRI post mortem human brain section studies have reported single slice pixel sizes of 300 x 300 µm (Castillo *et al.*, 1996; Smith *et al.*, 2012). After optimisation of the scan sequence, pixel sizes of 39 x 39 µm were achieved, using a slice thickness of 125 µm. The slice thickness could be reduced further but was limited by the control computer for the scanner and also the time taken for each scan, which was around 12 hours per section.

Only a representative sample of images has been included here to demonstrate the features that can be seen across the group of post mortem samples.

Figure 46 shows an example of a post mortem section from a non-lesioned region of the temporal lobe. This image clearly shows the intact cellular structure of this region, but also shows a very low contrast between the grey and white matter within the section. This will be discussed and explained in Section 8.5.

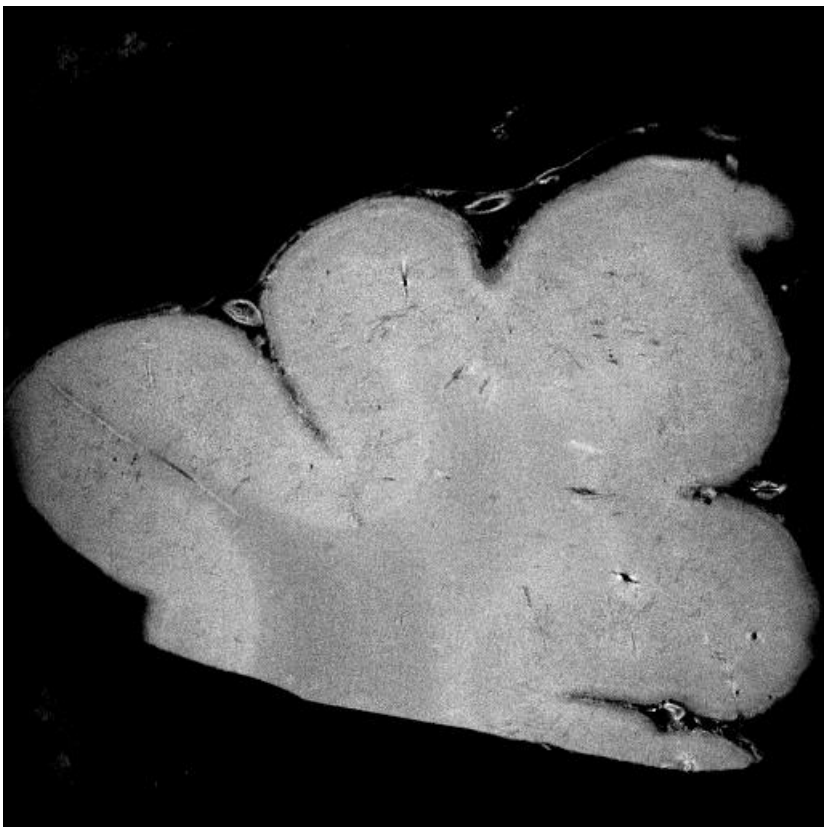

Figure 46. Ultra-high-resolution MRI scan with 39µm x 39µm x 125 µm voxels using a brain section from a non-lesioned area of brain from a patient with the m.3243A>G point mutation after mounting it in hydrogel.

The reporting of no visible lesions on the post mortem brain section did not necessarily correlate with a lack of structural change in the post mortem brain section, as is demonstrated by Figure 47, in which microvacuolation can clearly be seen within the cortical tissue.

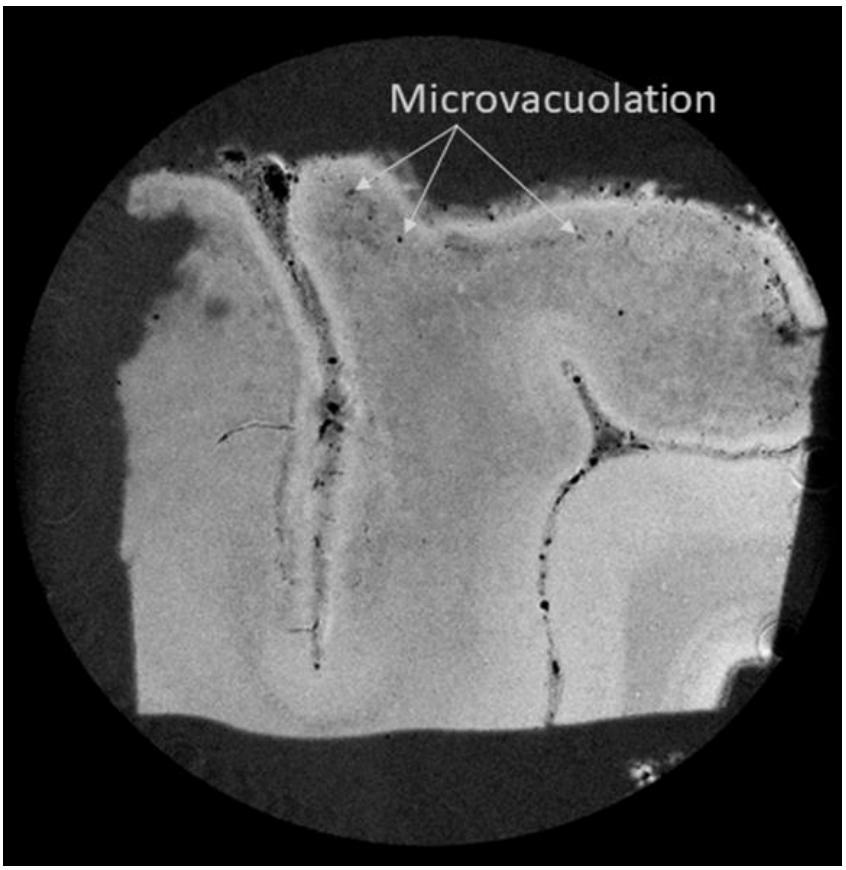

Figure 47. Ultra-high-resolution MRI scan with 39 µm x 39 µm x 125 µm voxels using a brain section from a non-lesioned area of brain from a patient with the m.3243A>G point mutation after mounting it in hydrogel.

Other post mortem sections showed very clear evidence of being lesioned, and this was even more apparent after carrying out the MRI scan as there are regions underneath the top cortical layers that have disintegrated entirely. It is not clear from these images whether the disintegration is of one of the cortical layers, or the underlying white matter, or a combination of the two.

Figure 48. Ultra-high-resolution MRI scan with 40 µm x 40µ x 125 µm voxels using a brain section from a lesioned area of brain from a patient with the m.3243A>G point mutation after mounting it in hydrogel.

8.4 Quantitative T1 mapping

The output quantitative T_1 maps were given a multi-coloured scale as this showed very clearly the boundary between the white (yellow and dark green) and grey (light green, blue, and red) matter in the post mortem section. Although the structural image did not provide good contrast between the two tissue types, quantitative T_1 mapping does provide very good contrast, as seen in Figure 49. There appears to be some evidence of differentiation between the cortical layers, but these are not clearly defined in these sections. It should be noted that individual pixel sampling was carried out on each image to verify which part of the scale they sit on. In Figure 49, the grey matter T_1 values were confirmed to lie in region of 0.1-0.15 ms.

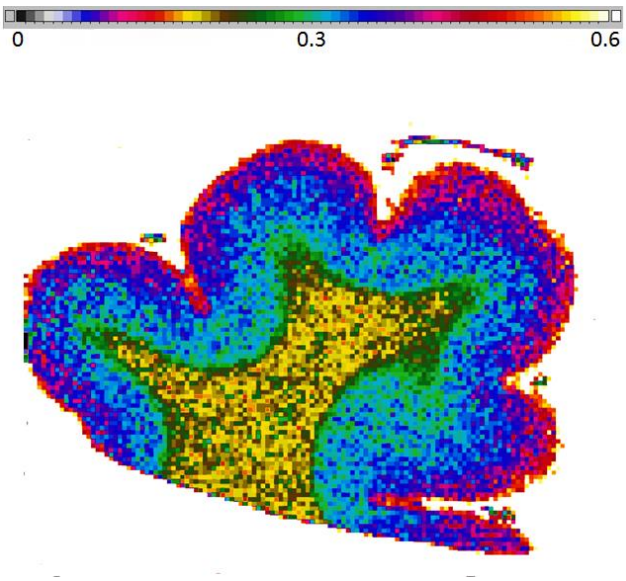

Figure 49. Quantitative T1 map showing the variation of T1 (in seconds) in a post mortem section of fixed brain tissue after mounting in hydrogel from a non-lesioned area of brain from a patient with the m.3243A>G point mutation.

The effect of neurodegeneration can also be clearly seen in the quantitative T_1 map of the lesioned section shown in Figure 48. Where the brain tissue has degenerated, there is literally nothing left and these areas have been filled with hydrogel and so have the same T_1 value as the surrounding fluid.

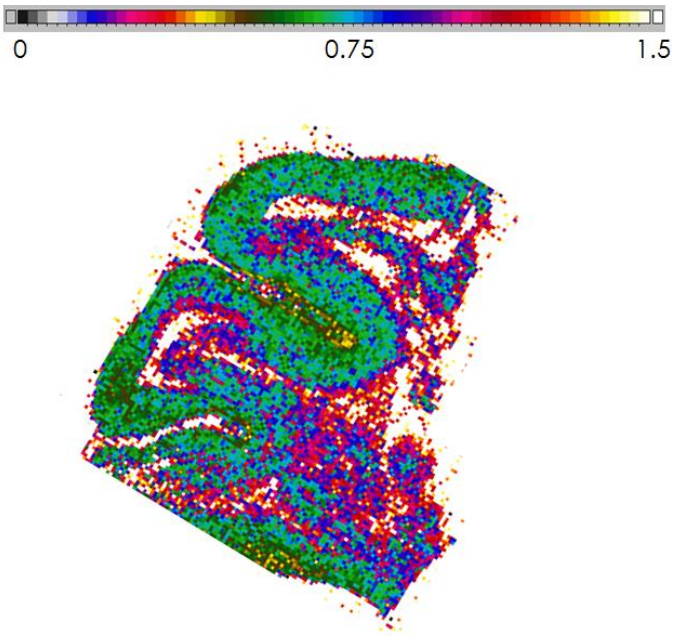

Figure 50. Quantitative T1 map showing the variation of T1 (in seconds) in a post mortem section of fixed brain tissue after mounting in hydrogel from a lesioned area of brain from a patient with the m.3243A>G point mutation.

				Layer (T1 in s)						Fixed
				1	2+3	4	5+6	WM		
Patient 1	m.3243A>G	Frontal	Non-lesioned	1.18	0.79	0.9	0.54	0.35		7mnths
		Occipital	Lesioned	0.99	0.74	0.68	0.54	0.37		
		Occipital	Non-lesioned	0.99	0.76	0.7	0.53	0.37		
		Temporal	Lesioned	0.83	0.68	0.62	0.52	0.36	Significant WM degradation	
Patient 2	Multiple mtDNA deletions	Frontal	Non-lesioned	0.47	0.37	0.33	0.28	0.21		4yrs
		Occpital	Non-lesioned	0.43	0.34	0.3	0.26	0.19		
		Temporal	Non-lesioned	0.44	0.34	0.31	0.26	0.19		
Patient 3	*POLG*	Frontal	Non-lesioned	0.51	0.45	0.4	0.31	0.18		4yrs
		Occpital	Non-lesioned	0.68	0.43	0.38	0.28	0.28		
		Temporal	Lesioned	0.54	0.46	0.41	0.31	0.19		
Patient 4	m.8344A>G	Frontal	Non-lesioned	0.43	0.43	0.39	0.33	0.23		4yrs
		Occpital	Non-lesioned	0.7	0.6	0.65	0.4	0.24	Vacuolated IV = 0.6-0.77	
		Temporal	Lesioned	0.47	0.63	1.2	0.7	0.83	Vacuolated IV = 1.0-1.5 Significant WM degradation	
		Temporal	Non-lesioned	0.63	0.45	0.4	0.33	0.25		
Patient 5	*POLG*	Frontal	Non-lesioned	0.5	0.45	0.4	0.33	0.24		5yrs
		Occpital	Non-lesioned	0.51	0.41	0.37	0.3	0.24		
		Temporal	Non-lesioned	0.75	0.47	0.41	0.36	0.28		
Patient 6	m.3243A>G	Frontal	Non-lesioned	0.49	0.39	0.36	0.3	0.23		3yrs
		Occpital	Non-lesioned	0.45	0.34	0.3	0.26	0.2		
		Temporal	Non-lesioned	0.5	0.43	0.37	0.3	0.21		
Patient 7	m.8344A>G	Frontal	Non-lesioned	0.49	0.43	0.39	0.34	0.23		9yrs
		Occipital	Non-lesioned	0.43	0.37	0.33	0.3	0.24		
Control 1	Control	Frontal	Non-lesioned	0.41	0.34	0.31	0.28	0.25		8yrs
		Occipital	Non-lesioned	0.82	0.42	0.36	0.3	0.24		
		Temporal	Non-lesioned	0.42	0.36	0.33	0.27	0.22		
Control 2	Control	Frontal	Non-lesioned	0.42	0.36	0.32	0.27	0.18		9yrs
		Occipital	Non-lesioned	0.4	0.3	0.25	0.27	0.17		
		Temporal	Non-lesioned	0.43	0.33	0.29	0.26	0.18		

Table 30. Showing the average T1 values for each layer of the cortex in each post mortem section.

The T_1 values for Patient 1 in Table 30 are clearly larger than for all of the other samples and this is due to these sections only being fixed and not being mounted in hydrogel. The physical differences between the two processes of fixation and mounting in hydrogel are large as the fixation process leaves all of the original material in situ, but through the application of formalin bonds are formed that stabilise the tissue and reduce T_1 values from those of unfixed tissue, whereas when tissue is mounted in hydrogel all of the lipids are stripped out of the section, which has the effect of shortening the T_1 values even further making it difficult to obtain high-quality very high-resolution MRI scans.

8.5 Discussion

To date there has been very little work carried out that attempts to identify neuropathological correlates for MRI features. This has mostly been because of the lack of techniques for the staining of thick tissue sections combined with limited spatial resolution of MRI scanning. With the development of the CLARITY technique for the processing, staining and imaging of thick brain slices of up to 500 µm, compared to the usual 5-10 µm in standard neuropathological staining techniques, along with up to 9 T MRI scanners becoming more prevalent, particularly in the form of pre-clinical scanners, the opportunity to finally begin to carry out multimodal imaging and analysis of post mortem tissues is finally here.

Figure 48 and Figure 50 clearly show the end state of the lesion process and it could be argued that these regions are perhaps of the least utility due to the significant degeneration and tissue loss. Once brain tissue has reached this point there is little point in correlating the features with *in vivo* scans as entire cortical layers have already been completely destroyed and so any correlation in these specific areas will be between whatever substance is now filling that gap. In the case of the *in vivo* brain it will be CSF, in the post mortem sections it will be formalin solution, air, or a buffer solution. It is of far more interest, and use, to study the cellular changes occurring in regions where lesions are not obvious, but there are changes actively occurring, as in Figure 47, but even in this case we only know that there was no visible lesion recorded during the post mortem and not whether there would have been a lesion, or any other visible MRI changes, identified on an MRI scan. This highlights the first issue that the development of this multi-disciplinary technique faces, which is the lack of longitudinal image and data collection throughout the life of a patient, through to the study of post mortem sections of the brain.

The second issue highlighted by the sections that were available to scan as part of this piece of work is that they had already been mounted in hydrogel, which was initially seen as desirable as this reduced the number of CLARITY processing steps that had to be carried out on each section post-MRI and was believed to increase the chances of a successful image registration. Unlike the fixation process, in which the changes caused to the brain tissue by the process are relatively well documented, the effects of mounting brain sections in hydrogel are not well understood from an MRI perspective. In fixed brain tissue, the T_1 values of grey and white matter are similar, although much shorter, than an *in vivo* brain, which means that the grey matter T_1 value will be larger than for white matter (Tofts, 2003). My work has shown that mounting a brain section in hydrogel not only significantly shortens the T_1 values, which makes optimising a sequence much more difficult and also limits the resolution compared to a fixed section with longer T_1 values, it also affects grey and white matter to different extents so that the grey matter in a section will end up with T values lower than those of the white matter and so the contrast is not only reduced, but also inverted compared to both fixed post mortem brain sections and *in vivo* brains.

The fact that my brain sections had already been mounted in hydrogel is clearly a very large limiting factor to this work, but despite that it was still possible to optimise a very high resolution 7 T MRI scan sequence to provide output images with very good signal to noise ratios, and considering the very short T_1 values a reasonable contrast between grey and white matter. To take this work forwards effectively would require optimisation of a high-resolution scan sequence using fixed brain tissue sections as this could not only provide greater contrast images, but also the potential for either reduced scanning times or increased resolution.

Attempting to register MRIs with neuropathological images initially appeared to be something that could be achieved, despite the disparity in the resolution of the images. However, a closer inspection of the CLARITY protocols highlighted a number of issues, but by far the biggest issue was the amount of movement of each section that occurred during the processing. With the development of possible techniques for carrying out CLARITY on 500 µm thick sections of brain tissue, there would have been a possibility to carry out MR imaging at this point, thus reducing the amount of movement between the MR imaging and the neuropathological imaging. After looking at the work I have carried out on this the changes to the brain tissue

caused by the mounting in hydrogel now precludes this, but there are far greater challenges to overcome due to the standard procedures for the rest of the processing.

CLARITY antibody staining, unlike standard thin section staining that is carried out with tissue mounted on a slide, is carried out with the sections floating freely in solution to allow the antibodies to penetrate the entire section. Therefore, attempting to get a stained brain section onto an imaging slide in the same orientation and without significant warping or physical distortion is virtually impossible unless there is a large feature within the slice that is, at an absolute minimum, around 80 μm in size for the MR imaging to be able to resolve, according to the Nyquist theorem. In practice there are additional image processing methods that have been developed for coregistration to pathology that may provide options to develop and optimise registration protocols for the brain to take this work forwards (Orczyk *et al.*, 2012; Antunes *et al.*, 2018).

Despite the very clear need for neuropathological correlates for MR imaging, I have identified that the practicalities of achieving the gold standard of fully registered MR and neuropathological images is currently not trivial to achieve and much development of CLARITY processing techniques would have to be carried out to achieve this. Even without this gold standard there is a great deal of work that could be carried out to being to more fully investigate the cellular changes within post mortem brain sections that could involve ultra-high resolution of fixed brain sections followed by standard neuropathological techniques that could begin to provide neuropathological correlates for observed MRI changes.

Quantitative T_1 mapping, although it suffers from the same T_1 value reduction issues as the structural imaging, may provide an easier method to gain further insights into the brains of patients with mitochondrial disease, both through the high resolution quantitative T_1 mapping of post mortem brain sections, but also ‘reverse engineering’ these to provide more information about the *in vivo* brain, particularly in relation to any changes that are observed within the cortex, which I showed in Chapter 6 to be significantly affected by the onset of stroke-like episodes.

The reason I have identified quantitative T_1 mapping as potentially useful source of information is because the T_1 values of tissue are directly related to properties of the tissue, such as the amount of CSF, cellular make-up, water binding within the tissue,

and also the concentration of macromolecules (Gowland and Stevenson, 2003). The benefit of using T_1 values over T_1-weighted images is that T1-weighted images have a lot more contributing factors in order to produce grey scale contrast images. Quantitative T_1 mapping not only provides a better contrast between tissue types, it also provides the quantitative difference between them as well, which means that differences between controls, carriers, and patients with MELAS can be quantified and also potentially investigated further using other MR techniques, such as looking at metabolite ADCs. Quantitative T_1 mapping of *in vivo* brains could also provide a clinical baseline, much in the same way as TPV and cortical thickness has been used in chapters 5 and 6, so that clinically significant changes in T_1 values could be identified and used in conjunction with other brain measures in longitudinal studies to ascertain the order and the extent of observable MR changes during the progression of mitochondrial disease in anyone carrying the m.3243A>G point mutation to gain a much more in depth understanding of the range of individual differences and perhaps begin to pinpoint any regions where protective mechanisms appear to be in effect.

In this chapter I have begun a discussion on the way forward for a multi-disciplinary approach to investigating mitochondrial disease with a view to achieving a much greater mechanistic understanding that may underpin future therapeutic strategy development. While it is one thing to discuss the methods required, it is another to put in place the systematic data collection required to achieve the greatest understanding, and until both standardised methods and a systematic approach are in place we shall find difficulties in making step changes in our understanding of mitochondrial disease.

Chapter 9. Final Discussion

9.1 MRI studies of the brain

This study was begun with a very small amount of published work on volumetric analysis using MRI in relation to adult individuals with the m.3243A>G point mutation and mitochondrial disease, which was a difficult starting point considering the complex, multisystemic, and unpredictable nature of mitochondrial disease. Therefore I had to develop testable hypotheses from a range of different sources whilst also keeping in mind that there may be quantitative information available that had not yet been identified. There was also the issue of a lack of standardised methods, patient selection, or patient grouping when carrying out quantitative volumetric work on MRI scans of the brains of people either just carrying a mitochondrial mutation through to those with a fully definable phenotype. The published studies also generally do not provided clinical details of patients, so it is often unclear how, or why they have been grouped as they have.

The complexity of mitochondrial disease, along with its multisystemic nature, make a systematic approach absolutely vital in order to obtain enough comparable data to be able to draw useful, and accurate, conclusions. Therefore the main aim of this thesis was to establish validated and justified methods to carry out an initial systematic volumetric analysis of both carriers and patients with MELAS to allow the formulation of more specific testable hypotheses both for further investigation within later work for this thesis, and also for future work in the form of highlighting specific regions of interest for the development of neuropathological correlates of structural MRI scans as well as regions to investigate further using both structural and functional MRI techniques.

9.1.i Volumetric

During the course of this thesis, I developed a number of protocols to systematically process T_1-weighted high-resolution structural brain MRI scans. I began by carrying out the time-consuming accuracy validation for these high-resolution anatomical T_1-weighted scans, which allowed me to justify and validate the use of FSL 5.0 for the global segmentation of tissues within this study as the comparison with the segmentation results of manual segmentation were matched closely (Chapter 4). However, it should be noted that there has yet to be a global comparison between

MRI segmentation volumes and actual volumes defined through pathological dissection so this work does not necessarily imply that the selection of segmentation software provides the ‘correct’ volumes, but does provide justification for making that selection based on the observable and measurable properties of the MRI scans available. One of the overarching comments for all of the segmentation work is that all of these segmentation protocols require scans to be high resolution, and also high contrast, thus leading to scans using protocols such as SPACE are not suitable for these analysis methods, although they may be favoured by radiologists due to the increased contrast between brain tissue and pathology, and this is an important takeaway point from this study to inform any future volumetric work (Okada *et al.*, 2011).

The method developed for global segmentation provides a straightforward methodology, which if combined with additional work to standardise scans between scanners and sites, could provide the basis for a much larger database for the study of individuals with mitochondrial disease. The systematic review (Chapter 2) highlighted the lack of standardised reporting, which leads to the loss of valuable information that is perhaps not deemed important enough to make it into a publication with a strict word limit, and the differences in the reported information makes it extremely difficult to combine or compare studies.

The global segmentation showed that, within the cohort of individuals with the m.3243A>G point mutation, TICV was strongly correlated with a clinical history of stroke-like episodes, and that this could potentially be used as a surrogate measure of susceptibility to the onset of stroke-like episodes in younger carriers of the m.3243A>G point mutation. The initial assumption that head circumference could potentially provide a much simpler surrogate measure in adults was quickly called into question after carrying out correlation calculations. The use of adult head circumferences to assess the percentile a person sits in is also problematic as there is currently no accepted percentile definition.

The TPV measurements showed that patients with MELAS showed high levels of atrophy compared to both the control and carrier groups, which supports the anecdotal clinical evidence of a link between high levels of atrophy and a clinical history of stroke-like episodes. The rate of atrophy was also touched-upon with a piece of work using two patients with a MELAS diagnosis for whom longitudinal

scans were available (although they were not part of the main cohort). The results from this study showed that atrophy can be very fast, decimating the brain tissue volume with around a 25% reduction over 8 - 10 years. While other generic lifestyle factors known to cause accelerated brain shrinkage, such as drinking alcohol, smoking, and diabetes, are important to consider, the mechanisms are very different as the rate of atrophy only increases slowly over decades, and even then the volume loss is only around half of that seen in patients with mitochondrial disease.

This fact makes identifying those susceptible to stroke-like episodes, and therefore also this rapid atrophy, an important endeavour if this process is to be understood to allow preventative treatments to be developed. To date, the atrophy associated with neurodegeneration in patients with mitochondrial disease has only been monitored visually, but this does not provide an accurate assessment of either the rate, or the true volume loss.

The very small, again opportunistic, longitudinal study of atrophy scans indicates that understanding the mechanisms for the onset of rapid atrophy are likely to be closely linked to the onset of stroke-like episodes as the brain volumes were normal for the head size and age at the first scan, but there is currently no information to suggest whether there is a causal relationship between the two, so the only way to increase characterisation of these changes is to being to carry out longitudinal, quantitative monitoring of brain volumes.

Looking at the results for GM and WM volumes in Figure 32 and Figure 33 it is clear that despite the individual differences, there are clear differences between the control and carrier groups, even in the absence of obvious neurological symptoms that equate to carriers of the m.3243A>G point mutation having a smaller percentage of GM, and higher percentage of white matter, in the make-up of their brain tissue.

The regional analysis of GM in the form of cortical thickness allowed me to carry out a systematic investigation of brain regions and to identify which regions are significantly thinner in carriers as well as in patients with MELAS. Perhaps one of the most surprising results is the observation that the precentral, paracentral, and postcentral gyri are significantly thinner in carriers than in controls and this results does fit with clinical reporting of movement disorders and a slow mental processing speed across both carriers and patients with MELAS. One area that has the cortical thickness preserved in both carriers and patients with MELAS is the frontal pole and

this region warrants further attention to ascertain if there is some sort of compensatory mechanism in place protecting this particular area. Other than the areas already mentioned, the occipital and parietal lobes are not significantly different between controls and carriers. This is in stark contrast to the temporal lobe, in which a number of regions are significantly thinner in carriers of the m.3243A>G point mutation compared to controls. These differences are most pronounced in the entorhinal cortex, fusiform gyrus, and temporal pole. It is important to note that these changes are seen even in the carriers who have no reported symptoms. However, even from this starting point of being significantly thinner in carriers than in controls, the temporal lobe undergoes further thinning, of around 10%, along with all of the other lobes after the onset of stroke-like episodes. Therefore, the existence of these differences between carrier and control brains are unlikely to be directly related to the onset of stroke-like episodes without some other type of mechanism being present as well.

As has already been mentioned, this study was only able to take a snapshot of the brains of everyone who had scans. This means that this study is not able to provide any information regarding the starting state of the brain of each person, or to provide an insight into any changes that happen over time that may provide key information about any causal processes that lead to some people with the m.3243A>G point mutation going on to develop stroke-like episodes and rapid atrophy.

The complex nature of mitochondrial disease and the extremely large individual variations suggests that the only way to get a true perspective on neurological disease progression is to carry out quantitative analysis, not only of brain volumes, but also on other quantitative measures that can be made of the brain, such as quantitative T_1 values, connectivity analysis, functional analysis using fMRI, along with non-scanning quantitative measures such as cognitive function tests. This clearly places a large assessment and analysis burden against carrying out this type of monitoring, but the inaccessibility of the brain and the rapid neurodegeneration suffered by MELAS patients is unlikely to be any better understood until this type of quantitative, longitudinal analysis is introduced.

9.1.ii TBSS

TBSS is a method for carrying out analysis across the whole of the brain to assess whether there are significant variations in FA between either different groups, or between different time points for an individual.

The TBSS analysis that was carried out looked at the differences between the carrier and MELAS groups. The control group utilised in the other sections of the study could not be used as they did not have a DTI scan taken as part of their scanning protocol. While this limited the group comparisons that could be made, it also highlighted the importance of having understanding of the analysis techniques prior to recruiting participants and collecting the scans for analysis. The aims of the analysis also need to be clearly defined as in this study it was only possible to compare the carrier group to the group with MELAS, which could only provide information on generic differences between the two and it was not possible to extract any information on individual differences and the extent to which these may have affected the group comparison.

While the results gave a couple of regions of interest that appear to be significantly different between groups, there were indications, in the form of many small regions of significantly different FA, distributed globally throughout the brain that potentially many regions may show altered FA but these are specific to individuals and only small patches of these are highlighted in the groupwise analysis.

With the increased understanding of what this technique is and what it shows, there are obvious improvements that can be made in improving future scan collection and analysis. The two biggest factors that will have an impact upon the outputs are:

- Increase in the numbers of participants in each group to much better ascertain whether there are any true group differences between controls, carriers, and patients with MELAS.
- Carry out longitudinal DTI scans of all three groups so that changes within an individual brain can be assessed over time. This will provide information on:
    - FA changes that occur in a healthy brain to inform what size of change is clinically significant,

- FA changes that are observed in carriers who will eventually fall into one of two categories, those who do not go on to develop stroke-like episodes and rapid atrophy, and those do,
- FA changes associated with the rapid atrophy and ongoing stroke-like episodes in patients with MELAS.

This method allows for generic analysis to be carried out across the whole brain, but more detailed analysis of white matter tracts and connectivity is also possible, and highly recommended, as specific regions of interest are defined in the volumetric analysis, and also potentially in future fMRI work. This again will require careful assessment of the scan requirements for each type of analysis prior to the capture of the scans, or possibly even prior to the recruitment of the participants.

9.1.iii Ultra-high-resolution MRI scanning

As this project has developed it has become clear that complete answers about any aspect of mitochondrial disease are highly unlikely to come from a single imaging modality. Perhaps the most obvious pairing to make is that of neuropathological staining and MRI, but until recently there have been practical issues preventing co-registration of imagery.

Every imaging and analysis modality in this research area is moving towards quantitative analysis, but the development of complementary techniques is still very much in its infancy.

This study identified an opportunity to carry out initial development of an ultra-high-resolution MRI scanning protocol on a 7 T pre-clinical scanner that would potentially allow registration with a CLARITY image that would be generated after the MRI scanning had completed and after subsequent staining of a target of interest had been carried out.

During the work there were a number of key issues that were highlighted that are very important if this work is to be taken forward and the desired multi-modal imaging is to be achieved:

- The MRI scans must be carried out prior to the tissue sections being mounted in hydrogel as the stripping out of the lipids reduces the T_1 values to such an extent that the desired image spatial resolution is not possible to achieve and

this also has the knock-on effect that the images are not easily relatable to any *in vivo* scans,

- The treatment of the tissue sections during the rest of the CLARITY process currently requires the tissue section to be free to move within various solutions. This movement away from the original position in which the MRI scan is done creates a huge challenge in the image registration process and either features need to be identified that will allow some sort of algorithmic registration to be carried out, or development of a CLARITY process that allows the tissue section to remain flat and in the MRI scan position.

The challenges of achieving this type of image registration should not be underestimated as it has recently been found that there is an entire PhD studentship dedicated to this exact subject.

Despite the challenges identified within this section of the study, good progress was made in understanding the capabilities and limitations of using a 7 T pre-clinical scanner to generate ultra-high-resolution MRIs of post mortem tissue. The pixel resolution achieved was 39 μm^2, which is almost small enough to begin to think about attempting to register the images against neuropathological images, but the thickness of the image slice was too large, at 125 µm. These limits were mostly imposed by the effects of the hydrogel on the tissue sample and the reduction of T_1 values to a fraction of those found in fixed tissue and it should be expected that these limits can be relatively easily surpassed using fixed tissue samples with similar scanning protocols.

The full effects of mounting the tissue samples in hydrogel did not become apparent until quantitative T_1 mapping was carried out on each section. This highlighted the reduction in T_1 values and also that the grey and white matter had been affected very differently by the process, which ultimately led to an inversion of the expected relationship between the T_1 values in each type of matter. This, again, highlights the importance of carrying out quantitative measurement and analysis as it provides a much greater level of detail, and therefore a greater potential contribution to the understanding of an observation or process, than qualitative analysis.

The quantitative T_1 mapping also showed the benefits of carrying out quantitative analysis as, even in the hydrogel-affected samples, it was possible to differentiate

between the different cortical layers, as well as seeing a clear boundary between the grey and white matter, which was not always obvious in the qualitative MRIs.

Multi-disciplinary investigation of tissue samples was last attempted in the early 90s, but neither the neuropathological methods nor the MRI scan protocols were at a stage where the desired outputs could be achieved. These are now in place and it is time to bring multiple disciplines together and align the aims and outputs to increase the amount of information it is possible to extract from the captured data.

9.2 Implications of this study

The implications of this study are that just being a carrier of the m.3243A>G point mutation is enough to lead to significant differences in the brain compared to healthy controls. Some of these changes affect every single person with the mutation, and so these are unlikely to be directly correlated with the later development of stroke-like episodes, unless there are threshold values. The changes in the brains of carriers of the m.3243A>G point mutation are not always what would be expected, for example the higher values for FA found in this study, the percentage of the brain cavity filled with brain tissue, and the significantly thinner cortex in the pre-, para-, and post-central gyrus that has not been reported previously. This study has shown the potential for structural MRI analysis to provide novel information about the effects of carrying the m.3243A>G point mutation, as well as demonstrating the devastating speed of atrophy that generally accompanies the occurrence of stroke-like episodes and the absolute importance of the opportunity to either delay or prevent the onset by identifying a predictive biomarker. Head size, in the form of TICV, appears to be a potentially easy to measure predictor of disease severity in carriers of the m3243A>G, and therefore also of potential susceptibility to stroke-like episodes.

However, perhaps the biggest implication of this study is that we are only just beginning to identify and pursue the techniques required to gain a solid understanding of the mechanisms associated with mitochondrial disease and why the disease is so heterogeneous in nature even within a single genotype.

9.3 Study Limitations

This section summarises the limitations of this study that have not been detailed in Section 9.1.

Chapter 4 – Accuracy of segmentation software

This work, although providing justification for the choice of software used in this specific study, is perhaps not valid for scans from other scanners, or using alternative MRI protocols for anatomical imaging of the brain. The study also only compared the segmentation results produced by a single individual. For a more robust validation, the manual segmentation would need to be carried out my multiple people. This study also only considered two of the possible options for global segmentation. Although these are the two pieces of software most often used for global segmentation, it could be argued that FreeSurfer should also have been included, and also the validation extended to validation the regional volumes produced by FreeSurfer, however time constraints led to this option not being taken.

The major consideration to be taken forwards is that there is currently no segmentation software, or method, that has been fully validated and confirmed to accurately and repeatably represent the actual tissue differences within the brain. This lack of validated segmentation method is compounded by the lack of a standard MRI scanning protocol for anatomical scans, and the increasing use of alternative protocols for enhanced tumour and lesion contrast in place of the preferred MPRAGE scan protocols that are optimised for healthy tissue classification.

Chapter 5 and 6 – Global and Regional segmentation

The volumetric work in this this section of the study set out a straightforward protocol to follow to measure and analyse brain volumes. The initial concept of grouping together all participants carrying the m.3243A>G point mutation was quickly seen to be inadequate and that there are significant differences between those with diagnoses of MELAS, and those without. This indicates that much more thought and preparation needs to go into the selection of study participants to be able to gain the most information from the work carried out.

This phase of work specifically used hypotheses that allow for the use of smaller sample sizes with the aim of providing more clinically relevant results. This approach was successful for this study, but more subtle, but still clinically significant differences may have been missed due to the lack of power.

The inclusions of patients with lesions led to them having to be removed from much of the analysis as there are currently no effective methods to analyse global volumes

while taking into account the effects of the presence of the lesions due to misclassification of those areas.

The lack of 3D anatomical MRI scan history for any of the participants of this study meant that the results from the analysis carried out had to be compared between participant groups. This lack of history means that vital information about the starting point of each person was not available, so a true measure of their changes could not be assessed. To begin to put together more meaningful change observations, longitudinal scans will need to be taken from the point of identification of the genetic diagnosis so that in addition to group comparisons, individual comparisons with their previous scans can also be made.

Chapter 7 – TBSS

There are a number of learning points that came out of this section of the study. The first is that the use of DTI scans is not straightforward and that both the scan protocols and the analysis methods have to be carefully selected along with having a sound understanding of how the analysis methods treat the recorded data.

This method could provide a particularly powerful longitudinal analysis method as one of the analysis options is to specifically compare the current measure of fractional anisotropy against previously recorded measures for an individual. This, like the volumetric methods, could provide valuable information about how the brain of an individual changes over time, which then allows more insight to be gained on the variation in progression patterns, symptom onset, and also overall severity.

There are techniques that allow much more detailed analysis of white matter tracts to be undertaken, but these have a significant time burden associated with them and also require very specific regions of interest to be identified to optimise the analysis techniques. The identification of the temporal pole as a key region of interest in both carriers and patients with MELAS, provides the first definitive area that could be investigated as it is known that it is affected in all carriers of the m.3243A>G point mutation, but what is unknown is whether there are additional connectivity, or network, differences that may facilitate development of stroke-like episodes.

There is also an ongoing debate about whether it is better to use DTI or DKI scans. Each one has advantages and disadvantages and these need to be better explored

to identify which method could provide the most useful information about the brains of people with the m.3243A>G point mutation.

Chapter 8 – Ultra-high-resolution 7 T MRI of post mortem brain sections

It is clear that the greatest limitation in this work was the fact that the brain sections that were available had already been mounted in hydrogel, which had removed the lipids from the sections. This significantly altered the physical properties of the tissue making it difficult to obtain the highest quality MRI scans. If the scans were to be carried out prior to mounting in hydrogel the resolution limits of the ultra-high-resolution scanning would be increased, and it would also be possible to get much more useful information about the cortical layers using higher resolution quantitative T_1 mapping. To date, the capabilities of a 7 T pre-clinical MRI scanner have not been pushed to their limits, but in the future higher field scanners should be considered should these limits need to be pushed further to obtain the resolution required to achieve true image registration with CLARITY stained tissue sections.

To fully take this work forwards the cellular targets for the neuropathological staining would need to be defined and the CLARITY process optimised.

The biggest challenge for researchers in this area is currently finding a way to achieve image registration between the CLARITY images and MRIs. The CLARITY process, as it stands, requires the section to be suspended in solutions containing the required antibodies, and the MRI scans are taken prior to this, so the key problem to solve to take this forwards is how to reorient, or prevent movement of, the section to allow the images to be fully registered to each other. Once this problem is resolved, this will provide an incredibly powerful analysis technique to potentially allow analysis at the post mortem cellular level to be ultimately applied to *in vivo* imaging to understand and assess real-time changes in cellular function.

9.4 Concluding remarks

In conclusion, the methods presented in this thesis form a starting point for a standardisation of MRI processing that can be used across the mitochondrial disease population, while the data has expanded upon current knowledge by systematically looking at the structural properties of the brains of individuals harbouring the m.3243A>G point mutation and may have allowed the identification of TICV as a surrogate marker for susceptibility to stroke-like episodes. To effectively achieve a

greater level of understanding larger sample sizes, longitudinal studies, and an emphasis on quantitative measurement and analysis that are clinically significant, are required in all areas with a multi-disciplinary approach being identified as the most effective way to achieve significant progression in the understanding of mitochondrial disease.

Chapter 10. References

Abe, K., Yoshimura, H., Tanaka, H., Fujita, N., Hikita, T. and Sakoda, S. (2004) 'Comparison of conventional and diffusion-weighted MRI and proton MR spectroscopy in patients with mitochondrial encephalomyopathy, lactic acidosis, and stroke-like events', Neuroradiology, 46(2), pp. 113-117.

Abe, O., Okubo, T., Hayashi, N., Saito, N., Iriguchi, N., Shirouzu, I., Kojima, Y., Masumoto, T., Ohtomo, K. and Sasaki, Y. (2000) 'Temporal changes of the apparent diffusion coefficients of water and metabolites in rats with hemispheric infarction: Experimental study of transhemispheric diaschisis in the contralateral hemisphere at 7 tesla', Journal of Cerebral Blood Flow and Metabolism, 20(4), pp. 726-735.

Alberts, B., Johnson, A., Morgan, D., Raff, M., Roberts, K. and Walter, P. (2008) Molecular Biology of the Cell. 5th edn. New York: Garland Science.

Alvim, M.K.M., Coan, A.C., Campos, B.M., Yasuda, C.L., Oliveira, M.C., Morita, M.E. and Cendes, F. (2016) 'Progression of gray matter atrophy in seizure-free patients with temporal lobe epilepsy', Epilepsia, 57(4), pp. 621-629.

Amedi, A., Malach, R., Hendler, T., Peled, S. and Zohary, E. (2001) 'Visuo-haptic object-related activation in the ventral visual pathway', Nature Neuroscience, 4(3), pp. 324-330.

Anderson, S., Bankier, A.T., Barrell, B.G., Debruijn, M.H.L., Coulson, A.R., Drouin, J., Eperon, I.C., Nierlich, D.P., Roe, B.A., Sanger, F., Schreier, P.H., Smith, A.J.H., Staden, R. and Young, I.G. (1981) 'Sequence and Organization of the Human Mitochondrial Genome', Nature, 290(5806), pp. 457-465.

Antunes, J., Viswanath, S., Brady, J. T., Crawshaw, B., Ros, P., Steele, S., Delaney, C. P., Paspulati, R., Willis, J., Madabhushi, A. (2018) ‘Coregistration of Preoperative MRI with Ex Vivo Mesorectal Pathology Specimens to Spatially Map Post-Treatment Changes in Rectal Cancer onto In Vivo Imaging: Preliminary Findings’, Acta Radiol., 25(7), pp. 833-841.

Apostolova, L.G., White, M., Moore, S.A. and Davis, P.H. (2005) 'Deep white matter pathologic features in watershed regions - A novel pattern of central nervous system involvement in MELAS', Archives of Neurology, 62(7), pp. 1154-1156.

Aribisala, B.S., He, J.B. and Blamire, A.M. (2011) 'Comparative Study of Standard Space and Real Space Analysis of Quantitative MR Brain Data', Journal of Magnetic Resonance Imaging, 33(6), pp. 1503-1509.

Ashburner, J. and Friston, K.J. (2000) 'Voxel-based morphometry - The methods', Neuroimage, 11(6), pp. 805-821.

Ashburner, J. and Friston, K.J. (2001) 'Why voxel-based morphometry should be used', Neuroimage, 14(6), pp. 1238-1243.

Ashburner, J. and Friston, K.J. (2005) 'Unified segmentation', Neuroimage, 26(3), pp. 839-851.

Bakker, C.J.G. and Vriend, J. (1984) 'Multi-Exponential Water Proton Spin-Lattice Relaxation in Biological Tissues and its Implications for Quantitative NMR Imaging', Physics in Medicine and Biology, 29(5), pp. 509-518.

Bale, S.J., Amos, C.I., Parry, D.M., and Bale, A.E. (1991) ‘Relationship between head circumference and height in normal adults and in the nevoid basal cell carcinoma syndrome and neurofibromatosis type I’, Am. J. Med. Genet, 40, pp. 206-210.

Barakovic, M., Girard, G., Romascano, D.P.R., Patino Lopez, J.R., Descoteaux, M., Innocenti, G., Jones, D.K., Thiran, J.-P. and Daducci, A. 'Assessing feasibility and reproducibility of a bundle-specific framework on in vivo axon diameter estimates at 300mT/m', ISMRM. Paris, France, 2018.

Barral, J.K., Gudmundson, E., Stikov, N., Etezadi-Amoli, M., Stoica, P. and Nishimura, D.G. (2010) 'A Robust Methodology for In Vivo T-1 Mapping', Magnetic Resonance in Medicine, 64(4), pp. 1057-1067.

Battaglini, M., Jenkinson, M. and De Stefano, N. (2012) 'Evaluating and reducing the impact of white matter lesions on brain volume measurements', Human Brain Mapping, 33(9), pp. 2062-2071.

Bereiterhahn, J. and Voth, M. (1994) 'Dynamices of Mitochondria in Living Cells - Shape Changes, Dislocations, Fusion, and Fission of Mitochondria', Microscopy Research and Technique, 27(3), pp. 198-219.

Betts, J., Jaros, E., Perry, R.H., Schaefer, A.M., Taylor, R.W., Abdel-All, Z., Lightowlers, R.N. and Turnbull, D.M. (2006) 'Molecular neuropathology of MELAS: level of heteroplasmy in individual neurones and evidence of extensive vascular involvement', Neuropathology and Applied Neurobiology, 32(4), pp. 359-373.

Bi, K.L., Baehring, J.M. and Lesser, R.L. (2006) 'Evolution of brain imaging abnormalities in mitochondrial encephalomyopathy with lactic acidosis and stroke-like episodes', Journal of Neuro-Ophthalmology, 26(4), pp. 251-256.

Biberacher, V., Schmidt, P., Keshavan, A., Boucard, C. C., Righart, R., Sämann, P., Preibisch, C., Fröbel, D., Aly, L., Hemmer, B., Zimmer, C., Henry, R. G., Mühlau, M. (2016), 'Intra- and interscanner variability of magnetic resonance imaging based volumetry in multiple sclerosis', NeuroImage, 142, pp. 188-197.

Biessels, G.J. and Reijmer, Y.D. (2014) 'Brain Changes Underlying Cognitivie Dysfunction in Diabetes: What Can We Learn From MRI?', Diabetes, 63, pp. 2244-2252.

Birkl, C., Langkammer, C., Golob-Schwarzl, N., Leoni, M., Haybaeck, J., Goessler, W., Fazekas, F. and Ropele, S. (2016) 'Effects of formalin fixation and temperature on MR relaxation times in the human brain', NMR in Biomedicine, 29(4), pp. 458-465.

Birky, C.W. (1994) 'Relaxed and Stringent Genomes - Why Cytoplasmic Genes Don't Obey Mendel's Laws', Journal of Heredity, 85(5), pp. 355-365.

Blamire, A. M., Rowe, J. G., Styles, P., McDonald, B. (1999) 'Optimising imaging parameters for the post-mortem MRI of human brain', Acta Radiol., 40, pp. 593-597

Block, K.T. (2018) ISMRM. Paris, France.

Boczonadi, V. and Horvath, R. (2014) 'Mitochondria: Impaired mitochondrial translation in human disease', International Journal of Biochemistry & Cell Biology, 48, pp. 77-84.

Bodini, B., Branzoli, F., Poirion, E., Garcia-Lorenzo, D., Didier, M., Maillart, E., Socha, J., Bera, G., Lubetzki, C., Ronen, I., Lehericy, S. and Stankoff, B. (2018)

'Dysregulation of energy metabolism in multiple sclerosis measured in vivo with diffusion-weighted spectroscopy', Multiple Sclerosis Journal, 24(3), pp. 313-321.

Boesch, P., Weber-Lotfi, F., Ibrahim, N., Tarasenko, V., Cosset, A., Paulus, F., Lightowlers, R.N. and Dietrich, A. (2011) 'DNA repair in organelles: Pathways, organization, regulation, relevance in disease and aging', Biochimica Et Biophysica Acta-Molecular Cell Research, 1813(1), pp. 186-200.

Bogenhagen, D. and Clayton, D.A. (1977) 'Mouse L-Cell Mitochondrial-DNA Molecules are Selected Randomly for Replication Throughout Cell-Cycle', Cell, 11(4), pp. 719-727.

Bookstein, F.L. (2001) '"Voxel-based morphometry" should not be used with imperfectly registered images', Neuroimage, 14(6), pp. 1454-1462.

Boorman, E.D. and Rushworth, M.F.S. (2009) 'Conceptual Representation and the Making of New Decisions', Neuron, 63(6), pp. 721-723.

Bourbon-Teles, J., Bells, S., Jones, D.K., Coulthard, E., Rosser, A. and Metzler-Baddeley, C. (2017) 'Myelin breakdown in human Huntington's disease: Multi-modal evidence from diffusion MRI and quantitative magnetization transfer', Neuroscience.

Bowen, J., Richards, T. and Maravilla, K. (1998) 'MR imaging and proton MR spectroscopy in A-to-G substitution at nucleotide position 3243 of leucine transfer RNA', American Journal of Neuroradiology, 19(2), pp. 231-234.

Branzoli, F., Ercan, E., Webb, A. and Ronen, I. (2014) 'The interaction between apparent diffusion coefficients and transverse relaxation rates of human brain metabolites and water studied by diffusion- weighted spectroscopy at 7 T', Nmr in Biomedicine, 27(5), pp. 495-506.

Brown, D.T., Samuels, D.C., Michael, E.M., Turnbull, D.M. and Chinnery, P.F. (2001) 'Random genetic drift determines the level of mutant mtDNA in human primary oocytes', American Journal of Human Genetics, 68(2), pp. 533-536.

Brown, G.K. and Squier, M.V. (1996) 'Neuropathology and pathogenesis of mitochondrial diseases', Journal of Inherited Metabolic Disease, 19(4), pp. 553-572.

Brown, T.A., Cecconi, C., Tkachuk, A.N., Bustamante, C. and Clayton, D.A. (2005) 'Replication of mitochondrial DNA occurs by strand displacement with alternative

light-strand origins, not via a strand-coupled mechanism', Genes & Development, 19(20), pp. 2466-2476.

Brown, W.M., George, M. and Wilson, A.C. (1979) 'Rapid Evolution of Animal Mitochondrial-DNA', Proceedings of the National Academy of Sciences of the United States of America, 76(4), pp. 1967-1971.

Busby, K.M.D., Cole, T., Matthews, J.N.S., and Goodship, J.A. (1992) 'Centiles for adult head circumference', Archives of Disease in Childhood, 67, pp. 1286-1287.

Calkins, M.J. and Reddy, P.H. (2011) 'Assessment of newly synthesized mitochondrial DNA using BrdU labeling in primary neurons from Alzheimer's disease mice: Implications for impaired mitochondrial biogenesis and synaptic damage', Biochimica Et Biophysica Acta-Molecular Basis of Disease, 1812(9), pp. 1182-1189.

Cantor-Rivera, D., Baxter, J.S.H., de Ribaupierrre, S., Lau, J.C., Mirsattari, S.M., Goubran, M., Burneo, J.G., Steven, D.A., Peters, T.M. and Khan, A.R. (2016) 'Individual feature maps: a patient-specific analysis tool with applications in temporal lobe epilepsy', International Journal of Computer Assisted Radiology and Surgery, 11(1), pp. 53-71.

Cash, D.M., Frost, C., Iheme, L.O., Unay, D., Kandemir, M., Fripp, J., Salvado, O., Bourgeat, P., Reuter, M., Fischl, B., Lorenzi, M., Frisoni, G.B., Pennec, X., Pierson, R.K., Gunter, J.L., Senjem, M.L., Jack, C.R., Guizard, N., Fonov, V.S., Collins, D.L., Modat, M., Cardoso, M.J., Leung, K.K., Wang, H.Z., Das, S.R., Yushkevich, P.A., Malone, I.B., Fox, N.C., Schott, J.M. and Ourselin, S. (2015) 'Assessing atrophy measurement techniques in dementia: Results from the MIRIAD atrophy challenge', Neuroimage, 123, pp. 149-164.

Castillo, J., Rodriguez, J.R., Corredera, E., Alvarex, J.M., Purmar, J.M. and Noya, M. (1996) 'White matter high-signal areas on MRI associated with chronic hypoxia', European Journal of Neurology, 3(6), pp. 533-538.

Cavalier-Smith, T. (2006) 'Origin of mitochondria by intracellular enslavement of a photosynthetic purple bacterium', Proceedings of the Royal Society B-Biological Sciences, 273(1596), pp. 1943-1952.

Chen, H.C. and Chan, D.C. (2004) 'Mitochondrial dynamics in mammals', Current Topics in Developmental Biology, Vol 59, 59, pp. 119-+.

Chen, H.C. and Chan, D.C. (2009) 'Mitochondrial dynamics-fusion, fission, movement, and mitophagy-in neurodegenerative diseases', Human Molecular Genetics, 18, pp. R169-R176.

Chenevert, T. (2018) ISMRM. Paris, France.

Chi, C.S., Lee, H.F., Tsai, C.R., Lee, H.J. and Chen, L.H. (2010) 'Clinical Manifestations in Children With Mitochondrial Diseases', Pediatric Neurology, 43(3), pp. 183-189.

Chiang, S.R., Levin, H.S., Wilde, E. and Haneef, Z. (2016) 'White matter structural connectivity changes correlate with epilepsy duration in temporal lobe epilepsy', Epilepsy Research, 120, pp. 37-46.

Chinnery, P.F., Elliott, C., Green, G.R., Rees, A., Coulthard, A., Turnbull, D.M. and Griffiths, T.D. (2000a) 'The spectrum of hearing loss due to mitochondrial DNA defects', Brain, 123, pp. 82-92.

Chinnery, P.F., Howell, N., Lightowlers, R.N. and Turnbull, D.M. (1997) 'Molecular pathology of MELAS and MERRF - The relationship between mutation load and clinical phenotypes', Brain, 120, pp. 1713-1721.

Chinnery, P.F., Thorburn, D.R., Samuels, D.C., White, S.L., Dahl, H.H.M., Turnbull, D.M., Lightowlers, R.N. and Howell, N. (2000b) 'The inheritance of mitochondrial DNA heteroplasmy: random drift, selection or both?', Trends in Genetics, 16(11), pp. 500-505.

Choi, S.Y., Kim, Y., Oh, S.W., Jeong, S.H. and Kim, J.S. (2012) 'Pursuit-Paretic and Epileptic Nystagmus in MELAS', Journal of Neuro-Ophthalmology, 32(2), pp. 135-138.

Chrysostomou, A., Grady, J.P., Laude, A., Taylor, R.W., Turnbull, D.M. and Lax, N.Z. (2016) 'Investigating complex I deficiency in Purkinje cells and synapses in patients with mitochondrial disease', Neuropathology and Applied Neurobiology, 42(5), pp. 477-492.

Chu, Z., Wilde, E.A., Hunter, J.V., McCauley, S.R., Bigler, E.D., Troyanskaya, M., Yallampalli, R., Chia, J.M. and Levin, H.S. (2010) 'Voxel-Based Analysis of Diffusion

Tensor Imaging in Mild Traumatic Brain Injury in Adolescents', American Journal of Neuroradiology, 31(2), pp. 340-346.

Ciafaloni, E., Ricci, E., Shanske, S., Moraes, C.T., Silvestri, G., Hirano, M., Simonetti, S., Angelini, C., Donati, M.A., Garcia, C., Martinuzzi, A., Mosewich, R., Servidei, S., Zammarchi, E., Bonilla, E., Devivo, D.C., Rowland, L.P., Schon, E.A. and Dimauro, S. (1992) 'MELAS - Clinical-Features, Biochemistry, and Molecular-Genetics', Annals of Neurology, 31(4), pp. 391-398.

Clare, S. and Jezzard, P. (2001) 'Rapid T-1 mapping using multislice echo planar imaging', Magnetic Resonance in Medicine, 45(4), pp. 630-634.

Clark, J.M., Marks, M.P., Adalsteinsson, E., Spielman, D.M., Shuster, D., Horoupian, D. and Albers, G.W. (1996) 'MELAS: Clinical and pathologic correlations with MRI, xenon/CT, and MR spectroscopy', Neurology, 46(1), pp. 223-227.

Clayton, D.A. (1982) 'Replication of Animal Mitochondrial-DNA', Cell, 28(4), pp. 693-705.

Coan, A.C., Campos, B.M., Yasuda, C.L., Kubota, B.Y., Bergo, F.P.G., Geurreiro, C.A.M. and Cendes, F. (2014) ‘Frequent Seizures Are Associated with a Network of Gray Matter Atrophy in Temporal Lobe Epilepsy with or without Hippocampal Sclerosis’, PLOS One, 9(1), pp. 1-9.

Course, M.M. and Wang, X. (2016) 'Transporting Mitochondria in Neurons [version 1; referees: 2 approved]', F1000Research, 5(F1000 Faculty Rev).

Craven, L., Tuppen, H.A., Greggains, G.D., Harbottle, S.J., Murphy, J.L., Cree, L.M., Murdoch, A.P., Chinnery, P.F., Taylor, R.W., Lightowlers, R.N., Herbert, M. and Turnbull, D.M. (2010) 'Pronuclear transfer in human embryos to prevent transmission of mitochondrial DNA disease', Nature, 465(7294), pp. 82-U89.

Cree, L.M., Samuels, D.C., Lopes, S., Rajasimha, H.K., Wonnapinij, P., Mann, J.R., Dahl, H.H.M. and Chinnery, P.F. (2008) 'A reduction of mitochondrial DNA molecules during embryogenesis explains the rapid segregation of genotypes', Nature Genetics, 40(2), pp. 249-254.

D'Arceuil, H. and de Crespigny, A. (2007) 'The effects of brain tissue decomposition on diffusion tensor imaging and tractography', Neuroimage, 36(1), pp. 64-68.

Dale, A.M., Fischl, B. and Sereno, M.I. (1999) 'Cortical surface-based analysis - I. Segmentation and surface reconstruction', Neuroimage, 9(2), pp. 179-194.

Daw, N.D., Courville, A.C. and Touretzky, D.S. (2006) 'Representation and timing in theories of the dopamine system', Neural Computation, 18(10), pp. 2582-2582.

Dawe, R.J., Bennett, D.A., Schneider, J.A., Vasireddi, S.K. and Arfanakis, K. (2009) 'Post mortem MRI of Human Brain Hemispheres: T-2 Relaxation Times During Formaldehyde Fixation', Magnetic Resonance in Medicine, 61(4), pp. 810-818.

De Vos, K.J., Grierson, A.J., Ackerley, S. and Miller, C.C.J. (2008) 'Role of axonal transport in neurodegenerative diseases', in Annual Review of Neuroscience. Palo Alto: Annual Reviews, pp. 151-173.

Debernard, L., Melzer, T.R., Alla, S., Eagle, J., Van Stockum, S., Graham, C., Osborne, J.R., Dalrymple-Alford, J.C., Miller, D.H. and Mason, D.F. (2015) 'Deep grey matter MRI abnormalities and cognitive function in relapsing-remitting multiple sclerosis', Psychiatry Res, 234(3), pp. 352-61.

Deelchand, D.K., Auerbach, E.J. and Marjanska, M. (2018) 'Apparent diffusion coefficients of the five major metabolites measured in the human brain in vivo at 3T', Magnetic Resonance in Medicine, 79(6), pp. 2896-2901.

Deheshi, S., Dabiri, B., Fan, S., Tsang, M. and Rintoul, G.L. (2015) 'Changes in Mitochondrial Morphology Induced by Calcium or Rotenone in Primary Astrocytes Occur Predominantly Through ROS-Mediated Remodeling', Journal of Neurochemistry, 133(5), pp. 684-699.

Desikan, R.S., Segonne, F., Fischl, B., Quinn, B.T., Dickerson, B.C., Blacker, D., Buckner, R.L., Dale, A.M., Maguire, R.P., Hyman, B.T., Albert, M.S. and Killiany, R.J. (2006) 'An automated labeling system for subdividing the human cerebral cortex on MRI scans into gyral based regions of interest', Neuroimage, 31(3), pp. 968-980.

DiMauro, S. (2006) 'Mitochondrial diseases: An update', Journal of Inherited Metabolic Disease, 29, pp. 6-6.

DiMauro, S. and Schon, E.A. (2003) 'Mechanisms of disease: Mitochondrial respiratory-chain diseases', New England Journal of Medicine, 348(26), pp. 2656-2668.

Dinkelacker, V., Valabregue, R., Thivard, L., Lehericy, S., Baulac, M., Samson, S. and Dupont, S. (2015) 'Hippocampal-thalamic wiring in medial temporal lobe epilepsy: Enhanced connectivity per hippocampal voxel', Epilepsia, 56(8), pp. 1217-1226.

Durand-Dubief, F., Belaroussi, B., Armspach, J.P., Dufour, M., Roggerone, S., Vukusic, S., Hannoun, S., Sappey-Marinier, D., Confavreux, C. and Cotton, F. (2012) 'Reliability of Longitudinal Brain Volume Loss Measurements between 2 Sites in Patients with Multiple Sclerosis: Comparison of 7 Quantification Techniques', American Journal of Neuroradiology, 33(10), pp. 1918-1924.

Duriez, Q., Crivello, F., and Mazoyer, B. (2014) ‘Sex-related and tissue-specific effects of tobacco smoking on brain atrophy: assessment in a large longitudinal cohort of healthy elderly’, frontiers in Aging Neuroscience, 6(299), pp. 1-17.

El-Hattab, A.W., Adesina, A.M., Jones, J. and Scaglia, F. (2015) 'MELAS syndrome: Clinical manifestations, pathogenesis, and treatment options', Molecular Genetics and Metabolism, 116(1-2), pp. 4-12.

El-Khamisy, S.F. and Caldecott, K.W. (2007) 'DNA single-strand break repair and spinocerebellar ataxia with axonal neuropathy-1', Neuroscience, 145(4), pp. 1260-1266.

Elson, J.L., Samuels, D.C., Turnbull, D.M. and Chinnery, P.F. (2001) 'Random intracellular drift explains the clonal expansion of mitochondrial DNA mutations with age', American Journal of Human Genetics, 68(3), pp. 802-806.

Ercan, A.E., Techawiboonwong, A., Versluis, M.J., Webb, A.G. and Ronen, I. (2015) 'Diffusion-weighted chemical shift imaging of human brain metabolites at 7T', Magnetic Resonance in Medicine, 73(6), pp. 2053-2061.

Fabrizi, G.M., Cardaioli, E., Grieco, G.S., Cavallaro, T., Malandrini, A., Manneschi, L., Dotti, M.T., Federico, A. and Guazzi, G. (1996) 'The A to G transition at nt 3243 of the mitochondrial tRNA(Leu)(UUR) may cause an MERRF syndrome', Journal of Neurology Neurosurgery and Psychiatry, 61(1), pp. 47-51.

Falkenberg, M., Gaspari, M., Rantanen, A., Trifunovic, A., Larsson, N.G. and Gustafsson, C.M. (2002) 'Mitochondrial transcription factors B1 and B2 activate transcription of human mtDNA', Nature Genetics, 31(3), pp. 289-294.

Fedorov, A., Beichel, R., Kalpathy-Cramer, J., Finet, J., Fillion-Robin, J.C., Pujol, S., Bauer, C., Jennings, D., Fennessy, F., Sonka, M., Buatti, J., Aylward, S., Miller, J.V., Pieper, S. and Kikinis, R. (2012) '3D Slicer as an image computing platform for the Quantitative Imaging Network', Magnetic Resonance Imaging, 30(9), pp. 1323-1341.

Fischl, B. and Dale, A.M. (2000) 'Measuring the thickness of the human cerebral cortex from magnetic resonance images', Proceedings of the National Academy of Sciences of the United States of America, 97(20), pp. 11050-11055.

Fischl, B., Salat, D.H., Busa, E., Albert, M., Dieterich, M., Haselgrove, C., van der Kouwe, A., Killiany, R., Kennedy, D., Klaveness, S., Montillo, A., Makris, N., Rosen, B. and Dale, A.M. (2002) 'Whole brain segmentation: Automated labeling of neuroanatomical structures in the human brain', Neuron, 33(3), pp. 341-355.

Fischl, B., van der Kouwe, A., Destrieux, C., Halgren, E., Segonne, F., Salat, D.H., Busa, E., Seidman, L.J., Goldstein, J., Kennedy, D., Caviness, V., Makris, N., Rosen, B. and Dale, A.M. (2004) 'Automatically parcellating the human cerebral cortex', Cerebral Cortex, 14(1), pp. 11-22.

Floros, V.I., Pyle, A., Dietmann, S., Wei, W., Tang, W.W.C., Irie, N., Payne, B., Capalbo, A., Noli, L., Coxhead, J., Hudson, G., Crosier, M., Strahl, H., Khalaf, Y., Saitou, M., Ilic, D., Surani, M.A. and Chinnery, P.F. (2018) 'Segregation of mitochondrial DNA heteroplasmy through a developmental genetic bottleneck in human embryos', Nature Cell Biology, 20(2), pp. 144-+.

FMRIB (2015) FSL - FMRIB Software Library v5.0 [Computer program].

Freeborough, P.A., Fox, N.C. and Kitney, R.I. (1997) 'Interactive algorithms for the segmentation and quantitation of 3-D MRI brain scans', Computer Methods and Programs in Biomedicine, 53(1), pp. 15-25.

Freund, W., Faust, S., Birklein, F., Gaser, C., Wunderlich, A.P., Muller, M., Billich, C., Juchems, M.S., Schmitz, B.L., Gron, G. and Schutz, U.H. (2012) 'Substantial and reversible brain gray matter reduction but no acute brain lesions in ultramarathon runners: experience from the TransEurope-FootRace Project', BMC Medicine, 10, p. 11.

Friston, K.J. (2007) 'Statistical Parametric Mapping', in Penny, W., Friston, K.J., Ashburner, J., Kiebel, S. and Nichols, T. (eds.) Statistical Parametric Mapping: The Analysis of Functional Brain Images. Academic Press.

Fromont, I., Nicoli, F., Valero, R., Felician, O., Lebail, B., Lemur, Y., Mancini, J., Paquis-Flucklinger, V., Cozzone, P.J. and Vialettes, B. (2009) 'Brain anomalies in maternally inherited diabetes and deafness syndrome', Journal of Neurology, 256(10), pp. 1696-1704.

Gadda, D., Mazzoni, L.N., Pasquini, L., Busoni, S., Simonelli, P. and Giordano, G.P. (2017) 'Relationship between Apparent Diffusion Coefficients and MR Spectroscopy Findings in High-Grade Gliomas', Journal of Neuroimaging, 27(1), pp. 128-134.

Garcia-Finana, M., Cruz-Orive, L.M., Mackay, C.E., Pakkenberg, B. and Roberts, N. (2003) 'Comparison of MR imaging against physical sectioning to estimate the volume of human cerebral compartments', Neuroimage, 18(2), pp. 505-516.

Garcia-Finana, M., Keller, S.S. and Roberts, N. (2009) 'Confidence intervals for the volume of brain structures in Cavalieri sampling with local errors', Journal of Neuroscience Methods, 179(1), pp. 71-77.

Geuze, E., Vermetten, E. and Bremner, J.D. (2005) 'MR-based in vivo hippocampal volumetrics: 1. Review of methodologies currently employed', Molecular Psychiatry, 10(2), pp. 147-159.

Giles, R.E., Blanc, H., Cann, H.M. and Wallace, D.C. (1980) 'Maternal Inheritance of Human Mitochondrial-DNA', Proceedings of the National Academy of Sciences of the United States of America-Biological Sciences, 77(11), pp. 6715-6719.

Goetz, P., Blamire, A., Rajagopalan, B., Mackay, C. and Cadoux-Hudson, T.A.D. (2004) 'Evidence for neuro-plasticity after traumatic brain injury: A prospective 2-year magnetic resonance study', Journal of Neurotrauma, 21(9), pp. 1336-1336.

Goldman, J.G., Stebbins, G.T., Dinh, V., Bernard, B., Merkitch, D., deToledo-Morrell, L. and Goetz, C.G. (2014) 'Visuoperceptive region atrophy independent of cognitive status in patients with Parkinson's disease with hallucinations', Brain, 137, pp. 849-859.

Good, C.D., Scahill, R.I., Fox, N.C., Ashburner, J., Friston, K.J., Chan, D., Crum, W.R., Rossor, M.N. and Frackowiak, R.S.J. (2002) 'Automatic differentiation of anatomical patterns in the human brain: Validation with studies of degenerative dementias', Neuroimage, 17(1), pp. 29-46.

Goodfellow, J.A., Dani, K., Stewart, W., Santosh, C., McLean, J., Mulhern, S. and Razvi, S. (2012) 'Mitochondrial myopathy, encephalopathy, lactic acidosis and stroke-like episodes: an important cause of stroke in young people', Postgraduate Medical Journal, 88(1040), pp. 326-334.

Gorman, G.S., Grady, J.P. and Turnbull, D.M. (2015a) 'Mitochondrial Donation - How Many Women Could Benefit?', New England Journal of Medicine, 372(9), pp. 885-887.

Gorman, G.S., Schaefer, A.M., Ng, Y., Gomez, N., Blakely, E.L., Alston, C.L., Feeney, C., Horvath, R., Yu-Wai-Man, P., Chinnery, P.F., Taylor, R.W., Turnbull, D.M. and McFarland, R. (2015b) 'Prevalence of Nuclear and Mitochondrial DNA Mutations Related to Adult Mitochondrial Disease', Annals of Neurology, 77(5), pp. 753-759.

Gorman, G. S., Chinnery, P. F., DiMauro, S., Hirano, M., Koga, Y., McFarland, R., Suomalainen, A., Thorburn, D. R., Zeviani, M., Turnbull, D. M. (2016) ‘Mitochondrial diseases’, Nature Reviews: Disease Primers, 2, pp. 1-22

Goubran, M., Hammond, R.R., de Ribaupierre, S., Burneo, J.G., Mirsattari, S., Steven, D.A., Parrent, A.G., Peters, T.M. and Khan, A.R. (2015) 'Magnetic Resonance Imaging and Histology Correlation in the Neocortex in Temporal Lobe Epilepsy', Annals of Neurology, 77(2), pp. 237-250.

Gowland, P.A. and Stevenson, V.L. (2003) 'T1: the Longitudinal Relaxation Time', in Tofts, P. (ed.) Quantitative MRI of the Brain: Measuring Changes Caused by Disease. Chichester: Joh Wiley & Sons Ltd.

Grady, J.P., Picket, S.J., Ng, Y.S., Alston, C.L., Blakely, E.L., Hardy, S.A., Feeney, C.L., Bright, A.A., Schaefer, A.M., Gorman, G.S., McNally, R.J.Q., Taylor, R.W., Turnbull, D.M., and McFarland, R. (2018) ‘mtDNA heteroplasmy level and copy number indicate disease burden in m.3243A>G mitochondrial disease’, EMBO Mol. Med., 10(6), e8262 pp. 1-13.

Gronenschild, E., Habets, P., Jacobs, H.I.L., Mengelers, R., Rozendaal, N., van Os, J. and Marcelis, M. (2012) 'The Effects of FreeSurfer Version, Workstation Type, and Macintosh Operating System Version on Anatomical Volume and Cortical Thickness Measurements', PLOS One, 7(6), p. 13.

Gross, N.J. and Rabinowitz, M. (1969) 'Synthesis of new strands of mitochondrial and nuclear deoxyribonucleic acid by semiconservative replication', J Biol Chem, 244(6), pp. 1563-6.

Haas, R. and Dietrich, R. (2004) 'Neuroimaging of mitochondrial disorders', Mitochondrion, 4(5-6), pp. 471-490.

Haast, R.A.M., Ivanov, D., Ijsselstein, R.J.T., Sallevelt, S., Jansen, J.F.A., Smeets, H.J.M., de Coo, I.F.M., Formisano, E. and Uludag, K. (2018) 'Anatomic & metabolic brain markers of the m.3243A > G mutation: A multi-parametric 7T MRI study', Neuroimage-Clinical, 18, pp. 231-244.

Haider, L., Simeonidou, C., Steinberger, G., Hametner, S., Grigoriadis, N., Deretzi, G., Kovacs, G.G., Kutzelnigg, A., Lassmann, H. and Frischer, J.M. (2014) 'Multiple sclerosis deep grey matter: the relation between demyelination, neurodegeneration, inflammation and iron', Journal of Neurology Neurosurgery and Psychiatry, 85(12), pp. 1386-1395.

Hanna, M.G., Vaughan, J.R., Silburn, P.A., Davis, P.T.G., Greenhall, R.C.D., Squier, M.V., Mills, K.R., Renowden, S. and Sellar, A. (1997) 'Two unusual clinical presentations of the mitochondrial DNP, A3243G point mutation in adult neurological practice', Journal of Neurology Neurosurgery and Psychiatry, 62(5), pp. 544-546.

Hatefi, Y. (1985) 'The Mitochondrial Electron-Transport and Oxidative-Phosphorylation System', Annual Review of Biochemistry, 54, pp. 1015-1069.

Hegde, M.L., Izumi, T. and Mitra, S. (2012) 'Oxidized Base Damage and Single-Strand Break Repair in Mammalian Genomes: Role of Disordered Regions and Posttranslational Modifications in Early Enzymes', in Doetsch, P.W. (ed.) Mechanisms of DNA Repair. San Diego: Elsevier Academic Press Inc, pp. 123-153.

Helenius, J., Soinne, L., Perkio, J., Salonen, O., Kangasmaki, A., Kaste, M., Carano, R.A.D., Aronen, H.J. and Tatlisumak, T. (2002) 'Diffusion-weighted MR imaging in

normal human brains in various age groups', American Journal of Neuroradiology, 23(2), pp. 194-199.

Hirano, M., Ricci, E., Koenigsberger, M.R., Defendini, R., Pavlakis, S.G., Devivo, D.C., Dimauro, S. and Rowland, L.P. (1992) 'MELAS - An Original Case and Clinical-Criteria for Diagnosis', Neuromuscular Disorders, 2(2), pp. 125-135.

Holt, I.J. and Reyes, A. (2012) 'Human Mitochondrial DNA Replication', Cold Spring Harbor Perspectives in Biology, 4(12), p. 15.

Hong, H., Yao, L., Zhao, X.J. and IEEE (2009) A study of human brain structural connectivity based on diffusion tensor imaging in Alzheimer's disease. New York: IEEE.

Horvath, R., Hudson, G., Ferrari, G., Futterer, N., Ahola, S., Lamantea, E., Prokisch, H., Lochmuller, H., McFarland, R., Ramesh, V., Klopstock, T., Freisinger, P., Salvi, F., Mayr, J.A., Santer, R., Tesarova, M., Zeman, J., Udd, B., Taylor, R.W., Turnbull, D., Hanna, M., Fialho, D., Suomalainen, A., Zeviani, M. and Chinnery, P.F. (2006) 'Phenotypic spectrum associated with mutations of the mitochondrial polymerase gamma gene', Brain, 129, pp. 1674-1684.

Hubbard, N.A., Turner, M.P., Ouyang, M.H., Himes, L., Thomas, B.P., Hutchison, J.L., Faghihahmadabadi, S., Davis, S.L., Strain, J.F., Spence, J., Krawczyk, D.C., Huang, H., Lu, H.Z., Hart, J., Frohman, T.C., Frohman, E.M., Okuda, D.T. and Rypma, B. (2017) 'Calibrated Imaging Reveals Altered Grey Matter Metabolism Related to White Matter Microstructure and Symptom Severity in Multiple Sclerosis', Human Brain Mapping, 38(11), pp. 5375-5390.

Iizuka, T., Sakai, F., Kan, S. and Suzuki, N. (2003) 'Slowly progressive spread of the stroke-like lesions in MELAS', Neurology, 61(9), pp. 1238-1244.

Iizuka, T., Sakai, F., Suzuki, N., Hata, T., Tsukahara, S., Fukuda, M. and Takiyama, Y. (2002) 'Neuronal hyperexcitability in stroke-like episodes of MELAS syndrome', Neurology, 59(6), pp. 816-824.

Ikawa, M., Yoneda, M., Muramatsu, T., Matsunaga, A., Tsujikawa, T., Yamamoto, T., Kosaka, N., Kinoshita, K., Yamamura, O., Hamano, T., Nakamoto, Y. and Kimura, H. (2013) 'Detection of preclinically latent hyperperfusion due to stroke-like episodes by

arterial spin-labeling perfusion MRI in Patients with MELAS', Mitochondrion, 13(6), pp. 676-680.

Imamura, H., Matsumoto, R., Takaya, S., Nakagawa, T., Shimotake, A., Kikuchi, T., Sawamoto, N., Kunieda, T., Mikuni, N., Miyamoto, S., Fukuyama, H., Takahashi, R. and Ikeda, A. (2016) 'Network specific change in white matter integrity in mesial temporal lobe epilepsy', Epilepsy Research, 120, pp. 65-72.

Jeurissen, B., Leemans, A., Tournier, J.D., Jones, D.K. and Sijbers, J. (2013) 'Investigating the Prevalence of Complex Fiber Configurations in White Matter Tissue with Diffusion Magnetic Resonance Imaging', Human Brain Mapping, 34(11), pp. 2747-2766.

Johnson, C.P., Follmer, R.L., Oguz, I., Warren, L.A., Christensen, G.E., Fiedorowicz, J.G., Magnotta, V.A. and Wemmie, J.A. (2015) 'Brain abnormalities in bipolar disorder detected by quantitative T1 rho mapping', Molecular Psychiatry, 20(2), pp. 201-206.

Kamiya, H. (2003) 'Mutagenic potentials of damaged nucleic acids produced by reactive oxygen/nitrogen species: approaches using synthetic oligonucleotides and nucleotides', Nucleic Acids Research, 31(2), pp. 517-531.

Kan, H.E., Techawiboonwong, A., van Osch, M.J.P., Versluis, M.J., Deelchand, D.K., Henry, P.G., Marjanska, M., van Buchem, M.A., Webb, A.G. and Ronen, I. (2012) 'Differences in apparent diffusion coefficients of brain metabolites between grey and white matter in the human brain measured at 7 T', Magnetic Resonance in Medicine, 67(5), pp. 1203-1209.

Kaneda, H., Hayashi, J.I., Takahama, S., Taya, C., Lindahl, K.F. and Yonekawa, H. (1995) 'Elimination of Paternal Mitochondrial-DNA in Intraspecific Crosses During Early Mouse Embryogenesis', Proceedings of the National Academy of Sciences of the United States of America, 92(10), pp. 4542-4546.

Kasparek, T.R. and Humphrey, T.C. (2011) 'DNA double-strand break repair pathways, chromosomal rearrangements and cancer', Seminars in Cell & Developmental Biology, 22(8), pp. 886-897.

Keller, S.S., O'Muircheartaigh, J., Traynor, C., Towgood, K., Barker, G.J. and Richardson, M.P. (2014) 'Thalamotemporal impairment in temporal lobe epilepsy: A

combined MRI analysis of structure, integrity, and connectivity', Epilepsia, 55(2), pp. 306-315.

Keller, S.S. and Roberts, N. (2010) 'Measurement of brain volume using MRI: software, techniques, choices and prerequisites (vol 87, pg 127, 2009)', Journal of Anthropological Sciences, 88, pp. 251-251.

Keller, S.S., Wieshmann, U.C., Mackay, C.E., Denby, C.E., Webb, J. and Roberts, N. (2002) 'Voxel based morphometry of grey matter abnormalities in patients with medically intractable temporal lobe epilepsy: effects of side of seizure onset and epilepsy duration', Journal of Neurology Neurosurgery and Psychiatry, 73(6), pp. 648-656.

Khosravizadeh, P. and Teimournezhad, S. (2011) ‘Handedness and Lateralisation of the Brain’, Brain, 2(1), pp. 11-16.

Kikinis, R., Pieper, S. and Vosburgh, K. (2014) 3D Slicer: A Platform for Subject-Specific Image Analysis, Visualization, and Clinical Support.

Kim, H.J., Im, K., Kwon, H., Lee, J.M., Kim, C., Kim, Y.J., Jung, N.Y., Cho, H., Ye, B.S., Noh, Y., Kim, G.H., Ko, E.D., Kim, J.S., Choe, Y.S., Lee, K.H., Kim, S.T., Lee, J.H., Ewers, M., Weiner, M.W., Na, D.L. and Seo, S.W. (2015) 'Clinical effect of white matter network disruption related to amyloid and small vessel disease', Neurology, 85(1), pp. 63-70.

Kim, S.H., Akbarkhodjaeva, Z.A., Jung, I. and Kim, J.S. (2016) 'Eye movement and vestibular dysfunction in mitochondrial A3243G mutation', Neurological Sciences, 37(7), pp. 1159-1162.

Kitamura, M., Yatsuga, S., Abe, T., Povalko, N., Saiki, R., Ushijima, K., Yamashita, Y. and Koga, Y. (2016) 'L-Arginine intervention at hyper-acute phase protects the prolonged MRI abnormality in MELAS', Journal of Neurology, 263(8), pp. 1666-1668.

Kobayashi, Z., Tsunemi, T., Miake, H., Tanaka, S., Watabiki, S. and Morokuma, Y. (2005) 'A mother and a child with maternally inherited diabetes and deafness (MIDD) showing atrophy of the cerebrum, cerebellum and brainstem on magnetic resonance imaging (MRI)', Internal Medicine, 44(4), pp. 328-331.

Koechlin, E., Danek, A., Brunod, Y. and Grafman, J. (2002) 'Medial prefrontal and subcortical mechanisms underlying the acquisition of motor and cognitive action sequences in humans', Neuron, 35(2), pp. 371-381.

Koga, Y., Povalko, N., Nishioka, J., Katayama, K., Kakimoto, N. and Matsuishi, T. (2010) 'MELAS and L-arginine therapy: pathophysiology of stroke-like episodes', in Wei, Y.H., Tzeng, C.R. and Lee, H.M. (eds.) Mitochondrial Research in Translational Medicine. Malden: Wiley-Blackwell, pp. 104-110.

Kolb, S.J., Costello, F., Lee, A.G., White, M., Wong, S., Schwartz, E.D., Messe, S.R., Ellenbogen, J., Kasner, S.E. and Galetta, S.L. (2003) 'Distinguishing ischemic stroke from the stroke-like lesions of MELAS using apparent diffusion coefficient mapping', Journal of the Neurological Sciences, 216(1), pp. 11-15.

Kugler, P. (1992) 'Mitochondrial-Enzymes Related to Glutamate and GABA-Metabolism in the Hippocampus of Young and Aged Rats - A quantitative histochemical study', Neurochemical Research, 17(2), pp. 179-185.

Lam, A.D., Deck, G., Goldman, A., Eskandar, E.N., Noebels, J., Cole, A.J. (2017) ‘Silent Hippocampal Seizures and Spikes Identified by Foramen Ovale Electrodes in Alzheimer’s Disease’, Nat. Med., 23(6), pp. 678-680.

Lampinen, B., Szczepankiewicz, F., Martensson, J., van Westen, D., Sundgren, P.C. and Nilsson, M. (2017) 'Neurite density imaging versus imaging of microscopic anisotropy in diffusion MRI: A model comparison using spherical tensor encoding', Neuroimage, 147, pp. 517-531.

Larsen, N.B., Rasmussen, M. and Rasmussen, L.J. (2005) 'Nuclear and mitochondrial DNA repair: similar pathways?', Mitochondrion, 5(2), pp. 89-108.

Larsson, N.G. and Clayton, D.A. (1995) 'Molecular genetic aspects of human mitochondrial disorders', Annual Review of Genetics, 29, pp. 151-178.

Lax, N.Z. (2011) Understanding the mechanisms of neurodegeneration in mitochondrial disease. Thesis (Ph. D.) - University of Newcastle upon Tyne, 2011.

Lax, N.Z., Gorman, G.S. and Turnbull, D.M. (2017) 'Review: Central nervous system involvement in mitochondrial disease', Neuropathology and Applied Neurobiology, 43(2), pp. 102-118.

Lax, N.Z., Grady, J., Laude, A., Chan, F., Hepplewhite, P.D., Gorman, G., Whittaker, R.G., Ng, Y., Cunningham, M.O. and Turnbull, D.M. (2016) 'Extensive respiratory chain defects in inhibitory interneurones in patients with mitochondrial disease', Neuropathology and Applied Neurobiology, 42(2), pp. 180-193.

Lax, N.Z., Hepplewhite, P.D., Reeve, A.K., Nesbitt, V., McFarland, R., Jaros, E., Taylor, R.W. and Turnbull, D.M. (2012a) 'Cerebellar Ataxia in Patients With Mitochondrial DNA Disease: A Molecular Clinicopathological Study', Journal of Neuropathology and Experimental Neurology, 71(2), pp. 148-161.

Lax, N.Z., Pienaar, I.S., Reeve, A.K., Hepplewhite, P.D., Jaros, E., Taylor, R.W., Kalaria, R.N. and Turnbull, D.M. (2012b) 'Microangiopathy in the cerebellum of patients with mitochondrial DNA disease', Brain, 135, pp. 1736-1750.

Lebois, A. (2014) Brain microstructure mapping using quantitative and diffusion MRI. (Ph. D.) Universite Paris-Sud., 2014.

Lee, H., Park, J.H., Seo, I., Park, S.H. and Kim, S. (2014) 'Improved application of the electrophoretic tissue clearing technology, CLARITY, to intact solid organs including brain, pancreas, liver, kidney, lung, and intestine', Bmc Developmental Biology, 14, p. 7.

Levin, H.S., Wilde, E.A., Chu, Z.L., Yallampalli, R., Hanten, G.R., Li, X.Q., Chia, J., Vasquez, A.C. and Hunter, J.V. (2008) 'Diffusion tensor imaging in relation to cognitive and functional outcome of traumatic brain injury in children', Journal of Head Trauma Rehabilitation, 23(4), pp. 197-208.

Li, Y.X., Lin, J., Sun, C., Zhao, C.B. and Li, H.Q. (2017) 'Increased Cerebral Blood Flow as a Predictor of Episodes in MELAS Using Multimodal MRI', Journal of Magnetic Resonance Imaging, 46(3), pp. 915-918.

Lin, M.Y. and Sheng, Z.H. (2015) 'Regulation of mitochondrial transport in neurons', Experimental Cell Research, 334(1), pp. 35-44.

Lipton, M.L., Gellella, E., Lo, C., Gold, T., Ardekani, B.A., Shifteh, K., Bello, J.A. and Branch, C.A. (2008) 'Multifocal White Matter Ultrastructural Abnormalities in Mild Traumatic Brain Injury with Cognitive Disability: A Voxel-Wise Analysis of Diffusion Tensor Imaging', Journal of Neurotrauma, 25(11), pp. 1335-1342.

Liu, Z., Zheng, D., Wang, X., Zhang, J., Xie, S., Xiao, J. and Jiang, X. (2011a) 'Apparent Diffusion Coefficients of Metabolites in Patients with MELAS Using Diffusion-Weighted MR Spectroscopy', American Journal of Neuroradiology, 32(5), pp. 898-902.

Liu, Z.H., Liu, X.W., Hui, L.H., Zhao, D.H., Wang, X.Y., Xie, S., Xiao, J.X. and Jiang, X.X. (2011b) 'The appearance of ADCs in the non-affected areas of the patients with MELAS', Neuroradiology, 53(4), pp. 227-232.

Llopis, J., McCaffery, J.M., Miyawaki, A., Farquhar, M.G. and Tsien, R.Y. (1998) 'Measurement of cytosolic, mitochondrial, and Golgi pH in single living cells with green fluorescent proteins', Proceedings of the National Academy of Sciences of the United States of America, 95(12), pp. 6803-6808.

Lott, M.T. (2018) MITOMAP: A Human Mitochondrial Genome Database. Available at: http://www.mitomap.org (Accessed: 18th September 2018).

Lott, M.T., Leipzig, J.N., Derbeneva, O., Xie, H.M., Chalkia, D., Sarmady, M., Procaccio, C. and Wallace, D.C. (2013) 'mtDNA Variation and Analysis Using MITOMAP and MITOMASTER', Current Protocols in Bioinformatics, 1(123), p. 4.

Maclaren, J., Han, Z.Y., Vos, S.B., Fischbein, N. and Bammer, R. (2014) 'Reliability of brain volume measurements: A test-retest dataset', Scientific Data, 1, p. 9.

Majamaa-Voltti, K.A.M., Winqvist, S., Remes, A.M., Tolonen, U., Pyhtinen, J., Uimonen, S., Karppa, M., Sorri, M., Peuhkurinen, K. and Majamaa, K. (2006) 'A 3-year clinical follow-up of adult patients with 3243A > G in mitochondrial DNA', Neurology, 66(10), pp. 1470-1475.

Malhotra, K. and Liebeskind, D.S. (2016) 'Imaging of MELAS', Current Pain and Headache Reports, 20(9), p. 8.

Margulis, L. (1971) 'Symbiosis and Evolution', Scientific American, 225(2), pp. 49-&.

Martin, W.F., Garg, S. and Zimorski, V. (2015) 'Endosymbiotic theories for eukaryote origin', Philosophical Transactions of the Royal Society B-Biological Sciences, 370(1678), p. 18.

Mason, P.A., Matheson, E.C., Hall, A.G. and Lightowlers, R.N. (2003) 'Mismatch repair activity in mammalian mitochondria', Nucleic Acids Research, 31(3), pp. 1052-1058.

Matsushita, M., Hosoda, K., Naitoh, Y., Yamashita, H. and Kohmura, E. (2011) 'Utility of diffusion tensor imaging in the acute stage of mild to moderate traumatic brain injury for detecting white matter lesions and predicting long-term cognitive function in adults Clinical article', Journal of Neurosurgery, 115(1), pp. 130-139.

Matthews, P.M., Brown, R.M., Morten, K., Marchington, D., Poulton, J. and Brown, G. (1995) 'Intracellular Heteroplasmy for Disease-Associated Point Mutations in mtDNA - Implications for Disease Expression and Evidence for Mitotic Segregation of Heteroplasmic Units of mtDNA', Human Genetics, 96(3), pp. 261-268.

McBride, H.M., Neuspiel, M. and Wasiak, S. (2006) 'Mitochondria: More than just a powerhouse', Current Biology, 16(14), pp. R551-R560.

McFarland, H. F. and Martin, R. (2007) ‘Multiple sclerosis: a complicated picture of autoimmunity’, Nature Immunology, 8, pp. 913-919.

McFarland, R., Taylor, R.W. and Turnbull, D.M. (2002) 'The neurology of mitochondrial DNA disease', Lancet Neurology, 1(6), pp. 343-351.

McFarland, R., Taylor, R.W. and Turnbull, D.M. (2010) 'A neurological perspective on mitochondrial disease', Lancet Neurology, 9(8), pp. 829-840.

Mervaala, E., Fohr, J., Kononen, M., Valkonen-Korhonen, M., Vainio, P., Partanen, K., Partanen, J., Tiihonen, J., Viinamaki, H., Karjalainen, A.K. and Lehtonen, J. (2000) 'Quantitative MRI of the hippocampus and amygdala in severe depression', Psychological Medicine, 30(1), pp. 117-125.

Miceli, G., Conti, G., Cianfoni, A., Di Giacopo, R., Zampetti, P. and Servidei, S. (2008) 'Acute auditory agnosia as the presenting hearing disorder in MELAS', Neurological Sciences, 29(6), pp. 459-462.

Minobe, S., Matsuda, A., Mitsuhashi, T., Ishikawa, M., Nishimura, Y., Shibata, K., Ito, E., Goto, Y., Nakaoka, T. and Sakura, H. (2015) 'Vasodilatation of multiple cerebral arteries in early stage of stroke-like episode with MELAS', Journal of Clinical Neuroscience, 22(2), pp. 407-408.

Mizukami, K., Sasaki, M., Suzuki, T., Shiraishi, H., Koizumi, J., Ohkoshi, N., Ogata, T., Mori, N., Ban, S. and Kosaka, K. (1992) 'Central-Nervous-System Changes in Mitochondrial Encephalomyopathy - Light and Electron-Microscopic Study', Acta Neuropathologica, 83(4), pp. 449-452.

Morfini, G.A., Burns, M., Binder, L.I., Kanaan, N.M., LaPointe, N., Bosco, D.A., Brown, R.H., Brown, H., Tiwari, A., Hayward, L., Edgar, J., Nave, K.A., Garberrn, J., Atagi, Y., Song, Y.Y., Pigino, G. and Brady, S.T. (2009) 'Axonal Transport Defects in Neurodegenerative Diseases', Journal of Neuroscience, 29(41), pp. 12776-12786.

Morgan-Hughes, J.A., Sweeney, M.G., Cooper, J.M., Hammans, S.R., Brockington, M., Schapira, A.H.V., Harding, A.E. and Clark, J.B. (1995) 'Mitochondrial-DNA (mtDNA) Diseases - Correlation of genotype to phenotype', Biochimica Et Biophysica Acta-Molecular Basis of Disease, 1271(1), pp. 135-140.

Mulder, E.R., de Jong, R.A., Knol, D.L., van Schijndel, R.A., Cover, K.S., Visser, P.J., Barkhof, F., Vrenken, H. and Alzheimers Dis Neuroimaging, I. (2014) 'Hippocampal volume change measurement: Quantitative assessment of the reproducibility of expert manual outlining and the automated methods FreeSurfer and FIRST', Neuroimage, 92, pp. 169-181.

Murphy, J. L., Ratnaike. T. E., Shang, E., Falkous, G., Blakely, E. L., Alston, C. L., Hickman, K., Chanter, H., Taivassalo, T., Haller, R. G., Taylor, R. W., Turbull, D. M. (2012) ‘Long term endurance training and deconditioning in patients with mitochondrial myopathy’, United Kingdom Neuromuscular Translational Research Conference, Conference Proceedings, pp. S24.

Najac, C., Branzoli, F., Ronen, I. and Valette, J. (2016) 'Brain intracellular metabolites are freely diffusing along cell fibers in grey and white matter, as measured by diffusion-weighted MR spectroscopy in the human brain at 7 T', Brain Structure & Function, 221(3), pp. 1245-1254.

Najac, C., Marchadour, C., Guillermier, M., Houitte, D., Slavov, V., Brouillet, E., Hantraye, P., Lebon, V. and Valette, J. (2014) 'Intracellular metabolites in the primate brain are primarily localized in long fibers rather than in cell bodies, as shown by diffusion-weighted magnetic resonance spectroscopy', Neuroimage, 90, pp. 374-380.

Neil, J.J. (2008) 'Diffusion imaging concepts for clinicians', Journal of Magnetic Resonance Imaging, 27(1), pp. 1-7.

Nekolla, S., Gneiting, T., Syha, J., Deichmann, R. and Haase, A. (1992) 'T1 Maps by K-Space Reduced Snapshot-Flash MRI', Journal of Computer Assisted Tomography, 16(2), pp. 327-332.

Nelson, A.R., Sweeney, M.D., Sagare, A.P. and Zlokovic, B.V. (2016) 'Neurovascular dysfunction and neurodegeneration in dementia and Alzheimer's disease', Biochimica Et Biophysica Acta-Molecular Basis of Disease, 1862(5), pp. 887-900.

Nelson, S.L. (2017) MELAS Syndrome Clinical Presentation. Available at: https://emedicine.medscape.com/article/946864-clinical (Accessed: February).

Newcombe, V.F.J., Outtrim, J.G., Chatfield, D.A., Manktelow, A., Hutchinson, P.J., Coles, J.P., Williams, G.B., Sahakian, B.J. and Menon, D.K. (2011) 'Parcellating the neuroanatomical basis of impaired decision-making in traumatic brain injury', Brain, 134, pp. 759-768.

Nguyen, A.K.D., Simard-Meilleur, A. A., Berthiaume, C., Godbout, R., and Mottron, L. (2012) ‘Head Circumference in Canadian Male Adults: Development of a Normalized Chart’, Int. J. Morphol, 30(4), pp. 1474-1480.

Niogi, S.N., Mukherjee, P., Ghajar, J., Johnson, C., Kolster, R.A., Sarkar, R., Lee, H., Meeker, M., Zimmerman, R.D., Manley, G.T. and McCandliss, B.D. (2008) 'Extent of microstructural white matter injury in postconcussive syndrome correlates with impaired cognitive reaction time: A 3T diffusion tensor imaging study of mild traumatic brain injury', American Journal of Neuroradiology, 29(5), pp. 967-973.

Nucifora, P.G.P., Verma, R., Lee, S.K. and Melhem, E.R. (2007) 'Diffusion-tensor MR Imaging and tractography: Exploring brain microstructure and connectivity', Radiology, 245(2), pp. 367-384.

O'Brien, T. (2003) 'Properties of human mitochondrial ribosomes', Iubmb Life, 55(9), pp. 505-513.

O'Doherty, J.P. (2007) 'Lights, camembert, action! The role of human orbitofrontal cortex in a encoding stimuli, rewards, and choices', in Schoenbaum, G., Gottfried,

J.A., Murray, E.A. and Ramus, S.J. (eds.) Linking Affect to Action: Critical Contributions of the Orbitofrontal Cortex. Oxford: Blackwell Publishing, pp. 254-272.

Oh-Hama, T. (1997) 'Evolutionary consideration on 5-aminolevulinate synthase in nature', Origins of Life and Evolution of the Biosphere, 27(4), pp. 405-412.

Ohama, E., Ohara, S., Ikuta, F., Tanaka, K., Nishizawa, M. and Miyatake, T. (1987) 'Mitochondrial Angiopathy in Cerebral Blood-Vessels of Mitochondrial Encephalomyopathy', Acta Neuropathologica, 74(3), pp. 226-233.

Ohsawa, Y., Hagiwara, H., Nishimatsu, S.I., Hirakawa, A., Kamimura, N., Ohtsubo, H., Fukai, Y., Murakami, T., Koga, Y., Goto, Y.I., Ohta, S. and Sunada, Y. (2018) 'Taurine supplementation for prevention of stroke-like episodes in MELAS: a multicentre, open-label, 52-week phase III trial', J Neurol Neurosurg Psychiatry.

Ohshita, T., Oka, M., Imon, Y., Watanabe, C., Katayama, S., Yamaguchi, S., Kajima, T., Mimori, Y. and Nakamura, S. (2000) 'Serial diffusion-weighted imaging in MELAS', Neuroradiology, 42(9), pp. 651-656.

Okada, T., Kanagaki, M., Yamamoto, A., Sakamoto, R., Kasahara, S., Morimoto, E., Iima, M., Mehemed, T., Nakajima, S. and Togashi, K. (2011) ‘Which to choose for volumetry: MPRAGE or SPACE?’, ISMRM Proceedings 2011

Oppenheim, C., Galanaud, D., Samson, Y., Sahel, M., Dormont, D., Wechsler, B. and Marsault, C. (2000) 'Can diffusion weighted magnetic resonance imaging help differentiate stroke from stroke-like events in MELAS?', Journal of Neurology Neurosurgery and Psychiatry, 69(2), pp. 248-250.

Orczyk, C., Mikheev, A., Rosenkrantz, A., Melamed, J., Taneja, S. S., Rusinek, H. (2012) ‘Imaging of prostate cancer: a platform for 3D co-registration of in-vivo MRI ex-vivo MRI and pathology’, Proc. SPIE 8316 – Medical Imaging, pp. 83162M.

Örmeci, A.R., Gürbüz, H., Ayata, A., and Çetin, H. (1997) ‘Adult Head Circumferences and Centiles’, Journal of Turgut Özal Medical Centre, 4(3), pp. 261-264.

Osborn, A.G. (2013) Osborn's Brain. Altona, Manitoba, Canada: Friesens.

Oscar-Berman, M. and Marinkovic, K. (2003) ‘Alcoholism and the Brain: An Overview’, Alcohol Research and Health, 27(2), pp. 125-134.

Palade, G.E. (1952) 'The fine structure of mitochondria', The Anatomical Record, 114(3), pp. 427-451.

Palombo, M., Shemesh, N., Ronen, I. and Valette, J. (2017) 'Insights into brain microstructure from in vivo DW-MRS', Neuroimage.

Park, C.B. and Larsson, N.G. (2011) 'Mitochondrial DNA mutations in disease and aging', Journal of Cell Biology, 193(5), pp. 809-818.

Park, M.Y. and Byun, J.Y. (2012) 'Understanding the Mathematics Involved in Calculating Apparent Diffusion Coefficient Maps', American Journal of Roentgenology, 199(6), pp. W784-W784.

Parry, A. and Matthews, P.M. (2003) 'Roles for imaging in understanding the pathophysiology, clinical evaluation, and management of patients with mitochondrial disease', Journal of Neuroimaging, 13(4), pp. 293-302.

Pavlakis, S.G., Phillips, P.C., Dimauro, S., Devivo, D.C. and Rowland, L.P. (1984) 'Mitochondrial Myopathy, Encephalopathy, Lactic-Acidosis, and Stroke-Like Episodes - A Distinctive Clinical Syndrome', Annals of Neurology, 16(4), pp. 481-488.

Pfefferbaum, A., Sullivan, E.V., Adalsteinsson, E., Garrick, T. and Harper, C. (2004) 'Post mortem MR imaging of formalin-fixed human brain', Neuroimage, 21(4), pp. 1585-1595.

Phillips, J., (2015) The Investigation of Axonal Pathology in the Cerebellum of Patients with Mitochondrial Disease. Thesis (Ph. D.) - University of Newcastle upon Tyne, 2015.

Phillips, J., Laude, A., Lightowlers, R., Morris, C.M., Turnbull, D.M. and Lax, N.Z. (2016) 'Development of passive CLARITY and immunofluorescent labelling of multiple proteins in human cerebellum: understanding mechanisms of neurodegeneration in mitochondrial disease', Scientific Reports, 6, p. 12.

Poguzhelskaya, E., Artamonov, D., Bolshakova, A., Vlasova, O. and Bezprozvanny, I. (2014) 'Simplified method to perform CLARITY imaging', Molecular Neurodegeneration, 9, p. 5.

Popescu, V., Klaver, R., Voorn, P., Galis-de Graaf, Y., Knol, D.L., Twisk, J.W.R., Versteeg, A., Schenk, G.J., Van der Valk, P., Barkhof, F., De Vries, H.E., Vrenken, H.

and Geurts, J.J.G. (2015) 'What drives MRI-measured cortical atrophy in multiple sclerosis?', Multiple Sclerosis Journal, 21(10), pp. 1280-1290.

Raffelt, D.A., Tournier, J.D., Smith, R.E., Vaughan, D.N., Jackson, G., Ridgway, G.R. and Connelly, A. (2017) 'Investigating white matter fibre density and morphology using pixel-based analysis', Neuroimage, 144, pp. 58-73.

Rajasimha, H.K., Chinnery, P.F. and Samuels, D.C. (2008) 'Selection against pathogenic mtDNA mutations in a stem cell population leads to the loss of the 3243A -> G mutation in blood', American Journal of Human Genetics, 82(2), pp. 333-343.

Ratnaike, T. E., Murphy, J., Krishnan, K. J., Taylor, R. W., Turnbull, D. M. (2012) ‘Changes in mitochondrial function over time and with exercise in patients with mitochondrial disease’, United Kingdom Neuromuscular Translational Research Conference, Conference Proceedings, pp. S25.

Reece, J.B. and Campbell, N.A. (2011) Campbell Biology. 9th edn. Boston: Benjamin Cummings / Pearson.

Reisert, M., Kellner, E., Dhital, B., Hennig, J. and Kiselev, V.G. (2017) 'Disentangling micro from mesostructure by diffusion MRI: A Bayesian approach', Neuroimage, 147, pp. 964-975.

Rieckmann, A., Van Dijk, K.R.A., Sperling, R.A., Johnson, K.A., Buckner, R.L. and Hedden, T. (2016) 'Accelerated decline in white matter integrity in clinically normal individuals at risk for Alzheimer's disease', Neurobiology of Aging, 42, pp. 177-188.

Roberts, N., Puddephat, M.J. and McNulty, V. (2000) 'The benefit of stereology for quantitative radiology', British Journal of Radiology, 73(871), pp. 679-697.

Rocca, M.A., Valsasina, P., Pagani, E., Bianchi-Marzoli, S., Milesi, J., Falini, A., Comi, G. and Filippi, M. (2011) 'Extra-Visual Functional and Structural Connection Abnormalities in Leber's Hereditary Optic Neuropathy', Plos One, 6(2), p. 10.

Rodriguez-Cruces, R. and Concha, L. (2015) 'White matter in temporal lobe epilepsy: clinico-pathological correlates of water diffusion abnormalities', Quantitative Imaging in Medicine and Surgery, 5(2), pp. 264-278.

Romero-Sierra, C. (1986) Neuroanatomy: A Conceptual Approach. 1st edn. New York: Churchill Livingstone.

Rorden, C. and Brett, M. (2000) ‘Stereotaxic display of brain lesions’, Behavioural Neurology, 12, pp. 191-200.

Rossier, M.F. (2006) 'T channels and steroid biosynthesis: in search of a link with mitochondria', Cell Calcium, 40(2), pp. 155-164.

Rossignol, R., Faustin, B., Rocher, C., Malgat, M., Mazat, J.P. and Letellier, T. (2003) 'Mitochondrial threshold effects', Biochemical Journal, 370, pp. 751-762.

Saneto, R.P., Friedman, S.D. and Shaw, D.W.W. (2008) 'Neuroimaging of mitochondrial disease', Mitochondrion, 8(5-6), pp. 396-413.

Sato, M. and Sato, K. (2013) 'Maternal inheritance of mitochondrial DNA by diverse mechanisms to eliminate paternal mitochondrial DNA', Biochimica Et Biophysica Acta-Molecular Cell Research, 1833(8), pp. 1979-1984.

Schmierer, K., Bizzi, A., Jackson, G., Punwani, S., Waldman, A., Tournier, D., Nilsson, M., Campbell, J., Jiang, X. and Veraart, J. (2018) ISMRM. Paris, France.

Schmierer, K., Thavarajah, J.R., An, S.F., Brandner, S., Miller, D.H. and Tozer, D.J. (2010) 'Effects of Formalin Fixation on Magnetic Resonance Indices in Multiple Sclerosis Cortical Gray Matter', Journal of Magnetic Resonance Imaging, 32(5), pp. 1054-1060.

Schmierer, K., Wheeler-Kingshott, C.A.M., Tozer, D.J., Boulby, P.A., Parkes, H.G., Yousry, T.A., Scaravilli, F., Barker, G.J., Tofts, P.S. and Miller, D.H. (2008) 'Quantitative magnetic resonance of postmortem multiple sclerosis brain before and after fixation', Magnetic Resonance in Medicine, 59(2), pp. 268-277.

Schneider, C.A., Rasband, W.S. and Eliceiri, K.W. (2012) 'NIH Image to ImageJ: 25 years of image analysis', Nature Methods, 9(7), pp. 671-675.

Seehaus, A., Roebroeck, A., Bastiani, M., Fonseca, L., Bratzke, H., Lori, N., Vilanova, A., Goebel, R. and Galuske, R. (2015) 'Histological validation of high-resolution DTI in human post mortem tissue', Frontiers in Neuroanatomy, 9, p. 12.

Shepherd, T., Prince, S.J.D. and Alexander, D.C. (2012) 'Interactive Lesion Segmentation with Shape Priors From Offline and Online Learning', IEEE Transactions on Medical Imaging, 31(9), pp. 1698-1712.

Shi, Y.H., Dierckx, A., Wanrooij, P.H., Wanrooij, S., Larsson, N.G., Wilhelmsson, L.M., Falkenberg, M. and Gustafsson, C.M. (2012) 'Mammalian transcription factor A is a core component of the mitochondrial transcription machinery', Proceedings of the National Academy of Sciences of the United States of America, 109(41), pp. 16510-16515.

Skulachev, V.P. (2001) 'Mitochondrial filaments and clusters as intracellular power-transmitting cables', Trends in Biochemical Sciences, 26(1), pp. 23-29.

Smith, E.E., Schneider, J.A., Wardlaw, J.M. and Greenberg, S.M. (2012) 'Cerebral microinfarcts: the invisible lesions', Lancet Neurology, 11(3), pp. 272-282.

Smith, S.M. (2002) 'Fast robust automated brain extraction', Human Brain Mapping, 17(3), pp. 143-155.

Smith, S.M., Jenkinson, M., Woolrich, M.W., Beckmann, C.F., Behrens, T.E.J., Johansen-Berg, H., Bannister, P.R., De Luca, M., Drobnjak, I., Flitney, D.E., Niazy, R.K., Saunders, J., Vickers, J., Zhang, Y.Y., De Stefano, N., Brady, J.M. and Matthews, P.M. (2004) 'Advances in functional and structural MR image analysis and implementation as FSL', Neuroimage, 23, pp. S208-S219.

Smith, S.M., Zhang, Y.Y., Jenkinson, M., Chen, J., Matthews, P.M., Federico, A. and De Stefano, N. (2002) 'Accurate, robust, and automated longitudinal and cross-sectional brain change analysis', Neuroimage, 17(1), pp. 479-489.

Smits, P., Smeitink, J. and van den Heuvel, L. (2010) 'Mitochondrial Translation and Beyond: Processes Implicated in Combined Oxidative Phosphorylation Deficiencies', Journal of Biomedicine and Biotechnology, p. 24.

Sparaco, M., Bonilla, E., Dimauro, S. and Powers, J.M. (1993) 'Neuropathology of Mitochondrial Encephalomyopathies due to Mitochondrial-DNA Defects', Journal of Neuropathology and Experimental Neurology, 52(1), pp. 1-10.

Spence, R.D., Kurth, F., Itoh, N., Mongerson, C.R.L., Wailes, S.H., Peng, M.S. and MacKenzie-Graham, A.J. (2014) 'Bringing CLARITY to gray matter atrophy', Neuroimage, 101, pp. 625-632.

Steffann, J., Frydman, N., Gigarel, N., Burlet, P., Ray, P.F., Fanchin, R., Feyereisen, E., Kerbrat, V., Tachdjian, G., Bonnefont, J.P., Frydman, R. and Munnich, A. (2006)

'Analysis of mtDNA variant segregation during early human embryonic development: a tool for successful NARP preimplantation diagnosis', Journal of Medical Genetics, 43(3), pp. 244-247.

Steinman, L. (1996) ‘Multiple Sclerosis: A Coordinated Immunological Attack against Myelin in the Central Nervous System’, Cell, 85(3), pp. 299-302.

Stejskal, E.O. and Tanner, J.E. (1965) 'Spin Diffusion Measurements: Spin Echoes in the Presence of a Time-Dependent Field Gradient', The Journal of Chemical Physics, 42(1).

Stewart, J.B. and Chinnery, P.F. (2015) 'The dynamics of mitochondrial DNA heteroplasmy: implications for human health and disease', Nature Reviews Genetics, 16(9), pp. 530-542.

Stewart, J.D., Horvath, R., Baruffini, E., Ferrero, I., Bulst, S., Watkins, P.B., Fontana, R.J., Day, C.P. and Chinnery, P.F. (2010) 'Polymerase gamma Gene POLG Determines the Risk of Sodium Valproate-Induced Liver Toxicity', Hepatology, 52(5), pp. 1791-1796.

Stierum, R.H., Dianov, G.L. and Bohr, V.A. (1999) 'Single-nucleotide patch base excision repair of uracil in DNA by mitochondrial protein extracts', Nucleic Acids Research, 27(18), pp. 3712-3719.

Stikov, N., Tardif, C., Barral, J.K., Levesque, I. and Pikes, G.B. (2011) 'T1 mapping: methods and challenges', Proceedings International Society for Magnetic Resonance in medicine, p. 1.

Styner, M. A., Charles, H. C., Park, J., Gerig, G. (2002) ‘Multisite validation of image analysis methods: assessing intra- and intersite variability’, SPIE Proceedings 4684 Medical Imaging: Image Processing.

Sue, C.M., Crimmins, D.S., Soo, Y.S., Pamphlett, R., Presgrave, C.M., Kotsimbos, N., Jean-Francois, M.J.B., Byrne, E. and Morris, J.G.L. (1998) 'Neuroradiological features of six kindreds with MELAS tRNA(Leu) A3243G point mutation: implications for pathogenesis', Journal of Neurology Neurosurgery and Psychiatry, 65(2), pp. 233-240.

Sutovsky, P., Moreno, R.D., Ramalho-Santos, J., Dominko, T., Simerly, C. and Schatten, G. (1999) 'Development - Ubiquitin tag for sperm mitochondria', Nature, 402(6760), pp. 371-372.

Suzuki, Y., Iizuka, T., Kobayashi, T., Nishikawa, T., Atsumi, Y., Kadowaki, T., Oka, Y., Kadowaki, H., Taniyama, M. and Hosokawa, K. (1997) 'Diabetes mellitus associated with the 3243 mitochondrial tRNA(Leu(UUR)) mutation: Insulin secretion and sensitivity', Metabolism-Clinical and Experimental, 46(9), pp. 1019-1023.

Tanahashi, C., Nakayama, A., Yoshida, M., Ito, M., Mori, N. and Hashizume, Y. (2000) 'MELAS with the mitochondrial DNA 3243 point mutation: a neuropathological study', Acta Neuropathologica, 99(1), pp. 31-38.

Tanji, K., Kunimatsu, T., Vu, T.H. and Bonilla, E. (2001) 'Neuropathological features of mitochondrial disorders', Seminars in Cell & Developmental Biology, 12(6), pp. 429-439.

Tarnopolsky, M. (2016) 'Exercise and Nutrition Therapy for Mitochondrial Disease', mitoAction. Available at: http://www.mitoaction.org/blog/exercise-nutrition.

Tatlisumak, T., Putaala, J., Innila, M., Enzinger, C., Metso, T.M., Curtze, S., von Sarnowski, B., Amaral-Silva, A., Jungehulsing, G.J., Tanislav, C., Thijs, V., Rolfs, A., Norrving, B., Fazekas, F., Suomalainen, A. and Kolodny, E.H. (2016) 'Frequency of MELAS main mutation in a phenotype-targeted young ischemic stroke patient population', Journal of Neurology, 263(2), pp. 257-262.

Taylor, P.N., Kaiser, M. and Dauwels, J. (2014) 'Structural connectivity based whole brain modelling in epilepsy', Journal of Neuroscience Methods, 236, pp. 51-57.

Taylor, R.W. and Turnbull, D.M. (2005) 'Mitochondrial DNA mutations in human disease', Nature Reviews Genetics, 6(5), pp. 389-402.

Tofts, P. (2003) Quantitative MRI of the Brain. Chichester: John Wiley & Sons Ltd.

Tomer, R., Ye, L., Hsueh, B. and Deisseroth, K. (2014) 'Advanced CLARITY for rapid and high-resolution imaging of intact tissues', Nature Protocols, 9(7), pp. 1682-1697.

Tovi, M. and Ericsson, A. (1992) 'MEASUREMENTS OF T1 AND T2 OVER TIME IN FORMALIN-FIXED HUMAN WHOLE-BRAIN SPECIMENS', Acta Radiologica, 33(5), pp. 400-404.

Tschampa, H.J., Urbach, H., Greschus, S., Kunz, W.S. and Kornblum, C. (2013) 'Neuroimaging characteristics in mitochondrial encephalopathies associated with the m.3243A > G MTTL1 mutation', Journal of Neurology, 260(4), pp. 1071-1080.

Tsujikawa, K., Senda, J., Yasui, K., Hasegawa, Y., Hoshiyama, M., Katsuno, M. and Sobue, G. (2016) 'Distinctive distribution of brain volume reductions in MELAS and mitochondrial DNA A3243G mutation carriers: A voxel-based morphometric study', Mitochondrion, 30, pp. 229-235.

Tsujikawa, T., Yamamoto, T., Ikawa, M., Yoneda, M. and Kimura, H. (2012) 'Crossed cerebellar hyperperfusion after MELAS attack followed up by whole brain continuous arterial spin labeling perfusion imaging', Acta Radiologica, 53(2), pp. 220-222.

Tuppen, H.A.L., Blakely, E.L., Turnbull, D.M. and Taylor, R.W. (2010) 'Mitochondrial DNA mutations and human disease', Biochimica Et Biophysica Acta-Bioenergetics, 1797(2), pp. 113-128.

Turken, A.U., Whitfield-Gabrieli, S., Bammer, R., Baldo, J.V., Dronkers, N.F. and Gabrieli, J.D.E. (2008) 'Cognitive processing speed and the structure of white matter pathways: Convergent evidence from normal variation and lesion studies', Neuroimage, 42(2), pp. 1032-1044.

Tzoulis, C. and Bindoff, L.A. (2009) 'Serial Diffusion Imaging in a Case of Mitochondrial Encephalomyopathy, Lactic Acidosis, and Stroke-Like Episodes', Stroke, 40(2), pp. E15-E17.

Tzoulis, C., Henriksen, E., Miletic, H. and Bindoff, L.A. (2017) 'No evidence of ischemia in stroke-like lesions of mitochondrial POLG encephalopathy', Mitochondrion, 32, pp. 10-15.

Uehara, R., Yamashita, K., Hiwatashi, A., Togao, O., Kikuchi, K., Yokoyama, J., Matsuse, D., Yoshiura, T. and Honda, H. (2014) 'Intravoxel incoherent motion magnetic resonance imaging findings in the acute phase of MELAS: a case report', Brain and Behavior, 4(6), pp. 798-800.

Ungerleider, L.G. and Mishkin, M. (1982) Two Cortical Visual Systems. Cambridge: MIT Press.

Valette, J., Ligneul, C., Marchadour, C., Najac, C. and Palombo, M. (2018) 'Brain Metabolite Diffusion from Ultra-Short to Ultra-Long Time Scales: What Do We Learn, Where Should We Go?', Frontiers in Neuroscience, 12, p. 6.

Van De Pavert, S.H.P. (2017) Grey matter pathology in multiple sclerosis: in vivo and post mortem magnetic resonance imaging studies. University College London.

van der Toorn, A., Dijkhuizen, R.M., Tulleken, C.A.F. and Nicolay, K. (1996) 'Diffusion of metabolites in normal and ischemic rat brain measured by localized H-1 MRS', Magnetic Resonance in Medicine, 36(6), pp. 914-922.

van Ginneken, B. (2018) ISMRM. Paris, France.

Velasco-Annis, C., Akhondi-Asl, A., Stamm, A. and Warfield, S.K. (2018) 'Reproducibility of Brain MRI Segmentation Algorithms: Empirical Comparison of Local MAP PSTAPLE, FreeSurfer, and FSL-FIRST', Journal of Neuroimaging, 28(2), pp. 162-172.

Virtanen, S.M., Lindroos, M.M., Majamaa, K., Nuutila, P., Borra, R.J. and Parkkola, R. (2011) 'Voxelwise Analysis of Diffusion Tensor Imaging and Structural MR Imaging in Patients with the m.3243A > G Mutation in Mitochondrial DNA', American Journal of Neuroradiology, 32(3), pp. 522-526.

Vollmar, C., O'Muircheartaigh, J., Barker, G. J., Symms, M. R., Thompson, P., Kumari, V., Duncan, J. S., Richardson, M. P., Koepp, M. J. (2010) 'Identical, but not the same: Intra-site and inter-site reproducibility of fractional anisotropy measures on two 3.0 T scanners', NeuroImage, 51(4-4) pp. 1384-1394.

Waehnert, M.D., Dinse, J., Schafer, A., Geyer, S., Bazin, P.L., Turner, R. and Tardif, C.L. (2016) 'A subject-specific framework for in vivo myeloarchitectonic analysis using high resolution quantitative MRI', Neuroimage, 125, pp. 94-107.

Wallace, D.C. (2010) 'Mitochondrial DNA Mutations in Disease and Aging', Environmental and Molecular Mutagenesis, 51(5), pp. 440-450.

Wang, C.X. and Youle, R.J. (2009) 'The Role of Mitochondria in Apoptosis', in Annual Review of Genetics. Palo Alto: Annual Reviews, pp. 95-118.

Weber, K., Wilson, J.N., Taylor, L., Brierley, E., Johnson, M.A., Turnbull, D.M. and Bindoff, L.A. (1997) 'A new mtDNA mutation showing accumulation with time and

restriction to skeletal muscle', American Journal of Human Genetics, 60(2), pp. 373-380.

Whelan, C.D., Altmann, A., Botía, J.A., Jahanshad, N., Hibar, D.P., Absil, J., Alhusaini, S., Alvim, M.K.M., Auvinen, P., Bartolini, E., Bergo, F.P.G., Bernardes, T., Blackmon, K., Braga, B., Caligiuri, M.E., Calvo, A., Carr, S.J., Chen, J., Chen, S., Cherubini, A., David, P., Domin, M., Foley, S., França, W., Haaker, G., Isaev, D., Keller, S.S., Kotikalapudi, R., Kowalczyk, M.A., Kuzniecky, R., Langner, S., Lenge, M., Leyden, K.M., Liu, M., Loi, R.Q., Martin, P., Mascalchi, M., Morita, M.E., Pariente, J.C., Rodríguez-Cruces, R., Rummel, C., Saavalainen, T., Semmelroch, M.K., Severino, M., Thomas, R.H., Tondelli, M., Tortora, D., Vaudano, A.E., Vivash, L., von Podewils, F., Wagner, J., Weber, B., Yao, Y., Yasuda, C.L., Zhang, G., Bargalló, N., Bender, B., Bernasconi, N., Bernasconi, A., Bernhardt, B.C., Blümcke, I., Carlson, C., Cavalleri, G.L., Cendes, F., Concha, L., Delanty, N., Depondt, C., Devinsky, O., Doherty, C.P., Focke, N.K., Gambardella, A., Guerrini, R., Hamandi, K., Jackson, G.D., Kälviäinen, R., Kochunov, P., Kwan, P., Labate, A., McDonald, C.R., Meletti, S., O'Brien, T.J., Ourselin, S., Richardson, M.P., Striano, P., Thesen, T., Wiest, R., Zhang, J., Vezzani, A., Ryten, M., Thompson, P.M., Sisodiya, S.M. (2018) ‘Structural brain abnormalities in the common epilepsies assessed in a worldwide ENIGMA study’, Brain, 141(2), pp. 391-408.

Wick, M., Nagatomo, Y., Prielmeier, F. and Frahm, J. (1995) 'Alteration of Intracellular Metabolite Diffusion in Rat-Brain in vivo During Ischemia and Reperfusion', Stroke, 26(10), pp. 1930-1933.

Wood, E.T., Ercan, E., Sati, P., Cortese, I.C.M., Ronen, I. and Reich, D.S. (2017) 'Longitudinal MR spectroscopy of neurodegeneration in multiple sclerosis with diffusion of the intra-axonal constituent N-acetylaspartate', Neuroimage-Clinical, 15, pp. 780-788.

Yakubovskaya, E., Guja, K.E., Eng, E.T., Choi, W.S., Mejia, E., Beglov, D., Lukin, M., Kozakov, D. and Garcia-Diaz, M. (2014) 'Organization of the human mitochondrial transcription initiation complex', Nucleic Acids Research, 42(6), pp. 4100-4112.

Yang, C.Y., Liu, H.M., Chen, S.K., Chen, Y.F., Lee, C.W. and Yeh, L.R. (2016) 'Reproducibility of Brain Morphometry from Short-Term Repeat Clinical MRI Examinations: A Retrospective Study', Plos One, 11(1), p. 15.

Yasui, A., Yajima, H., Kobayashi, T., Eker, A.P.M. and Oikawa, A. (1992) 'Mitochondrial-DNA Repair by Photolyase', Mutation Research, 273(2), pp. 231-236.

Yoneda, M., Ikawa, M., Arakawa, K., Kudo, T., Kimura, H., Fujibayashi, Y. and Okazawa, H. (2012) 'In vivo functional brain imaging and a therapeutic trial of L-arginine in Patients with MELAS', Biochimica Et Biophysica Acta-General Subjects, 1820(5), pp. 615-618.

Yong-Hing, C.J., Obenaus, A., Stryker, R., Tong, K. and Sarty, G.E. (2005) 'Magnetic resonance imaging and mathematical modeling of progressive formalin fixation of the human brain', Magnetic Resonance in Medicine, 54(2), pp. 324-332.

Youle, R.J. and van der Bliek, A.M. (2012) 'Mitochondrial Fission, Fusion, and Stress', Science, 337(6098), pp. 1062-1065.

Zhang, J., Guo, J.H., Fang, W.H., Jun, Q.L. and Shi, K.L. (2015) 'Clinical features of MELAS and its relation with A3243G gene point mutation', International Journal of Clinical and Experimental Pathology, 8(10), pp. 13411-13415.

Zhang, J., Liu, H., Luo, S.Y., Lu, Z., Chavez-Badiola, A., Liu, Z.T., Yang, M.X., Merhi, Z., Silber, S.J., Munne, S., Konstantinidis, M., Wells, D., Tang, J.J. and Huang, T.S. (2017) 'Live birth derived from oocyte spindle transfer to prevent mitochondrial disease (vol 34, pg 361, 2017)', Reproductive Biomedicine Online, 35(6), pp. 750-750.

Zhang, Y.Y., Brady, M. and Smith, S. (2001) 'Segmentation of brain MR images through a hidden Markov random field model and the expectation-maximization algorithm', Ieee Transactions on Medical Imaging, 20(1), pp. 45-57.

Zheng, D.D., Liu, Z.H., Fang, J., Wang, X.Y. and Zhang, J. (2012) 'The Effect of Age and Cerebral Ischemia on Diffusion-Weighted Proton MR Spectroscopy of the Human Brain', American Journal of Neuroradiology, 33(3), pp. 563-568.

Zhu, T., Liu, X.X., Gaugh, M.D., Connelly, P.R., Ni, H.Y., Ekholm, S., Schifitto, G. and Zhong, J.H. (2009) 'Evaluation of Measurement Uncertainties in Human Diffusion Tensor Imaging (DTI)-Derived Parameters and Optimization of Clinical DTI Protocols With a Wild Bootstrap Analysis', Journal of Magnetic Resonance Imaging, 29(2), pp. 422-435.

Appendix A – Global Segmentation Procedure Details

A.1 Segmentation of global tissue volumes

Segmentation of the MRI scan images to produce the global tissue volumes was carried out using the FSL FMRIB's Automated Segmentation Tool (FAST) (Zhang *et al.*, 2001) as justified by the work carried out in Chapter 4 regarding the accuracy of the volumetric outputs.

Stage 1: Skull stripping was carried out using the FSL Brain Extraction Tool (BET) (Smith, 2002) using the following settings:

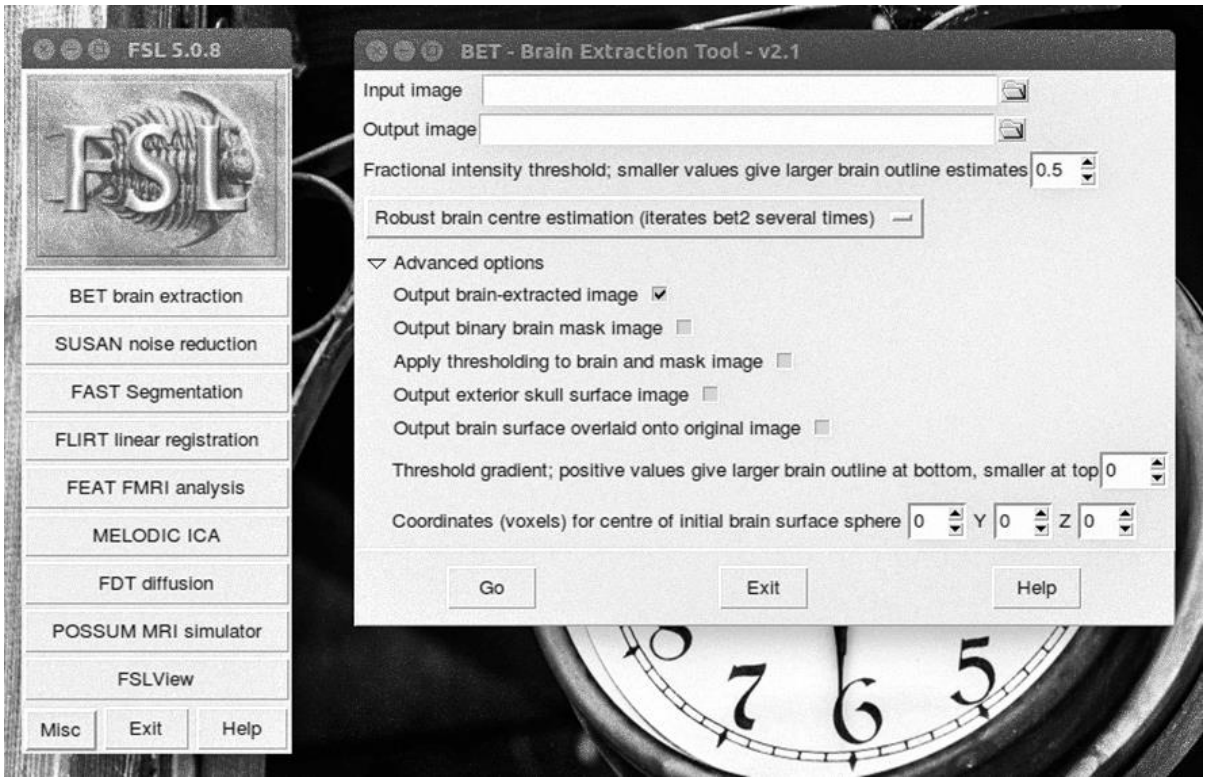

Figure 51. Screen capture of the FSL BET GUI (reproduced here with the permission of the FMRIB FSL Development Group, Oxford University).

Input file = original .nii file

Output file = original-brain.nii.gz file

Fractional intensity threshold was optimised to provide the most accurate removal of the skull, leaving the entire brain cavity intact. It was found that for all of the high-resolution scans this should be set to 0.5.

The extraction protocol used was: Robust brain centre estimation (iterates bet2 several times), where bet2 is the basic brain extraction tool algorithm.

The extracted brain file was then examined using FSLView to assess the accuracy of the brain extraction to ensure that all of the brain was present. The brain-extracted image would then be further used in the segmentation process using the FSL FAST.

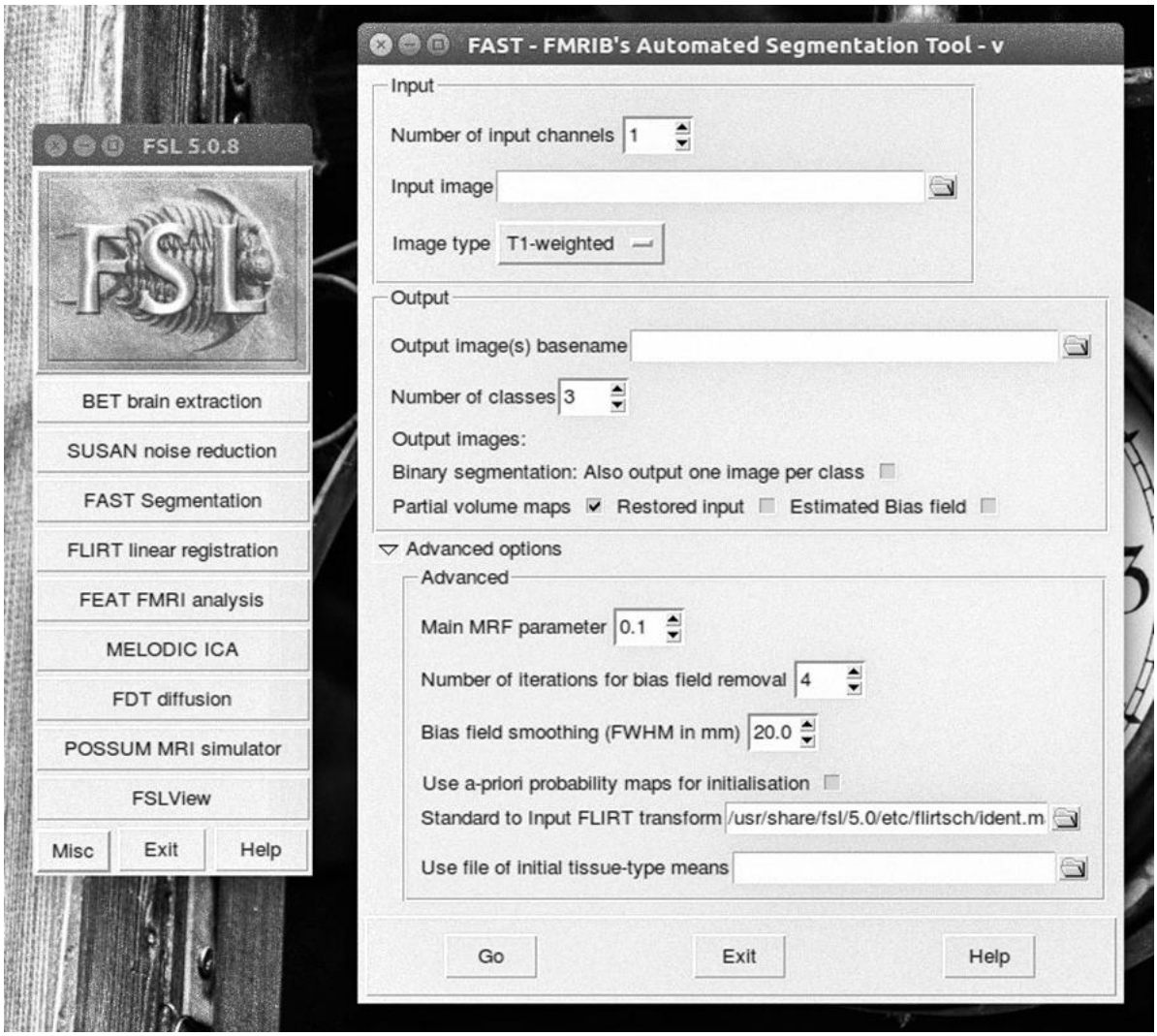

Figure 52. Screen capture of the FSL FAST GUI (reproduced here with the permission of the FMRIB FSL Development Group, Oxford University).

Leave all settings as is, except increase number of iterations to 5.

3 output files created, one for each of the tissue types:

pve_0 = CSF

pve_1 = GM

pve_2 = WM

The segmentation for each individual was then assessed using FSLView, loading up the extracted brain file and overlaying each of the segmented classifications on top to ensure that the segmentation was ok.

The volumetric measurement for each of these is then extracted using the command line prompt:

fslstats file_pve_0.nii.gz –M –V

To obtain the volume in mm^3 of each tissue type, the first and third of the returned values must be multiplied by each other.

Appendix B – TBSS Protocol Details

TBSS Protocol

Pre-processing for 17 NCL patients

Select only the first average of the scan taken by using the following commands in the FSL terminal:

fslroi input_file.nii.gz output_file.nii.gz 0 65

Select the second average:

fslroi input_file.nii.gz output_file.nii.gz 65 65

Open bval and bvec files in Excel and take out second average ‘a’ values (they are the same for both averages).

Create a new folder for each input .nii file with a copy of the bval and bvec file.

Carry out eddy current correction:

eddy_correct input_file.nii ecc.nii 0

Rotate bvecs:

fdt_rotate_bvecs input.bvec rot.bvec ecc.ecclog

Note that bvecs must be rotated for each individual DTI .nii file as the eddy current correction will be different for each one.

Open the FSL GUI.

Run brain extraction (BET):

Input file is ecc.nii (BET will only take the b0 scan to run the BET on), leave output file to populate automatically, set the fractional intensity to 0.25, use the ‘Robust brain centre estimation’, and check the ‘Output binary mask image’ option in the ‘Advanced’ section.

Open FSLView and carry out a manual check of the brain extraction to ensure that the whole brain has been selected, but that there is no excessive material around the

brain. If either case is encountered modify the fractional intensity value (lower value = more volume included, higher value = smaller volume included).

Run DTIFIT:

Select ‘FDT Diffusion’

In the dropdown menu at the top of the box select ‘DTIFIT Reconstruction diffusion tensors’

Select ‘Specify input files manually’.

Diffusion weighted data = ecc.nii

BET binary brain mask = ecc_brain_mask.nii

Output basename: Automatically populates

Gradient directions = rot.bvec

B values = file_name.bval

Once DTIFIT has been run on all of the files required, collect all of the FA files into a single folder ensuring that each group (i.e. controls, carriers, patients) have a different identifier at the beginning of the FA filename.

Pre-TBSS processing stages

From within the folder of FA files run the follow:

*tbss_1_preproc *.nii.gz*

This creates a new folder called ‘FA’, along with another called ‘origdata’ that will contain all of the original FA files.

Once tbss_1 has run, open the FA folder, then open the ‘slicesdir’ folder. If the processing has been successful all of the strips will show DTI images. If any do not show images and are blank, this indicates that there has been a problem with the processing and that the processing needs to be run again.

Then run

tbss_2_reg –T

to align all of the FA images to the FMRIB58_FA standard space.

tbss_3_postreg –S

to bring all of the subjects into MNI152 space.

View the skeleton output in the stats folder (mean_FA) to assess what the most suitable threshold is for the next stage. This is used to remove noise from outside the white matter. The threshold can most often be set at 0.2.

tbss_4_prestats 0.2

to apply the thresholding.

Pre-TBSS DTI Batch Processing

Each .nii DTI file should be in its own folder with a copy of all.bvec and all.bval. The script then carries out eddy current correction, b vector rotation, brain extraction on the b0 scan, and finally the DTIFIT process. This will output a number of files but the FA is the file required for TBSS.

Shell script to automate the pre-TBSS DTI processing:

#!/bin/sh

eddy_correct file_in.nii ecc.nii 0

fdt_rotate_bvecs all.bvec rot.bvec ecc.ecclog

bet ecc.nii ecc_brain.nii –R –f 0.25 –g 0 –m

dtifit --data=ecc.nii.gz --out=dti --mask=ecc_brain_mask.nii.gz --bvecs=rot.bvec --bvals=all.bval

done

TBSS

To run TBSS a general linear matrix (GLM) needs to be generated. This can be carried out by opening the FSL GUI and using the GLM option in the Misc tab. It is easiest to create this within the ‘stats’ folder of the current analysis folder.

The group sizes used in the statistical analysis were as follows:

Carriers (10) – Patients (8) = Total 18

In all cases two EVs were used with group 1 being the first named group above, and group 2 being the second named group.

Four contrasts were used for each analysis with values as shown in brackets and the control-carrier group used as an example:

1. Carrier FA > MELAS FA (1, -1)
2. MELAS FA > Carrier FA (-1, 1)
3. Carrier mean FA (1, 0)
4. MELAS mean FA (0, 1)

The matrix should be then be saved in the stats folder as e.g. CaME for the above example, which then generates a number of files that will be used in the next stage.

The final step is to run ‘randomise’ to carry out the analysis using the following command line, where ‘n’ is the number of permutations:

randomise -i all_FA_skeletonised -o tbss -m mean_FA_skeleton_mask -d GLM_matrix_name.mat -t GLM_matrix_name.con -n 5000 –T2 -V

The number of permutations used in this analysis was 5000, however this should be considered the minimum for each of the larger datasets and if time and processing facilities permit, larger n values should be used for large datasets such as these.